T H E U N I V E R S I T Y O F T U L S A

THE GRADUATE SCHOOL

ANALYTICAL SOLUTIONS FOR PRESSURE TRANSIENT ANALYSIS OF INJECTION, FALLOFF AND FLOWBACK DATA FOR TWO-PHASE FLOW PROBLEMS

by
Cíntia Gonçalves Machado

A dissertation submitted in partial fulfillment of
the requirements for the degree of Doctor of Philosophy
in the Discipline of Petroleum Engineering

The Graduate School
The University of Tulsa

2018

T H E U N I V E R S I T Y O F T U L S A

THE GRADUATE SCHOOL

ANALYTICAL SOLUTIONS FOR PRESSURE TRANSIENT ANALYSIS OF INJECTION, FALLOFF AND FLOWBACK DATA FOR TWO-PHASE FLOW PROBLEMS

by
Cíntia Gonçalves Machado

A DISSERTATION

APPROVED FOR THE DISCIPLINE OF

PETROLEUM ENGINEERING

By Dissertation Committee

Albert Coburn Reynolds Jr., Chair
Rami Mustafa Younis
Mustafa Onur
Christian Constanda

ABSTRACT

Cíntia Gonçalves Machado (Doctor of Philosophy in Petroleum Engineering)

Analytical Solutions for Pressure Transient Analysis of Injection, Falloff and Flowback Data for Two-Phase Flow Problems

Directed by Albert Coburn Reynolds Jr.

210 pp., Chapter 5: Discussions and Conclusions

(301 words)

In the petroleum industry, well testing is a common practice. A well test consists of wellbore pressure and flow rate data acquisition to estimate parameters that govern flow in the reservoir rock. Well tests give insight into the oil and gas field production potential and profitability, allow the estimation of reservoir parameters and inform the decision of whether a well needs to be stimulated. Multiphase flow is the norm in petroleum reservoirs, where water - but also gas and gas dissolved in or alternated with water - injection is commonly used to displace oil to a producing well. An injection-falloff test consists of a period of fluid injection into an reservoir, followed by a period of shut-in (zero flow rate). Injection-falloff testing is particularly important for offshore reservoirs containing high amount of harmful gases like carbon dioxide and sulfur dissolved in the oil. In this environment, a conventional test (production test) on an exploratory well cannot be run because the emission of these gases to the atmosphere is harmful to the environment; hence, there is a need to develop techniques for analyzing pressure data from injection-falloff tests. If we can return a well to production subsequent to an injection-falloff test, then during the flowback period, the sandface will be exposed to a range of water saturations. Consequently, the wellbore pressure during the flowback period must be influenced by the changing water saturation in the near wellbore region and hence must contain information about the two-phase oil-water relative permeability and capillary pressure curves. This work presents a procedure to

generate analytical solutions to model multiphase tests involving different physical processes to provide an accurate and fast forward-model for well test analysis of injection-falloff and injection-falloff-production tests, considering hysteresis and capillary pressure effects on the wellbore pressure response.

"The Guide is definitive. Reality is frequently inaccurate."

— Douglas Adams in *The Restaurant at the End of the Universe*

ACKNOWLEDGEMENTS

I would like to thank my advisor, Dr. Albert Reynolds, for his guidance and patience through this journey. His integrity, hard work and search for perfection will always be an example in my life. I want to thank my professors, Dr. Younis, Dr. Miska, Dr. Chen, Dr. Zhang, Dr. Constanda, Dr. Shahvali, Dr. Redner, Dr. Crunkleton, Dr. Forouzanfar and Dr. Lu for all the interesting lectures and assignments along with some challenging life-lessons. I shall also thank Dr. Onur; and this covers the dissertation committee. I thank the department staff, Judy, Loreta and Rhonda, for unremittingly being here to help and support us. Likewise, let me not forget to thank Mike Stafford and his coffee and I should not neglect to thank Helen, who - besides keeping our building habitable and erasing our unimportant derivations - had never abstained us of a warm good morning smile. My special thanks goes to my dear friends for always making me feel at home and safeguarded: Ranran, Sepide, Bailian, Rocky, Shaho, Soham, Ruslan, Walter, Niyati, Gosha, Shanshan, Emilio, Reza, Javad, Taşansu, Thiana and whoever else that might be reading this and thinking I have forgotten you. And finally, yet importantly, I thank my family for constantly reminding me to enjoy the strawberries of life and my boyfriend Enrique, to whom I dedicate this dissertation, for invariably pushing me hard and continually bringing me back to reality. This research was conducted under the auspices of TUPREP, the Tulsa University Petroleum Reservoir Exploitation Projects, and it was prepared with financial support from the Coordination for the Improvement of Higher Education Personnel (CAPES) within the Ministry of Education - Brazil.

A mi cariño.

TABLE OF CONTENTS

LIST OF TABLES

LIST OF FIGURES

CHAPTER 1

INTRODUCTION

"Isso de começar não é fácil.
Muito mais simples é acabar.
Pinga-se um ponto final e pronto;
ou então escreve-se um latinzinho: FINIS.
Mas começar é terrível."
— "Emília" in *Memórias de Emília* by Monteiro Lobato

1.1 Background and Literature Review

In the petroleum industry, well testing is a common practice which consists of wellbore pressure and flow rate data acquisition to estimate parameters that govern flow in the porous media, i.e., the reservoir rock which stores the hydrocarbons. Well tests give an insight into the oil and gas field production potential and profitability, allow the estimation of reservoir parameters and provide the information necessary to decide whether a well needs to be stimulated. Estimated parameters can also be used to calibrate the reservoir simulation model, used to describe these reservoirs and forecast their performance as well as to maximize the productivity of the wells.

Multiphase flow is the norm in petroleum reservoirs and an injection-falloff test consists of a period of water or gas injection into an oil reservoir, technique known as waterflooding or gasflooding that is commonly used to displace oil to a producing well, followed by a period of shut-in (zero wellbore flow rate) (Figs. 1.1a, 1.1b and 1.1c). Data from an injection-falloff test can be used to estimate reservoir rock absolute permeability, skin zone permeability, i.e., the permeability in the damaged/stimulated zone around the well, and

the end-point mobilities. Injection and falloff are important tests on reservoirs containing high amount of harmful gases like carbon dioxide and sulfur dissolved in the oil, which make conventional production testing in the exploratory phase of offshore fields development inviable.

The injection-falloff-production test was originally proposed in Chen et al. [30] and Chen et al. [31] as a well test for the in situ estimation of two-phase relative permeability curves to be used for simulating multiphase flows in porous media. Chen et al. [29, 30, 31] and Machado and Reynolds [67] showed that if the well is produced after the injection-falloff test (Fig. 1.1d), the sandface will be exposed to a range of water saturations. Consequently, the wellbore pressure must be influenced by the changing water saturation in the near wellbore region and hence must contain information about the two-phase oil-water relative permeability curves. In essence, the injection-falloff-production test is a three-stage well test for the in situ estimation of oil-water relative permeability curves, absolute permeability and the skin factor. Chen et al. [30] developed an approximate semi-analytical solution for the saturation distribution during the flowback period of an IFPT, using the front tracking approach [15, 16, 56] by applying Euler's method to the find the shock path numerically. Although this solution gives saturation distributions and pressure data that are in excellent agreement with corresponding results from a reservoir simulator, the saturation solution of Chen et al. [31] is not consistent with the mathematical theory of waves and his analysis procedure requires very small time steps to get an accurate shock path. In this work, we correct this deficiency; in fact, we show that the weak solution we construct for the saturation equation for the flowback period by applying the method of characteristics satisfies the Oleinik entropy condition [74] and hence is unique. Another novel feature of our work is that we allow the governing relative permeabilities during the flow back period (drainage) curves and their end points (points at critical saturations) to be different from the relative permeabilities during injection (imbibition curves). Note; we have assumed throughout this work a water-wet reservoir. Chen et al. [32] have given a few suggestions on how to run these test in practice, as the use of flowmeters before fluid separation for better metering

accuracy and the use of artificial lift systems, as an electrical submersible pump, to keep the total flow rate stable.

In this work, we show how to generate a semi-analytical solution for the wellbore pressure response during an the injection-falloff-production test (IFPT). In the pursuance of modeling the IFPT, the Buckley-Leverett equation is used to determine the water saturation distribution in the reservoir as a function of time by assuming a one-dimensional homogeneous medium containing incompressible fluids. The corresponding pressure solution can be obtained by integrating the expression for the pressure gradient, given by Darcy's law, from the wellbore radius to infinity while assuming an infinite-acting reservoir. To actually evaluate this integral which represents the pressure solution, however, we must first solve for water saturation. Because Darcy's law does not assume incompressible flow, the pressure solution is transient and does not assume incompressible flow even though the saturation profile is generated from a Buckley-Leverett solution. It is also important to note that the analytical solution for pressure is derived under the assumption that the "steady-state theory" developed by [98] applies. For a water-oil system, where water is injected at a constant rate, this steady-state theory does not assume that steady-state flow exists throughout the reservoir; instead it assumes that, the following three conditions hold throughout the infinite-acting radial flow period, (i) at any time t, there is a radius $r_{ss}(t)$ such that the total flow rate $(q_t(r,t))$ as a function of r, is approximately constant for $r_w \leq r \leq r_{ss}(t)$, (ii) that $r_{ss}(t)$ increases as t increases and (iii) that any time t, the radius $r_{f,inj}(t)$ of the water front (radius of the zone invaded by water) satisfies $r_{f,inj}(t) < r_{ss}(t)$, i.e., the zone in which two phases are mobile is within the zone in which the profile of the total flow rate is constant. The analytical solution we generate does not require knowledge of $r_{ss}(t)$, only that $r_{f,inj}(t) < r_{ss}(t)$. This is fortunate because determining $r_{ss}(t)$ at a given time t would require defining $r_{ss}(t)$ as the maximum radius at which $q_t(r_{ss}(t),t) \approx q_t(r_w,t)$ where, $q_t(r_w,t)$ is equal to the wellbore injection/production rate, and then, determining $r_{ss}(t)$ would depend on defining precisely what $q_t(r_{ss}(t),t) \approx q_t(r_w,t)$ means. The so-called steady-state theory is only approximate because, given a fixed time $\hat{t} > 0$, and the corresponding $r_{ss}(\hat{t})$, it implies that for any time

$t > \hat{t}$, the total flow rate out of the volume between $[r_w, r_{ss}(\hat{t})]$ is equal to the total flow rate into the volume, i.e., equal to the injection/production rate. These two rates cannot be exactly equal unless total compressibility is zero so the steady-state theory is approximate. Based on this preceding discussion, intuition suggests that the assumption of the existence of the steady-state zone is more tenuous if the total compressibility of the system is large. However, this steady-state assumption has been shown to yield accurate semi-analytical pressure solutions even for gas-condensate systems [99]. For a gas-condensate reservoir, the steady-state assumption must be interpreted to mean the total mass rate into and the total mass rate out of the steady-state zone are equal. While steady-state theory (conditions (i) (ii) and (iii)) can only be verified using numerical solutions, [79] has given a semi-theoretical argument that for any reasonable values of reservoir parameters, assumption (iii) will hold, i.e., the radius of the two-phase flow zone will always be within the steady-state zone.

The Thompson and Reynolds [98] steady-state approach has been used previously to generate approximate solution for injection-falloff testing [79, 82, 13], but these papers did not consider a production test conducted subsequent to the falloff test. For injection tests, Peres and Reynolds [79] developed an semi-analytical solution for the wellbore pressure during water injection for both horizontal and vertical wells using the Thompson and Reynolds [98] steady-state theory. In the vertical well case, Peres and Reynolds [79] showed that their solution yields the injection solution of Bratvold and Horne [17] provided one makes the Bratvold and Horne assumption that the injection solution is a unique function of the Boltzmann transform which is valid for a finite wellbore radius well except at early times. Bratvold and Horne [17] as well as Abbaszadeh and Kamal [1] generated an approximation to the falloff pressure response by analogy with the shut-in solution for a single-phase composite reservoir, whereas Peres et al. [82] approximated the falloff pressure solution by applying superposition in an approximate way. None of these authors cited in this paragraph used data to approximate in situ relative permeabilities curves. However, under their assumption that the pressure and saturation are functions of the Boltzmann transform, Serra et al. [91] and Al-Khalifa et al. [4] showed that it is possible to obtain effective permeabilities from a

drawdown test of a homogeneous reservoir under two-phase flow (oil and gas) conditions; this idea that was pursued further by Hatzignatiou and Reynolds [49] under the assumption that the true in situ relative permeabilities can be accurately represented by Standing [96] or Corey [37] equations.

This work focus on developing a procedure to generate analytical and semi-analytical solution to model injection-falloff and and injection-falloff-production tests by showing how to solve the nonlinear system of partial differential equations arising in testing of injection wells in different scenarios of multiphase flow and physical phenomena. The analytical and semi-analytical solutions developed here can be used to match pressure and water flow rate data from an injection-falloff tests or injection-falloff-production tests, and this provides an accurate and fast forward model compared to a numerical model, which requires extraordinarily small time steps and a highly refined radial grid around the well to generate an accurate solution. Water injection is commonly used to displace oil to a producing well, but we also consider the in injection of gas or gas dissolved in water.

Regarding the injection of gas dissolved in water, Pope [84] presented an analytical solution to saturation and concentration distributions during carbonated water injection into an oil reservoir, but he ignored the CO_2 adsorption phenomenon and the dependence of the water-oil surface tension on carbon dioxide concentration in his solution. Bedrikovetsky [11] presented an analytical solution to the hyperbolic system that governs oil displacement by chemical solutions considering the phenomena that Pope [84] neglected, but none of these authors cited in this paragraph has considered the effect of CO_2 in the wellbore pressure response as in Machado et al. [69, 70].

1.2 Research Objectives and Dissertation Outline

1.2.1 Research Objectives

The objectives of this research can be delineated as follows:

1. To develop a procedure to generate analytical and semi-analytical solutions to model

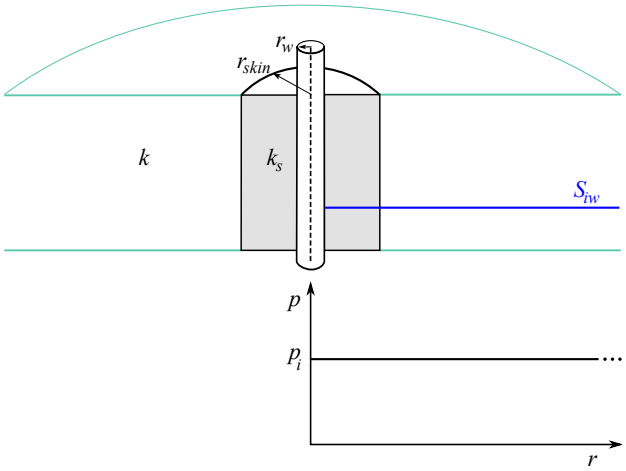

(a) Reservoir is assumed to be at rest at the beginning of the test with constant pressure and immobile water saturation distribution.

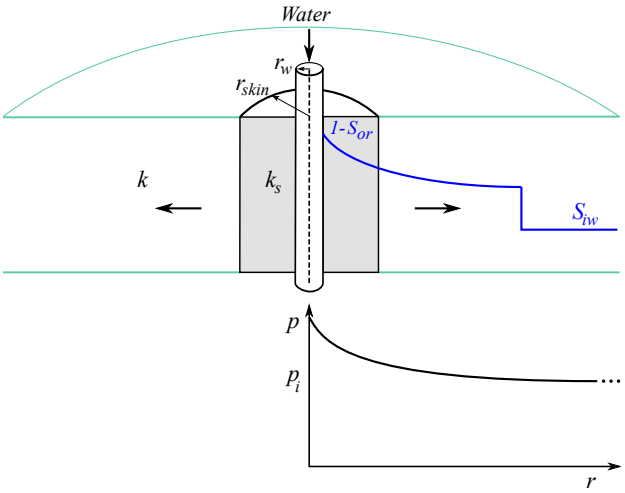

(b) Water is injected at constant flow rate leading to pressure change that propagates from the well.

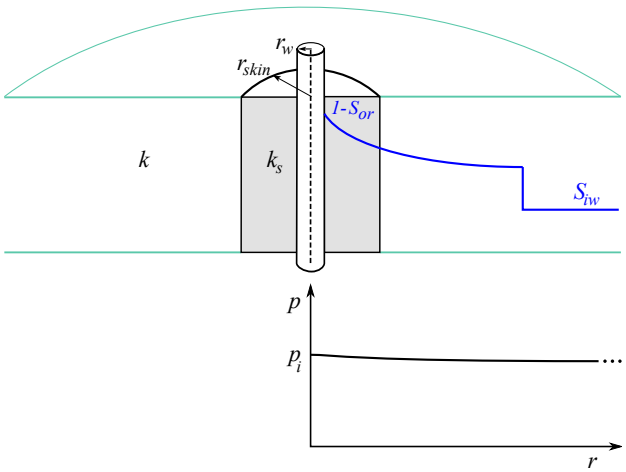

(c) The well is shut and the wellbore pressure tends to return to initial condition while the saturation does not change assuming that capillary pressure effects are negligible.

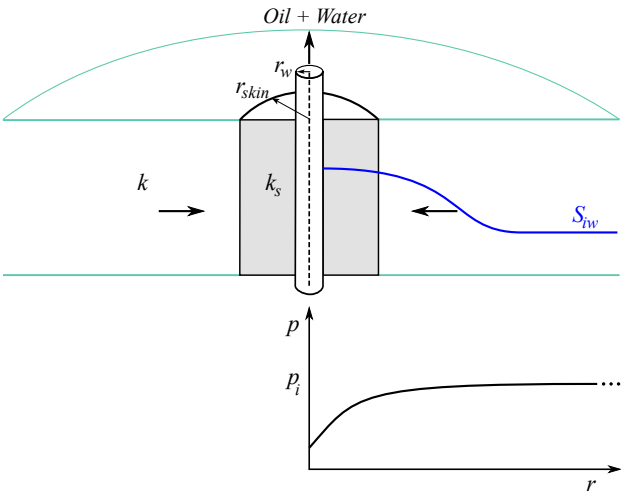

(d) Fluids are produced at constant total flow rate causing a pressure drop in the wellbore. Water-oil ratio (WOR) varies during the flowback period, and a range of saturations is observed at the sandface as a function of time.

Figure 1.1: Sketch of the Injection-Falloff-Production Test.

wellbore pressure response during injection-falloff and and injection-falloff-production tests involving different physical processes.

2. Consider hysteresis effects in the relative permeability curves, i.e., allow the governing relative permeabilities during the flowback period to be different from the relative permeabilities during injection, with water as the injected fluid.

3. Incorporate capillary pressure effects on the wellbore pressure response during injection-falloff and and injection-falloff-production tests.

4. To investigate whether that we can match data from injection-falloff and injection-falloff-production tests using the solutions developed and its derivatives to estimate absolute permeability, skin factor, in-situ relative permeabilities and capillary pressure curves.

1.2.2 Dissertation outline

This dissertation contains 5 chapters that proceed as follows:

In Chapter 2, we present a procedure to generate semi-analytical solutions for the wellbore pressure response during an injection-falloff-production test which allows the governing relative permeabilities during the flow back period to be different from the relative permeabilities during injection.The weak solution we construct for the saturation equation for the flowback period satisfies the Oleinik entropy condition [74] and hence is unique [7]. By comparing results with those from a commercial simulator, we show that our approximate semi-analytical solution yields an accurate prediction of the saturation profile and bottom-hole pressure during an IFPT. Finally, we show that our analytical model can be used to match pressure and water flow rate data from an synthetic multiphase well test in order to estimate absolute permeability, skin factor and the parameters for in-situ relative permeabilities..

In Chapter 3, we extend of the work presented in Chapter 2 to include capillary pressure effects and investigate the effect of this phenomenon when estimating reservoir

parameters from multiphase well test data.

In Chapter 4, we present a continuation of the previous solutions by considering the possibility of a component being dissolved in the injected water. We develop an approximate analytical solution for wellbore pressure response during a gas injection and falloff well test in a reservoir containing oil and immobile gas considering the temperature difference between the injected fluid and the reservoir. The gas component in the solution can be any gas, where the oil industry usually injects carbon dioxide, nitrogen or lean gas. After validating our solution by comparing the bottom-hole pressure data calculated from the analytical model with the bottom-hole pressure obtained from a commercial numerical simulator GEM, we show that our solution can be used as the forward model in a least-squares optimization algorithm in order to estimate skin factor, reservoir absolute permeability and end-point relative permeabilities.

We summarize the main results of this study and present recommendations for future work in Chapter 5.

In the Appendix 1, we show the numerical details to compute the solutions developed in this work while in Appendix 2 we provide the analytical derivatives for the solution presented in Chapter 2.

CHAPTER 2

ANALYTICAL SOLUTION OF PRESSURE RESPONSE DURING IFPT

"No intelligent idea can gain general acceptance unless some stupidity is mixed in with it."

— Fernando Pessoa

In this chapter, we show how to develop a semi-analytical solution for the wellbore pressure response during an the injection-falloff-production test (IFPT). In the pursuance of modeling the IFPT, the Buckley-Leverett equation is used to determine the water saturation distribution in the reservoir as a function of time by assuming a one-dimensional homogeneous medium containing incompressible fluids. The corresponding pressure solution can be obtained by integrating the expression for the pressure gradient, given by Darcy's law, from the wellbore radius to infinity while assuming an infinite-acting reservoir. To actually evaluate this integral which represents the pressure solution, however, we must first solve for water saturation. Because Darcy's law does not assume incompressible flow, the pressure solution is transient and does not need to assume incompressible flow even though the saturation profile is generated from a Buckley-Leverett solution.

As mentioned in Chapter 1, the injection-falloff-production test was originally proposed in Chen et al. [30] and Chen et al. [31] as a well test for the in situ estimation of two-phase relative permeability curves to be used for simulating multiphase flows in porous media. Chen et al. [30] did developed an approximate semi-analytical solution for the saturation distribution during the flowback period of an IFPT, using the front tracking approach [15, 16, 56] by applying Euler's method to the find the shock path numerically. Although this solution gives saturation distributions and pressure data that are in excellent agreement

with corresponding results from a reservoir simulator, the saturation solution of Chen et al. [31] is not consistent with the mathematical theory of waves and his analysis procedure requires very small time steps to get an accurate shock path. In this work, we correct this deficiency; in fact, we show that the weak solution we construct for the saturation equation for the flowback period by applying the method of characteristics satisfies the Oleinik entropy condition and hence is unique. Another novel feature of our work is that we allow the governing relative permeabilities during the flow back period (drainage) curves and their end-points (points at critical saturations) to be different from the relative permeabilities during injection (imbibition curves).

2.1 Mathematical model

In this section, we present the semi-analytical solution for the wellbore pressure during an Injection-Falloff-Production Test. As depicted in Fig. 1.1, the IFPT problem can be decoupled into three stages - injection, falloff and production. At the beginning of the test, the reservoir is assumed to be at a constant initial pressure with water saturation equal to irreducible water saturation. First, water is injected at a constant flow rate leading to a pressure change that propagates outward from the well. Then, the well is shut; and the wellbore pressure tends to return to its initial condition while the saturation does not change assuming that capillary pressure effects are negligible. Subsequently, fluids are produced at constant total flow rate causing a pressure drop in the wellbore; this period is the production or flowback period. The water-oil ratio (WOR) varies during the flowback period, and a range of saturations is observed at the sandface as a function of time. For each of these stages (three tests), the nonlinear PDE's that describe the flow of oil and water are solved for the water saturation distribution ($S_w(r,t)$), for a sequence of times and then solved for pressure.

2.1.1 Saturation Profile

We assume a one-dimensional radial flow. The mass balance equation, in radial

coordinates, leads to the following [21] equation:

$$\frac{\partial S_w}{\partial t} + \frac{\theta q_t}{2\pi r h \phi} \frac{df_w(S_w)}{dS_w} \frac{\partial S_w}{\partial r} = 0, \tag{2.1}$$

which is a first order nonlinear hyperbolic equation. Throughout, we assume porosity (ϕ) is homogeneous. q_t is the total liquid rate in RB/D; r and h, respectively, represent the radius and reservoir thickness in feet ; θ represents in general a unit conversion factor where in the oil field units used here, $\theta = 5.6146/24$; time, t, is in hours. Neglecting capillary and gravity effects, the water fractional flow curve is

$$f_w(S_w) = \frac{\frac{k_{rw}(S_w)}{\mu_w}}{\frac{k_{rw}(S_w)}{\mu_w} + \frac{k_{ro}(S_w)}{\mu_o}}, \tag{2.2}$$

where the water and oil viscosities (μ_w and μ_o) are in centipoise and assumed to be constant. For simplicity, we assume relative permeabilities are represented by the power-law model, also known as the modified Brooks-Corey functions [19], given by

$$k_{rw} = a_w \left(\frac{S_w - S_{iw}}{1 - S_{iw} - S_{or}} \right)^{n_w} \tag{2.3}$$

and

$$k_{ro} = a_o \left(\frac{1 - S_w - S_{or}}{1 - S_{iw} - S_{or}} \right)^{n_o}, \tag{2.4}$$

where $a_w = k_{rw}(S_w = 1 - S_{or})$, $a_o = k_{ro}(S_w = S_{iw})$, $0 < a_w < 1$ (for a water-wet reservoir), a_o is defined as 1, the exponents n_o and n_w to range from 1 to 6. S_{or} denotes residual oil saturation, and S_{iw} denotes irreducible water saturation. Although we have assumed a power-law model, our solution does not require any specific form of the relative permeability curves, but to estimate the relative permeabilities from measured pressure data by nonlinear regression, the relative permeability function must be parameterized because nonlinear regression routine is inherently a parameter estimation procedure; the parametrization could be quite general, for example using B-splines [28, 31, 43]. Defining the oil and water

mobilities, respectively by

$$\lambda_o = \frac{k_{ro}}{\mu_o} \tag{2.5}$$

and

$$\lambda_w = \frac{k_{rw}}{\mu_w}, \tag{2.6}$$

it follows that

$$\frac{df_w}{dS_w} = \frac{\frac{d\lambda_w}{dS_w}}{(\lambda_o + \lambda_w)} - \frac{\lambda_w\left(\frac{d\lambda_w}{dS_w} + \frac{d\lambda_o}{dS_w}\right)}{(\lambda_o + \lambda_w)^2}. \tag{2.7}$$

From

$$\frac{d\lambda_o}{dS_w} = \frac{n_o a_o}{\mu_o}\left(\frac{1 - S_w - S_{iw}}{1 - S_{iw} - S_{or}}\right)^{n_o - 1} = n_o \lambda_o \left(\frac{1 - S_{iw} - S_{or}}{1 - S_w - S_{iw}}\right), \tag{2.8}$$

$$\frac{d\lambda_w}{dS_w} = \frac{a_w n_w}{\mu_w}\left(\frac{S_w - S_{iw}}{1 - S_{iw} - S_{or}}\right)^{n_w - 1} = n_w \lambda_w \left(\frac{1 - S_{iw} - S_{or}}{S_w - S_{iw}}\right) \tag{2.9}$$

and Eq. 2.2, Eq. 2.7 can be rewritten as

$$\frac{df_w}{dS_w} = n_w f_w \left(\frac{1 - S_{iw} - S_{or}}{S_w - S_{iw}}\right) - f_w \left[n_w f_w \left(\frac{1 - S_{iw} - S_{or}}{S_w - S_{iw}}\right) + n_o f_o \left(\frac{1 - S_{iw} - S_{or}}{1 - S_w - S_{iw}}\right)\right]. \tag{2.10}$$

Using $f_o = 1 - f_w$, Eq. 2.10 can be rearranged as

$$\frac{df_w}{dS_w} = (f_w - f_w^2)\left[n_w - n_o \left(\frac{S_w - S_{iw}}{1 - S_w - S_{or}}\right)\right]. \tag{2.11}$$

Taking the derivate of Eq. 2.11 with respect to S_w, yields

$$\frac{d^2 f_w}{dS_w^2} = (1 - 2f_w)\frac{f_w}{dS_w}\left[n_w - n_o \left(\frac{S_w - S_{iw}}{1 - S_w - S_{or}}\right)\right]. \tag{2.12}$$

Fig. 2.1 shows a plot of f_w and $\frac{df_w}{dS_w}$ for the case where initial water saturation, S_{wi}, is equal to the irreducible water saturation, S_{iw}.

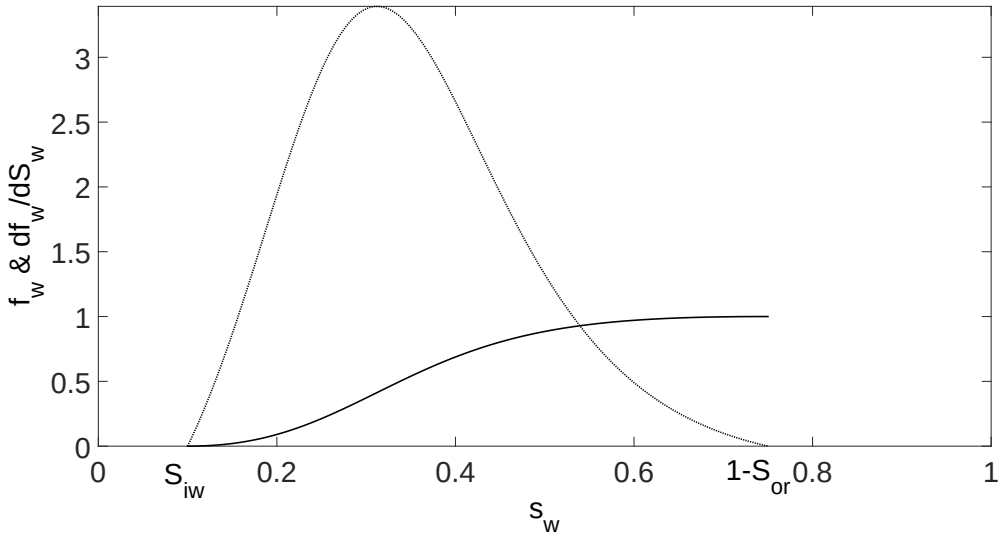

Figure 2.1: Water fractional flow curve (dark solid curve) and its derivative (dotted curve).

The injection period of the IFPT is represented by the following Riemann problem,

$$\begin{cases} \frac{\partial S_w}{\partial t} + \frac{\theta q_{inj}}{2\pi r h \phi} \frac{\partial f_w(S_w)}{\partial r} = 0, \\ S_w(r,0) = \begin{cases} 1 - S_{or}, & r^2 \leqslant r_w^2 \\ S_{iw}, & r^2 > r_w^2, \end{cases} \end{cases} \tag{2.13}$$

where $q_{inj} > 0$ during the injection period. Problem Eq. 2.13 has the unique admissible entropy weak solution for a S-shaped water fractional flow curve (monotonically increasing function with a single inflection point) can be obtained by the application of the Method of Characteristics and is given by [21],

$$S_w(r,t) = \begin{cases} 1 - S_{or}, & r^2 \leqslant \frac{\theta q_{inj}}{\pi h \phi} \frac{df_w(1-S_{or})}{dS_w} t + r_w^2 \\ \left(\frac{df_w}{dS_w}\right)^{-1} \left(\frac{\pi h \phi}{\theta q_{inj}} \frac{(r^2 - r_w^2)}{t}\right), & \frac{\theta q_{inj}}{\pi h \phi} \frac{df_w(1-S_{or})}{dS_w} t < r^2 - r_w^2 \leqslant \frac{\theta q_{inj}}{\pi h \phi} \frac{df_w(S_{wf})}{dS_w} t \\ S_{iw}, & r^2 > \frac{\theta q_{inj}}{\pi h \phi} \frac{df_w(S_{wf})}{dS_w} t + r_w^2, \end{cases} \tag{2.14}$$

where S_{wf} represents the water front saturation, expressed in the implicit form as

$$\frac{df_w(S_{wf})}{dS_w} = \frac{f_w(S_{wf}) - f_w(S_{iw})}{S_{wf} - S_{iw}}. \tag{2.15}$$

Note this solution consists of a uniform region at the injection well saturation condition, $1 - S_{or}$, a family of rarefaction waves followed by a stable shock wave and then a uniform region at initial saturation, S_{iw}. The details of this solution can be found in [21]. Fig. 2.2 shows the shock jump slope tangent to the fractional flow curve at $S_w = S_{wf}$ and the saturation distribution in the reservoir at a some time t. The rarefaction waves family spans from $1 - S_{or}$ to S_{wf} from r_w to $r = 25$ ft, the water front position, i.e., the shock front position, r_s. Ahead of the water front position, there is immobile water.

During the falloff stage, to determine the saturation and the total mobility distributions, it is assumed that there is no fluid movement in the reservoir, which is reasonable because we neglect the effects of capillary pressure, gravitational force and fluid compressibilities. Consequently, to compute the water saturation profile during the production period of the IFPT, we need to solve the following Cauchy problem:

$$\begin{cases} \frac{\partial S_w(r,\Delta t_{prod})}{\partial t} + \frac{\theta q_{t,prod}}{2\pi r h \phi} \frac{\partial f_w(S_w(r,\Delta t_{prod}))}{\partial r} = 0 \\ S_w(r,0) = S_w(r,t_{inj}) \end{cases} \tag{2.16}$$

which has a weak solution because the initial condition ($S_w(r,0)$), which is given by the saturation distribution at the end of the injection period ($S_w(r,t_{inj})$), is bounded and measurable [7]. Here, t_{inj} is the total time at the end of the injection period and Δt_{prod} denotes the time during production with $\Delta t_{prod} = 0$ at the beginning of the production period, and $q_{t,prod} < 0$.

For the purpose of applying the method of characteristics to solve the initial value problem given by Eq. 2.16, Eq. 2.1 can be rewritten as

$$\frac{\partial S_w}{\partial t} + \frac{\theta q_{t,prod}}{\pi h \phi} \frac{df_w(S_w)}{dS_w} \frac{\partial S_w}{\partial (r^2)} = 0. \tag{2.17}$$

The total derivative of water saturation with respect to time is given by

$$\frac{dS_w(r^2(t),t)}{dt} = \frac{\partial S_w}{\partial t} + \frac{\partial S_w}{\partial (r^2)} \frac{d(r^2)}{dt}. \tag{2.18}$$

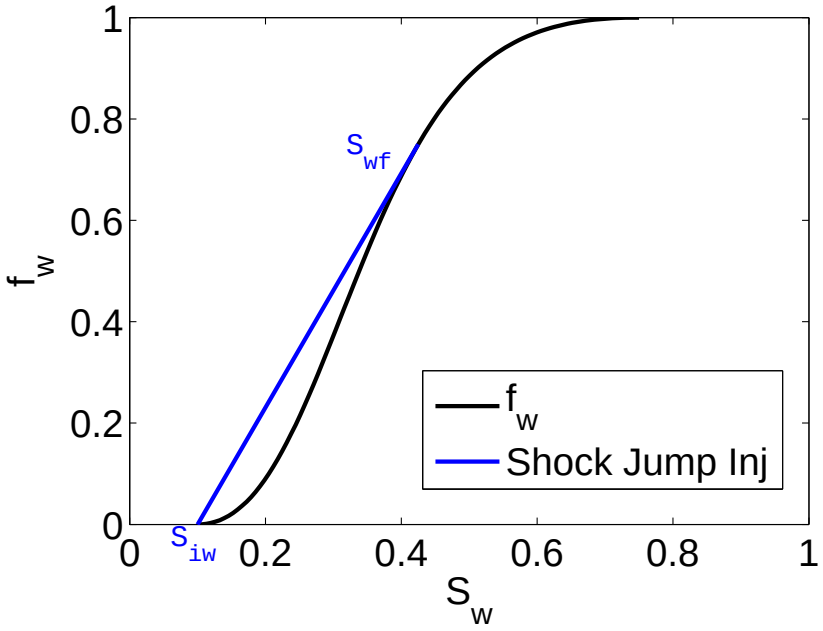

(a)

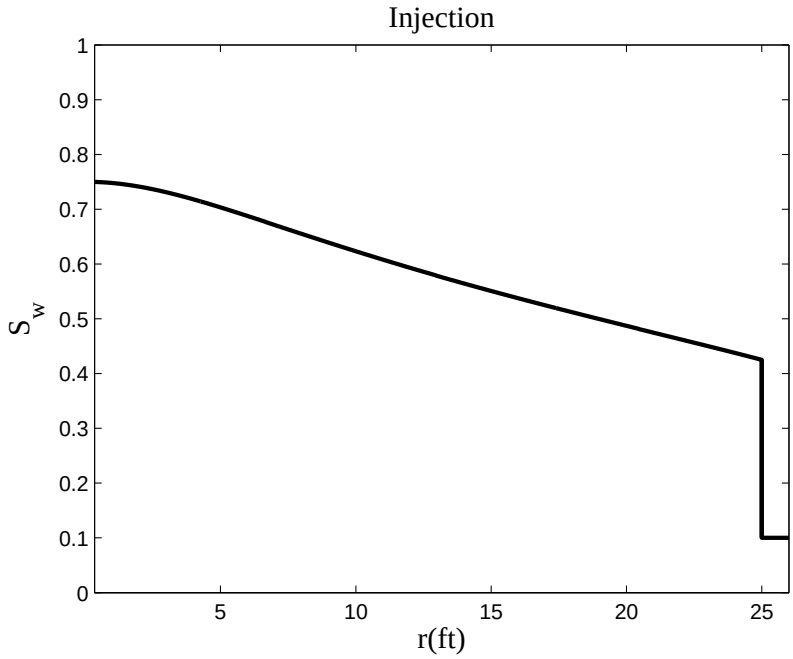

(b)

Figure 2.2: The shock jump slope tangent (blue curve) to the S-shaped fractional flow curve at $S_w = S_{wf}$ (a) and the saturation profile in the reservoir at a some time t (b). he rarefaction waves family spans from $1 - S_{or}$ to S_{wf} from r_w to $r = 25$ ft, the water front position, i.e., the shock front position, $r_{f,nj}$. Ahead of the water front position, there is immobile water.

When $\frac{dS_w}{dt} = 0$, the right hand side of Eq. 2.18 must be equal to the left hand side of Eq. 2.17 and it then follows easily that

$$\frac{dr^2}{dt} = \frac{\theta q_{t,prod}}{\pi h \phi} \frac{df_w(S_w)}{dS_w}, \tag{2.19}$$

where $\frac{dr^2}{dt}$ defines the speed of the saturation waves. Also along any characteristic curve defined by Eq. 2.19, $\frac{dS_w}{dt} = 0$, implies that S_w is constant along this curve. Solving Eq. 2.19, we find the characteristic curve

$$r^2(\xi, t) = \frac{\theta q_{t,prod}}{\pi h \phi} \frac{df_w(S_w(\xi, t_{inj}))}{dS_w}(t - t_{foff}) + \xi \tag{2.20}$$

for any starting point (ξ, t_{foff}) in the (r^2, t) plane. Here, $t = \Delta t_{prod} + t_{foff}$. Since during production $q_{t,prod} < 0$, the radius decreases as time increases. Note that in Figs. 2.3a, 2.3b and 2.3c, the falloff period is not considered, since we assumed no fluid motion during falloff. Therefore, the time at which production actually begins corresponds to the total time, t_{foff}, which is the total elapsed time since the beginning of the injection test and is greater than 16 hours. Then, the production time would be the time t represented in those figures plus the falloff period duration. If we propagate the waves from the initial condition for the Cauchy problem given in Eq. 2.16 - $S_w(r, 0) = S_w(r, t_{inj})$ - in the r-t diagram using Eq. 2.20, we see that there is a region which contain no characteristics. Fig. 2.3a shows the construction of these characteristic curves in the rt-plane, where the bottom curves are for injection ($0 \leq t \leq 16$) and the top curves are for flowback ($t > 16$). If we fill this "void" of information with rarefaction waves by applying Eq. 2.20 from the initial saturation to the front saturation (S_{wf}), we will see that the rarefactions curves of the expansion waves will cross the rarefaction lines of the compression waves, as a consequence of the inflection point in the fractional flow curve between those two saturations (Fig. 2.3b), i.e., there is a saturation discontinuity, or shock, between those two families of waves (Fig. 2.3c). The shock is a jump in saturation and the shock speed must satisfy the Rankine-Hugoniot condition,

i. e., we must have [66]

$$\frac{dr_s^2}{dt} = \frac{\theta q_t}{\pi h \phi} \frac{[f_w]}{[S_w]} \equiv \frac{\theta q_{t,prod}}{\pi h \phi} \frac{[f_w(S_w^-) - f_w(S_w^+)]}{[S_w^- - S_w^+]}, \tag{2.21}$$

where r_s is the shock position, while S_w^- and S_w^+ are the saturations downstream and upstream of the shock, respectively.

The above discussion indicates that if we apply Eq. 2.20 to obtain the saturation profile, we obtain a multivalued saturation function which is non-physical. This happens because, as we can notice from a S-shaped of the water fractional flow curve, some waves traveling to the producer well have higher speed than some waves corresponding to large saturations which are also traveling to the well. Consequently, the slower waves are caught up to by the faster ones immediately, causing a gradient catastrophe, i. e., a discontinuity in the solution at the beginning of the production period. The resulting discontinuous solution, must satisfy the weak form of Eq. 2.1, i. e.,

$$\begin{aligned} &\int_0^\infty \int_0^\infty \big(S_w(r,t)T_t(r,t) + f_w(r,t)T_r(r,t)\big) 2\pi r dr dt \\ &+ \int_0^\infty S_w(r,0)T(r,0)2\pi r dr + \int_0^\infty f_w(0,t)T(0,t)2\pi dt = 0, \end{aligned} \tag{2.22}$$

for every test function T(r,t). Eq. 2.22 was obtained following the derivations presented in [58] for the weak form in Cartesian coordinates. To qualify as a test function, T(r,t) must have compact support and the derivatives T_r and T_t must exist and be continuous for all (r,t) [58].

A question that arises now is how to determine the shock that satisfies the weak form of Buckley-Leverett conservation equation (Eq. 2.22) and the Oleinik entropy condition for the flowback period. To satisfy the weak form of the Buckley-Leverett equation, the area under the discontinuous saturation profile (weak solution) must be the same as the area under the multivalued wave profile, which we know satisfies conservation of mass. For that

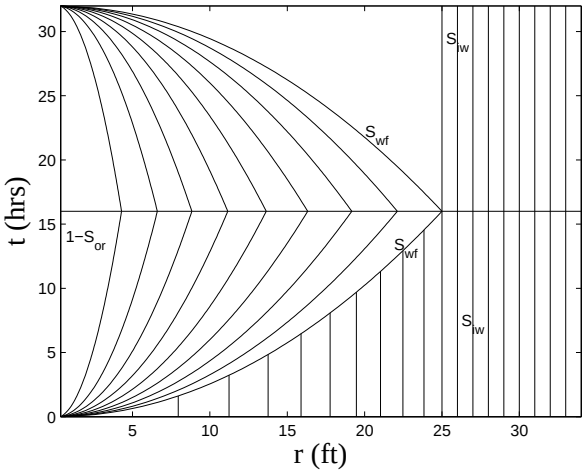

(a) Characteristic curves of the injection period, composed of a family of rarefaction waves, a shock and a region of constant saturation equal to S_{iw}, and their propagation during the production period ($t > 16$ hours).

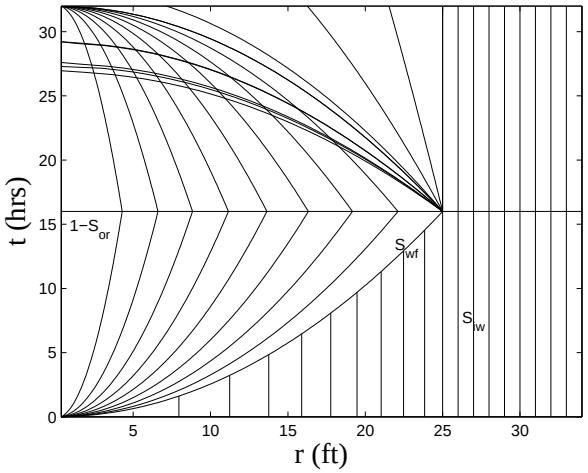

(b) Characteristic curves of the injection period and their propagation during the production period showing a gradient catastrophe when a family of rarefaction waves is inserted.

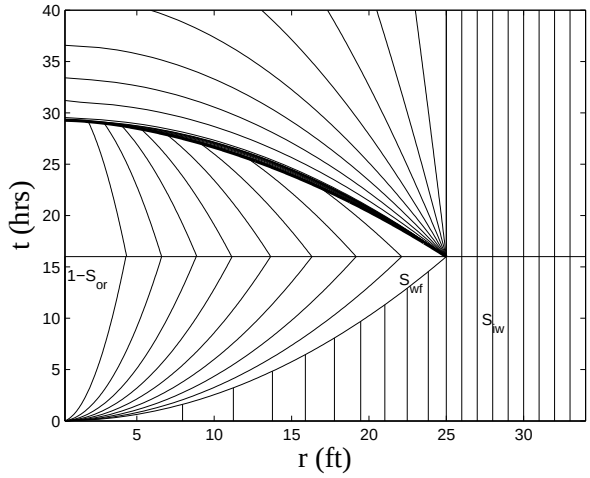

(c) Characteristic curves of the IFPT problem. The production period ($t \geq 16$ hrs) is composed of a family of compression waves, a shock, a family of rarefaction waves and a region of constant saturation.

Figure 2.3: Construction of the characteristic curves of the IFPT problem in the rt-plane. The falloff period is omitted since it is assumed there is no fluid movement during falloff.

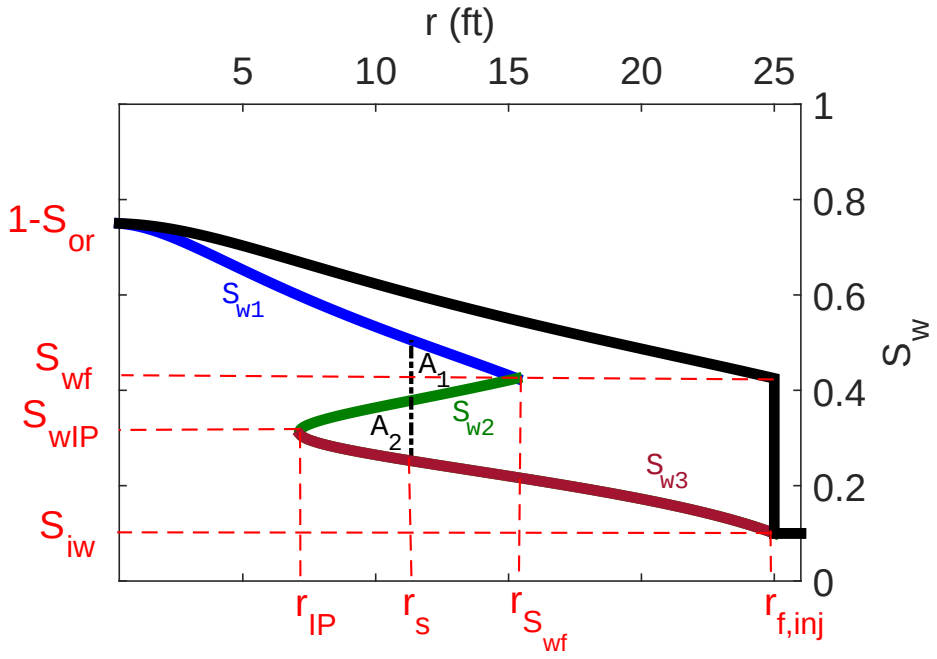

Figure 2.4: Cross section of the non-physical saturation profile in radial coordinates at some time during the production period before the oil front breakthrough. The "area equality" method is applied to construct the shock position at each time during the production period before the shock breakthrough. The saturation profile is divided into three curves: $S_{w1}(r,t) \in [S_w(r_w,t), S_{wf}]$ (blue solid curve), $S_{w2}(r,t) \in [S_{wIP}, S_{wf}]$ (green solid curve) and $S_{w3}(r,t) \in [S_{wIP}, S_{iw}]$ (brown solid curve). The black solid curve represents the saturation profile in the end of the injection period.

to be true, the area of the lobes of the multivalued profile cut by the shock (dashed line in Fig. 2.4) must be the same [102]. Specifically, if we divide the saturation profile for the production stage (flowback period) in Fig. 2.4 into three curves: $S_{w1}(r,t) \in [S_w(r_w,t), S_{wf}]$, $S_{w2}(r,t) \in [S_{wIP}, S_{wf}]$ and $S_{w3}(r,t) \in [S_{wIP}, S_{iw}]$, where S_{wIP} is the inflection point (IP) of the water fractional flow curve and S_{wf} is the shock saturation during injection period, the conservation law implies that at any time t we must have

$$\int_{r_s}^{r_{S_{wf}}} (S_{w1} - S_{w2}) 2\pi r dr = \int_{r_{IP}}^{r_s} (S_{w2} - S_{w3}) 2\pi r dr, \tag{2.23}$$

where r_s is the shock position at a time t so that $A_1 = A_2$ (Fig. 2.4), where $r_{S_{wf}} = r(S_{wf}, t)$ and $r_{IP} = r(S_{wIP}, t)$. To obtain the shock position expression for the flowback period,

Eq. 2.23 can be rearranged as

$$\int_{r_s^2}^{r_{S_{wf}}^2} S_{w1} d(r^2) - \int_{r_{IP}^2}^{r_{S_{wf}}^2} S_{w2} d(r^2) + \int_{r_{IP}^2}^{r_s^2} S_{w3} d(r^2) = 0. \tag{2.24}$$

We can evaluate each integral in Eq. 2.24 by the following integration by parts formula:

$$\int_a^b S_{wj} d(r^2) = S_{wj}(r,t) r^2 |_a^b - \int_{S_{wj}(a)}^{S_{wj}(b)} r^2 dS_{wj}, \quad j = 1, 2, 3. \tag{2.25}$$

Substituting the expression for r given by Eq. 2.20 into Eq. 2.25 gives

$$\int_a^b S_{wj} d(r^2) = S_{wj}(r,t) r^2 |_a^b - \int_{S_{wj}(a)}^{S_{iw}(b)} \left(r_{inj}^2 + \frac{\theta q_{t,prod} \Delta t_{prod}}{\pi h \phi} \frac{df_w}{dS_{wj}} \right) dS_{wj}. \tag{2.26}$$

Eq. 2.26 applies at for any time t greater than the time at which the falloff period ends. We neglect any changes in the saturation profile during the falloff period. The saturation radius position at the end of the injection period (r_{inj}) is defined as

$$r_{inj}^2 \equiv r_{inj}^2(S_{w1}, t_{inj}) = r_w^2 + \frac{\theta q_{inj} t_{inj}}{\pi h \phi} \frac{df_w(S_{w1})}{dS_{w1}} \tag{2.27}$$

for curve S_{w1} and as

$$r_{inj}^2(S_{w2,3}, t_{inj}) \equiv r_{f,inj}^2 = r_w^2 + \frac{\theta q_{inj} t_{inj}}{\pi h \phi} \frac{df_w(S_{wf})}{dS_{w2,3}} \tag{2.28}$$

for curves S_{w2} and S_{w3}, where $r_{f,inj}$ is the radius of the water front at the end of injection period. By using Eqs. 2.27 and 2.28 in Eq. 2.26 with $j = 1$ and inserting $S_{w1}(r_s, t) = S_w^+$

and $S_{w3}(r_s,t) = S_w^-$ in the resulting equation, we obtain

$$I \equiv \int_{r_s^2}^{r^2_{S_{wf}}} S_{w1} d(r^2) = S_{wf} r^2_{f,inj} - S_w^+ r_s^2 - \int_{S_w^+}^{S_{wf}} \left(r_w^2 + \frac{\theta q_{inj} t_{inj}}{\pi h \phi} \frac{df_w(S_{w1})}{dS_{w1}} + \frac{\theta q_{t,prod} \Delta t_{prod}}{\pi h \phi} \frac{df_w(S_{w1})}{dS_{w1}} \right) dS_{w1}, \quad (2.29)$$

and by integrating the last term in Eq. 2.29, it follows that

$$I \equiv S_{wf} r^2_{f,inj} - S_w^+ r_s^2 - r_w^2 (S_{wf} - S_w^+) - \frac{\theta (q_{inj} t_{inj} + q_{t,prod} \Delta t_{prod})}{\pi h \phi} (f_w(S_{wf}) - f_w(S_w^+)). \quad (2.30)$$

For the second term in Eq. 2.24, we use Eq. 2.26 with $i = 2$ to obtain

$$II \equiv - \int_{r_{IP}^2}^{r_{S_w^2}} S_{w2} d(r^2) = S_{wIP} r^2_{IP} - S_{wf} r_w^2 - \int_{S_{wf}}^{S_{wIP}} \left(r_w^2 + \frac{\theta q_{inj} t_{inj}}{\pi h \phi} \frac{df_w(S_{wf})}{dS_w} + \frac{\theta q_{t,prod} \Delta t_{prod}}{\pi \phi h} \frac{df_w(S_{w2})}{dS_{w2}} \right) dS_{w2}, \quad (2.31)$$

and after integrating, it follows that

$$II \equiv S_{wIP} r^2_{IP} - S_{wf} r^2_{f,inj} - \left(r_w^2 + \frac{\theta q_{inj} t_{inj}}{\pi h \phi} \frac{df_w(S_{wf})}{dS} \right) (S_{wIP} - S_{wf}) - \frac{\theta q_{t,prod} \Delta t_{prod}}{\pi \phi h} (f_w(S_{wIP}) - f_w(S_{wf})). \quad (2.32)$$

For the third term of Eq. 2.24, we use Eq. 2.26 with $i = 3$ to obtain

$$III \equiv \int_{r_{IP}^2}^{r_s^2} S_{w3} d(r^2) = r_s^2 S_w^- - r_{IP}^2 S_{wIP} - \int_{S_{wIP}}^{S_w^-} \left(r_w^2 + \frac{\theta q_{inj} t_{inj}}{\pi \phi h} \frac{df_w(S_{wf})}{dS_w} + \frac{\theta q_{t,prod} \Delta t_{prod}}{\pi h \phi} \frac{df_w(S_{w3})}{dS_{w3}} \right) dS_{w3} \quad (2.33)$$

which after integrating yields

$$III \equiv r_s^2 S_w^- - r_{IP}^2 S_{wIP} - \left(r_w^2 + \frac{\theta q_{inj} t_{inj}}{\pi h \phi} \frac{df_w(S_{wf})}{dS} \right) (S_w^- - S_{wIP}) - \frac{\theta q_{t,prod} \Delta t_{prod}}{\pi h \phi} (f_w(S_w^-) - f_w(S_{wIP})). \quad (2.34)$$

From Eq. 2.24, $I + II + III = 0$, which is equivalent to

$$r_s^2 (S_w^- - S_w^+) - r_w^2 (S_w^- - S_w^+) - \frac{\theta q_{t,prod} \Delta t_{prod}}{\pi h \phi} (f_w(S_w^-) - f_w(S_w^+)) - \frac{\theta q_{inj} t_{inj}}{\pi h \phi} (f_w(S_{wf}) - f_w(S_w^+) - \frac{df_w(S_{wf})}{dS} (S_{wf} - S_w^-)) = 0 \quad (2.35)$$

and finally, solving Eq. 2.35 for r_s, gives

$$r_s(\Delta t_{prod}) = \left\{ r_w^2 + \frac{\theta q_{t,prod} \Delta t_{prod}}{\pi h \phi} \frac{[f_w(S_w^-) - f_w(S^+)]}{[S_w^- - S_w^+]} + \frac{\frac{\theta q_{inj} t_{inj}}{\pi h \phi} [f_w(S_{wf}) - f_w(S_w^+) - (S_{wf} - S_w^-) \frac{df_w}{dS_w}(S_{wf})]}{[S_w^- - S_w^+]} \right\}^{\frac{1}{2}}. \quad (2.36)$$

subject to the bounds

$$r_w \leq r_s \leq r_{f,inj}. \quad (2.37)$$

Because gravity, capillarity and compressibilities effects are neglected when computing S_w, $S_w = S_{iw}$ for $r > r_{f,inj(t_{inj})}$, which means we have only single-phase flow of oil for any $r > r_{f,inj}(t_{inj})$. Here, S_w^+ is the saturation ahead of the shock and S_w^- is the saturation

behind the shock, both located at r_s at Δt_{prod}, where during production the shock is moving towards the wellbore ,i.e, in the negative r-direction. This pair of saturations determines the instantaneous shock speed, via the standard formula; see Eq. 2.45 which is presented later. In addition to Eq. 2.36, we also know that the compression wave ahead of the shock is defined by

$$r_{inj}^2(S_w^+, t_{inj}) - r_s^2(\Delta t_{prod}) = -\frac{\theta q_{t,prod} \Delta t_{prod}}{\pi h \phi} \frac{df_w}{dS_w}(S_w^+), \tag{2.38}$$

which is obtained from Eq. 2.20 at $t = \Delta t_{prod}$ with $\tau = 0$ and $\xi = r^2(S_w^+, t_{foff})$; i.e., ξ is the position where the shock saturation S_w^+ exists at the end of the falloff, which is the same time as the beginning of production. Since at $\Delta t_{prod} = 0$ we have a saturation distribution from $1 - S_{or}$ at the well to S_{wf} at the water front and the shock moves towards the well during production, S_w^+ cannot be smaller than S_{wf}, which means that Eq. 2.38 is subject to the bounds

$$S_{wf} \leq S_w^+(r_s, \Delta t_{prod}) \leq 1 - S_{or}. \tag{2.39}$$

The expansion wave behind the shock also comes from Eq. 2.20 at $t = \Delta t_{prod}$ with $\tau = 0$, but in this case, ξ is the shock front position at the end of the injection period:

$$r_{inj}^2(S_{wf}, t_{inj}) - r_s^2(\Delta t_{prod}) = -\frac{\theta q_{t,prod} \Delta t_{prod}}{\pi h \phi} \frac{df_w}{dS_w}(S_w^-), \tag{2.40}$$

subject to the bounds

$$S_{iw} \leq S_w^-(r_s, \Delta t_{prod}) \leq S_{wIP}. \tag{2.41}$$

Note; here the inflection point saturation, S_{wIP}, is the upper bound. From the multivalued function (Fig. 2.4), it is clear that there are three saturations located at the shock position, but we need only to find S_w^+ and S_w^-, the highest and lowest saturations, respectively. The values of $S_w^-(t)$, $S_w^+(t)$ and $r_s(t)$ can be found by solving numerically the system of equations given by Eqs. 2.36, 2.38 and 2.40 at each total time t during the flowback period. After"oil" breakthrough, i.e., after the shock reaches the producing well, the saturation distribution will be obtained from curve S_{w3}, i.e., from the expansion wave. Note that at oil breakthrough,

$r_s = r_w$, therefore we set $r_s = r_w$ in Eqs. 2.36, 2.38 and 2.40 and solve for Δt_{prod}, S_w^- and S_w^+ at breakthrough, where this Δt_{prod} represents the time of breakthrough itself.

The shock is a jump in saturation that must satisfy the Rankine-Hugoniot condition, which can be derived from the integral form of Eq. 2.1, i.e., the mass balance equation

$$\frac{d}{dt}\int_{a^2}^{b^2} S_w(r,t)\pi d(r^2) = \frac{\theta q_{t,prod}}{\phi h}(f_w(a,t) - f_w(b,t)), \tag{2.42}$$

which we split into two regions for a fixed point $(r_s(t), t) \in (a, b)$ to obtain

$$\frac{d}{dt}\Big(\int_{a^2}^{r_s^{2-}} S_w(r,t)\pi d(r^2) + \int_{r_s^{2+}}^{b^2} S_w(r,t)\pi d(r^2)\Big) = \frac{\theta q_{t,prod}}{\phi h}(f_w(a,t) - f_w(b,t)), \tag{2.43}$$

where $r_s^- = r_s - \epsilon$ and $r_s^+ = r_s + \epsilon$, with constant ϵ. Applying Leibniz rule in the integrals of Eq. 2.43 and dividign by π gives

$$\int_{a^2}^{r_s^{2-}} \frac{\partial S_w(r,t)}{\partial t} d(r^2) + S_w(r_s^{2-},t)\frac{dr_s^{2-}}{dt} + \int_{r_s^{2+}}^{b^2} \frac{\partial S_w}{\partial t}(r,t) d(r^2) - S_w(r_s^{2+},t)\frac{dr_s^{2+}}{dt} = \frac{\theta q_{t,prod}}{\phi \pi h}(f_w(a,t) - f_w(b,t)), \tag{2.44}$$

Letting $a \to r_s^-$, $b \to r_s^+$ and $\epsilon \to 0$ in Eq. 2.44 and simplifying,

$$\frac{dr_s^2}{dt} = \frac{\theta q_{t,prod}}{\phi \pi h}\frac{[f_w]}{[S_w]} = \frac{\theta q_{t,prod}}{\pi \phi h}\frac{[f_w(S_w^-) - f_w(S_w^+)]}{[S_w^- - S_w^+]}, \tag{2.45}$$

which is the Rankine-Hugoniot condition. By taking the partial derivative with respect to time of Eq. 2.36

$$\frac{\partial r_s^2}{\partial t}(\Delta t_{prod}) = \frac{\theta q_{t,prod}}{\pi \phi h}\frac{[f_w(S_w^-) - f_w(S_w^+)]}{[S_w^- - S_w^+]}. \tag{2.46}$$

To prove that the solution developed satisfies the Rankine-Hugoniot condition, we can take

the total derivative of r_s^2 with respect to time,

$$\frac{dr_s^2}{dt}(\Delta t_{prod}) = \frac{\partial r_s^2}{\partial t} + \frac{\partial r_s^2}{\partial S_w^-}\frac{dS_w^-}{dt} + \frac{\partial r_s^2}{\partial S_w^+}\frac{dS_w^+}{dt}, \tag{2.47}$$

and because $\frac{dS_w^-}{dt}(r,t) = 0$ and $\frac{dS_w^+}{dt}(r,t) = 0$ since along any characteristic curve defined by Eq. 2.19, $\frac{dS_w}{dt} = 0$, it follows that

$$\frac{dr_s^2}{dt}(\Delta t_{prod}) = \frac{\partial r_s^2}{\partial t}(\Delta t_{prod}), \tag{2.48}$$

which shows that Eq. 2.46 is the same as Eq. 2.45. Using Eq. 2.20 from $1 - S_{ro}$ to S_{iw}, we can plot the non-physical multivalued saturation profile for the flowback (Fig. 2.5). Fig. 2.6 shows the saturation profile during the production period until the breakthrough time obtained by applying the area equality shocking fitting method, where the shock jumps are represented in the fractional flow curve in Fig. 2.7.

Unlike the injection period, we have an unstable shock, i.e., the shock saturations ($S_w^-(t)$ and $S_w^+(t)$) are not constant with time. This phenomenon occurs because the shock speed is higher than the speed of the saturations ahead of it and it is lower than the speed of saturations behind it. Consequently, the shock is caught up to by the waves behind it and the shock catches up to the waves ahead of it, thus increasing the jump in saturation and reducing the speed of the shock. This can be seen in Fig. 2.6, which shows the saturation at the end of the falloff period and some specified saturation profiles obtained during the production period up to breakthrough. These profiles were obtained by applying the area equality shocking fitting method, where the shock jumps are represented in the fractional flow curve in Fig. 2.7. These shock jumps in addition to satisfying the weak form of the conservation equation, they also satisfy the Oleinik entropy condition [74], which is given by

$$\frac{f_w(S_w^-) - f_w(S_w)}{S_w^- - S_w} \geq \frac{f_w(S_w^-) - f_w(S^+)}{S_w^- - S_w^+} \geq \frac{f_w(S_w) - f_w(S^+)}{S_w - S_w^+}, \tag{2.49}$$

as we can see in Fig. 2.8a and 2.8b, for any $S_w \in (S_w^-, S_w^+)$, and thus the solution that we

have constructed is the unique admissible entropy solution, according to the Theorem of Uniqueness presented in [7]. Thus, we can conclude that the saturation distribution solution during the production period consists of a $(1 - S_{or}) - S_w^+ \rightarrow S_w^- - S_{iw}$ configuration, where $-$ represents a rarefaction fan and $\rightarrow$ represents a shock or discontinuity. In another words, the solution consists of a family of compression waves, an unstable shock wave, a family of rarefaction waves and a uniform region at initial condition, S_{iw}. Translating into the language of mathematics, the unique weak solution for the flowback period has the form

$$S_w(r, \Delta t_{prod}) = \begin{cases} S_{w1}(r, \Delta t_{prod}) = \left(\frac{df_w}{dS_w}\right)^{-1}\left(\frac{\pi h\phi}{\theta q_{t,prod}} \frac{r_{inj}^2(S_w, t_{inj}) - r^2}{\Delta t_{prod}}\right), & r_w^2 \leq r^2 \leqslant r_s^2(\Delta t_{prod}) \\ S_{w3}(r, \Delta t_{prod}) = \left(\frac{df_w}{dS_w}\right)^{-1}\left(\frac{\pi h\phi}{\theta q_{t,prod}} \frac{r_{inj}^2(S_{wfInj}, t_{inj}) - r^2}{\Delta t_{prod}}\right), & r_s^2(\Delta t_{prod}) < r^2 < r_{f,inj}^2 \\ S_{iw}, & r_{f,inj}^2 \leq r^2, \end{cases} \tag{2.50}$$

where $S_{w1}(r, \Delta t_{prod})$ represents the family of compression waves ahead the shock position and $S_{w3}(r, \Delta t_{prod})$ represents the family of expansion/rarefaction waves behind of it.

By analogy to the injection Riemann problem, one might think that during production period, the shock speed would also be tangent to the water fractional flow curve, i.e.,

$$\frac{df_w(S_w^-)}{dS_w} = \frac{[f_w(S_w^-) - f_w(S_w^+)]}{[S_w^- - S_w^+]}. \tag{2.51}$$

Eq. 2.51 was assumed to hold in [30], but we show that, in general, Eq. 2.51 is not valid. Substituting r_s^2 from Eq. 2.40 into Eq. 2.36, after squaring both sides of Eq. 2.36, yields

$$\begin{aligned} r_{inj}^2(S_{wf}, t_{inj}) - \frac{\theta q_{t,prod}\Delta t_{prod}}{\pi h\phi}\frac{df_w(S_w^-)}{dS_w} = r_w^2 - \frac{\theta q_{t,prod}\Delta t_{prod}}{\pi h\phi}\frac{[f_w(S_w^-) - f_w(S^+)]}{[S_w^- - S_w^+]} \\ + \frac{\frac{\theta q_{inj} t_{inj}}{\pi\phi h}[f_w(S_{wf}) - f_w(S_w^+) - \frac{df_w(S_{wf})}{dS_w}(S_{wf} - S_w^-)]}{[S_w^- - S_w^+]}, \end{aligned} \tag{2.52}$$

which is equivalent to

$$r_w^2 + \frac{\theta q_{inj} t_{inj}}{\pi h \phi} \frac{df_w(S_{wf})}{dS_w} - \frac{\theta q_{t,prod} \Delta t_{prod}}{\pi h \phi} \frac{df_w(S_w^-)}{dS_w} = r_w^2 - \frac{\theta q_{t,prod} \Delta t_{prod}}{\pi h \phi} \frac{[f_w(S_w^-) - f_w(S_w^+)]}{[S_w^- - S_w^+]} + \frac{\frac{\theta q_{inj} t_{inj}}{\pi h \phi} [f_w(S_{wf}) - f_w(S_w^+) - \frac{df_w(S_{wf})}{dS_w}(S_{wf} - S^-)]}{[S_w^- - S_w^+]}, \tag{2.53}$$

since $r_{inj}^2(S_{wf}, t_{inj}) = r_w^2 + \frac{\theta q_{inj} t_{inj}}{\pi h \phi} \frac{df_w(S_{wf})}{dS_w}$. Eq. 2.53 can be rearranged to obtain

$$- \frac{\theta q_{t,prod} \Delta t_{prod}}{\pi h \phi} \frac{df_w}{dS_w}(S_w^-) = - \frac{\theta q_{t,prod} \Delta t_{prod}}{\pi \phi h} \frac{[f_w(S_w^-) - f_w(S_w^+)]}{[S_w^- - S_w^+]} + \frac{\frac{\theta q_{inj} t_{inj}}{\pi h \phi} [f_w(S_{wf}) - f_w(S_w^+) - \frac{df_w(S_{wf})}{dS_w}(S_{wf} - S^-)] - \frac{df_w(S_{wf})}{dS_w}(S_w^- - S_w^+)}{[S_w^- - S_w^+]}, \tag{2.54}$$

or, equivalently,

$$- \frac{\theta q_{t,prod} \Delta t_{prod}}{\pi h \phi} \frac{df_w}{dS_w}(S_w^-) = - \frac{\theta q_{t,prod} \Delta t}{\pi h \phi} \frac{[f_w(S_w^-) - f_w(S_w^+)]}{[S_w^- - S_w^+]} + \frac{\frac{\theta q_{inj} t_{inj}}{\pi h \phi} (f_w(S_{wf}) - f_w(S_w^+) - \frac{df_w(S_{wf})}{dS_w} S_{wf} + \frac{df_w(S_{wf})}{dS_w} S_w^+)}{[S_w^- - S_w^+]}. \tag{2.55}$$

By simply grouping the terms that are multiplied by $\frac{df_w(S_{wf})}{dS_w}$, we obtain

$$- \frac{\theta q_{t,prod} \Delta t_{prod}}{\pi h \phi} \frac{df_w}{dS_w}(S_w^-) = - \frac{\theta q_{t,prod} \Delta t_{prod}}{\pi h \phi} \frac{[f_w(S_w^-) - f_w(S_w^+)]}{[S^- - S^+]} + \frac{\frac{\theta q_{inj} t_{inj}}{\pi h \phi} (f_w(S_{wf}) - f_w(S_w^+) - \frac{df_w(S_{wf})}{dS_w}(S_{wf} - S_w^+)}{[S_w^- - S_w^+]}, \tag{2.56}$$

which is equivalent to

$$- \frac{\theta q_{t,prod} \Delta t_{prod}}{\pi h \phi} \frac{df_w}{dS_w}(S^-) = - \frac{\theta q_{t,prod} \Delta t_{prod}}{\pi h \phi} \frac{[f_w(S^-) - f_w(S^+)]}{[S_w^- - S_w^+]} + \frac{\theta q_{inj} t_{inj}}{\pi h \phi [S_w^- - S_w^+]} \left(f_w(S_{wf}) - f_w(S^+) - \frac{df_w(S_{wf})}{dS_w} [S_{wf} - S^+] \right). \tag{2.57}$$

From Eq. 2.57, we can see that Eq. 2.51 is true if and only if

$$\frac{[f_w(S_{wf}) - f_w(S_w^+)]}{[S_{wf} - S_w^+]} = \frac{df_w(S_{wf})}{dS_w}, \tag{2.58}$$

which is not possible for the S-shaped fractional flow curve, since the segment between S_{wf} and S_w^+ is concave. Consequently, Eq. 2.51 does not hold for the flowback solution, i.e., Eq. 2.51 is not consistent with Eqs. 2.36, 2.38 and 2.40, meaning that the shock speed is not the slope of an tangent line to the water fractional flow curve. Distinct from injection, in the production (flowback) period, we have an unstable shock, which results from the non-uniform saturation distribution at the beginning of the production period. The speed of the saturations behind the oil front are higher than the speed of the shock itself, which has higher speed than the saturations ahead of it. Consequently, the shock is caught up to by the waves behind it and also catches up to the waves ahead of it.

Note on Hysteresis Effects: It is important to note that in our model, the fluid saturation distribution for the IFPT can indeed be determined assuming two different fractional curves (Fig. 2.9b), which arise as a consequence of two sets of relative permeability curves, imbibition and drainage (Fig. 2.9a). In this case, as we can see in Fig. 2.9b, the speed of each saturation wave during production will be different than the speed of the corresponding wave from the injection period. After applying the area equality shocking fitting method, we can find the saturation profile from the end of the falloff period until breakthrough (Fig. 2.10), where the shock jumps in the fractional flow curve are shown in Fig. 2.11. In this case, the speed of the compression wave ahead of the shock is higher than the speed of the expansion wave behind the water front during the injection, so the saturation at $r = r_w$ will not be constant and equal to $1 - S_{or}$ at times prior to breakthrough. In fact, the oil saturation at the sandface drops below $1 - S_{or}$ as soon as production begins.

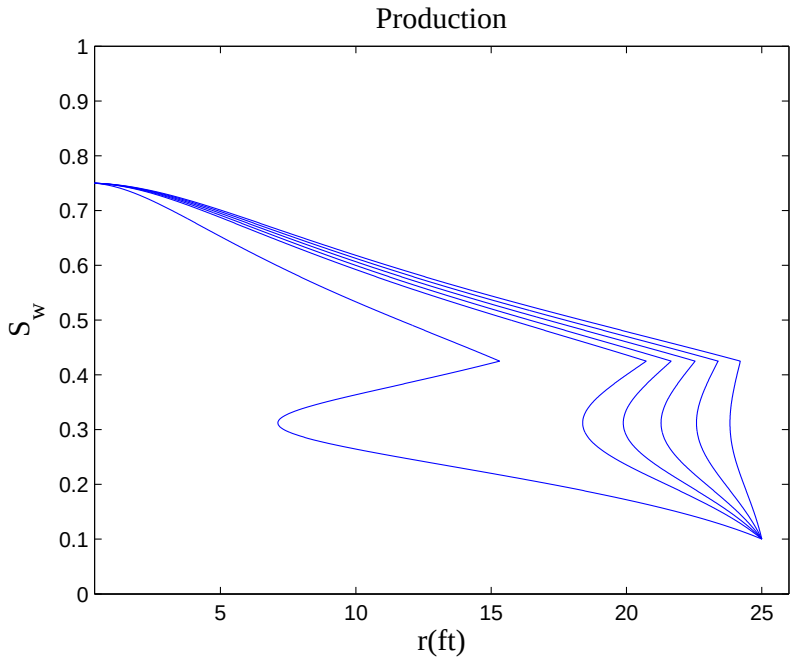

Figure 2.5: Non-physical multivalued saturation profile during production until BT.

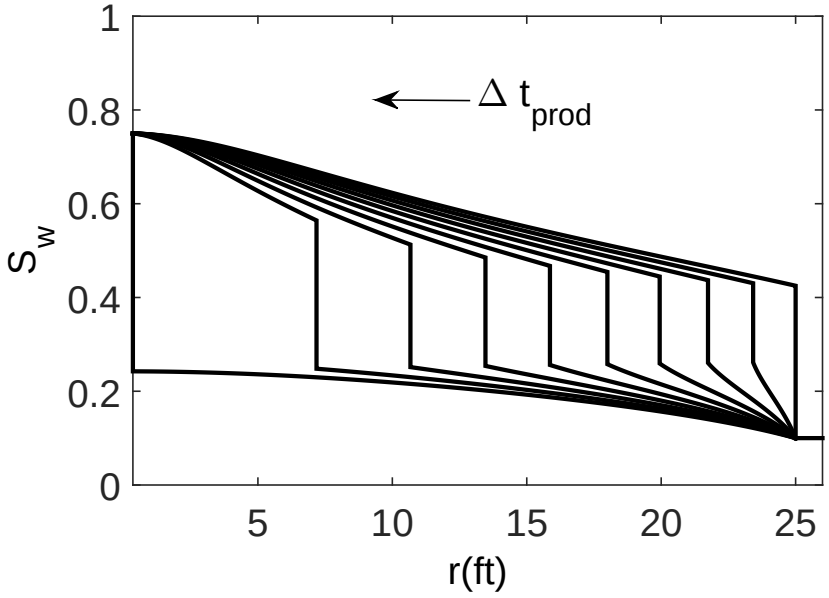

Figure 2.6: Saturation profiles during production - where the flow direction is from right to left - for different times from $\Delta_{prod} = 0$ (outer curve, to the right) to oil front breakthrough time (inner curve, to the left).

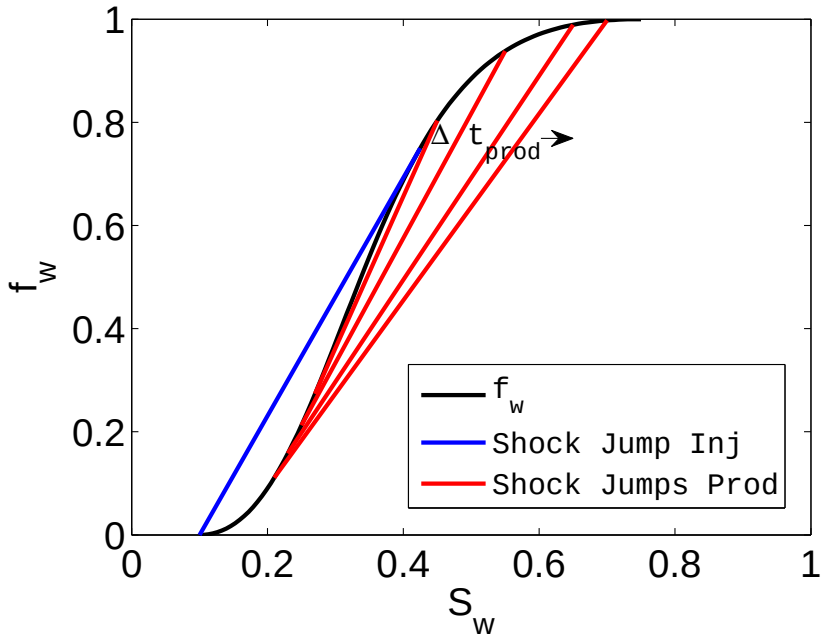

Figure 2.7: Shock jumps in the water fractional flow curve (solid black line) during flowback (solid red lines) determined by the area equality method. The blue solid line is the shock jump during the injection period, which is tangent to the f_w curve at the point S_{wf}.

2.1.2 Wellbore Pressure History

As mentioned previously, after finding the saturation distribution, we can obtain the wellbore pressure by applying the pressure solutions presented by [82, 28, 31].

Injection: During injection at a constant flow rate $q_{inj} = q_t(r_w, t)$ RB/D, where $t = 0$ at the beginning of the water injection, by integrating Darcy's law as in [98] and [79], the bottom hole pressure difference from the reservoir initial pressure (p_i) can be expressed as

$$\Delta p_{wf}(t) = p_{wf}(t) - p_i = \int_{r_w}^{\infty} \frac{\alpha q_t(r,t)}{h\lambda_t(r,t)k(r)} \frac{dr}{r}, \tag{2.59}$$

where α is a unit conversion factor with $\alpha = 141.2$ when oil field units are used. For injection, $q_{inj} > 0$ and

$$k(r) = \begin{cases} k_{skin}, & r_w < r \leq r_{skin} \\ k, & r > r_{skin}, \end{cases} \tag{2.60}$$

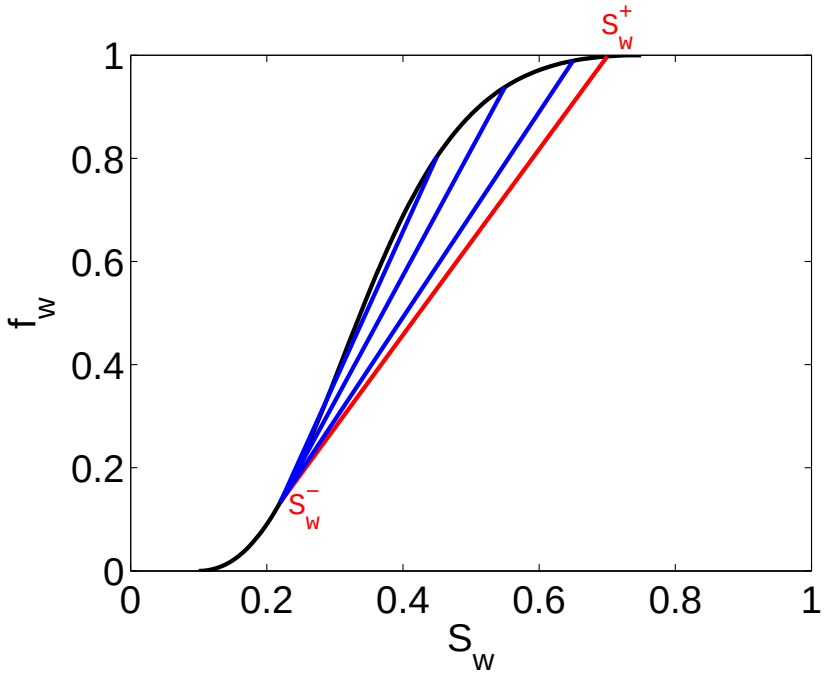

(a) If we draw lines connecting $f_w(S_w^-)$ with all points $f_w(S_w)$ where $S_w \in (S_w^-, S_w^+)$ (blue lines) in the water fractional flow curve (black curve), we can show that the first inequality Oleinik entropy condition (Eq. 2.49) is satisfied, i.e., those lines have a greater slope than $\frac{f_w(S_w^-)-f_w(S^+)}{S_w^- - S_w^+}$ (red line).

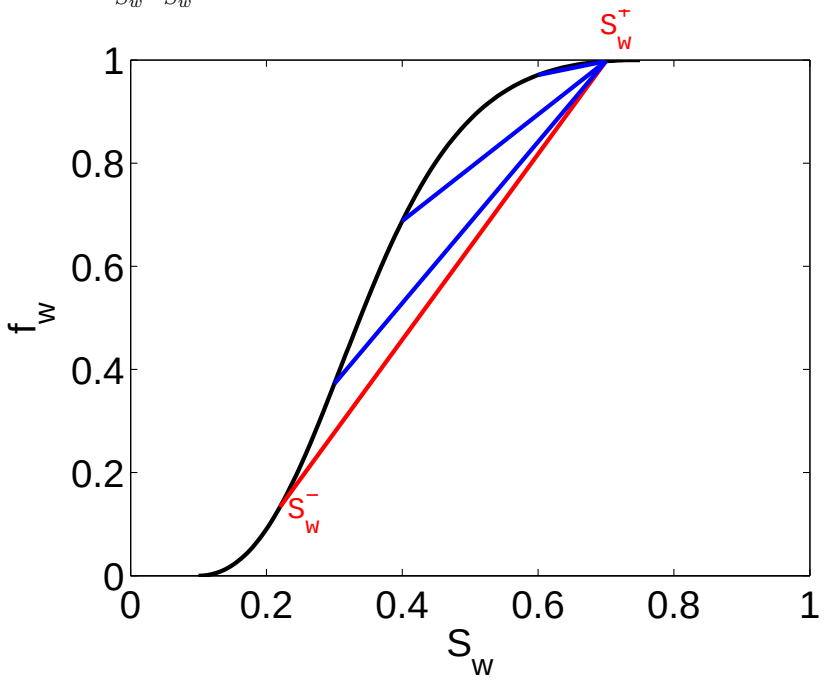

(b) If we draw lines connecting $f_w(S_w^+)$ with all points $f_w(S_w)$ where $S_w \in (S_w^-, S_w^+)$ (blue lines) in the water fractional flow curve (black curve), we can show that the second inequality in Oleinik entropy condition (Eq. 2.49) is satisfied, i.e., those lines have a smaller slope than $\frac{f_w(S_w^-)-f_w(S^+)}{S_w^- - S_w^+}$ (red line).

Figure 2.8: A graphical representation of the Oleinik entropy condition.

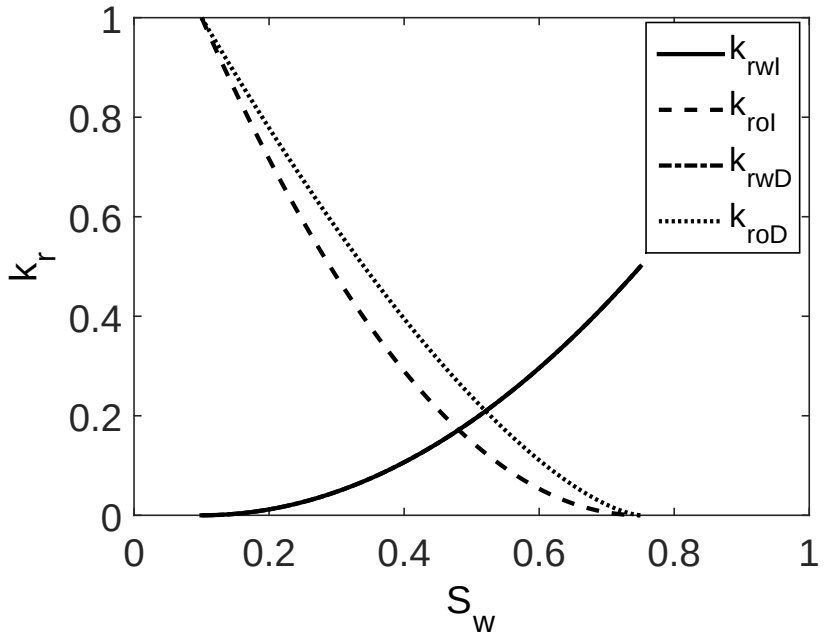

(a) Drainage and imbibition water/oil relative permeability curves.

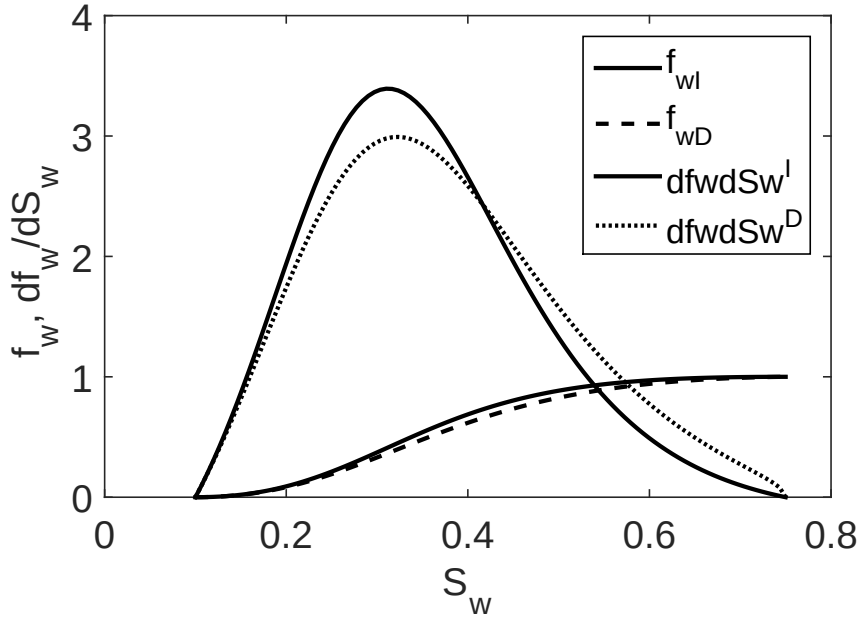

(b) Drainage and imbibition water fractional flow curves and its derivatives.

Figure 2.9: Hysteresis in the relative permeability curves and its effects on the water fractional flow curve.

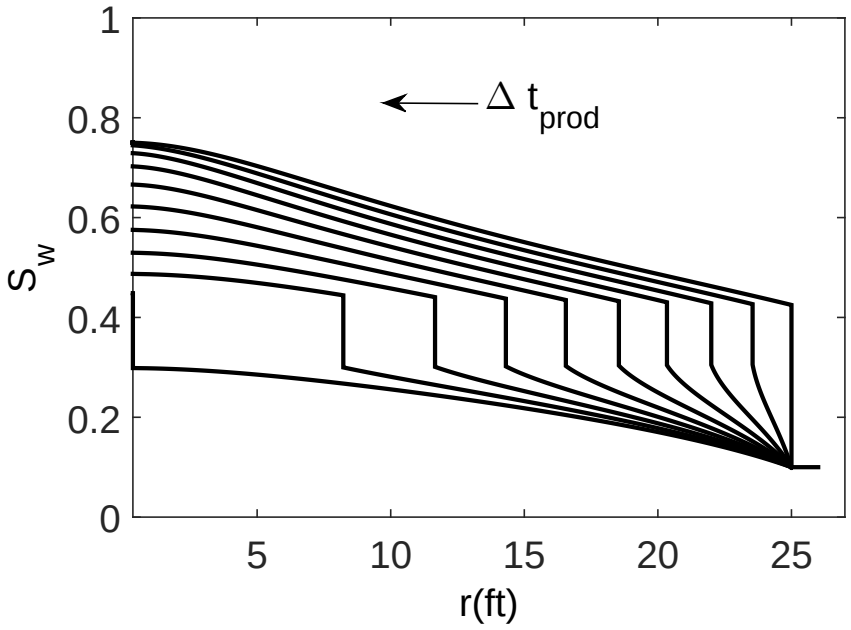

Figure 2.10: Saturation profile during production period using distinct fractional flow curves for imbibition and drainage periods.

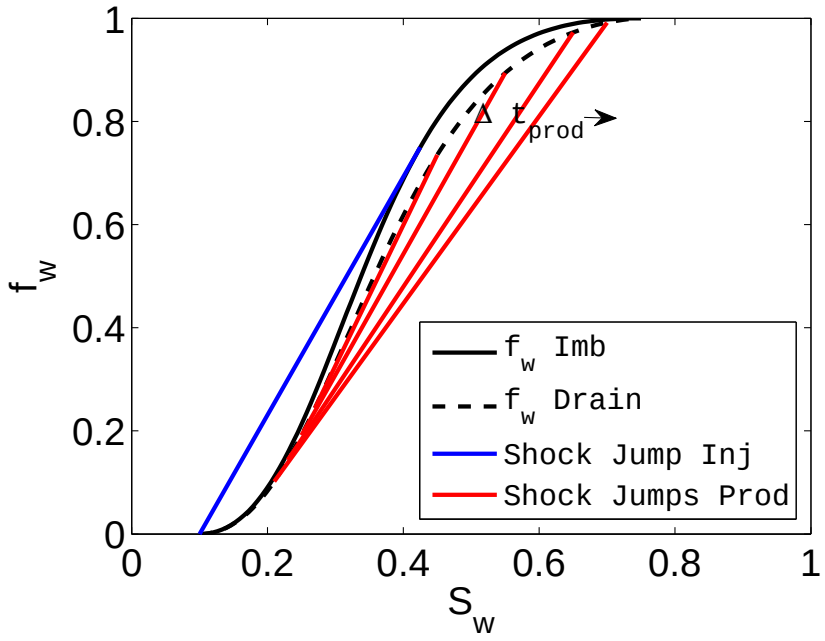

Figure 2.11: Shock jumps during injection and flowback using different fractional flow curves for imbibition and drainage periods.

where r_{skin} is the radius of the damaged zone and k_{skin} is the permeability in the skin zone.

Let $r_{f,inj}(t)$ be the radius of the water front at injection time t. Using the Thompson and Reynolds [98] steady theory, which assumes that, $q_t(r,t) = q_{inj}$, for $r \leq r_{f,inj}(t)$, Eq. 2.59 becomes

$$\Delta p_{wf}(t) = \frac{\alpha q_{inj}}{h} \int_{r_w}^{r_{f,inj}(t)} \frac{1}{\lambda_t(r,t)k(r)} \frac{dr}{r} + \frac{\alpha}{h} \int_{r_{f,inj}(t)}^{\infty} \frac{q_t(r,t)}{\lambda_t(r,t)k(r)} \frac{dr}{r}, \tag{2.61}$$

Adding and subtracting the term

$$\frac{\alpha}{h} \int_{r_w}^{r_{f,inj}(t)} \frac{q_{inj}}{\hat{\lambda}_o k(r)} \frac{dr}{r},$$

where $\hat{\lambda}_o = \frac{k_{ro}(S_{iw})}{\mu_o}$ is the endpoint oil mobility at $S_w = S_{iw}$, Eq. 3.228 can be rewritten as

$$\begin{aligned}\Delta p_{wf}(t) =& \frac{\alpha}{h} \int_{r_w}^{\infty} \frac{q_t(r,t)}{\hat{\lambda}_o(r,t)k(r)} \frac{dr}{r} + \frac{\alpha q_{inj}}{h} \int_{r_w}^{r_{f,inj}(t)} \left(\frac{1}{\lambda_t(r,t)} - \frac{1}{\hat{\lambda}_o} \right) \frac{dr}{k(r)r} \\ =& \Delta \hat{p}_o(t) + \frac{\alpha q_{inj}}{h} \int_{r_w}^{r_{f,inj}(t)} \left(\frac{1}{\lambda_t(r,t)} - \frac{1}{\hat{\lambda}_o} \right) \frac{dr}{k(r)r}. \end{aligned} \tag{2.62}$$

Throughout, $\Delta \hat{p}_o(t)$ is the single-phase oil transient pressure drop, the known pressure drop solution that is obtained if we inject oil into an oil reservoir. The single-phase oil transient pressure drop ($\Delta \hat{p}_o$) can be approximated as

$$\Delta \hat{p}_o(t) = p_{wf,o}(t) - p_i = \frac{\alpha q_{inj}}{kh\hat{\lambda}_o} \left[\frac{1}{2} \ln \left(\frac{\beta k \hat{\lambda}_o t}{\phi \hat{c}_{to} r_w^2} \right) + 0.4045 + s \right], \tag{2.63}$$

where is β is a unit conversion factor which in oil field units is 0.0002637 and

$$\hat{c}_{to} = c_o(1 - S_{iw}) + c_w S_{wi} + c_r. \tag{2.64}$$

Falloff: During falloff, assuming that the saturation distribution remains constant and equal to the distribution at the end of injection period ($S_w(r, \Delta t_{foff}) = S_w(r, t_{inj})$) so that

$$\lambda_t(r, \Delta t_{foff}) = \lambda_t(r, t_{inj}) = \frac{k_{rw}(S_w(r, t_{inj}))}{\mu_w} + \frac{k_{ro}(S_w(r, t_{inj}))}{\mu_o}. \tag{2.65}$$

Following [82, 28, 31], the bottom hole pressure drop can be expressed as

$$\Delta p_{ws}(\Delta t_{foff}) = p_{ws}(\Delta t_{foff}) - p_i = \int_{r_w}^{\infty} \frac{\alpha q_s(r, \Delta t_{foff})}{h\lambda_t(r, t_{inj})k(r)} \frac{dr}{r}, \tag{2.66}$$

where $\Delta t_{foff} = 0$ at the beginning of the falloff period and $p_{ws}(\Delta t_{foff})$ denotes the falloff pressure at time Δt_{foff}. Eq. 2.66 can be rewritten as

$$\Delta p_{ws}(\Delta t_{foff}) = \frac{\alpha}{h} \int_{r_w}^{r_{f,inj}(t_{inj})} \frac{q_s(r, \Delta t_{foff})}{\lambda_t(r, t_{inj})k(r)} \frac{dr}{r} + \frac{\alpha}{h} \int_{r_{f,inj}(t_{inj})}^{\infty} \frac{q_s(r, \Delta t_{foff})}{\lambda_t(r, t_{inj})k(r)} \frac{dr}{r}, \tag{2.67}$$

where $q_s(r, \Delta t_{foff})$ is the total flow rate profile at shut-in time, Δt_{foff}. Following Peres et al. [81] and Chen [28], we add and subtract the term

$$\frac{\alpha}{h} \int_{r_w}^{r_{f,inj}(t)} \frac{q_{os}(r, \Delta t_{foff})}{\hat{\lambda}_o k(r)} \frac{dr}{r}$$

to Eq. 2.67 and rearrange the resulting equation to obtain

$$\begin{aligned}
&\Delta p_{ws}(\Delta t_{foff}) = p_{ws}(\Delta t_{foff}) - p_i \\
&= \int_{r_w}^{\infty} \frac{\alpha q_s(r, \Delta t_{foff})}{h\hat{\lambda}_o k(r)} \frac{dr}{r} + \frac{\alpha}{h\hat{\lambda}_o} \int_{r_w}^{r_{f,inj}(t_{inj})} \left(\frac{\hat{\lambda}_o}{\lambda_t(r, t_{inj})} q_s(r, \Delta t_{foff}) - q_{os}(r, \Delta t_{foff}) \right) \frac{1}{k(r)} \frac{dr}{r} \\
&= \Delta \hat{p}_{os}(\Delta t_{foff}) + \frac{\alpha}{h\hat{\lambda}_o} \int_{r_w}^{r_{f,inj}(t_{inj})} \left(\frac{\hat{\lambda}_o}{\lambda_t(r, t_{inj})} q_s(r, \Delta t_{foff}) - q_{os}(r, \Delta t_{foff}) \right) \frac{1}{k(r)} \frac{dr}{r}.
\end{aligned} \tag{2.68}$$

Here $q_s(r, \Delta t_{foff}) = q_{os}(r, \Delta t_{foff})$ in the uninvaded zone, i.e., for $r > r_{f,inj}(t_{inj})$, where $q_{os}(r, \Delta t_{foff})$ is the single-phase rate profile obtained during falloff after injecting oil at the rate q_{inj} [82]. Since we are considering only infinite-acting behavior, where the single oil phase pressure drop that would be obtained if we had injected oil and then shut the well can be defined from the superposition of two constant sandface flow rates solutions, i.e.,

$$\Delta\hat{p}_{os}(r, \Delta t_{foff}) = \Delta\hat{p}_o(r, t_{inj} + \Delta t_{foff}) - \Delta\hat{p}_o(r, \Delta t_{foff}), \tag{2.69}$$

which gives

$$\Delta\hat{p}_{os}(r, \Delta t_{foff}) = p_{wf,o}(\Delta t_{foff}) - p_i = \frac{\alpha q_{inj}}{2kh\hat{\lambda}_o} \ln\left(\frac{t_{inj} + \Delta t_{foff}}{\Delta t_{foff}}\right), \tag{2.70}$$

with the rate schedule

$$q_t(r_w, t) = \begin{cases} q_{inj} > 0, & 0 < t \leq t_{inj} \\ 0, & t_{inj} < t \leq t_{inj} + t_{foff}, \end{cases} \tag{2.71}$$

where t_{foff} is the total time at the end of the falloff period and $\Delta t_{foff} = 0$ at the beginning of the falloff period. As rate superposition applies for single-phase flow, following Peres et al. [81] and Chen [28], we use rate superposition to approximate the rate profiles as

$$q_s(r, \Delta t_{foff}) = q_{inj}\left[\exp\left(-\frac{\phi c_t(r, t_{inj})r^2}{4\beta k\lambda_t(r, t_{inj})(t_{inj} + \Delta t_{foff})}\right) - \exp\left(-\frac{\phi c_t(r, t_{inj})r^2}{4\beta k\lambda_t(r, t_{inj})\Delta t_{foff}}\right)\right] \tag{2.72}$$

and the single oil phase flow rate

$$q_{os}(r, \Delta t_{foff}) = q_{inj}\left[\exp\left(-\frac{\phi\hat{c}_{to}r^2}{4\beta k\hat{\lambda}_o(t_{inj} + \Delta t_{foff})}\right) - \exp\left(-\frac{\phi\hat{c}_{to}r^2}{4\beta k\hat{\lambda}_o\Delta t_{foff}}\right)\right], \tag{2.73}$$

with

$$c_t(r, t_{inj}) = c_o S_o(r, t_{inj}) + c_w S_w(r, t_{inj}) + c_r. \tag{2.74}$$

Production: During production at a constant flow rate $q_{prod} = q_t(r_w, \Delta t_{prod})$ RB/D, where $\Delta t_{prod} = 0$ at the beginning of the flowback period, the bottom hole pressure drop can be expressed as [28, 31]

$$\Delta p_{wf}(\Delta t_{prod}) = p_i - p_{wf}(\Delta t_{prod}) = -\int_{r_w}^{\infty} \frac{\alpha q_t(r, \Delta t_{prod})}{h\lambda_t(r, \Delta t_{prod})k(r)} \frac{dr}{r}, \tag{2.75}$$

Let $r_{f,inj}$ be the radius of the water front at the end of injection period, then for any time Δt_{prod}, such that, $q_t(r,t) = q_{prod}$ for $r \leq r_{f,inj}(t_{inj})$, Eq. 2.75 becomes

$$\Delta p_{wf}(\Delta t_{prod}) = -\frac{\alpha q_{prod}}{h} \int_{r_w}^{r_{f,inj}(t_{inj})} \frac{1}{\lambda_t(r, \Delta t_{prod})k(r)} \frac{dr}{r} - \frac{\alpha}{h} \int_{r_{f,inj}(t_{inj})}^{\infty} \frac{q_t(r, \Delta t_{prod})}{\lambda_t(r, \Delta t_{prod})k(r)} \frac{dr}{r}, \tag{2.76}$$

where the Thompson and Reynolds [98] steady-state theory was applied to calculate the pressure drop with time in each stage of well testing by integrating Darcy's equation, ignoring capillary and gravitational effects. Obviously, the former assumption is not valid for the whole production process. However, as shown by Chen [28], the steady-state solution will be reached in a short time after the production starts, if the injected water bank is not extensive. By adding and subtracting the term

$$\frac{\alpha}{h} \int_{r_w}^{r_{f,inj}(t_{inj})} \frac{q_{prod}}{\hat{\lambda}_o k(r)} \frac{dr}{r},$$

where $\hat{\lambda}_o$ is the endpoint oil mobility at $S_w = S_{wi}$, which means that $\lambda_t(r, \Delta t_{prod}) = \hat{\lambda}_o$ for $r > r_{f,inj}$, Eq. 2.76 can be rewritten as

$$\begin{aligned}\Delta p_{wf}(\Delta t_{prod}) &= -\frac{\alpha q_{prod}}{h}\int_{r_w}^{r_{f,inj}(t_{inj})}\left(\frac{1}{\lambda_t(r,\Delta t_{prod})}-\frac{1}{\hat{\lambda}_o}\right)\frac{dr}{k(r)r}-\frac{\alpha}{h}\int_{r_w}^{\infty}\frac{q_t(r,\Delta t_{prod})}{\hat{\lambda}_o k(r)}\frac{dr}{r}\\ &= -\Delta\hat{p}_{op}(\Delta t_{prod})-\frac{\alpha q_{prod}}{h\hat{\lambda}_o}\int_{r_w}^{r_{f,inj}(t_{inj})}\left(\frac{\hat{\lambda}_o}{\lambda_t(S_w(r,\Delta t_{prod}))}-1\right)\frac{1}{k(r)}\frac{dr}{r},\end{aligned} \tag{2.77}$$

where we have assumed that Δt_{prod} is sufficiently large so that $q_t(r, \Delta t_{prod}) = q_{prod}$ for $r \geq r_{f,inj}(t_{inj})$. The single-phase oil solution that would be obtained if we had injected oil into a oil reservoir, shut the well and the produced it, $\Delta\hat{p}_{op}(\Delta t_{prod})$, can be determined by the superposition of three constant sandface flow rate solutions, i.e.,

$$\begin{aligned}\Delta\hat{p}_{op}(\Delta t_{prod}) =&\Delta\hat{p}_o(r, t_{inj}+t_{foff}+t_{inj})-\Delta\hat{p}_o(r, t_{foff}+\Delta t_{prod})\\ &+\frac{\alpha q_{prod}}{kh\hat{\lambda}_o}\left[\frac{1}{2}\ln\left(\frac{\beta k\hat{\lambda}_o t}{\phi\hat{c}_{to}r_w^2}\right)+0.4045+s\right],\end{aligned} \tag{2.78}$$

which gives

$$\begin{aligned}\Delta\hat{p}_{op}(\Delta t_{prod}) = &\frac{\alpha}{kh\hat{\lambda}_o}\left\{\frac{q_{inj}}{2}\ln\left(\frac{t_{inj}+t_{foff}+\Delta t_{prod}}{t_{foff}+\Delta t_{prod}}\right)\right.\\ &\left.+q_{prod}\left[\frac{1}{2}\ln\left(\frac{\beta k\hat{\lambda}_o}{\phi\hat{c}_{to}r_w^2}\Delta t_{prod}\right)+0.4045+s\right]\right\},\end{aligned} \tag{2.79}$$

with the rate schedule:

$$q_t(r_w,t)=\begin{cases}q_{inj}>0, & 0<t\leq t_{inj}\\ 0, & t_{inj}<t\leq t_{foff}\\ q_{prod}<0, & t>t_{foff}.\end{cases} \tag{2.80}$$

Figs. 2.12 and 2.13 show the bottomhole pressure behavior for the IFPT with and

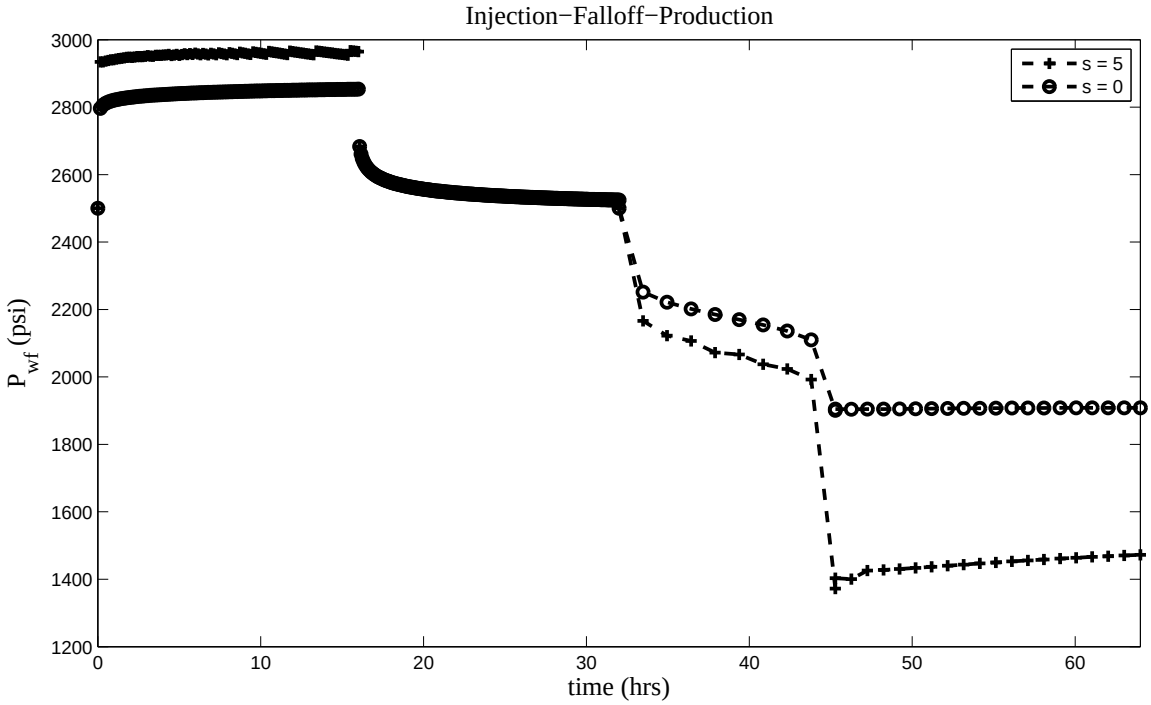

Figure 2.12: Wellbore pressure during IFP well testing with and without skin effect.

without skin and hysteresis effects, respectively.

2.2 Validation

"There he is, bent over the page, with a monocle in his right eye, wholly devoted to the noble but rugged task of ferreting out the error."

— "Brás Cubas"

in *Memórias Póstumas de Brás Cubas* by Machado de Assis

The semi-analytical solution developed for the IFPT was compared with the solution from the commercial numerical simulator IMEX, using the properties shown in Table 2.1. To obtain IMEX results which matched our semi-analytical, we were forced to use very small time steps as well as highly refined radial grids in the IMEX simulator. In the results shown, we set the grid size in the area invaded by injected water equal to 0.01 ft then increased it geometrically by the factor of 1.013 until reaching the outer radius of the reservoir. We choose an initial time step of 10^{-7} days to get convergence at the first time step and then

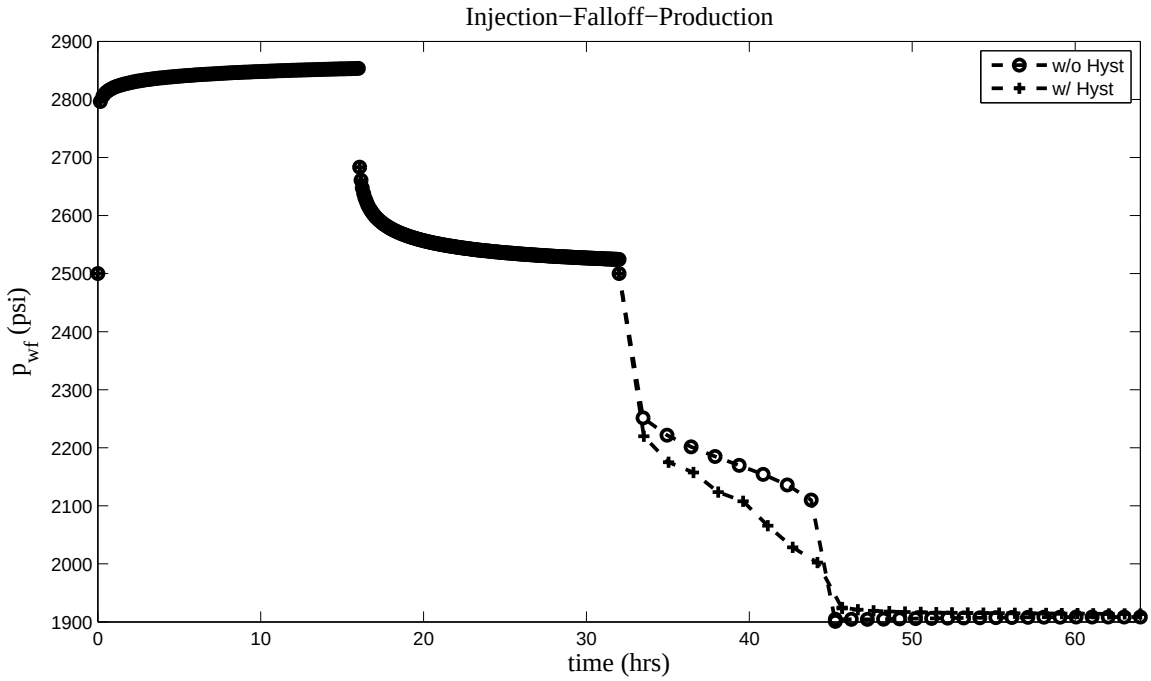

Figure 2.13: Wellbore pressure during IFP well testing with and without hysteresis effect.

increase the time step geometrically using a factor of 1.05. After each rate change, we reinitialized the time step to 10^{-7} days and then increased it again using 1.05 as the time step multiplier. Fig. 2.14 compares the bottom hole pressure obtained from our analytical solution with the reservoir simulation results and Fig. 2.15 presents the comparison between the saturation profiles from IMEX and our analytical solution. Note the two sets of results are in excellent agreement.

Although the assumption of the steady-state zone has been verified previously for injection and production tests, Figures 2.16a and 2.16b are provided to illustrate the feasibility of using the steady-state theory for both the injection and flowback periods. Note that these two figures show the relationship between the water saturation and total flow rate profile at two different times during injection and production; these results were generated from a reservoir simulator using fine spatial grids and small time steps. Both figures show that the total rate profile is approximately constant in a region close to the wellbore and that the radius of the region in which the total rate is constant increases with time. Moreover, as illustrated in Fig. 2.16a, the computational results show that for $t > 0$ hours, the two-phase

flow region lies with the constant total rate steady-state zone. However, in Fig. 2.16b, we see that, flowback period, the total rate is not constant inside the two-phase zone until sometime after 0.3 hour where in this plot, $t = 0$ corresponds to the time as which the production period begins. The fact that steady-state theory is not applicable at very early-times during the production period emanates from the fact that, when the production begins, there is already a sizable region where two-phase are mobile due to the preceding water injection period.

Table 2.1: Reservoir, rock and fluid properties for simulation and analytical solution.

Property	Value	Unit
q_{inj}	3000	RB/DAY
q_{prod}	-3000	RB/DAY
h	60	ft
r_w	0.35	ft
r_e	6800	ft
k	300	md
s	0	
a_w	0.5	
a_o	1	
n_w	2	
n_{oI}	2	
n_o	1.5	
S_{iw}	0.1	
S_{or}	0.25	
p_i	2500	psi
ϕ	0.22	
B_o	1.003	RB/STB
B_w	1.002	RB/STB
c_o	8.0×10^{-6}	ft
c_w	3.02×10^{-6}	ft
c_r	5.0×10^{-6}	ft
μ_o	3.0	cp
μ_w	0.5	cp
t_{inj}	16	h
t_{foff}	32	h
t_{prod}	56	h

Using the saturation profile at the end of the water injection as the initial condition, we showed that the saturation profile in the reservoir at different production times can be

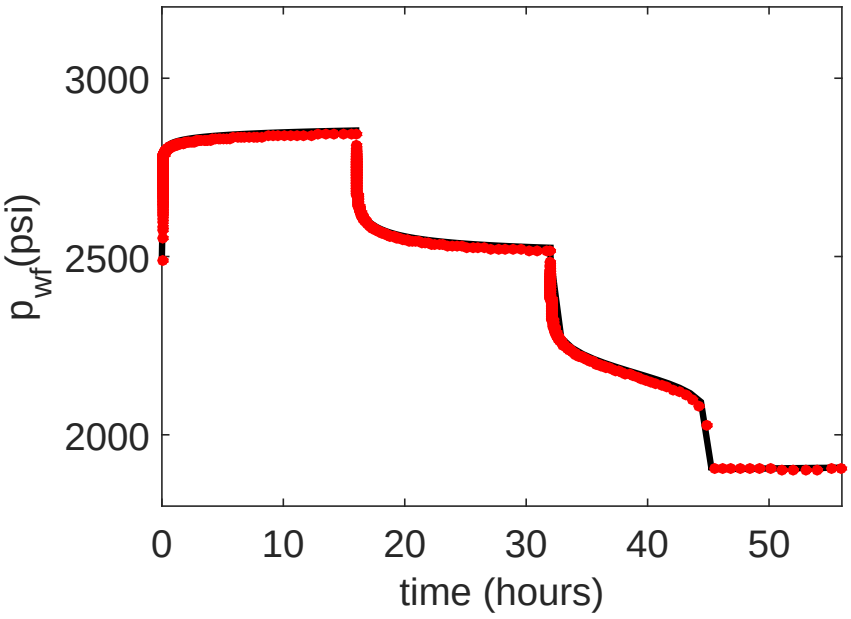

Figure 2.14: Bottomhole pressure during an IFPT, analytical solution (dark solid curve) versus simulation results (red circle curve). Here, $t_{inj} = 16$ h, $t_{foff} = 32$ h and $t_{prod} = 56$ h

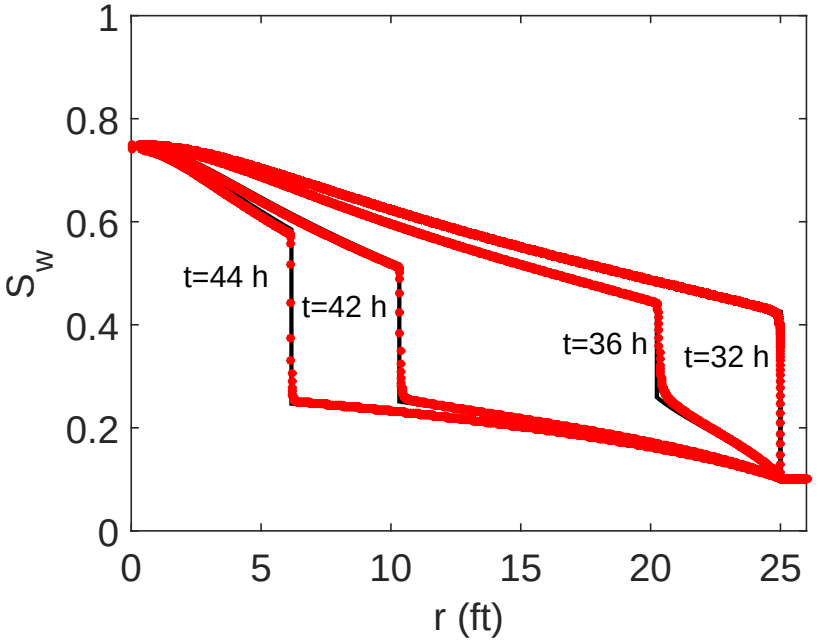

Figure 2.15: Saturation profile during flowback period, analytical solution (dark solid curve) versus simulation results (red circles).

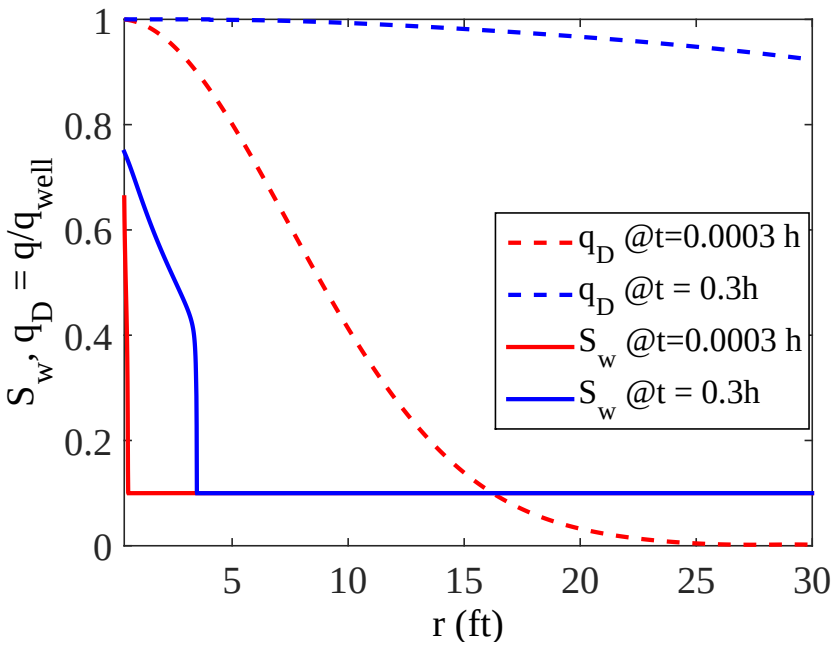

(a)

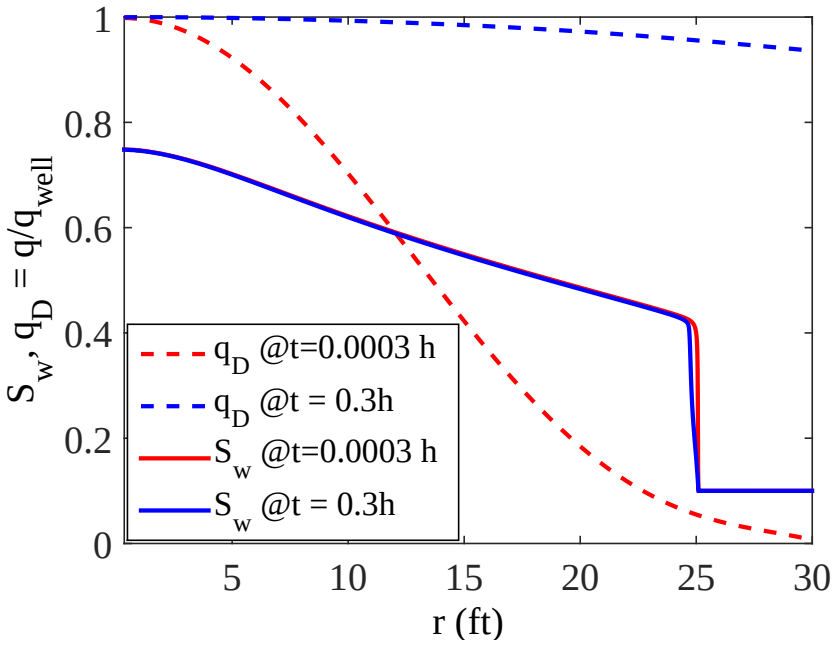

(b)

Figure 2.16: Relationship between water saturation and total flow rate profile during injection (a) and production (b).

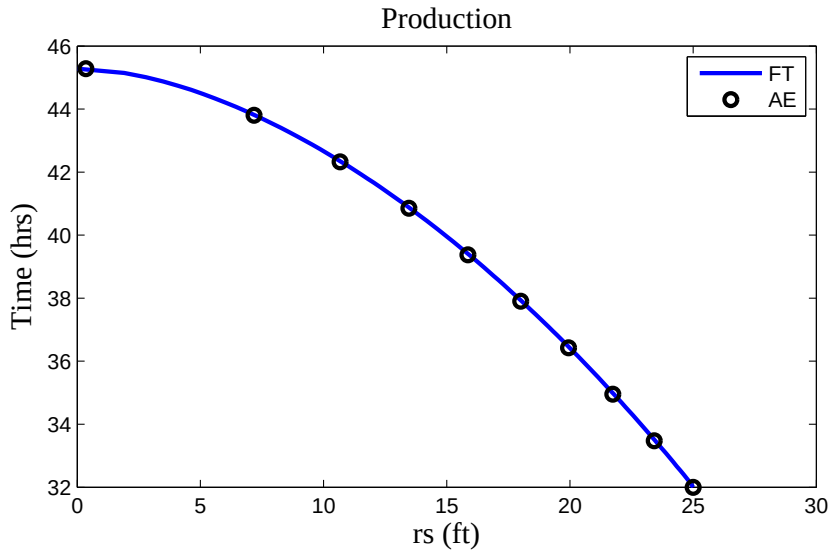

Figure 2.17: Comparison of shock path obtained from front tracking (FT) and area equality (EA) shocking fitting methods.

obtained. Figs. 2.17 and 2.18 compare the solution we obtained based on area equality with the front tracking method which has as its basis the integration of Eq. 2.45.

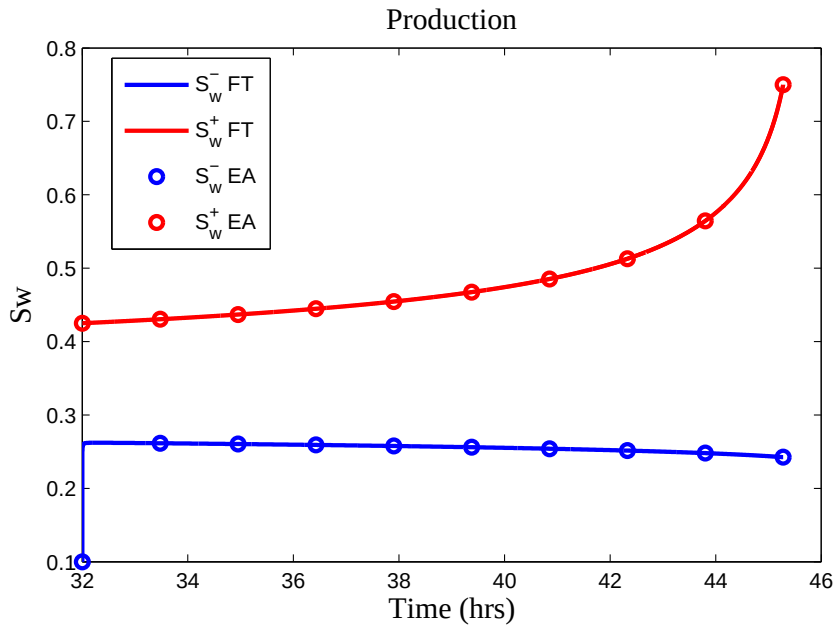

Figure 2.18: Comparison of shock saturations obtained from front tracking (FT) and area equality (EA) shocking fitting methods.

In the front tracking approach, Euler's method can be applied to find the shock path

numerically, with initial conditions given by

$$IC : S_w^-(r,0) = S_{iw}, \quad S_w^+(r,0) = S_{wf}, \quad r_s(0) = r_{f,inj}. \tag{2.81}$$

We assume that shock speed is constant throughout each time step ($\Delta t^n = t^n - t^{n-1}$), and integrating Eq. 2.45 over the time step gives the change in the radius square of the shock over the time step Δt^n,

$$\Delta r_s^2(t^n) \equiv r_s^2(t^n) - r_s^2(t^{n-1}) = \frac{\theta q_{t,prod} \Delta t}{\pi h \phi} \frac{[f_w(S_w^-(t^{n-1})) - f_w(S_w^+(t^{n-1}))]}{[S_w^-(t^{n-1}) - S_w^+(t^{n-1})]}. \tag{2.82}$$

From Eq. 2.82, it follows that the updated shock position squared at the end of the time step is given by,

$$r_s^2(t^n) = r_s^2(t^{n-1}) + \frac{\theta q_{t,prod} \Delta t}{\pi h \phi} \frac{[f_w(S_w^-(t^{n-1})) - f_w(S_w^+(t^{n-1}))]}{[S_w^-(t^{n-1}) - S_w^+(t^{n-1})]}. \tag{2.83}$$

Given r_s^2, S_w^- and S_w^+ can be obtained by solving

$$r_{inj}^2(S_w^+, t_{inj}) - r_s^2(t^n) = -\frac{\theta q_{t,prod} t^n}{\pi h \phi} \frac{df_w}{dS_w}(S_w^+(t^n)) \tag{2.84}$$

and

$$r_{inj}^2(S_{wf}, t_{inj}) - r_s^2(t^n) = -\frac{\theta q_{t,prod} t^n}{\pi h \phi} \frac{df_w}{dS_w}(S_w^-(t^n)), \tag{2.85}$$

for $\frac{df_w}{dS_w}(S_w^+(t^n))$ and $\frac{df_w}{dS_w}(S_w^-(t^n))$ and then S_w^+ and S_w^- can be computed from the water fractional flow derivative curve. The only disadvantage of this method is that it is necessary to use a small time step to obtain an accurate shock path because the method assumes Δt^n is sufficiently small so the shock speed does not change within the time step. The best approach (less expensive computationally) to use depends on the amount of data to be matched in the well testing application. If successive data points in time are closely spaced so that very small time steps must be used to predict data at observations, the front-tracking procedure would be more efficient than the area equality method.

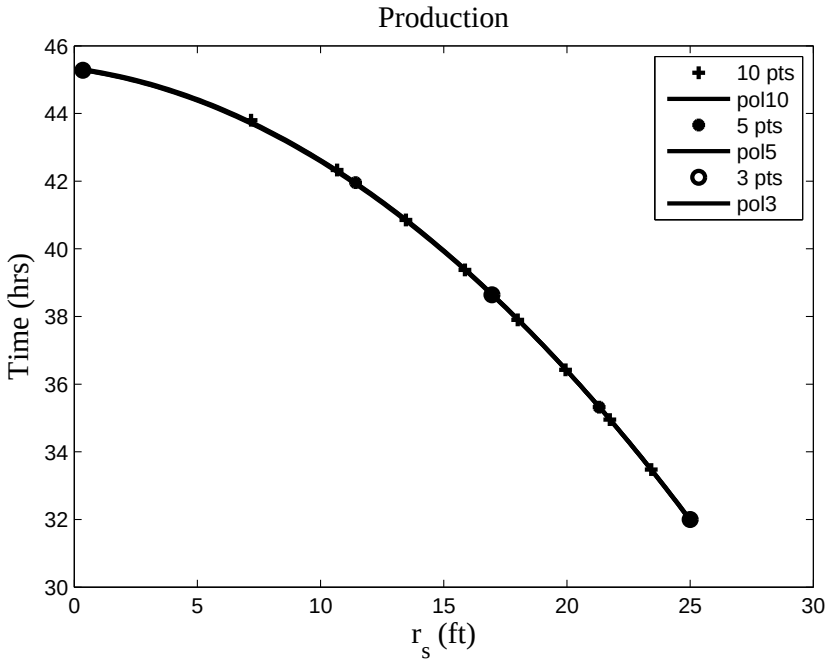

Figure 2.19: Shock path for the production period obtained from quadratic polynomial fitting.

Fig. 2.19 shows the shock path for the production period obtained from quadratic polynomial fitting using 10, 5 and 3 points obtained from the area equality approach. As we can see, by only solving the system of Eqs. 2.36, 2.38 and 2.40 at one point $(r_s(t), t)$ with time $t = 0$ at the beginning of the production period and fitting a quadratic curve, $r_s(t) = at^2 + bt + c$, by using also the initial and breakthrough points, we can find the shock path for the whole flowback period. We can use this polynomial curve to determine $r_s(t)$ at each data time, and then apply Eqs. 2.38 and 2.40 to find S_w^- and S_w^+.

2.3 Example

"The reader, like his fellows, doubtless prefers action to reflection,
and doubtless he is wholly in the right.
So we shall get to it."
— "Brás Cubas"
in *Memórias Póstumas de Brás Cubas* by Machado de Assis

In this section, we exemplify how the analytical solutions developed in this chapter

can be applied to estimate reservoir parameters. In the example presented here, we match pressure data generated from commercial numerical reservoir simulators by using nonlinear regression where our analytical solution is the forward model. The model parameters to be estimated are the absolute permeability, the skin factor and the coefficients and exponents in power law relative permeability curves; the critical saturations are assumed to be known since, as discussed previously in this Chapter 2, the work of [28] indicates that it cannot always obtain good estimates of the critical saturations.

The approximate analytical and semi-analytical solutions for the wellbore pressure presented here and in the next two chapters can be used as the forward model when analyzing pressure data by nonlinear regression (assisted history matching). In this procedure, starting with an initial guess for reservoir parameters, we minimize the least-squares objective function,

$$O(\vec{m}) = \frac{1}{2}\sum_{k=1}^{N_d} \frac{(p_{wf,obs}(t_k) - p_{wf}(\vec{m}, t_k))}{\sigma_k^2}, \tag{2.86}$$

where the model parameters to be estimated are the components of the vector $\vec{m}$, N_d is the number of observed pressure data used for analysis, where $p_{wf,obs}(t_k)$, $k = 1, 2, \cdots N_d$ denote these measured pressure data, $0 < t_1 < \cdots < t_{N_d}$ represent the times of these observations; $p_{wf}(\vec{m}, t_k)$ denotes the corresponding pressure computed from our analytical solution at time t_k for the current estimate of $\vec{m}$, and σ_k^2 denotes the variance of the measurement error at time t_k. In our procedure, we minimize the objective function using the Trust-Region-Reflective Least Squares Algorithm (TRR) algorithm [35] to obtain an estimates of $\vec{m}$ so that $p_{wf}(\vec{m}, t_k)$ honors the observed data, $p_{wf,obs}(t_k)$ for $k = 1, 2, \cdots, N_d$. The TRR algorithm requires upper and lower bounds on all variables; these bounds may be specified arbitrarily but should of course be such that the resulting bounds cover all physically plausible values of the parameters. Convergence of the TRR algorithm is assumed when the relative change in the objective function between two successive iterations is less than a specified tolerance, ϵ. In our example, with $\epsilon = 10^{-6}$, i.e., for convergence we require that $|O(\vec{m}^{k+1}) - O(\vec{m}^k)| \leq 10^{-6}$. The overall history-matching (nonlinear regression) procedure is illustrated in Fig. 2.20. If

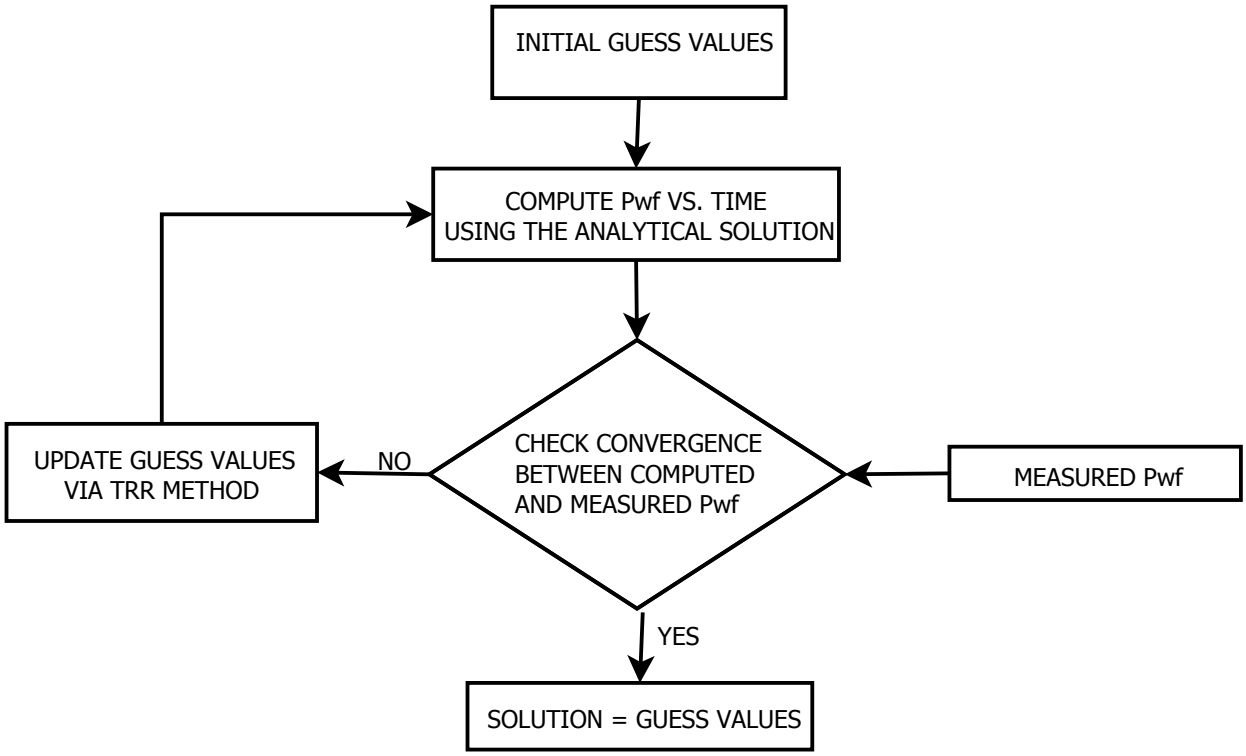

Figure 2.20: Data analysis procedure.

all σ_k's are equal, they can be deleted from the definition of the objective function without changing the values of corresponding minimizing parameters.

In this example, we applied our semi-analytical approximate solution as a forward model to estimate absolute permeability, skin factor and relative permeability parameters for the rock and fluid properties described in Table 2.1. The observed well pressure data with time $(p_{wf,obs}(t_k), k = 1, ..., n)$ were obtained from an IFPT simulation using a commercial numerical simulator by adding uncorrelated Gaussian noise with mean zero and variance 1 psi^2 and using data only for times more than 0.5 hour after each flow rate change to avoid matching data that might be masked by wellbore storage. The model parameters to be estimated were the component of the vector $\vec{m}$, given by

$$\vec{m} = [k, s, a_w, n_w, n_{oI}, n_{oD}]^T, \tag{2.87}$$

Table 2.2: Parameter bounds for IFPT.

Parameter	k (md)	Skin Factor	a_w	n_w	n_{oI}	n_{oD}
Lower bound IFPT	5	-8	0.05	0.5	0.5	0.5
Upper bound IFPT	4000	25	1.00	4.5	4.5	4.5

where, as mentioned previously, the skin factor, s, is related to the skin permeability, k_s, via the Hawkins's formula [50], where the skin zone radius need to be fixed. The last four elements in $\vec{m}$ are the parameters for the relative permeabilities curves represented by the power law model given by Eqs. 2.3 and 2.4. It is important to note that the critical saturations could conceptually be included as parameters to be estimated when matching data by nonlinear regression; in fact, [28] showed that, for some examples, critical saturations can be reasonably estimated. However, as explained by [28], including critical saturations as parameters when matching data tends to make the problem more ill-conditioned and it can be difficult to resolve these parameters accurately. To reproduce the simple explanation provided by [28], we temporarily neglect hysteresis. Then if all parameters except endpoint saturations are fixed but S_{iw} and S_{or} are varied but the sum $S_{iw} + S_{or}$ is held constant, then the fractional flow curve is a function of the saturation change, $S_w - S_{iw}$; thus, if $c_o S_o + c_w S_w + c_r$ is close to constant, which is the case if $c_0 \approx c_w$, then the pressure response generated with one set of relative permeability curves can be well approximated with any other set of relative permeability curves obtained by shifting the original set by varying only S_{iw} and S_{or} keeping $S_{iw} + S_{or}$ constant. With this reasoning, it follows that it can be difficult to estimate accurate values of end-point saturations together with the parameters specified in Eq. 2.87 by matching pressure data.

Fig. 2.21 shows the bottom-hole pressure match for the IFPT data while Fig. 2.22 shows the estimated relative permeability curves, assuming hysteresis affects only the oil relative curve. Table 2.3 presents the values of model parameters estimated based on the set of bounds on parameters shown in Table 2.2.

(a)

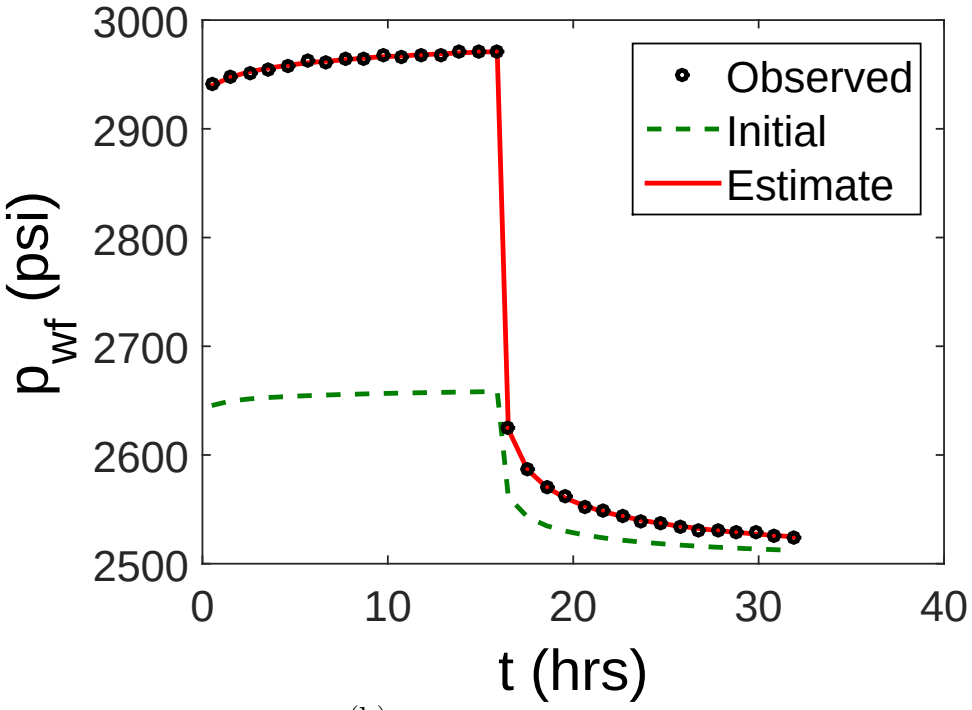

(b)

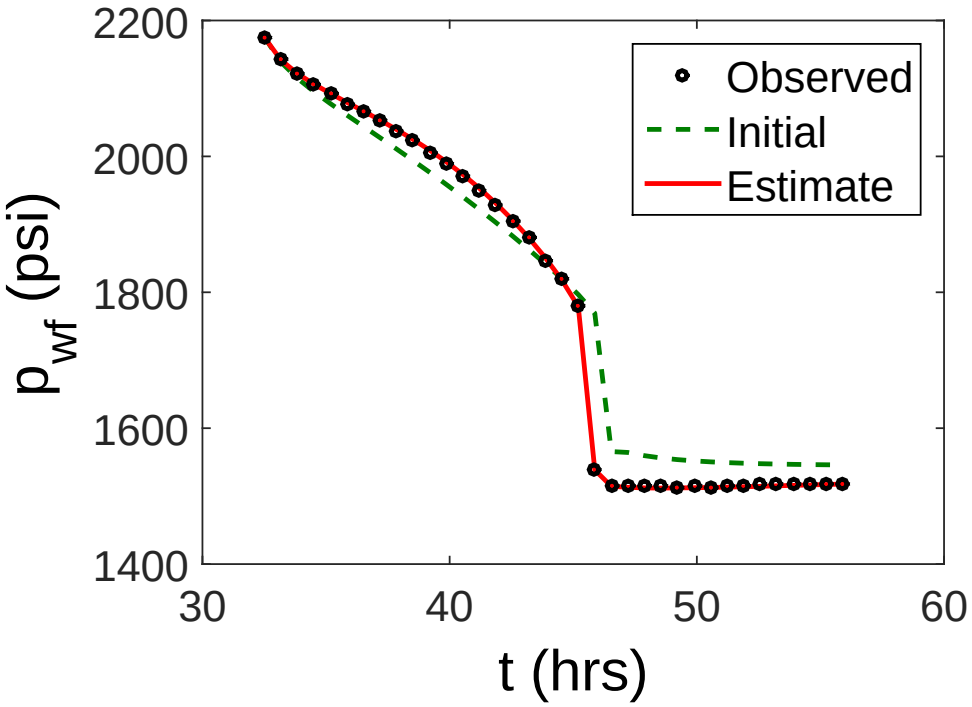

Figure 2.21: Data match for the IFPT test; (a) injection and falloff, (b) production (flow-back). The dashed green curves represent the computed pressure based on the initial guess for model parameters, the black circles the true noisy data and the red solid curves the data predicted from the estimated parameters.

Table 2.3: Estimated model parameters based on the approximate analytical solution of IFPT.

Parameter	k (md)	Skin Factor	a_w	n_w	n_{oI}	n_{oD}
True	300.00	5.00	0.50	2.00	2.00	1.50
Initial Guess	600.00	0.00	0.80	1.20	1.20	1.20
IFPT	298.92	4.43	0.48	1.79	2.11	1.52

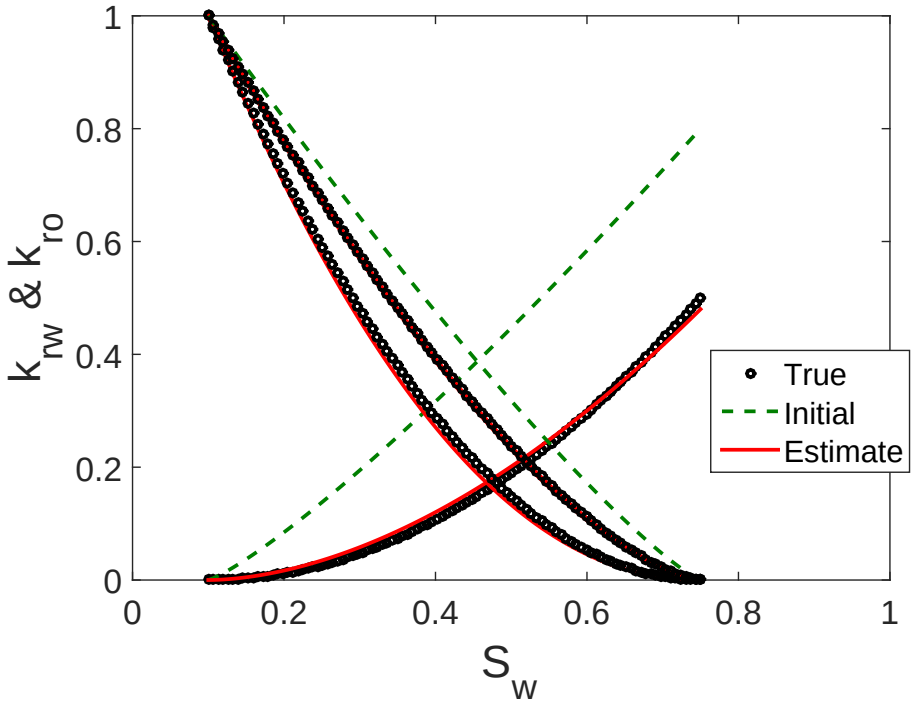

Figure 2.22: Estimated imbibition (black solid curves) and oil drainage (red solid curve) relative permeability curves based on model parameters obtained from IFPT data match. The green dashed lines represent the relative permeability curves computed based on the initial guess for model parameters and the circles, represents the true curves.

2.4 Note on Data Sensitivity

Through sensitivity analysis, derivations and examples, Nanba and Horne [71], Peres and Reynolds [77], Chen [28] have showed in details that data from an injection test can be used to estimate the reservoir rock absolute permeability, the skin zone permeability and the water end-point relative permeability. Although the flowback pressure data are necessary to estimate the drainage relative permeability curves parameters, Nanba and Horne [71] states that the imbibition curves and skin and absolute permeability can indeed be found uniquely from falloff tests data. However, although the falloff data are somewhat sensitive to the power law exponents, Nanba and Horne [71] have attributed themselves their successful examples on estimating imibibiton relative permeability curves to the fact that their data - synthetic data - were obtained from numerical simulation ignoring wellbore storage effects. Taking the derivative of Eq. 2.66 with respect to the logarithm of time, $\ln \Delta t_{foff}$, we have

$$\frac{\partial \Delta p_{ws}(\Delta t_{foff})}{\partial \ln \Delta t_{foff}} = \frac{\alpha}{h} \int_{r_w}^{\infty} \frac{1}{r} \frac{\partial q_s(r, \Delta t_{foff})}{\partial \ln \Delta t_{foff}} \frac{1}{k(r)\lambda_t(r, t_{inj})} dr, \tag{2.88}$$

Eq. 2.88 indicates that the pressure derivative at a given time during falloff reflects a weighted harmonic average of the permeability-total mobility. The regions in the reservoir where the total flow rate, q_s, is changing most rapidly with time is weighted most heavily. Consequently, the bottom-hole pressure data during falloff at the very earlier times - when the flow rate front (the position where the flow rate is changing abruptly from $q_s \approx 0$ to q_{inj}) is crossing the invaded zone - would reflect the fluid distribution in the invaded zone, i.e, , in a similar way the bottom-hole pressure would reflect the reservoir heterogeneities (as in [98]). If the measured data is distorted by wellbore storage effects, the relative permeability curve parameters information would most probably be masked. Chen [28] has showed that the addition of not only the production wellbore pressure response but also the oil rate (or water rate) together with injection-falloff pressure data to the wellbore pressure history matching process would lead to the correct estimation of imbibition parameters. Chen [28] recommends to cut off the very early times from falloff and production data to guarantee that no fragment

of the observed data is distorted by wellbore storage. In addition, Chen [28] recommends the use of the cumulative oil rate, given by

$$Q_o(t) = \int_{t_{foff}}^{t} (1 - f_w(r_w, t)) q_{prod} dt \tag{2.89}$$

instead of the instantaneous oil flow rate,

$$q_o(r_w, t) = (1 - f_w(r_w, t)) q_{prod}. \tag{2.90}$$

The derivative of the Eq. 2.89 with respect of the relative permeability curve parameters show smoother variations than the derivative of the Eq. 2.90. The cumulative oil rate is insensitive to skin and absolute permeabilities; remember that S_w (and consequently $f_w(S_w)$) is governed by the Buckley-Leverett equation (Eq. 2.1), which does not include permeability as a parameter. For a deeper discussion on the sensitivities of the injection-falloff-production test data to skin, absolute permeabilities and relative permeability curve parameters, please see Peres and Reynolds [77], Chen [28].

CHAPTER 3

PRESSURE RESPONSE DURING IFPT WITH CAPILLARY PRESSURE

"No meio do caminho tinha uma pedra..."

—Carlos Drummond de Andrade, *No Meio do Caminho*

"Why the devil couldn't it have been blue?"

— "Brás Cubas"

in *Memórias Póstumas de Brás Cubas* by Machado de Assis

In this chapter, we include capillary pressure effects in our semi-analytical model. In summary, we develop a semi-analytical approximate solution for the wellbore pressure response and the wellbore water/oil flow rates, which accounts for capillary and hysteresis effects. This solution can be used as a forward model during non-linear regression analysis to estimate in-situ rock-fluid properties from data collected during an injection-falloff-production (IFPT). If we simply use the saturation profile obtained during an IFPT without considering the dispersive effects caused by capillary pressure, we find a discrepancy between the saturation distributions with and without capillary pressure in terms of the calculated oil breakthrough time. As we can see in Fig. 3.1, when capillary pressure is neglected, the oil front takes longer to reach the wellbore during the flowback. This retardation is caused mainly by the difference between the saturation profiles at the beginning of the flowback, caused by the capillarity dispersive effect during injection and falloff (Fig. 3.16). Consequently, the wellbore pressure response is affected during the flowback in the breakthrough "period". The breakthrough period refers to the time interval when the saturation at the sandface changes rapidly. Fig. 3.2 compares the wellbore pressure history obtained from IMEX during an IFPT with and without capillary pressure. During flowback it is observed

a 200 psi discrepancy in the wellbore pressure when capillary pressure effects are neglected, this discrepancy represents 8% of the initial pressure, $p_i = 2500$ psi. The wellbore pressure data measured during this breakthrough period represent those data that are most sensitive to the relative permeability parameters. In addition, it is possible to estimate not only in-situ relative permeability curves but also in-situ capillary pressure curves from these data. The solutions presented assume infinite-acting radial flow from and to a fully-penetrating vertical well.

3.1 Mathematical model

We apply the method of matched asymptotic expansions to solve the one-dimensional saturation convection-dispersion equation, a non-linear pseudo-parabolic partial differential equation. This equation is one of the governing equations for two-phase flow in a porous media when including capillary pressure effects, for the specific initial and boundary conditions arising when injecting water in an infinite radial piecewise homogeneous horizontal medium containing oil and water. The method of matched asymptotic expansions combines inner and outer expansions to construct the global solution. In here, the outer expansion corresponds to the solution of the nonlinear first-order hyperbolic equation obtained when the dispersion effects driven by capillary pressure became negligible. This equation has a monotonic flux function with an inflection point; and its weak solution can be found by applying the method of characteristics. The inner expansion corresponds to the shock layer, which is modeled as a traveling wave obtained by a stretching transformation of the partial differential equation. If the total flow rate becomes equal to zero as in a falloff test, the saturation convection-dispersion equation reduces to a non-linear parabolic equation, which contains only a dispersion (diffusion) term. In this case, we find a closed form solution for the saturation by applying the perturbation theory together with a Green‘s function, treating the non-linearity as a source term. By combining the solution for saturation with the so-called Thompson-Reynolds steady-state theory, one can obtain an approximate analytical solution for the wellbore pressure.

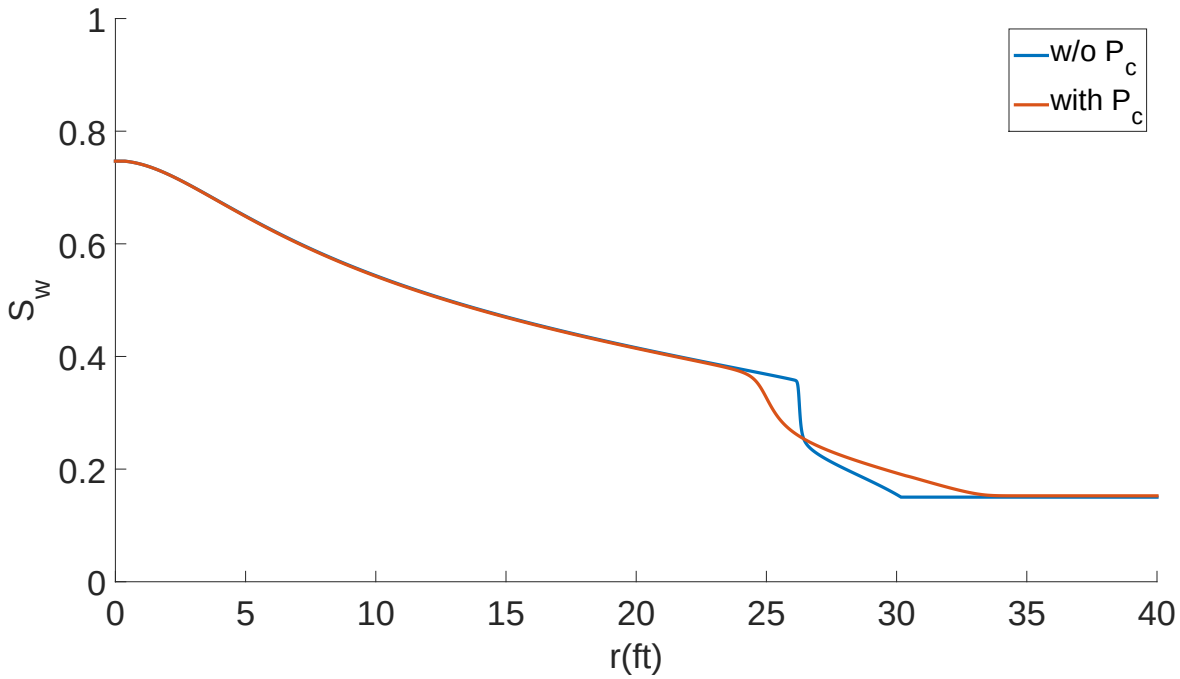

(a)

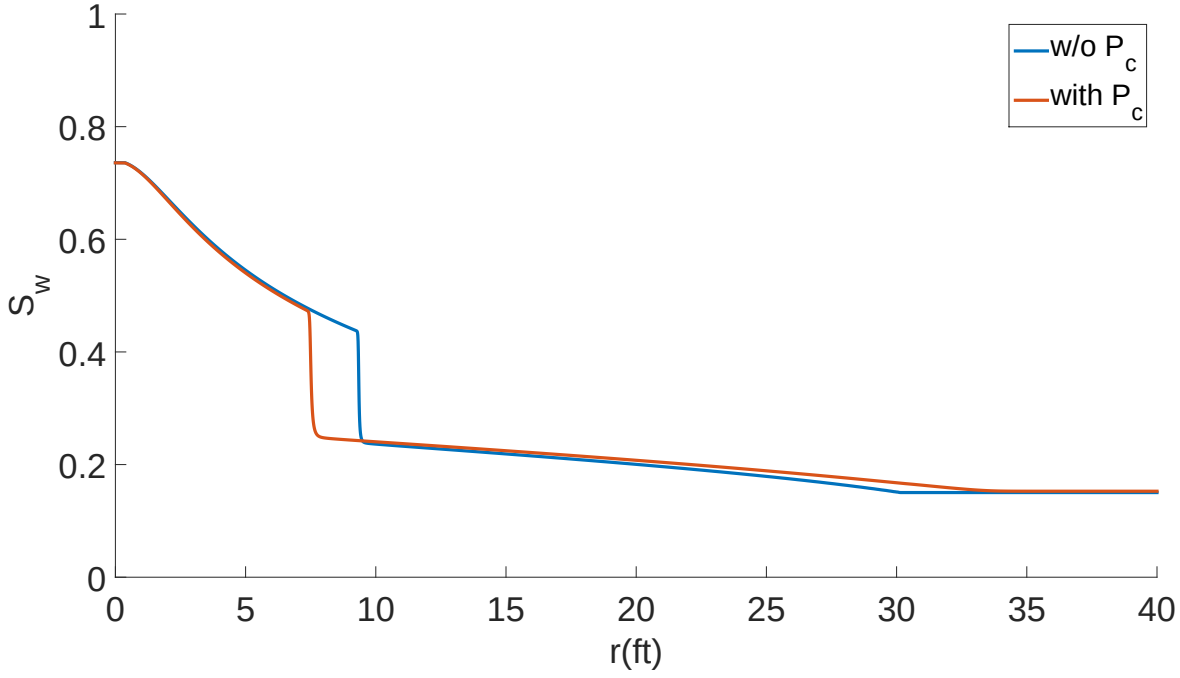

(b)

Figure 3.1: Saturation profile after 3 hours (a) and 12 hours (b) flowing back with and without capillary pressure from IMEX. Note, the saturation profile at the end of the falloff, i.e., the initial condition for the flowback for the cases with and without p_c are distinct. To obtain these profiles we have run a full test (injection-falloff-production) with and without capillarity.

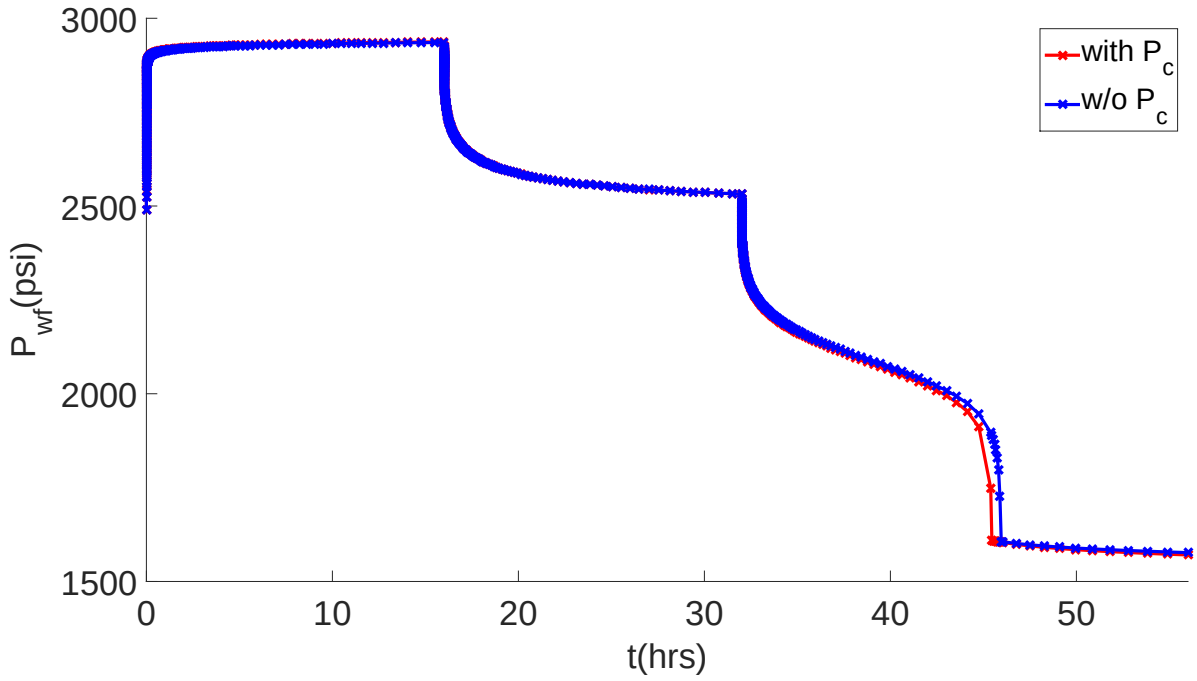

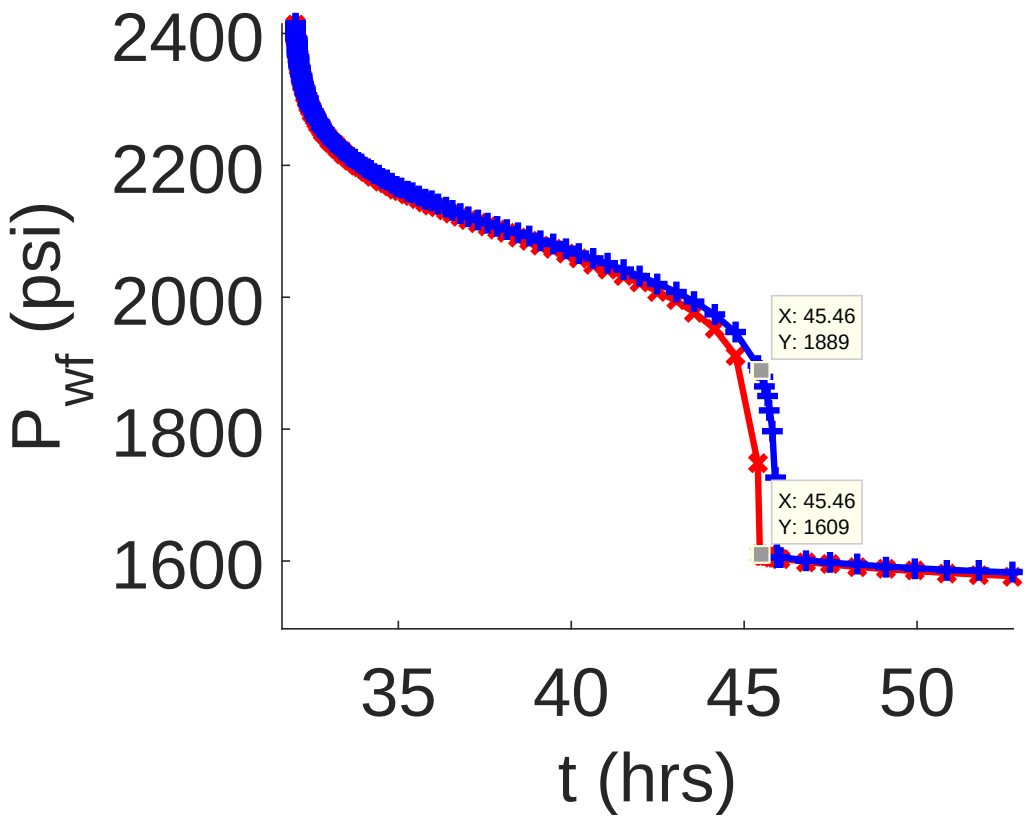

(a) (b)

Figure 3.2: Wellbore pressure history during an IFPT with versus without capillary pressure from IMEX (a) and the zoom in the wellbore pressure history during flowback (b) to show the discrepancy on pressure caused by neglecting capillary pressure effects. X corresponds to time while Y corresponds to pressure. At $X = 45.46$ there is a 200 psi discrepancy in the wellbore pressure when neglecting capillary pressure effects, which represents 8% of the initial pressure, 2500 psi.

3.1.1 Saturation Profile

Once again, let us start by finding the saturation distribution in the reservoir for each test period: injection, falloff and production. The water mass balance equation, in radial coordinates, leads to the following non-linear partial differential equation [21]:

$$\frac{\partial S_w}{\partial t} + \frac{\theta q_t}{2\pi r h \phi}\frac{\partial F_w(S_w)}{\partial r} = 0, \tag{3.1}$$

where throughout we assume porosity, ϕ, is homogeneous. q_t is the total liquid rate in RB/D; θ represents in general a unit conversion factor where in the oil field units used here, $\theta = 5.6146/24$; the reservoir thickness, h, and the radius, r , are in ft; time, t, is in hours. Let us use Darcy's equation in radial coordinates without gravity for the oil flow rate in RB/D is given by

$$q_o = -\frac{k(r)h\lambda_o(S_w)}{\alpha}\left(r\frac{\partial p_o}{\partial r}\right), \tag{3.2}$$

and the water flow rate (RB/D) is

$$q_w = -\frac{k(r)h\lambda_w(S_w)}{\alpha}\left(r\frac{\partial p_w}{\partial r}\right). \tag{3.3}$$

to find the water fractional flow, F_w. For field units used throughout, $\alpha = 141.2$. p_w and p_o are the water and oil phase pressures, respectively. The λ_w and λ_o are the water and oil mobilities, respectively, given by the ratio of the water/oil permeability (k_{rw} and k_{ro}), which are functions of the water saturation by the water/oil viscosity, μ_w and μ_o. We can subtract Eq. 3.3 from Eq. 3.2, to get

$$\frac{\alpha q_o}{k(r)h\lambda_o(S_w)} - \frac{\alpha q_w}{k(r)h\lambda_w(S_w)} = -\left(r\frac{\partial p_o}{\partial r} - r\frac{\partial p_w}{\partial r}\right). \tag{3.4}$$

Rearranging Eq. 3.4 and substitution the capillary pressure p_c given by the difference of the

oil pressure (p_o) and the water pressure (p_w), leads to

$$q_o - \frac{q_w \lambda_o(S_w)}{\lambda_w(S_w)} = -\frac{k(r)h\lambda_o}{\alpha}\left(r\frac{\partial p_c(S_w)}{\partial r}\right). \tag{3.5}$$

We assume throughout that water is the wetting phase. Dividing Eq. 3.5 by the total flow rate, q_t, yields

$$F_o - \frac{F_w \lambda_o(S_w)}{\lambda_w(S_w)} = -\frac{k(r)h\lambda_o(S_w)}{\alpha q_t}\left(r\frac{\partial p_c(S_w)}{\partial r}\right), \tag{3.6}$$

where F_o and F_w are the oil and water fractional flow given by $\frac{q_o}{q_t}$ and $\frac{q_w}{q_t}$, respectively. Finally, substituting $F_o = 1 - F_w$ in Eq. 3.6 and solving for F_w, we have the following expression for the water fractional flow including capillary pressure effects,

$$\begin{aligned} F_w(S_w) &= \frac{1 + \frac{k(r)h\lambda_o(S_w)}{\alpha q_t}\left(r\frac{\partial p_c}{\partial r}\right)}{1 + \frac{\lambda_o(S_w)}{\lambda_w(S_w)}} \\ &= \frac{1}{1 + \frac{\lambda_o(S_w)}{\lambda_w(S_w)}} + \frac{\frac{k(r)hk_{ro}}{\alpha q_t \mu_o}\left(r\frac{\partial p_c}{\partial r}\right)}{1 + \frac{\lambda_o(S_w)}{\lambda_w(S_w)}} \\ &= f_w + \epsilon r k(r) f_w(S_w) k_{ro}(S_w)\frac{\partial p_c(S_w)}{\partial r}, \end{aligned} \tag{3.7}$$

where f_w is the water mobility ratio (Fig. 2.1), i.e., the ratio of water mobility and the total mobility (λ_t), given by

$$f_w(S_w) = \frac{1}{1 + \frac{\lambda_o(S_w)}{\lambda_w(S_w)}} = \frac{\lambda_w(S_w)}{\lambda_o(S_w) + \lambda_w(S_w)}\frac{\lambda_w(S_w)}{\lambda_o(S_w) + \lambda_w(S_w)}, \tag{3.8}$$

which usually assumes a S-shape. ϵ is the perturbation parameter, defined by

$$\epsilon = \frac{h}{\alpha q_t \mu_o} \quad \left[\frac{T^2}{ML}\right] \tag{3.9}$$

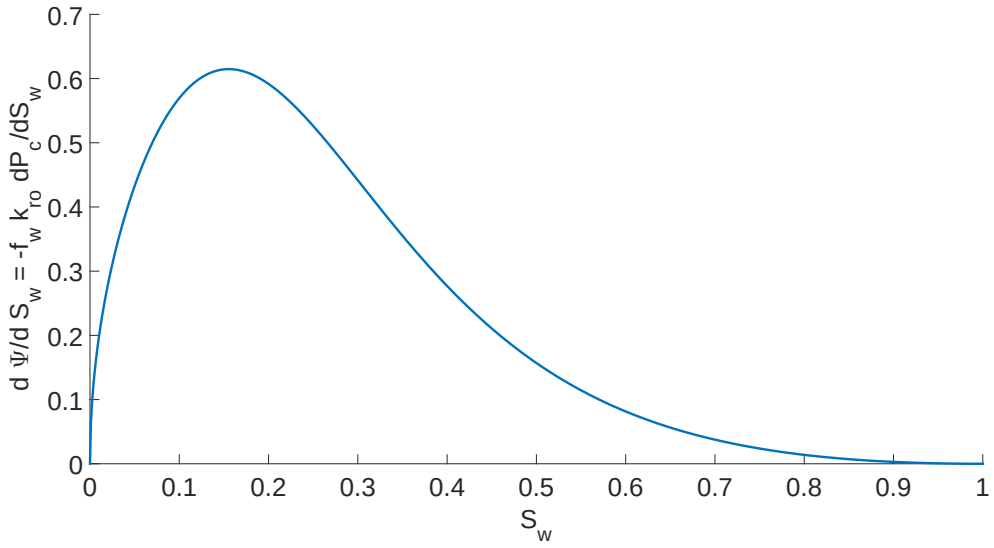

Figure 3.3: $\frac{d\Psi}{dS_w}$ versus water saturation.

and the permeability is a function of radius because we consider a skin damaged zone,

$$k(r) = \begin{cases} k_{\mathrm{s}}, & r_w \leq r < r_{\mathrm{skin}} \\ k, & r \geq r_{\mathrm{skin}}, \end{cases} \tag{3.10}$$

where r_w is the wellbore radius, r_{skin} is the radius of the damaged zone and k_{s} is the permeability in the skin zone. Grouping all the parameters the are function of water saturation, we can define (Fig. 3.3),

$$\frac{d\Psi}{dS_w}(S_w) = -f_w(S_w)k_{ro}(S_w)\frac{dp_c}{dS_w}(S_w), \tag{3.11}$$

and rewrite Eq. 3.12 as,

$$F_w(S_w) = f_w(S_w) - \epsilon r k(r)\frac{d\Psi(S_w)}{dS_w}\frac{\partial S_w}{\partial r}. \tag{3.12}$$

For simplicity, we use the Brooks and Corey model [20] given by,

$$p_c(S_w) = p_t\left(\frac{S_w - S_{iw}}{1 - S_{iw} - S_{or}}\right)^{-\frac{1}{\lambda}}, \tag{3.13}$$

to represent capillary pressure. Here S_{wi} is the immobile water saturation and S_{or} is the residual oil saturation. λ, where $0.4 \leq \lambda \leq 4.0$, is a measure of the pore size distribution (the greater the λ value, the more uniform is the pore size distribution) and p_t, the threshold pressure. The threshold pressure is a measure of the maximum pore size [53], i.e., the minimum capillary pressure at which a continuous nonwetting phase exists in the imbibition case and a continuous wetting phase exists in the drainage case [64]. The greater is the maximum pore size, smaller is the pressure threshold. According to Donaldson et al. [40], the extrapolation of the capillary pressure curve obtained from experimental data to $S_w = 1$ yields the correct threshold value. In practice, we introduce a small variable, sv, to limit the maximum value of p_c to a finite value, i.e., replace Eq. 3.13 by

$$p_c(S_w) = p_t\left(sv + \frac{S_w - S_{wi}}{1 - S_{wi} - S_{or}}\right)^{-\frac{1}{\lambda}}. \tag{3.14}$$

We can relate the relative permeabilities and the capillary pressure through the pore size distribution index, λ, by using the Purcell [85] model for the water phase (wetting phase),

$$k_{rw} = a_w\left(\frac{S_w - S_{iw}}{1 - S_{iw} - S_{or}}\right)^{\frac{2+\lambda}{\lambda}}, \tag{3.15}$$

and the Brooks and Corey [20] model for the oil phase (nonwetting phase) [65],

$$k_{ro} = \left(1 - \frac{S_w - S_{iw}}{1 - S_{iw} - S_{or}}\right)^2\left[1 - \left(\frac{S_w - S_{iw}}{1 - S_{iw} - S_{or}}\right)^{\frac{2+\lambda}{\lambda}}\right]. \tag{3.16}$$

The capillary pressure derivative is given by

$$\frac{dp_c(S_w)}{dS_w} = -\frac{1}{\lambda}p_t\left(sv + \frac{S_w - S_{wi}}{1 - S_{wi}}\right)^{-\frac{1}{\lambda}-1} = -\frac{p_c}{\lambda}\left(sv + \frac{S_w - S_{wi}}{1 - S_{wi} - S_{or}}\right)^{-1}, \tag{3.17}$$

and the second derivative is

$$\begin{aligned}\frac{d^2p_c(S_w)}{dS_w^2} &= \frac{1}{\lambda}\left(\frac{1}{\lambda}+1\right)p_t\left(sv+\frac{S_w-S_{wi}}{1-S_{wi}-S_{or}}\right)^{-\frac{1}{\lambda}-2} \\ &= -\frac{dp_c}{dS_w}\left(\frac{1}{\lambda}+1\right)\left(sv+\frac{S_w-S_{wi}}{1-S_{wi}-S_{or}}\right)^{-1} \\ &= p_c\left(\frac{1+\lambda}{\lambda^2}\right)\left(sv+\frac{S_w-S_{wi}}{1-S_{wi}-S_{or}}\right)^{-2}. \end{aligned} \tag{3.18}$$

Now that we have defined the fractional flow rate and its parameters, let us go back to our governing equation for saturation, Eq. 3.1. Inserting Eq. 3.12 into Eq. 3.1 leads to the Rapoport and Leas [86] equation,

$$\frac{\partial S_w}{\partial t}+\frac{\theta q_t}{2\pi rh\phi}\frac{\partial f_w}{\partial r}-\epsilon\frac{\theta q_t}{2\pi rh\phi}\frac{\partial}{\partial r}\left(rk(r)\frac{\partial \Psi}{\partial r}\right)=0. \tag{3.19}$$

For simplicity we can define

$$C=\frac{\theta q_t}{\pi h\phi} \tag{3.20}$$

and rewrite Eq. 3.19 as

$$\frac{\partial S_w}{\partial t}+\frac{C}{2r}\frac{\partial f_w}{\partial r}-\epsilon\frac{C}{2r}\frac{\partial}{\partial r}\left(rk(r)\frac{\partial \Psi}{\partial r}\right)=0, \tag{3.21}$$

which is the non-linear "pseudo-parabolic" governing equation for saturation.

Injection: Although the wellbore pressure during injection seems to be insensitive to capillarity effects (as can be seen in Fig. 3.2), i.e., insensitive to the accuracy of the calculated saturation distribution in the reservoir, knowledge of the correct saturation profile at the end of injection represents the initial condition for the falloff period (Fig. 3.4), and hence is required to calculate the saturation distribution during falloff. Let us start by inserting same common values for the parameters in Eq. 3.9 to have an idea of its order of magnitude,

$$\mathcal{O}(\epsilon)=\mathcal{O}\left(\frac{h}{\alpha q_t\mu_o}\right)\sim\mathcal{O}\left(\frac{10^1}{141.2\times10^3\times10^0}\right)\sim\mathcal{O}(10^{-5})<<1, \tag{3.22}$$

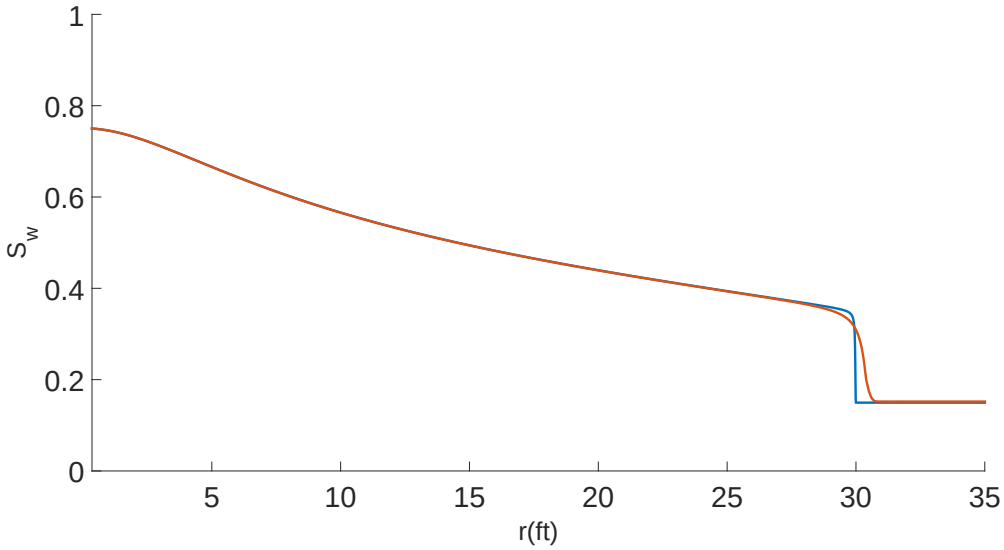

Figure 3.4: Saturation profile at the end of the injection period with (orange solid curve)and without capillary pressure (blue solid curve) from IMEX.

where we use $h \approx 10^1$, $q_t \approx 10^3$ and $\mu_o \approx 10^0$. We can see that epsilon is a very small number. By looking in approximate order of magnitude of each term in Eq. 3.21, we have

$$\mathcal{O}\left(\frac{\partial S_w}{\partial t}\right) \sim \mathcal{O}\left(\frac{\Delta S_w}{\Delta t}\right) \sim \mathcal{O}\left(\frac{10^0}{10^1}\right) \sim \mathcal{O}(10^{-1}), \tag{3.23}$$

$$\mathcal{O}(C) \sim \mathcal{O}\left(\frac{\theta q_t}{\pi h \phi}\right) \sim \mathcal{O}\left(\frac{\frac{5.6146}{24} \times 10^3}{3.14159 \times 10^1 \times 10^{-1}}\right) \sim \mathcal{O}(10^1), \tag{3.24}$$

$$\mathcal{O}\left(\frac{C}{2r}\frac{\partial f_w}{\partial r}\right) = \mathcal{O}\left(C\frac{\partial f_w}{\partial (r^2)}\right) \sim \mathcal{O}\left(C\frac{\Delta f_w}{\Delta (r^2)}\right) \sim \mathcal{O}\left(10^1 \times 10^1 \times \frac{10^0}{10^3}\right) \sim \mathcal{O}(10^{-1}) \tag{3.25}$$

and

$$\begin{aligned}\mathcal{O}\left(\epsilon\frac{C}{2r}\frac{\partial}{\partial r}\left(rk\frac{\partial\Psi}{\partial r}\right)\right) &\sim \mathcal{O}\left(\epsilon Ck\left(\frac{1}{2}\frac{\partial^2\Psi}{\partial r^2}+\frac{\partial\Psi}{\partial(r^2)}\right)\right)\\ &\sim \mathcal{O}\left(10^{-5}\times 10^{1}\times 10^{2}\left(\frac{1}{2}\frac{\Delta\Psi}{\Delta r^2}+\frac{\Delta\Psi}{\Delta r^2}\right)\right)\\ &\sim \mathcal{O}\left(10^{-5}\times 10^{1}\times 10^{2}\left(\frac{1}{2}\frac{10^{-1}}{10^{3}}+\frac{10^{-1}}{10^{3}}\right)\right)\\ &\sim \mathcal{O}(10^{-6}),\end{aligned} \tag{3.26}$$

where we use $k \approx 10^2 \approx$ constant and time is in the order of hours. We can see that last term, Eq. 3.26 is far smaller than the others (Eqs. 3.23 and 3.25). This suggests that the effect of the third term in Eq. 3.21 may be treated as a perturbation to the first-order hyperbolic equation [21], given by

$$\frac{\partial S_w}{\partial t}+\frac{C}{2r}\frac{\partial f_w}{\partial r}=0, \tag{3.27}$$

where f_w, the the ratio of the water mobility over total mobility, is considered to be a S-shaped function - a monotonically increasing function with a single inflection point - along this chapter. During injection, for a partially water wet reservoir, the capillary pressure dispersive effect will be non-negligible only in a small region around the water front (hypodispersion phenomenon) [6, 73] where the capillary pressure derivative and the saturation gradient are significant (Fig. 3.5.). The capillary pressure smears the water front during injection balancing the self-sharpening tendency of the shock. Yortsos and Fokas [105] have developed an exact analytical solution for linear waterflood including the effects of capillary pressure, but their solution is limited to a particular functional form to represent relative permeabilities and capillary pressure curves and does not consider radial flow, which makes their solution very restrictive. As done by Barenblatt et al. [8], Bedrikovetsky et al. [10] for Cartesian coordinates and by Deng and King [38] for streamlines and streamtubes, the perturbation caused by the capillary pressure effects can be modeled as a shock layer (water front) which moves with the same speed as the shock wave. By applying the method of matched asymptotic expansions [101, 52], Machado and Reynolds [68] combined the solu-

tion of the Buckley-Leverett equation (Eq. 3.27) with this steady travelling wave to generate an approximate solution of the Rappaport and Leas equation, i.e., the solution of the convection-dispersion saturation equation. To solve the Rapoport and Leas [86] equation for the injection period, with the following initial,

$$S_w(r,0) = S_{iw} \tag{3.28}$$

and boundary conditions,

$$F_w(S_w(r_w,t)) = f_w(S_w(r_w,t)) - \epsilon r_w k(r_w)\frac{d\Psi(S_w(r_w,t))}{dS_w}\frac{\partial S_w(r_w,t)}{\partial r} = 1 \tag{3.29}$$

and

$$\lim_{r\to\infty} S_w(r,t) = S_{iw}, \tag{3.30}$$

we divide the domain into two regions, outer and inner regions (Fig. 3.6), where the inner region, the region around the water front, is modeled as a shock layer which propagates with the same speed as the shock that would be obtained when $\epsilon \to 0$, i.e., when the capillary pressure effects are null. The combination of the self-sharping tendency of the shock ($S_{wf} > S_{iw}$) with the dispersive effect from the capillary pressure balance against each other leading to the shock layer [87]. King and Dunayevsky [57] presented the idea of using the method of matched asymptotic equations to solve the Rapoport-Leas equation while Bedrikovetsky et al. [10], Hussain et al. [54], Deng and King [38] showed how the mass balance could be used to present a closed solution for the saturation distribution. Hussain et al. [54] derived an approximate solution for the Rapoport and Leas [86] in Cartesian coordinates for both water and oil injection into a core considering end effects by also applying the method of matched asymptotic expansions. The method of asymptotic expansions uses the inner and outer saturation solutions combined with a matching function to obtain a composite solution which avoids abruptly switching from the outer to the inner solution or vice-versa. The inner and outer solutions are each capable of representing the real solution in two distinct

$$F_w = f_w + \epsilon r k f_w k_{ro} \boxed{\frac{dP_c}{dS_w}\frac{\partial S_w}{\partial r}}$$

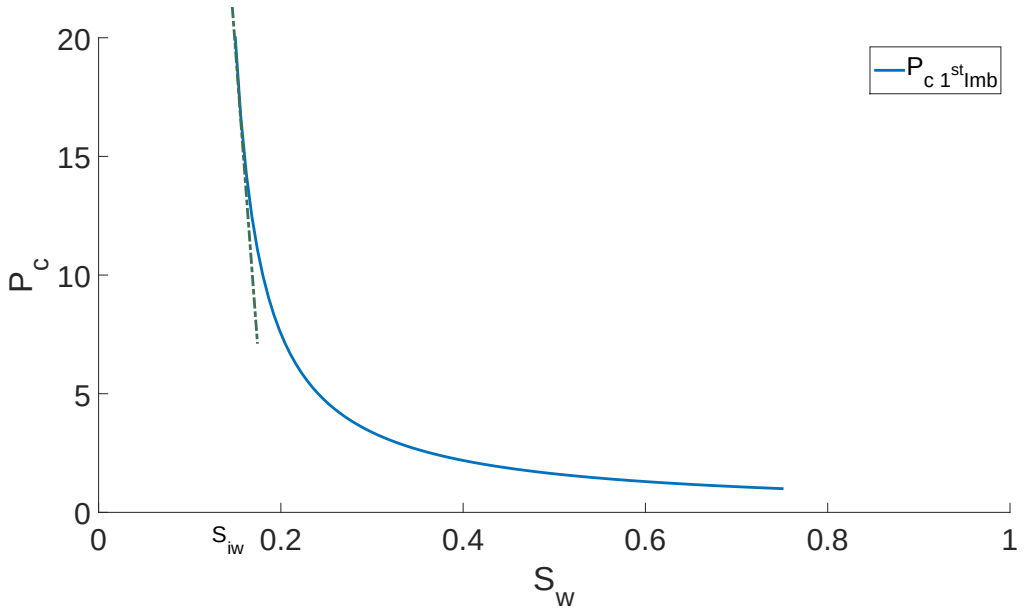

(a)

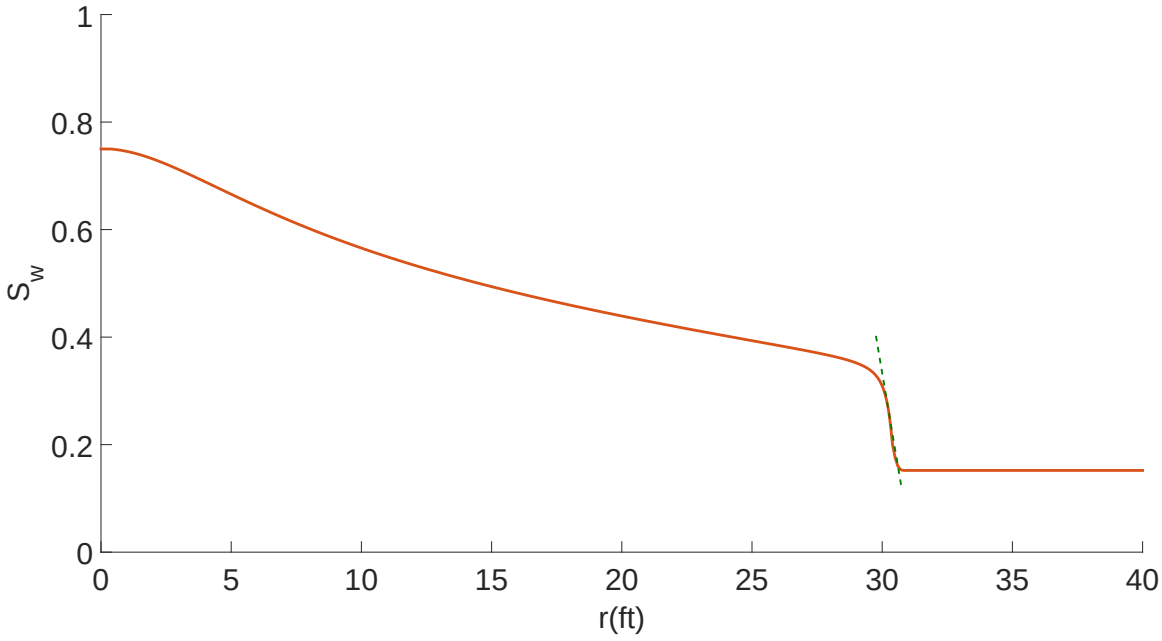

(b)

Figure 3.5: Capillary pressure curve (a) and saturation profile at the some time t during water injection (b). The dashed green lines represent the capillary pressure derivative (a) and the saturation gradient (b) at the water front.

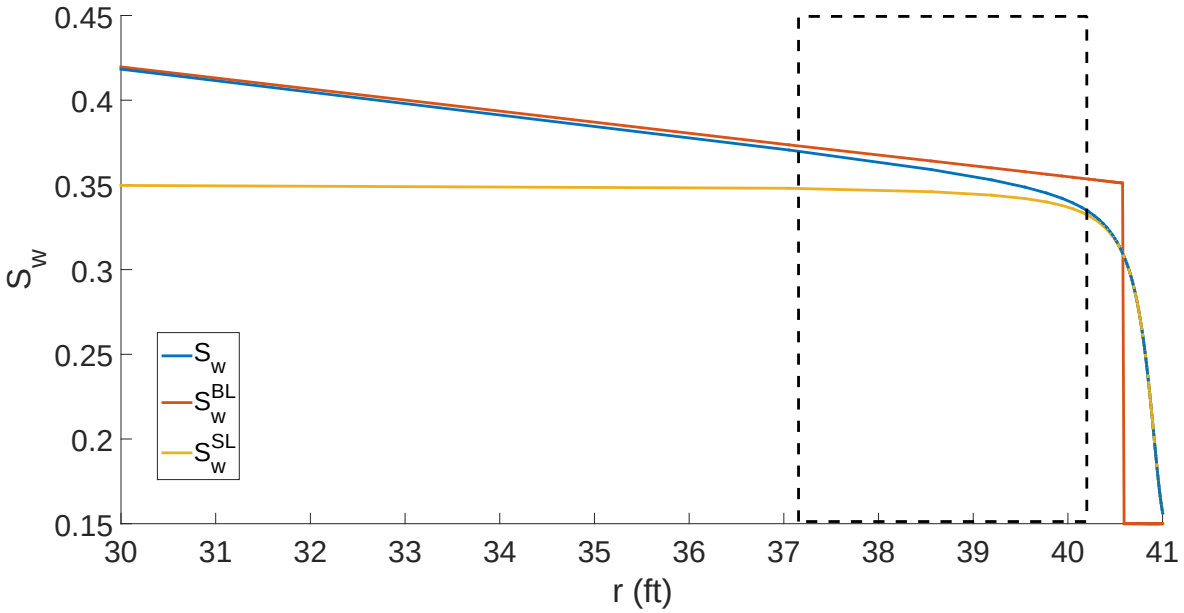

Figure 3.6: Saturation distribution in the reservoir (S_w) compared with the outer solution (S_w^{BL}) and the inner solution (S_w^{SL}). The dashed square show the saturation transition zone between the outer and the inner solution where none of these two solution are capable of approximate the true solution, S_w.

regions - the"inner region" and the "outer region" of the boundary layer (Fig. 3.6). Similarly, we approximate the saturation solution of Rapoport-Leas equation by forming a composite solution given by the combination of three saturations: S_w^{BL}, the solution obtained when the capillary pressure effects are neglected; S_w^{SL}, the saturation distribution in the shock layer obtained by magnifying the dispersion effects in the saturation governing equation; S_w^{SH}, the shock wave represented by a Heaviside function,

$$S_w(r,t) \simeq S_w^{BL}(r,t) + S_w^{SL}(r,t) - S_w^{SH}(r,t), \tag{3.31}$$

where BL stands for Buckley-Leverett, SL for Shock Layer and SH for Shock function.

Outer Solution, S_w^{BL} The outer solution, S_w^{BL}, is obtained by letting $\epsilon \to 0$ in Eq. 3.21,

$$S_w^{BL}(r,t) = \lim_{\epsilon \to 0,\ (r,t) \text{ fixed}} S_w(r,t,\epsilon). \tag{3.32}$$

That is the non-linear hyperbolic equation convection equation known as the Buckley-Leverett saturation equation which is obtained when capillary and gravity effects are neglected. Letting $\epsilon \to 0$ in Eq. 3.29, $F_w(S_w^{BL}(r_w,t)) = f_w(S_w^{BL}(r_w,t)) = 1$, which implies that we must have $S_w^{BL}(r_w,t) = 1 - S_{or}$. The well known unique admissible weak solution of this Riemann problem,

$$\begin{cases} \frac{\partial S_w^{BL}}{\partial t} + \frac{\theta q}{\phi 2\pi r h}\frac{\partial f_w(S_w^{BL})}{\partial r} = 0, & \\ S_w^{BL}(r_w,t) = 1 - S_{or}, & t > 0, \\ S_w^{BL}(r,0) = S_{iw}, & r_w \leq r \leq \infty, \end{cases} \tag{3.33}$$

can be obtained by the application of the Method of Characteristics and is given by [21]

$$S_w^{BL}(r,t) = \begin{cases} 1 - S_{or}, & r^2 \leqslant r_w^2 \\ \left(\frac{df_w}{dS_w}\right)^{-1}\left(\frac{\phi\pi h}{\theta q_t}\frac{(r^2 - r_w^2)}{t}\right), & r_w^2 < r^2 \leqslant r_w^2 + Dt \\ S_{iw}, & r^2 > Dt + r_w^2, \end{cases} \tag{3.34}$$

i.e., by a family of rarefaction waves, semi-shock wave and a constant saturation zone where water is immobile. The shock jump seen in the solution is caused by the S-shaped form of the fractional flow curve, which leads to a gradient catastrophe, and consequently a shock solution. This semi-shock has constant speed, satisfying the Rankine-Hugoniot condition [58],

$$D = \frac{\theta q_t}{\phi\pi h}\frac{[f_w(S_{wf}) - f_w(S_{iw})]}{[S_{wf} - S_{iw}]}, \tag{3.35}$$

where S_{wf} and S_{iw} are the shock saturations. In this case, to satisfy the conservation of mass, the shock speed should correspond to the slop of a tangent line to the water fractional flow curve, i.e.,

$$\frac{\theta q_t}{\phi\pi h}\frac{f_w(S_{wf}) - f_w(S_{iw})}{S_{wf} - S_{iw}} = \frac{\theta q_t}{\phi\pi h}\frac{df_w(S_{wf})}{dS_w}. \tag{3.36}$$

The details of this solution can be found in Buckley and Leverett [21]. Fig. 3.7 shows the shock jump slope tangent to the fractional flow curve at $S_w = S_{wf}$ and the saturation distribution in the reservoir at a some time t. The rarefaction waves family spans from $1 - S_{or}$

to S_{wf} from r_w to $r = 25$ ft, the water front position, i.e., the shock front position, r_s. Ahead of the water front position, there is immobile water. Fig. 3.8 compares this solution, the outer solution, with the true solution, there is, the convection-dispersion saturation profile. Here; we call the true solution the solution obtained from a numerical simulator.

Inner Solution, S_w^{SL} As mentioned, the inner solution intends to represent the saturation profile in the "inner" region around the water front, which a shock layer (a boundary layer) around the shock traveling with the same speed as the shock itself (Fig. 3.9). To find S_w^{SL}, we magnify the shock layer by using a stretching traveling wave coordinate [23]. Similarly as defined in Hussain et al. [54], Bedrikovetsky et al. [10], Deng and King [38],

$$w = w(r,t) = \frac{r^2 - r_s^2(t)}{\epsilon}, \tag{3.37}$$

where r_s is the shock front position,

$$r_s^2(t) = r_w^2 + \frac{\theta q_t}{\phi \pi h}\frac{df_w(S_{wf})}{dS_w}t = r_w^2 + CDt, \tag{3.38}$$

with C given by Eq. 3.20 and D by Eq. 3.35. w is zero at $r = r_s$ and goes to $\pm\infty$ as $\epsilon \to 0$. w is a moving coordinate traveling with the same speed as the shock which expands the length scale in the vicinity of shock. Note, in this case w is not a space variable but has the following dimension $w[\frac{L^3M}{T^2}]$. We wish to rewrite Eq 3.21 in term of moving coordinates, $(r,t) \to (w,\tau)$, where $\tau = \tau(t) = t$. To do so, we first use the chain rule to find the derivative s as follows

$$\frac{\partial S_w}{\partial t} = \frac{\partial S_w}{\partial \tau}\frac{d\tau}{dt} + \frac{\partial S_w}{\partial w}\frac{\partial w}{\partial t} = \frac{\partial S_w}{\partial \tau} - \frac{CD}{\epsilon}\frac{\partial S_w}{\partial w}, \tag{3.39}$$

$$\frac{\partial S_w}{\partial (r^2)} = \frac{\partial S_w}{\partial w}\frac{\partial w}{\partial (r^2)} = \frac{1}{\epsilon}\frac{\partial S_w}{\partial w} \tag{3.40}$$

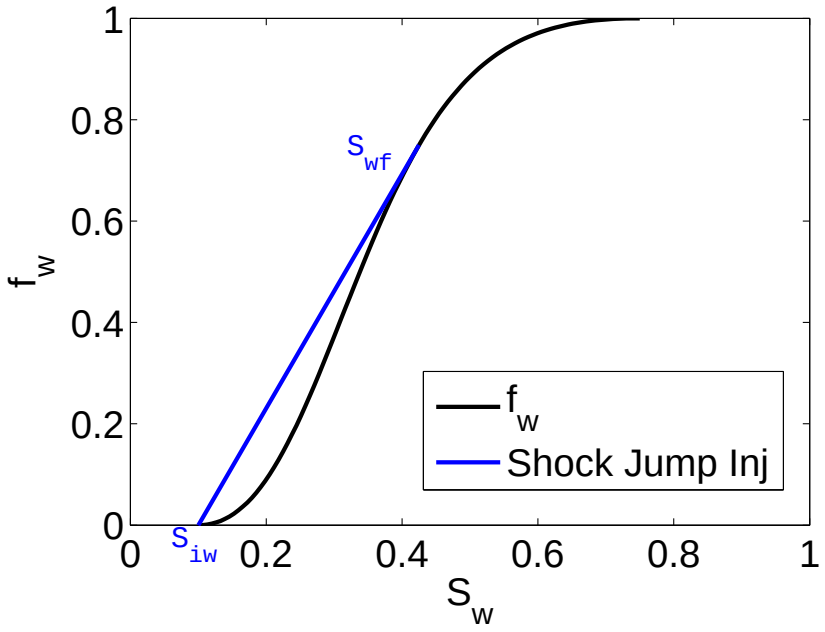

(a)

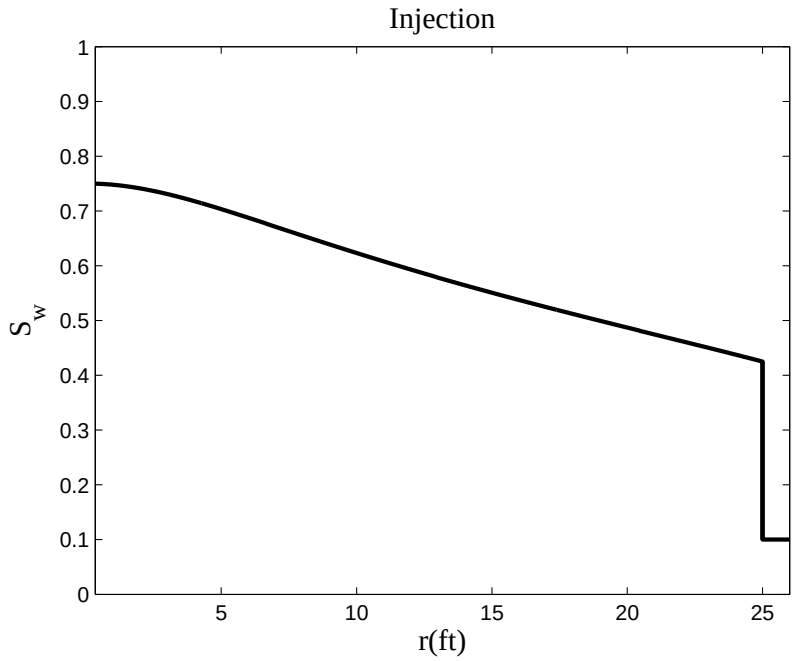

(b)

Figure 3.7: The shock jump slope tangent (blue curve) to the S-shaped fractional flow curve at $S_w = S_{wf}$ (a) and the saturation profile in the reservoir at a some time t (b). The rarefaction waves family spans from $1 - S_{or}$ to S_{wf} from r_w to $r = 25$ ft, the water front position, i.e., the shock front position, $r_{f,nj}$. Ahead of the water front position, there is immobile water.

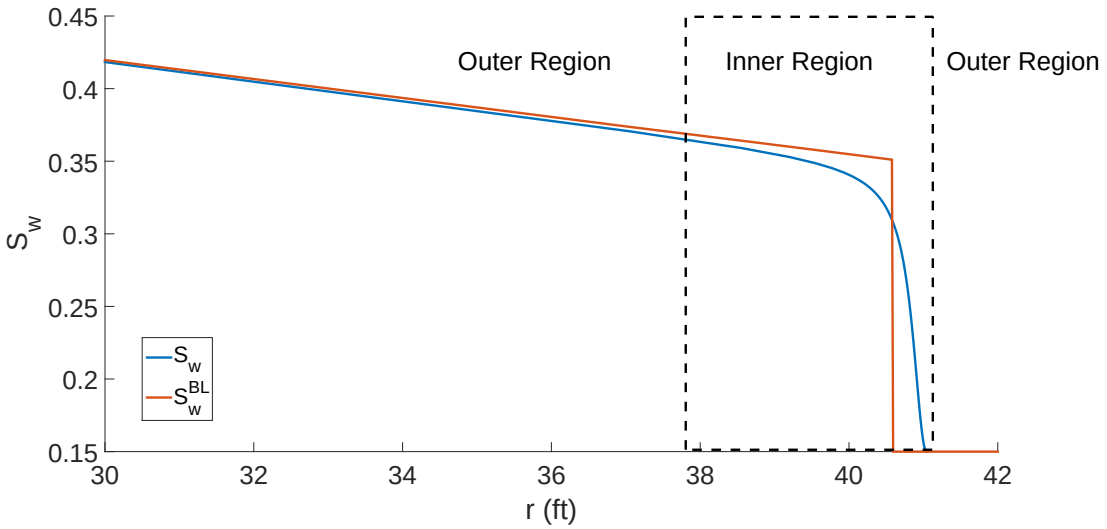

Figure 3.8: Saturation distribution during the injection period for the outer solution (S_w^{BL}), without capillary pressure, and for the true solution (S_w), with capillary pressure. Both profiles agree in the region far from the water front, the region outside the dashed square.

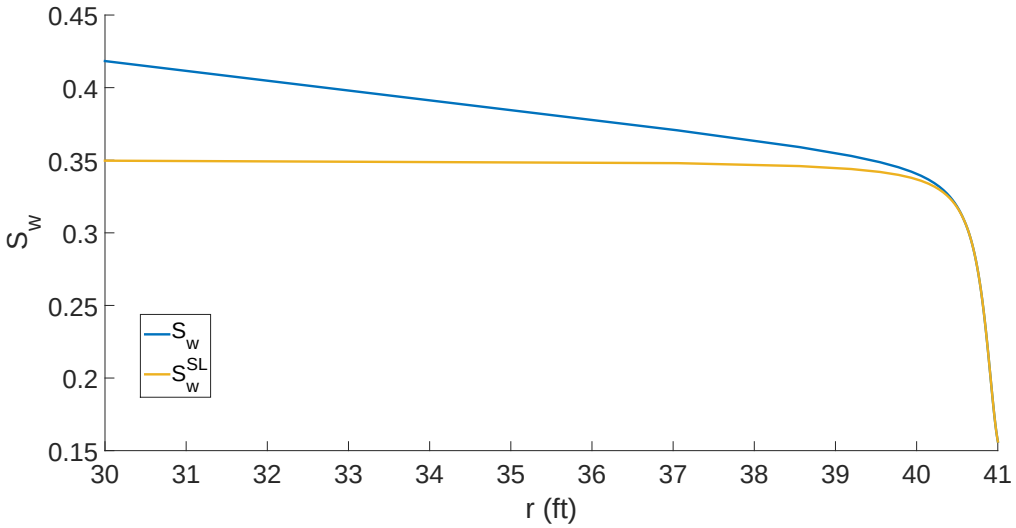

Figure 3.9: Saturation distribution during the injection period for the inner solution (S_w^{SL}), the travelling wave, and for the true solution (S_w), with capillary pressure. Both profiles agree in the region around the water front, i.e., in the shock boundary layer which we have defined as the inner region.

and

$$\frac{1}{2r}\frac{\partial}{\partial r}\left(rk\frac{\partial \Psi}{\partial r}\right) = \frac{1}{2r}\frac{d}{dw}\left(rk\frac{\partial \Psi}{\partial r}\right)\frac{\partial w}{\partial r} = \frac{2r}{\epsilon 2r}\frac{d}{dw}\left(rk\frac{\partial \Psi}{\partial w}\frac{\partial w}{\partial r}\right) = \frac{1}{\epsilon^2}\frac{\partial}{\partial w}\left(2r^2k(w)\frac{\partial \Psi}{\partial w}\right). \tag{3.41}$$

Using Eq. 3.39, Eq. 3.40 and Eq. 3.41, Eq 3.21 can be rewritten as follows

$$\frac{\partial S_w}{\partial \tau} - \frac{CD}{\epsilon}\frac{\partial S_w}{\partial w} + \frac{C}{\epsilon}\frac{\partial f_w}{\partial w} - \frac{C}{\epsilon}\frac{\partial}{\partial w}\left(2r^2k(r)\frac{\partial \Psi}{\partial w}\right) = 0. \tag{3.42}$$

Multiplying Eq. 3.42 by $\frac{\epsilon}{C}$ and using Eq. 3.37, Eq. 3.42 becomes

$$\frac{\epsilon}{C}\frac{\partial S_w}{\partial \tau} - D\frac{\partial S_w}{\partial w} + \frac{\partial f_w}{\partial w} - \frac{\partial}{\partial w}\left[2(\epsilon w + r_s^2(\tau))k(\epsilon w + r_s^2(\tau))\frac{\partial \Psi}{\partial w}\right] = 0. \tag{3.43}$$

The inner solution, S_w^{SL}, is obtained by letting $\epsilon \to 0$ in Eq. 3.43,

$$S_w^{SL}(w,\tau) = \lim_{\epsilon \to 0,(w,\tau)\text{ fixed}} S_w(\epsilon w + r_s^2(\tau), \tau, \epsilon), \tag{3.44}$$

as presented in Nayfeh [72]. Neglecting the terms of order ϵ in Eq. 3.43, yields

$$-D\frac{\partial S_w^{SL}}{\partial w} + \frac{\partial f_w}{\partial w} - \frac{\partial}{\partial w}\left(2r_s^2(\tau)k(r_s^2(\tau))\frac{\partial \Psi}{\partial w}\right) = 0. \tag{3.45}$$

Note that here we are treating the permeability k as function of the shock position radius, r_s, only, by assuming that in the limit of the inner solution, $\epsilon(r \to r_s(\tau))$. Intuitively, this assumption does not seem to be valid when the shock layer is crossing heterogeneities interfaces, i.e., interfaces between two different permeabilities zones. However, for the water injection in a field scale, the skin zone will be crossed by the water front in a very short time and we will only need to use the pseudo-parabolic equation (Eq. 3.21) to find saturation for the end of injection period (to be used as initial condition for falloff and flowback testes, as mentioned in the introduction). Consequently, we can simplify the problem as shown above. Integrating the ordinary differential equation given by Eq. 3.45 with respect to w for any

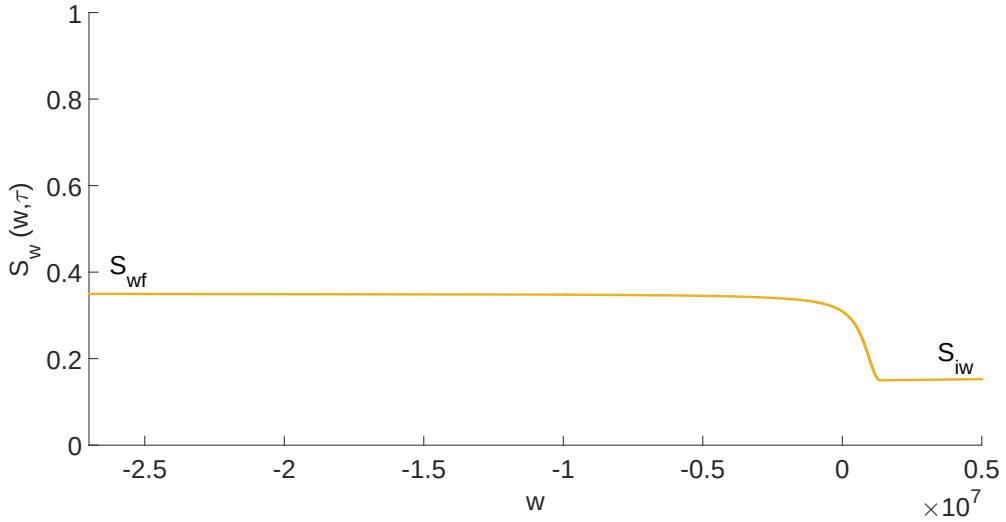

Figure 3.10: Travelling wave saturation distribution (inner solution), S_w^{SL} versus the moving coordinate w. S_w^{SL} goes asymptotically to the shock saturations S_{iw} and S_{wf} as w goes to $\pm\infty$.

fixed time τ and applying the chain rule, gives

$$-DS_w^{SL} + f_w(S_w^{SL}) - 2r_s^2(\tau)k(r_s^2(\tau))\frac{d\Psi(S_w^{SL})}{dS_w}\frac{\partial S_w^{SL}(w,\tau)}{\partial w} = a(\tau), \tag{3.46}$$

where $a(\tau)$ is a constant for the injection case, as we will show later. As mentioned, the inner solution is modeled as a travelling wave with a constant speed - the shock speed - and the boundary conditions (for the inner solution) given by

$$w \to \infty : \; S_w^{SL} = S_{iw}, \quad \frac{\partial S_w^{SL}}{\partial w} = 0 \tag{3.47}$$

and

$$w \to -\infty : \; S_w^{SL} = S_{wf}, \quad \frac{\partial S_w^{SL}}{\partial w} = 0, \tag{3.48}$$

as the inner solution goes asymptotically to the shock saturations (Fig. 3.10). This necessity of this behavior will be clearer very soon when we compare the inner solution with the matching saturation solution. Using the boundary condition given by Eq. 3.47 in Eq. 3.46

leads to,

$$a(\tau) = -DS_{iw}, \tag{3.49}$$

while using the boundary condition given by Eq. 3.48 yields,

$$a(\tau) = -DS_{wf} + f_w(S_{wf}), \tag{3.50}$$

implying

$$-D(S_{iw} - S_{wf}) - f_w(S_{wf}) = 0, \tag{3.51}$$

which it is indeed correct from the definition of D in Eq. 3.35. As we can see from Eq. 3.49 and 3.50, $a(\tau)$ is a constant and it will be called simply by a from now on. Substituting the constant a (Eq. 3.49) in Eq. 3.46 and dividing it by $D(S_{iw} - S_w^{SL}) + f_w(S_w^{SL})$, yields

$$2r_s^2(\tau)k(r_s^2(\tau))\frac{\frac{d\Psi(S_w^{SL})}{dS_w}}{D(S_{iw} - S_w^{SL}) + f_w(S_w^{SL})}\frac{\partial S_w^{SL}(w,\tau)}{\partial w} = 1. \tag{3.52}$$

Integrating Eq. 3.52 from $w_{well} = w(r_w, \tau)$ to any w at any time τ using the separation of variables method, gives us the relationship between any S_w^{SL} and w,

$$2r_s^2 k(r_s^2)\int_{S_w^{SL}(w_{well})}^{S_w^{SL}} \frac{\frac{d\Psi(S_w^{SL})}{dS_w}}{D(S_{iw} - S_w^{SL}) + f_w(S_w^{SL})} dS_w^{SL} = \int_{w_{well}}^{w} dw. \tag{3.53}$$

At $S_w^{SL} = S_{wf}$ and $S_w^{SL} = S_{iw}$, the integral in the left side diverges as the denominator goes to 0. This behavior is consistent with our boundary conditions assumptions for S_w^{SL} (Eqs. 3.47 and 3.48). Note, we still do not know the value of S_w^{SL} at w_{well}. To find a closed form for this problem, mass balance can be used, but first let us present the matching saturation, since this solution will be necessary for the mass balance.

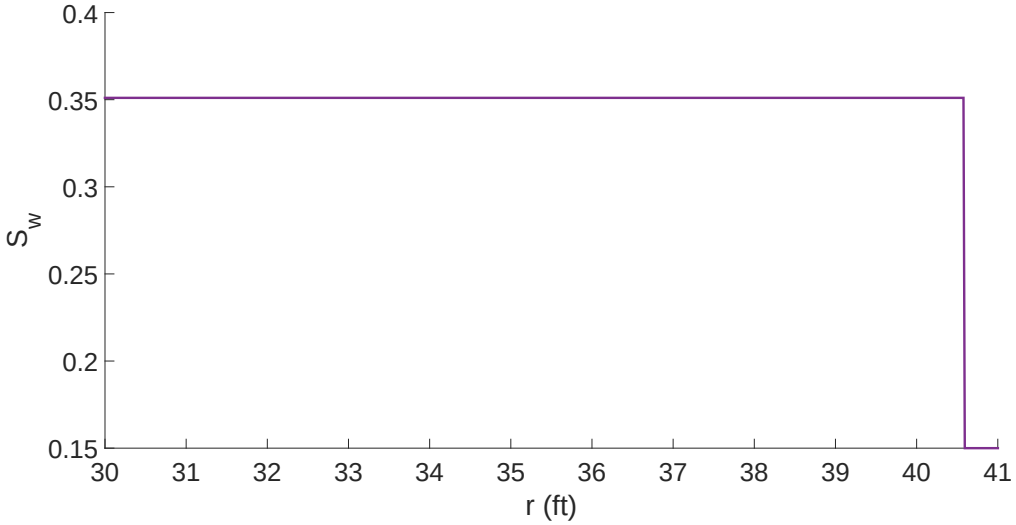

Figure 3.11: Matching saturation (S_w^{SH}) function.

Matching Solution, S_w^{SH} The matching saturation S_w^{SH} is defined using the matching principle by applying Prandtl's technique [72]:

$$\lim_{r^2 \to r_w^2 + CDt} S_w^{BL}(r,t) = \lim_{w \to \pm\infty} S_w^{SL}(w,t). \tag{3.54}$$

and in the injection case is given by,

$$S_w^{SH}(r,t) = \begin{cases} S_{iw}, & r^2 \geq r_s^2(t) = r_w^2 + CDt, \\ S_{wf}, & r_w^2 \leq r_s^2(t). \end{cases} \tag{3.55}$$

which is plotted in Fig. 3.11. Figs. 3.12 and 3.13 compare the matching saturation with the outer and inner solutions, respectively. As we were searching for, S_w^{SH} matches with the region outer solution in the inner region and with the inner solution in the outer solution, being able to subtract their effect in the composite solution in their "non-correspondents" zones.

Figs.3.14 compares the saturation distribution during the injection period for the true solution obtained from the numerical simulator IMEX with the outer solution, inner solution and the matching saturation while Fig. 3.15 shows saturation profile obtained by

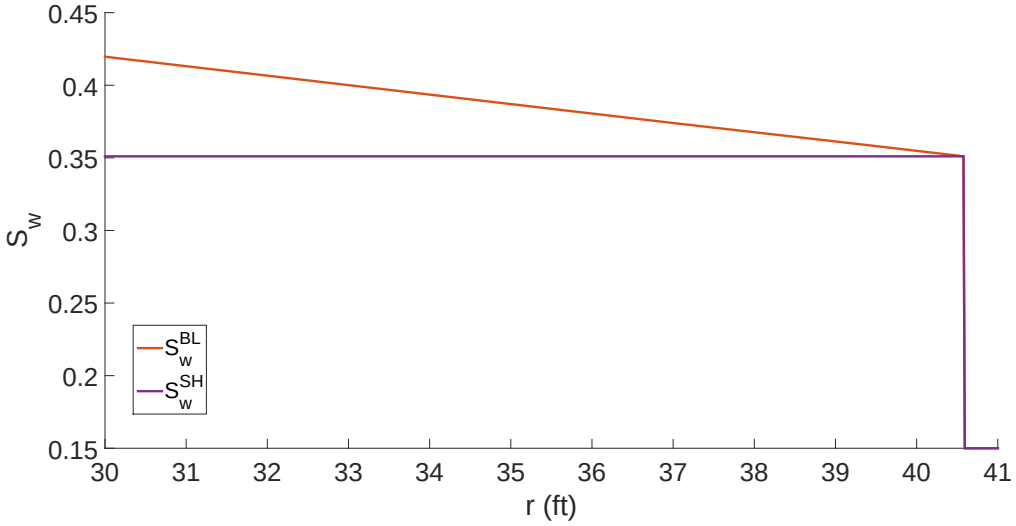

Figure 3.12: Saturation distribution without capillary pressure (outer solution), S_w^{BL}, and the matching saturation function, S_w^{SH}. S_w^{SH} matches with the region outer solution in the inner region, the region around the water front.

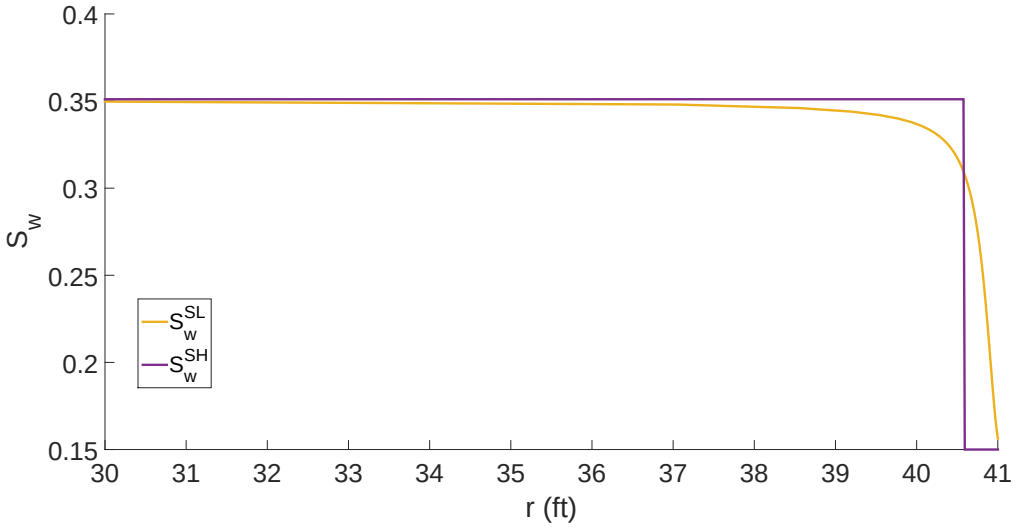

Figure 3.13: Travelling wave saturation distribution (inner solution), S_w^{SL} and the matching saturation function, S_w^{SH}. S_w^{SH} matches with the region inner solution in the outer region, the region far from the water front.

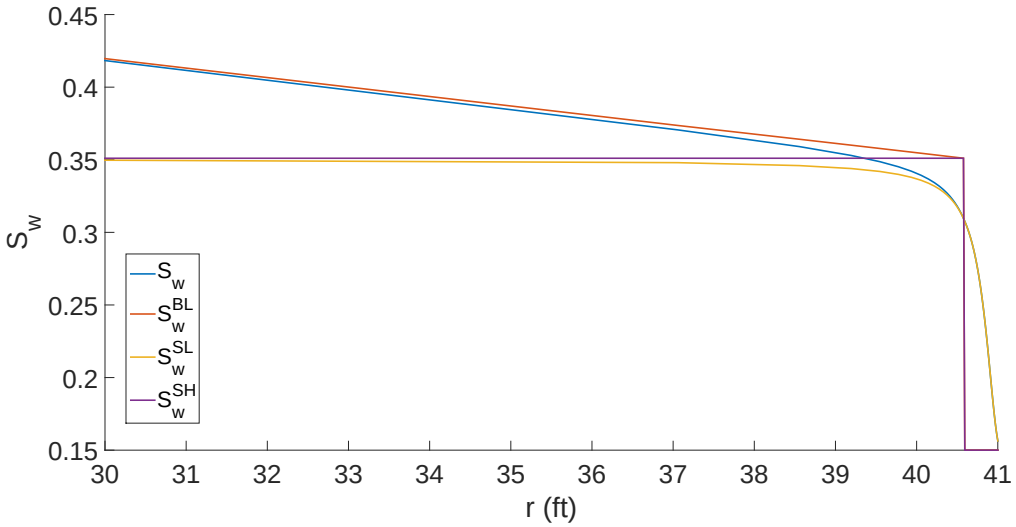

Figure 3.14: Saturation distribution during the injection period with (true solution) and without capillary pressure (outer solution), the travelling wave (inner solution) and the matching saturation.

the combination of the outer, inner and matching saturation (Eq. 3.31).

Material Balance Now that we have defined all the three saturations that composes the approximate solution for the convection-dispersion saturation equation, let us try to find a closed form for the saturation distribution based in the mass balance. Since both the Buckley-Leverett (S_w^{BL}) solution and the composite solution (S_w) must obey material balance, the two following equations must hold:

$$\int_{r_w^2}^{\infty} (S_w(r,t) - S_{iw})\pi hd(r^2) = q_t t \tag{3.56}$$

and

$$\int_{r_w^2}^{\infty} (S_w^{BL}(r,t) - S_{iw})\pi hd(r^2) = q_t t. \tag{3.57}$$

From Eqs. 3.31, 3.56 and 3.192 it follows that

$$\int_{r_w^2}^{\infty} (S_w^{BL} + S_w^{SL} - S_w^{SH} - S_{iw})\pi hd(r^2) = \int_{r_w^2}^{\infty} (S_w^{BL}(r,t) - S_{iw})\pi hd(r^2), \tag{3.58}$$

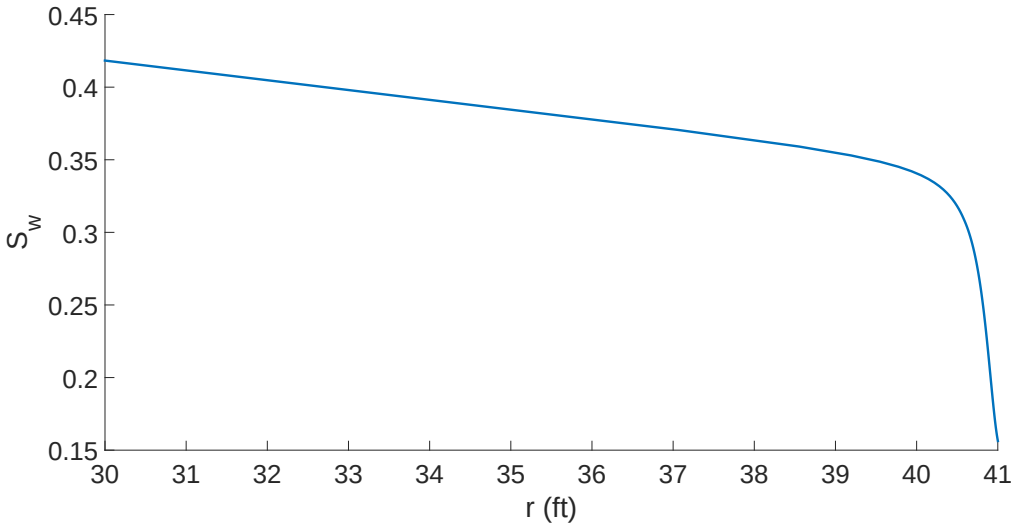

Figure 3.15: Saturation distribution during the injection period with capillary pressure which is composed by the outer, inner and matching saturation.

which, upon simplification gives

$$\int_{r_w^2}^{\infty} (S_w^{SL} - S_w^{SH}) d(r^2) = 0. \tag{3.59}$$

Rearranging Eq. 3.59 using Eq. 3.55 for S_w^{SH} gives

$$\begin{aligned} \int_{r_w^2}^{\infty} S_w^{SL} d(r^2) &= \int_{r_w^2}^{r_s^2} S_{wf} d(r^2) + \int_{r_s^2}^{\infty} S_{iw} d(r^2) \\ &= S_{wf}(r_s^2 - r_w^2) + \left(S_{iw} \int_{r_w^2}^{\infty} d(r^2) - S_{iw} \int_{r_w^2}^{r_s^2} d(r^2) \right). \end{aligned} \tag{3.60}$$

Using Eq. 3.38 in Eq. 3.60, it follows that

$$\int_{r_w^2}^{\infty} S_w^{SL} d(r^2) = (S_{wf} - S_{iw}) CDt + S_{iw} \int_{r_w^2}^{\infty} d(r^2). \tag{3.61}$$

Transforming Eq. 3.61 from $(r, t) \rightarrow (w, \tau)$ and using Eq. 3.37, Eq. 3.61 becomes

$$\epsilon \int_{-\frac{CD\tau}{\epsilon}}^{\infty} S_w^{SL}(w) dw = (S_{wf} - S_{iw}) CD\tau + \epsilon S_{iw} \int_{-\frac{CD\tau}{\epsilon}}^{\infty} dw. \tag{3.62}$$

From Eq. 3.52,

$$dw = 2r_s^2 k(r_s^2) \frac{\frac{d\Psi}{dS_w}}{D(S_{iw} - S_w^{SL}) + f_w} dS_w^{SL}. \tag{3.63}$$

Substituting Eq. 3.63 in Eq. 3.62 gives

$$\epsilon 2r_s^2 k(r_s^2) \int_{S_w^{SL}(-\frac{CD\tau}{\epsilon})}^{S_{iw}} S_w^{SL} \frac{\frac{d\Psi}{dS_w}}{D(S_{iw} - S_w^{SL}) + f_w} dS_w^{SL} = (S_{wf} - S_{iw}) CD\tau + \epsilon S_{iw} \int_{-\frac{CD\tau}{\epsilon}}^{\infty} dw. \tag{3.64}$$

Dividing Eq. 3.64 by ϵS_{iw} and solving the resulting equation for $\int_{-\frac{CD\tau}{\epsilon}}^{\infty} dw$ gives

$$\int_{-\frac{CD\tau}{\epsilon}}^{\infty} dw = \frac{2r_s^2 k(r_s^2)}{S_{iw}} \int_{S_w^{SL}(-\frac{CD\tau}{\epsilon})}^{S_{iw}} S_w^{SL} \frac{\frac{d\Psi}{dS_w}}{D(S_{iw} - S_w^{SL}) + f_w} dS_w^{SL} - \frac{(S_{wf} - S_{iw}) CD\tau}{\epsilon S_{iw}}. \tag{3.65}$$

Setting $S_w = S_{iw}$ in the upper limits of the integrals of Eq. 3.53 and exchanging the two sides of the equation yields,

$$\int_{-\frac{CD\tau}{\epsilon}}^{\infty} dw = 2r_s^2 k(r_s^2) \int_{S_w^{SL}(-\frac{CD\tau}{\epsilon})}^{S_{iw}} \frac{\frac{d\Psi}{dS_w}}{D(S_{iw} - S_w^{SL}) + f_w} dS_w^{SL}. \tag{3.66}$$

As the left sides of Eqs 3.65 and 3.66 are the same, the right sides of these two equations must be equal which gives

$$\begin{aligned} &2r_s^2 k(r_s^2) \int_{S_w^{SL}(-\frac{CD\tau}{\epsilon})}^{S_{iw}} \frac{\frac{d\Psi}{dS_w}}{D(S_{iw} - S_w^{SL}) + f_w} dS_w^{SL} = \\ &\frac{2r_s^2 k(r_s^2)}{S_{iw}} \int_{S_w^{SL}(-\frac{CD\tau}{\epsilon})}^{S_{iw}} S_w^{SL} \frac{\frac{d\Psi}{dS_w}}{D(S_{iw} - S_w^{SL}) + f_w} dS_w^{SL} - \frac{(S_{wf} - S_{iw}) CD\tau}{\epsilon S_{iw}}, \end{aligned} \tag{3.67}$$

Multiplying Eq. 3.67 by ϵS_{iw} and rearranging the resulting equation gives

$$2r_s^2 k(r_s^2) \epsilon \int_{S_w^{SL}(-\frac{CD\tau}{\epsilon})}^{S_{iw}} (S_w^{SL} - S_{iw}) \frac{\frac{d\Psi}{dS_w}}{D(S_{iw} - S_w^{SL}) + f_w} dS_w^{SL} = (S_{wf} - S_{iw}) CD\tau. \tag{3.68}$$

Once the value $S_w^{SL}(-\frac{CD\tau}{\epsilon})$ (i.e., the inner solution saturation in the wellbore, $S_w^{SL}(w_{well})$) is determined numerically by solving Eq. 3.68 using the bisection method [90] at each time τ, Eq. 3.53 is used to determine the saturation profile in the stabilized zone. It is important

to note that, as S_w^{SL} should reach S_{wf} and S_{iw} asymptotically as $w \to \pm\infty$, here we did not have to fix a finite distance in which the traveling wave would reach its open bounds as done by Bedrikovetsky et al. [10], Deng and King [38], Hussain et al. [54]. With our approach, as shown in the Section **Validation** (Fig. 3.26), we can obtain essentially a perfect match with the numerical solution, with a "smother" water front, which is expected from the dispersive effect of capillary pressure, contrary to the sharp transition between the saturation at the water front foot (r_{wf}) - which is the finite position at which water can be considered immobile - and the initial water saturation in the oil zone exhibited by solutions of previous authors.

Note on the Inner Boundary Condition As inner boundary condition during water injection, we assume that the water fractional flow is equal to 1 (Eq. 3.29). To satisfy the inner boundary condition, we allow $S_w(r_w, t)$ to be less than $1 - S_{or}$, which contradicts Chen [28] assumption that $S_w(r_w, t)$ must be equal to $1 - S_{or}$. Since $\frac{\partial S_w(r_w,t)}{\partial r} < 0$ and $\frac{d\Psi(S_w(r_w,t))}{dS_w} > 0$, the second term in the right side of Eq. 3.29,

$$F_w(S_w(r_w,,t)) = 1 = f_w(S_w(r_w,,t)) - \epsilon r_w k(r_w) \frac{d\Psi(S_w(r_w,t))}{dS_w} \frac{\partial S_w(r_w,t)}{\partial r}, \quad \text{(3.29 revisited)}$$

is greater than 0. Considering $f_w(S_w(r_w,,t)) \in [0,1]$ and that $-\epsilon r_w k(r_w) \frac{d\Psi(S_w(r_w,t))}{dS_w} \frac{\partial S_w(r_w,t)}{\partial r}$ can be estimated to be much less than one (vide the order of magnitude analysis presented earlier) outside the inner region, $1 - S_{or}$ is not the only saturation that satisfies Eq 3.29. When $S_w(r_w, t) = 1 - S_{or}$, from our approximate solution given by Eq. 3.31 at (r_w, t),

$$S_w(r_w,t) = 1 - S_{or} = S_w^{BL}(r_w,t) + S_w^{SL}(r_w,t) - S_w^{SH}(r_w,t) = 1 - S_{or} + S_w^{SL}(r_w,t) - S_{wf}, \quad (3.69)$$

we should have $S_w^{SL}(r_w, t) = S_{wf}$, which would not be possible since $S_w^{SL}(r, t) \to S_{wf}$ as $w \to \infty$, i.e., $S_w^{SL}(r_w, t) = S_w(\frac{-CDt}{\epsilon}, t) \neq S_{wf}$ unless when $\epsilon \to 0$ (when capillary pressure effects became negligible). Although it can be argued that $p_c \stackrel{!}{=} 0$ in the wellbore interface (at $r = r_w$) to guarantee pressure continuity, Van Duijn et al. [100] discussed several cases when pressure continuity is neither satisfied nor required. Using a Taylor expansion around

S_w^{BL}, we can approximate the water fractional flow as

$$F_w(S_w) \approx F_w(S_w^{BL} + S_w^{SL} - S_w^{SH}) \approx F_w(S_w^{BL}) + (S_w^{SL} - S_w^{SH})\frac{dF_w(S_w^{BL})}{dS_w}. \tag{3.70}$$

Since $S_w^{BL}(r_w, t) = 1 - S_{or} \implies F_w(S_w^{BL}(r_w, t)) = f_w(1 - S_{or}) = 1$ and $\frac{dF_w(S_w^{BL}(r_w,t))}{dS_w} = \frac{d\Psi(1-S_{or})}{dS_w} = 0$, $F_w(r_w, t) \approx 1$ in 3.70 and our approximation does satisfies Eq. 3.29, even though $S_w^{SL}(r_w, t) \neq S_w^{SH}(r_w, t)$. In our solution, $S_w^{SL}(r_w, t)$ does change with time and is smaller than S_{wf}. Consequently, $S_w(r_w, t) \neq (1 - S_{or})$, but slightly smaller than it and changes with time. Physically, is $S_w(r_w, t)$ indeed constant and equal $1-S_{or}$ during injection?

Falloff: During falloff, the total flow rate is assumed to be zero, leading to a non-linear dispersion equation for saturation [6]. We can treat this non-linearity as a source term, and by using a Green's function together with regular perturbation theory, we are able to develop a closed form approximate solution for the saturation distribution. Similarly to the injection period, during the falloff period, the wellbore pressure response is insensitive to the saturation change in the reservoir, but we need the profile at the end of the falloff to use as the initial condition for the production period.

As mentioned above, during falloff the convection term will be assumed to be negligible, since it is only not null in the multiphase zone for very early time period. As $q_t \to 0$, Eq. 3.19 becomes,

$$\frac{\partial S_w}{\partial t} - \frac{\theta}{2\pi\alpha r\phi\mu_o}\frac{\partial}{\partial r}\left(rk(r)\frac{\partial \Psi}{\partial r}\right) = 0. \tag{3.71}$$

Defining

$$\eta^0 = \frac{\theta}{2\pi\alpha\phi\mu_o}, \tag{3.72}$$

we can write in Eq. 3.71, as the following non-linear dispersion equation:

$$\frac{1}{r}\frac{\partial}{\partial r}\left(rk(r)\frac{d\Psi}{dS_w}\frac{\partial S_w}{\partial r}\right) = \frac{1}{\eta^0}\frac{\partial S_w}{\partial t}, \tag{3.73}$$

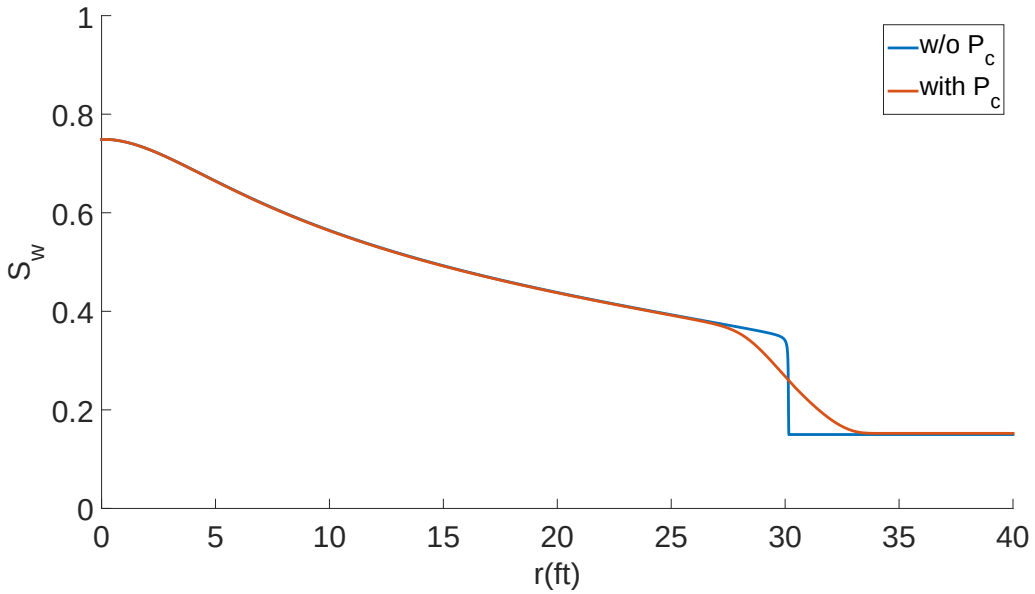

Figure 3.16: Saturation profile at the end of the falloff period with and without capillary pressure from IMEX.

with the following auxiliary conditions:

$$\begin{cases} S_w(r,0) = S_w(r,t_{inj}), & r_w \leq r \leq \infty, \\ S_w(r,t) = S_w(r,t_{inj}), & r_w \leq r \leq r_{skin}, \\ \lim_{r\to\infty} S_w = S_{iw}, & t \geq 0 \end{cases} \tag{3.74}$$

Note, the second condition of Eq. 3.74 assumes that the saturation dispersion will occur mainly in the area around the water front, and thus not affect the skin zone, which is true if the falloff period is sufficiently short, as we can see in Fig. 3.16. Analogous to the Al-Hussainy et al. [3] pseudo-pressure representation, we can define a pseudo-saturation [41, 36] by

$$m(S_w) = \int_{S_{iw}}^{S_w} \frac{d\Psi}{dS_w} dS_w \tag{3.75}$$

and then rewrite Eq. 3.73 in term of pseudo-saturation. Using the chain rule, to find

$$\frac{\partial m(S_w)}{\partial t} = \frac{d\Psi}{dS_w}\frac{\partial S_w}{\partial t} \tag{3.76}$$

and

$$\frac{\partial m(S_w)}{\partial r} = \frac{d\Psi}{dS_w}\frac{\partial S_w}{\partial r}. \tag{3.77}$$

Using Eqs. 3.76 and 3.77 in Eq. 3.73 gives

$$\frac{1}{r}\frac{\partial}{\partial r}\left(rk\frac{\partial m(S_w)}{\partial r}\right) = \frac{1}{\frac{d\Psi(S_w)}{dS_w}\eta^0}\frac{\partial m(S_w)}{\partial t}. \tag{3.78}$$

If we perform the integration in Eq. 3.75, we get

$$m(S_w) = \int_{S_{iw}}^{S_w}\frac{d\Psi}{dS_w}dS_w = \int_{\Psi(S_{iw})}^{\Psi(S_w)} d\Psi = \Psi(S_w) - \Psi(S_{iw}) \tag{3.79}$$

which means we can rewrite Eq. 3.78 as

$$\frac{1}{r}\frac{\partial}{\partial r}\left(rk\frac{\partial \Psi(S_w)}{\partial r}\right) = \frac{1}{\eta^0 H(S_w)}\frac{\partial \Psi(S_w)}{\partial t}, \tag{3.80}$$

where

$$H(S_w) = \frac{d\Psi(S_w)}{dS_w} \tag{3.81}$$

and the auxiliary conditions given by Eq. 3.74 as

$$\begin{cases} \Psi(r,0) = \Psi(S_w(r,t_{inj})) = f(r), & r_w \le r \le \infty, \\ \Psi(r,t) = f(r), & r_w \le r \le r_{skin} \text{ and } t \ge 0, \\ \lim_{r\to\infty}\Psi(r,t) = \Psi(S_{iw}), & t \ge 0. \end{cases} \tag{3.82}$$

Because of the second condition of Eq. 3.82, we only need to find the updated saturation profile at each time only from r_{skin} to ∞ , where $k(r) = k$. Let us define

$$\eta = k\eta_0 \tag{3.83}$$

and rewrite Eq. 3.80 as

$$\frac{1}{r}\frac{\partial}{\partial r}\left(r\frac{\partial \Psi(S_w)}{\partial r}\right) = \frac{1}{\eta H(S_w)}\frac{\partial \Psi(S_w)}{\partial t} \tag{3.84}$$

and modify Eq. 3.82 to obtain

$$\begin{cases} \Psi(r,0) = \Psi(S_w(r,t_{inj})) = f(r) & r_{skin} \le r \le \infty, \\ \Psi(r_{skin},t) = \Psi(S_w(r_{skin},0)) = f(r_{skin}), & t \ge 0, \\ \lim_{r\to\infty} \Psi(r,t) = \Psi(S_{iw}), & t \ge 0. \end{cases} \tag{3.85}$$

Note Eq. 3.85 means we need only to find the saturation distribution for $r_{skin} < r < \infty$ and assumes the falloff is short enough so that the water saturation in the skin zone does not change during falloff. Let us define,

$$\overline{H} = -\frac{\int_{S_{iw}}^{S_w(r_{skin},t_{inj})} f_w k_{ro} \frac{dP_c}{dS_w} dS_w}{S_w(r_{skin},t_{inj}) - S_{iw}} \tag{3.86}$$

and

$$H_{max} = \max H(S_w). \tag{3.87}$$

Note that $H(S_w)$ is bounded for a partially water wet rock (Fig. 3.3), thus the choice of defining a H_{max} seems appropriate for the modeling a hypodispersion phenomenon. We can add and subtract H_{max} from $H(S_w)$ in Eq. 3.84 and rearrange the result equation to obtain

$$(H_{max} + (H(S_w) - H_{max}))\frac{1}{r}\frac{\partial}{\partial r}\left(r\frac{\partial \Psi(S_w)}{\partial r}\right) = \frac{1}{\eta}\frac{\partial \Psi(S_w)}{\partial t}, \tag{3.88}$$

which after dividing by H_{max} can be further rearranged to obtain

$$\frac{1}{r}\frac{\partial}{\partial r}\left(r\frac{\partial \Psi(S_w)}{\partial r}\right) - \frac{1}{\eta H_{max}}\frac{\partial \Psi(S_w)}{\partial t} = \Lambda(S_w)\frac{1}{r}\frac{\partial}{\partial r}\left(r\frac{\partial \Psi(S_w)}{\partial r}\right), \tag{3.89}$$

where

$$\Lambda(S_w) = \frac{(H_{max} - H(S_w))}{H_{max}} \in [0, 1]. \tag{3.90}$$

From Eq. 3.79

$$\Psi(S_w) = \int_{S_{iw}}^{S_w} \frac{d\Psi}{dS_w} dS_w + \Psi(S_{iw}) \tag{3.91}$$

and we can define

$$\Delta\Psi(S_w) = \Psi(S_w) - \Psi(S_{iw}) = \int_{S_{iw}}^{S_w} \frac{d\Psi(S_w)}{dS_w} dS_w \tag{3.92}$$

or, dimensionless form

$$\Delta\Psi_D = \frac{\Psi(S_w) - \Psi(S_{iw})}{\Psi(S_w(r_{skin}, t_{inj})) - \Psi(S_{iw})} = \frac{\Delta\Psi(S_w)}{\Delta\Psi(S_w(r_{skin}, t_{inj}))}, \tag{3.93}$$

We can also define the dimensionless variables,

$$r_D = \frac{r}{r_w} \tag{3.94}$$

and

$$t_D = \frac{\eta H_{max} t}{r_w^2}, \tag{3.95}$$

Using Eqs. 3.93, 3.94 and 3.95, Eq. 3.89 and 3.85, respectively, can be rewritten as,

$$\frac{1}{r_D}\frac{\partial}{\partial r_D}\left(r_D \frac{\partial \Delta\Psi_D}{\partial r_D}\right) - \frac{\partial \Delta\Psi_D}{\partial t_D} = \Lambda(\Psi_D)\frac{1}{r_D}\frac{\partial}{\partial r_D}\left(r_D \frac{\partial \Delta\Psi_D}{\partial r_D}\right) \tag{3.96}$$

and

$$\begin{cases} \Delta\Psi_D(r_D, 0) = \frac{f(r_w r_D) - \Psi(S_{iw})}{\Psi(S_w(r_{skin}, t_{inj})) - \Psi(S_{iw})} = f_D(r_D), & r_{D,skin} \leq r_D \leq \infty \\ \Delta\Psi_D(r_{D,skin} = \frac{r_{skin}}{r_w}, t_D) = \frac{f(r_{skin}) - \Psi(S_{iw})}{\Psi(S_w(r_{skin}, t_{inj})) - \Psi(S_{iw})} = 1, & t_D \geq 0, \\ \lim_{r\to\infty} \Delta\Psi_D(r_D, t_D) = 0, & t_D \geq 0. \end{cases} \tag{3.97}$$

We can insert an artificially small number ϵ in Eq. 3.96,

$$\frac{1}{r_D}\frac{\partial}{\partial r_D}\left(r_D\frac{\partial \Delta\Psi_D}{\partial r_D}\right) - \frac{\partial \Delta\Psi_D}{\partial t_D} = \epsilon\Lambda(\Delta\Psi_D)\frac{1}{r_D}\frac{\partial}{\partial r_D}\left(r_D\frac{\partial \Delta\Psi_D}{\partial r_D}\right). \tag{3.98}$$

The regular perturbation theory can be used to solve Eq. 3.98 and then we can take the limit when $\epsilon \to 1$ of the resultant of the approximate solution of Eq. 3.98 to find an approximate solution for Eq, 3.96. Applying the Fundamental Theorem of Perturbation theory [72], the solution can be approximated as

$$\Delta\Psi_D(r_D, t_D) \simeq \Delta\Psi_D^0(r_D, t_D) + \epsilon\Delta\Psi_D^1(r_D, t_D) + \mathcal{O}(\epsilon^2), \tag{3.99}$$

which gives the approximation

$$\Delta\Psi_D(r_D, t_D) \simeq \begin{cases} f_D(r_D), & 1 \leq r_D < r_{D,skin} \\ \Delta\Psi_D^0(r_D, t_D) + \epsilon\Delta\Psi_D^1(r_D, t_D), & r \geq r_{D,skin}. \end{cases} \tag{3.100}$$

When $\epsilon \to 0$, $\Delta\Psi_D = \Delta\Psi_D^0$, where $\Delta\Psi_D^0$ the solution of the one-dimensional transient dispersion problem given by the following linear PDE

$$\frac{1}{r_D}\frac{\partial}{\partial r_D}\left(r_D\frac{\partial \Delta\Psi_D^0}{\partial r_D}\right) - \frac{\partial \Delta\Psi_D^0}{\partial t_D} = 0, \tag{3.101}$$

with auxiliary condition specified as

$$\begin{cases} \Delta\Psi_D^0(r_D, 0) = f_D(r_D), & r_{D,skin} \leq r_D \leq \infty, \\ \Delta\Psi_D^0(r_{D,skin}, t_D) = 1, & t \geq 0, \\ \lim_{r_D\to\infty} \Delta\Psi_D^0(r_D, t_D) = 0, & t \geq 0, \end{cases} \tag{3.102}$$

which can be solved in the Laplace domain applying the method of variation of parameters.

Applying the Laplace transform to Eq.3.101, yields

$$\frac{1}{r}\frac{\partial}{\partial r}\left(r\frac{\partial\overline{\Delta\Psi_D^0}}{\partial r}\right) = s\overline{\Delta\Psi_D^0} - f_D(r), \tag{3.103}$$

where s is the Laplace variable. Taking the Laplace transform of the last two conditions in Eq. 3.102 gives

$$\begin{cases} \overline{\Delta\Psi_D^0}(r_{D,skin}, s) = \frac{1}{s}, \\ \lim_{r_D\to\infty}\overline{\Delta\Psi_D^0}(r_D, s) = 0. \end{cases} \tag{3.104}$$

The solution of Eq. 3.103 is given by [39],

$$\begin{aligned}\overline{\Delta\Psi_D^0} =& C_1K_0(r_D\sqrt{s}) + C_2I_0(r_D\sqrt{s}) + K_0(r_D\sqrt{s})\int_{r_{D,skin}}^{r_D}(r'_D\sqrt{s})I_0(r'_D\sqrt{s})f_D(r'_D)dr'_D \\ &- I_0(r_D\sqrt{s})\int_{r_{D,skin}}^{r_D}(r'_D\sqrt{s})K_0(r'_D\sqrt{s})f_D(r'_D)dr'_D.\end{aligned} \tag{3.105}$$

Applying the second boundary condition of Eq. 3.104 to Eq. 3.105 and using $\lim_{x\to\infty}K_0(x) = 0$ [2], we have

$$\lim_{r_D\to\infty}\overline{\Delta\Psi_D^0} = \lim_{r_D\to\infty}\left[I_0(r_D\sqrt{s})\left(C_2 - \int_{r_{D,skin}}^{r_D}(r'_D\sqrt{s})K_0(r'_D\sqrt{s})f_D(r'_D)dr'_D\right)\right] = 0. \tag{3.106}$$

Because as $x\to\infty$, $I_0(x)\to\infty$ [2], Eq. 3.106 can hold only if

$$C_2 = \int_{r_{D,skin}}^{\infty} r'_D\sqrt{s}K_0(r'_D\sqrt{s})f_D(r'_D)dr'_D. \tag{3.107}$$

Applying the first boundary condition of Eq. 3.104 to Eq. 3.105, gives

$$\begin{aligned}\overline{\Delta\Psi_D^0}(r_{D,skin}, s) =& C_1K_0(r_{D,skin}\sqrt{s}) + C_2I_0(r_{D,skin}\sqrt{s}) \\ &+K_0(r_{D,skin}\sqrt{s})\int_{r_{D,skin}}^{r_{D,skin}} r'_D\sqrt{s}I_0(r'_D\sqrt{s})f_D(r'_D)dr'_D \\ &- I_0(r_{D,skin}\sqrt{s})\int_{r_{D,skin}}^{r_{D,skin}} r'_D\sqrt{s}K_0(r'_D\sqrt{s})f_D(r'_D)dr'_D = \frac{1}{s},\end{aligned} \tag{3.108}$$

which leads to,

$$C_1 = -\,C_2\frac{I_0(r_{D,skin}\sqrt{s})}{K_0(r_{D,skin}\sqrt{s})} + \frac{1}{sK_0(r_{D,skin}\sqrt{s})}. \tag{3.109}$$

Using Eqs. 3.107 and 3.109 in Eq. 3.105, we find that the zeroth solution in the Laplace space is then given by,

$$\begin{aligned}\overline{\Delta\Psi_D^0} = &-\frac{K_0(r_D\sqrt{s})I_0(r_{D,skin}\sqrt{s})}{K_0(r_{D,skin}\sqrt{s})}\int_{r_{D,skin}}^{\infty} r'_D\sqrt{s}K_0(r'_D\sqrt{s})f_D(r'_D)dr'_D \\ &+\frac{K_0(r_D\sqrt{s})}{sK_0(r_{D,skin}\sqrt{s})} + I_0(r_D\sqrt{s})\int_{r_{D,skin}}^{\infty} r'_D\sqrt{s}K_0(r'_D\sqrt{s})f_D(r'_D)dr'_D \\ &+K_0(r_D\sqrt{s})\int_{r_{D,skin}}^{r_D} r'_D\sqrt{s}I_0(r'_D\sqrt{s})f_D(r'_D)dr'_D \\ &-I_0(r_D\sqrt{s})\int_{r_{D,skin}}^{r_D} r'_D\sqrt{s}K_0(r'_D\sqrt{s})f_D(r'_D)dr'_D,\end{aligned} \tag{3.110}$$

which can be rearranged as,

$$\begin{aligned}\overline{\Delta\Psi_D^0} = K_0(r_D\sqrt{s})\Bigg(&\frac{1}{sK_0(r_{D,skin}\sqrt{s})} + \int_{r_{D,skin}}^{r_D} r'_D\sqrt{s}I_0(r'_D\sqrt{s})f_D(r'_D)dr'_D \\ &-\frac{I_0(r_{D,skin}\sqrt{s})}{K_0(r_{D,skin}\sqrt{s})}\int_{r_{D,skin}}^{\infty} r'_D\sqrt{s}K_0(r'_D\sqrt{s})f_D(r'_D)dr'_D\Bigg) \\ +I_0(r_D\sqrt{s})\Bigg(&\int_{r_{D,skin}}^{\infty} r'_D\sqrt{s}K_0(r'_D\sqrt{s})f_D(r'_D)dr'_D - \int_{r_{D,skin}}^{r_D} r'_D\sqrt{s}K_0(r'_D\sqrt{s})f_D(r'_D)dr'_D\Bigg).\end{aligned} \tag{3.111}$$

The solution in the real space is given by the inverse transform of Eq. 3.111, i.e.,

$$\Delta\Psi_D^0(r_D,t_D) = \mathcal{L}^{-1}\{\overline{\Delta\Psi_D^0}\}. \tag{3.112}$$

where this inverse will be obtained numerically using the Stehfest algorithm [97], presented in Appendix 1. To find $\Delta\Psi_D^1$, we have to also approximate

$$\frac{\partial\Delta\Psi_D(r_D,t_D)}{\partial t_D} \simeq \frac{\partial\Delta\Psi_D^0(r_D,t_D)}{\partial t_D} + \epsilon\frac{\partial\Delta\Psi_D^1(r_D,t_D)}{\partial t_D} + \mathcal{O}(\epsilon^2) \tag{3.113}$$

and

$$\frac{\partial \Delta\Psi_D(r_D,t_D)}{\partial r_D} \simeq \frac{\partial \Delta\Psi_D^0(r_D,t_D)}{\partial r_D} + \epsilon \frac{\partial \Delta\Psi_D^1(r_D,t_D)}{\partial r_D} + \mathcal{O}(\epsilon^2). \tag{3.114}$$

Starting with the definition of $H(S_w)$ and $\Delta\Psi_D$ in Eq. 3.81 and 3.93, respectively, and assuming that $H(S_{iw}) = \frac{d\Psi(S_{iw})}{dS_w} = 0$ for a partially water wet reservoir, we have

$$\begin{aligned}
\frac{d\Delta\Psi_D(r_D,t_D)}{dS_w} &= \frac{d}{dS_w}\left(\frac{\Psi(S_w(r_D,t_D)) - \Psi(S_{iw})}{\Psi(S_w(r_{D,skin},t_{D,inj})) - \Psi(S_{iw})}\right) \\
&= \frac{d}{dS_w}\left(\Delta\Psi(S_w(r_D,t_D))\Delta\Psi^{-1}(S_w(r_{D,skin},t_D)))\right) \\
&= \Delta\Psi^{-1}(r_{D,skin},t_{D,inj})H(\Delta\Psi_D(r_D,t_D)) \\
&\quad - \Delta\Psi^{-2}(r_{D,skin},t_{D,inj})H(\Delta\Psi_D(r_{D,skin},t_{D,inj}))\Delta\Psi(r_D,t_D).
\end{aligned} \tag{3.115}$$

Solving Eq. 3.115 for $H(\Delta\Psi_D(r_D,t_D))$ using Eq. 3.93, yields

$$H(\Delta\Psi_D(r_D,t_D)) = \Delta\Psi(r_{D,skin},t_{D,inj})\frac{d\Delta\Psi_D^0(r_D,t_D)}{dS_w} + H(\Delta\Psi_D(r_{D,skin},t_{D,inj}))\Delta\Psi_D^0(r_D,t_D) \tag{3.116}$$

Defining

$$H^0 = H(\Delta\Psi_D^0) = \Delta\Psi(r_{D,skin},t_{D,inj})\frac{d\Delta\Psi_D^1(r_D,t_D)}{dS_w} + H(\Delta\Psi_D(r_{D,skin},t_{D,inj}))\Delta\Psi_D^1(r_D,t_D) \tag{3.117}$$

and

$$H^1 = H(\Delta\Psi_D^1) = \Delta\Psi(r_{D,skin},t_{D,inj})\frac{d\Delta\Psi_D(r_D,t_D)}{dS_w} + H(\Delta\Psi_D(r_{D,skin},t_{D,inj}))\Delta\Psi_D(r_D,t_D), \tag{3.118}$$

we can approximate

$$
\begin{aligned}
H(\Delta\Psi_D(r_D,t_D)) &= \Delta\Psi(r_{D,skin},t_{D,inj})\frac{d\Delta\Psi_D(r_D,t_D)}{dS_w} + H(\Delta\Psi_D(r_{D,skin},t_{D,inj}))\Delta\Psi_D(r_D,t_D) \\
&\simeq \Delta\Psi(r_{D,skin},t_{D,inj})\left(\frac{d\Delta\Psi^0_D(r_D,t_D)}{dS_w} + \epsilon\frac{d\Delta\Psi^1_D(r_D,t_D)}{dS_w}\right) \\
&+ H(\Delta\Psi_D(r_{D,skin},t_{D,inj}))(\Delta\Psi^0_D(r_D,t_D) + \epsilon\Delta\Psi^1_D(r_D,t_D)) + \mathcal{O}(\epsilon^2) \\
&\simeq H(\Delta\Psi^0_D) + \epsilon H(\Delta\Psi^1_D) + \mathcal{O}(\epsilon^2) \\
&\simeq H^0 + \epsilon H^1 + \mathcal{O}(\epsilon^2)
\end{aligned} \tag{3.119}
$$

and rewrite Eq. 3.90 as

$$
\Lambda(\Delta\Psi_D(r_D,t_D)) = 1 - \frac{H}{H_{max}} \simeq 1 - \frac{H^0 + \epsilon H^1 + \mathcal{O}(\epsilon^2)}{H_{max}} = \Lambda(\Delta\Psi^0_D) - \epsilon\frac{H^1}{H_{max}}. \tag{3.120}
$$

Neglecting $\mathcal{O}(\epsilon^2)$ terms and substituting Eqs. 3.113, 3.114 and 3.120 in Eq. 3.98, yields

$$
\begin{aligned}
&\frac{1}{r_D}\frac{\partial}{\partial r_D}\left(r_D\frac{\partial\Delta\Psi^0_D}{\partial r_D} + \epsilon r_D\frac{\partial\Delta\Psi^1_D}{\partial r_D}\right) - \left(\frac{\partial\Delta\Psi^0_D}{\partial t_D} + \epsilon\frac{\partial\Delta\Psi^1_D}{\partial t_D}\right) \\
&= \epsilon\left(\Lambda(\Delta\Psi^0_D) - \epsilon\frac{H^1}{H_{max}}\right)\left[\frac{1}{r_D}\frac{\partial}{\partial r_D}\left(r_D\frac{\partial\Delta\Psi^0_D}{\partial r_D} + \epsilon r\frac{\partial\Delta\Psi^1_D}{\partial r}\right)\right]
\end{aligned} \tag{3.121}
$$

with

$$
\begin{cases}
\Delta\Psi^0_D(r_D,0) + \epsilon\Delta\Psi^1_D(r_D,0) = f_D(r_D), & r_{D,skin} \le r_D \le \infty, \\
\Delta\Psi^0_D(r_{D,skin},t_D) + \epsilon\Delta\Psi^1(r_{D,skin},t_D) = 1, & t_D \ge 0, \\
\lim_{r_D\to\infty}\Delta\Psi^0_D(r_D,t_D) + \epsilon\Delta\Psi^1(r_D,t_D) = 0, & t_D \ge 0.
\end{cases} \tag{3.122}
$$

For ϵ^1,

$$
\frac{1}{r_D}\frac{\partial}{\partial r_D}\left(r_D\frac{\partial\Delta\Psi^1_D}{\partial r_D}\right) - \frac{\partial\Delta\Psi^1_D}{\partial t_D} = \Lambda(\Delta\Psi^0_D)\frac{1}{r_D}\frac{\partial}{\partial r_D}\left(r_D\frac{\partial\Delta\Psi^0_D}{\partial r_D}\right), \tag{3.123}
$$

where

$$\begin{cases} \Delta\Psi_D^1(r_D,0)=0, & r_{D,skin}\leq r_D\leq\infty, \\ \Delta\Psi_D^1(r_{D,skin},t_D)=0, & t_D\geq 0, \\ \lim_{r_D\to\infty}\Delta\Psi_D^1(r_D,t_D)=0, & t_D\geq 0. \end{cases} \tag{3.124}$$

Following Barreto [9] and Sousa [95], Sousa et al. [94] derivations to solve the pressure diffusivity equation for gases, Eq. 3.123 can be rewritten in its integral form using a Green's function by treating the term on the right side of the Eq. 3.123 as a source term. We can then write Eq. 3.123 as

$$\frac{1}{r_D}\frac{\partial}{\partial r_D}\left(r_D\frac{\partial\Delta\Psi_D^1}{\partial r_D}\right)-\frac{\partial\Delta\Psi_D^1}{\partial t_D}=\tilde{q}(r_D,t_D), \tag{3.125}$$

where

$$\tilde{q}(r_D,t_D)=\Lambda(\Delta\Psi_D^0)\frac{1}{r_D}\frac{\partial}{\partial r_D}\left(r_D\frac{\partial\Delta\Psi_D^0}{\partial r_D}\right), \tag{3.126}$$

the associate Green's function problem is [42, 34]

$$\frac{1}{r_D}\frac{\partial}{\partial r_D}\left(r_D\frac{\partial G(r_D,r_{D0},t_D,t_{D0})}{\partial t_D}\right)-\frac{\partial G(r_D,r_{D0},t_D,t_{D0})}{\partial t_D}=\frac{\delta(r_D-r_{D0})\delta(t_D-t_{D0})}{2\pi r_D}, \tag{3.127}$$

where

$$\begin{cases} G(r_D,r_{D0},t_D,t_{D0})=0, & t_D<t_{D0} \\ G(r_{D,skin},r_{D0},t_D,t_{D0})=0 \\ \lim_{r_D\to\infty}G(r_D,r_{D0},t_D,t_{D0}))=0. \end{cases} \tag{3.128}$$

Note that the $\frac{1}{2\pi r_D}\delta(r_D-r_{D0})$ is the one-dimensional Dirac Delta function in cylindrical coordinates [42] and the term $\frac{1}{2\pi r_D}\delta(r_D-r_{D0})\delta(t_D-t_{D0})$ corresponds to a impulse at r_{D0} and t_{D0} (source position). Applying the Laplace transform [2] to Eq. 3.127 and to the boundary conditions, leads to

$$\frac{1}{r_D}\frac{\partial}{\partial r_D}\left(r_D\frac{\partial\overline{G}}{\partial r_D}\right)-s\overline{G}+G(r_D,r_{D0},t_D=0,t_{D0})=\frac{\delta(r_D-r_{D0})\exp(-st_{D0})}{2\pi r_D}, \tag{3.129}$$

with

$$\begin{cases} \overline{G}(r_{D,skin}, r_{D0}, s, t_{D0}) = 0 \\ \lim_{r_D \to \infty} \overline{G}(r_D, r_{D0}, s, t_{D0})) = 0. \end{cases} \tag{3.130}$$

Using the initial condition in Eq. 3.129, yields

$$\frac{1}{r_D}\frac{\partial}{\partial r_D}\left(r_D \frac{\partial \overline{G}}{\partial r_D}\right) - s\overline{G} = \frac{\delta(r_D - r_{D0})\exp(-st_{D0})}{2\pi r_D}. \tag{3.131}$$

We can solve Eq. 3.131 for any radius less than or greater than the source position, r_0, where the term on the right hand side of the equation is zero. For $r < r_0$, we have

$$\overline{G} = C_1 I_0(r_D\sqrt{s}) + C_2 K_0(r_D\sqrt{s}). \tag{3.132}$$

Applying the first boundary condition in Eq. 3.132 yields

$$\overline{G}(r_{D,skin}, r_{D0}, s, t_{D0}) = C_1 I_0(r_{D,skin}\sqrt{s}) + C_2 K_0(r_{D,skin}\sqrt{s}) = 0, \tag{3.133}$$

and thus,

$$C_1 = -C_2 \frac{K_0(r_{D,skin}\sqrt{s})}{I_0(r_{D,skin}\sqrt{s})}, \tag{3.134}$$

which gives,

$$\overline{G}(r_D, r_{D0}, s, t_{D0}) = C_2\left(- \frac{K_0(r_{D,skin}\sqrt{s})}{I_0(r_{D,skin}\sqrt{s})} I_0(r_D\sqrt{s}) + K_0(r_D\sqrt{s})\right), \tag{3.135}$$

for $r < r_0$. For $r > r_0$, we have

$$\overline{G} = C_3 I_0(r_D\sqrt{s}) + C_4 K_0(r_D\sqrt{s}). \tag{3.136}$$

Applying the second boundary condition,

$$\lim_{r_D \to \infty} \overline{G}(r_D, r_{D0}, s, t_{D0}) = \lim_{r_D \to \infty} \left(C_3 I_0(r_D\sqrt{s}) + C_4 K_0(r_D\sqrt{s})\right) = 0 \tag{3.137}$$

To $\overline{G}(r_D, r_{D0}, s, t_{D0})$ to be bounded, we must have $C_3 = 0$ and thus

$$\overline{G} = C_4 K_0(r_D\sqrt{s}) \tag{3.138}$$

for $r > r_0$, considering $\lim_{x\to\infty} K_0(x) \to 0$ and $\lim_{x\to\infty} I_0(x) \to \infty$. Since the Green's function must be continuous at r_0, it follows from Eqs. 3.135 and 3.138 that

$$C_2\left(-\frac{K_0(r_{D,skin}\sqrt{s})}{I_0(r_{D,skin}\sqrt{s})} I_0(r_{D0}\sqrt{s}) + K_0(r_{D0}\sqrt{s}) \right) = C_4 K_0(r_{D0}\sqrt{s}). \tag{3.139}$$

It follows immediately that

$$C_4 = C_2 \frac{\left(-\frac{K_0(r_{D,skin}\sqrt{s})}{I_0(r_{D,skin}\sqrt{s})} I_0(r_{D0}\sqrt{s}) + K_0(r_{D0}\sqrt{s}) \right)}{K_0(r_{D0}\sqrt{s})}. \tag{3.140}$$

Now only C_2 is left to be determined. If we integrate the ordinary differential equation given by Eq. 3.129 from r_{D0}^- to r_{D0}^+, we have

$$\int_{r_{D0}^-}^{r_{D0}^+} \frac{1}{r'_D}\frac{\partial}{\partial r'_D}\left(r'_D \frac{\partial \overline{G}}{\partial r'_D} \right) 2\pi r'_D dr'_D - \int_{r_{D0}^-}^{r_{D0}^+} s\overline{G} 2\pi r'_D dr'_D = \exp(-st_0) \int_{r_{D0}^-}^{r_{D0}^+} \frac{\delta(r'_D - r_{D0})}{2\pi r'_D} 2\pi r'_D dr'_D, \tag{3.141}$$

which gives

$$\left(r'_D \frac{\partial \overline{G}}{\partial r'_D} \right)|_{r_{D0}^-}^{r_{D0}^+} - \int_{r_{D0}^-}^{r_{D0}^+} s r'_D \overline{G} dr'_D = \frac{\exp(-st_{D0})}{2\pi}. \tag{3.142}$$

Taking the limit when $r_{D0}^-, r_{D0}^+ \to r_{D0}$, yields

$$\lim_{r_{D0}^-, r_{D0}^+ \to r_{D0}} \left(r'_D \frac{\partial \overline{G}}{\partial r'_D} \right)|_{r_{D0}^-}^{r_{D0}^+} = \frac{\exp(-st_{D0})}{2\pi}. \tag{3.143}$$

Taking the derivatives of Eqs. 3.135 and 3.138 with respect to r_{D0} using $\frac{dI_0(x)}{dx} = I_1(x)$ and

$\frac{dK_0(x)}{dx} = -K_1(x)$ and inserting the results into in Eq. 3.143, we have

$$C_2 \frac{\left(-\frac{K_0(r_{D,skin}\sqrt{s})}{I_0(r_{D,skin}\sqrt{s})} I_0(r_{D0}\sqrt{s}) + K_0(r_{D0}\sqrt{s}) \right)}{K_0(r_{D0}\sqrt{s})} r_{D0}\sqrt{s} K_1(r_{D0}\sqrt{s})$$
$$+ C_2 r_{D0}\sqrt{s} \left(-\frac{K_0(r_{skin}\sqrt{s})}{I_0(r_{D,skin}\sqrt{s})} I_1(r_{D0}\sqrt{s}) - K_1(r_{D0}\sqrt{s}) \right) = -\frac{\exp(-st_{D0})}{2\pi}, \tag{3.144}$$

which gives,

$$C_2 = \frac{\exp(-st_{D0})}{2\pi r_{D0}\sqrt{s} \frac{K_0(r_{D,skin}\sqrt{s})}{I_0(r_{D,skin}\sqrt{s})} \left(\frac{I_0(r_{D0}\sqrt{s})}{K_0(r_{D0}\sqrt{s})} K_1(r_{D0}\sqrt{s}) + I_1(r_{D0}\sqrt{s}) \right)}. \tag{3.145}$$

Substituting Eq. 3.145 in Eq. 3.140 gives

$$C_4 = \frac{\exp(-st_{D0}) \left(-\frac{K_0(r_{D,skin}\sqrt{s})}{I_0(r_{D,skin}\sqrt{s})} I_0(r_{D0}\sqrt{s}) + K_0(r_{D0}\sqrt{s}) \right)}{2\pi r_{D0}\sqrt{s} \frac{K_0(r_{D,skin}\sqrt{s})}{I_0(r_{D,skin}\sqrt{s})} \left(I_0(r_{D0}\sqrt{s}) K_1(r_{D0}\sqrt{s}) + I_1(r_{D0}\sqrt{s}) K_0(r_{D0}\sqrt{s}) \right)}. \tag{3.146}$$

Using the Wronskian given by

$$\mathcal{W}\{K_0(z)I_0(z)\} = I_0(z)K_1(z) + I_1(z)K_0(z) = \frac{1}{z}, \tag{3.147}$$

we can simplify Eqs. 3.107 and 3.146, respectively, to

$$C_2 = \frac{\exp(-st_{D0})}{2\pi} \frac{I_0(r_{D,skin}\sqrt{s})}{K_0(r_{D,skin}\sqrt{s})} K_0(r_{D0}\sqrt{s}). \tag{3.148}$$

and

$$C_4 = \frac{\exp(-st_{D0})}{2\pi} \left(\frac{I_0(r_{D,skin}\sqrt{s})}{K_0(r_{D,skin}\sqrt{s})} K_0(r_{D0}\sqrt{s}) - I_0(r_{D0}\sqrt{s}) \right). \tag{3.149}$$

Substituting Eq. 3.148 in Eq. 3.135, yields

$$\overline{G}(r_D, r_{D0}, s, t_{D0}) = \frac{\exp(-st_{D0})}{2\pi}\left(\frac{I_0(r_{D,skin}\sqrt{s})}{K_0(r_{D,skin}\sqrt{s})}K_0(r_D\sqrt{s}) - I_0(r_D\sqrt{s})\right)K_0(r_{D0}\sqrt{s}), \tag{3.150}$$

for $r < r_0$. Substituting Eq. 3.149 in Eq. 3.138, yields

$$\overline{G}(r_D, r_{D0}, s, t_{D0}) = \frac{\exp(-st_{D0})}{2\pi}\left(\frac{I_0(r_{D,skin}\sqrt{s})}{K_0(r_{D,skin}\sqrt{s})}K_0(r_{D0}\sqrt{s}) - I_0(r_{D0}\sqrt{s})\right)K_0(r_D\sqrt{s}), \tag{3.151}$$

for $r > r_0$. $\overline{G}$ can be inverted to give G in real space to find

$$\Delta\Psi^1_D(r_D, t_D) = 2\pi\int_0^{t_D}\int_{r_{D,skin}}^{\infty}\tilde{q}(r'_D, t'_D)G(r_D, r'_D, t_D, t'_D)r'_D dr'_D dt'_D. \tag{3.152}$$

Note; the first term in Eq. 3.150 and 3.151 have to be inverted numerically while the last term in these equations can be inverted analytically ([24] cited in[95]) using the translation property of Laplace transform [2]:

$$\begin{aligned}\mathcal{L}^{-1}\{-\frac{\exp(-st_{D0})}{2\pi}I_0(r_D\sqrt{s})K_0(r_{D0}\sqrt{s})\} = \mathcal{L}^{-1}\{-\frac{\exp(-st_{D0})}{2\pi}I_0(r_{D0}\sqrt{s})K_0(r_D\sqrt{s})\} = \\ = -\frac{1}{4\pi(t_D - t_{D0})}\exp\left(-\frac{r_D^2 + r_{D0}^2}{4(t_D - t_{D0})}\right)I_0\left(\frac{r_D r_{D0}}{2(t_D - t_{D0})}\right).\end{aligned} \tag{3.153}$$

Finally, taking the limit as $\epsilon \to 1$ in Eq. 3.100 [80], yields

$$\Delta\Psi_D(r_D, t_D) = \begin{cases} f_D(r_D), 1 \le r_D < r_{D,skin} \\ \Delta\Psi^0_D(r, t) + \Delta\Psi^1_D(r_D, t_D), r_D \ge r_{D,skin}. \end{cases} \tag{3.154}$$

The saturation distribution during falloff obtained here analytically does agree with numerical simulation results, as we will discuss in the Section **Validation** (Fig. 3.27).

Production: Fortunately - for modeling it, not for trying to estimate it - the capillary pressure effects cannot be noticed in the wellbore pressure response during injection, falloff and early times of production period, as showed in Fig. 3.2. Consequently, we can neglect the capillarity effects before the saturation wave breaking time (the breaking time is when the a gradient catastrophe occurs and a shock appears in the solution; more details will be given later), considering the injection time was sufficient long to guarantee that the wave breaks far from the wellbore. The last four curves (from left to right) in n Fig. 3.17 represent the saturation distribution in the reservoir at two times before the wave breaking time, with and without capillary pressure effects. We can see that for both times, the saturation profile with and without p_c coincides. In another hand, we observe that the capillary dispersive term in the Rapoport and Leas equation will became more and more negligible as the oil front moves closer to the wellbore. Similarly to the injection period, during the flowback, the capillary pressure dispersive effect will be non-negligible only in a small region around the water front where the saturation gradient are significant (Fig. 3.18(b)). But, dissimilarly, in this case, the capillary pressure derivative is not significant (Fig. 3.18(a)) - remember from Chapter 2 that during the flowback the shock saturations change with time and are always higher than the immobile water saturation. If we take a look in the Rapoport and Leas equation,

$$\frac{\partial S_w}{\partial t} + \frac{C}{2r}\frac{\partial}{\partial r}\left(f_w - \epsilon k \Psi\right) - \frac{\epsilon k C}{2}\frac{\partial^2 \Psi}{\partial r^2} = 0, \tag{3.155}$$

we see that as the radius decreases (flowback period), the convective term become more and more significant, while the dispersive term coefficient remains the same, making the saturation profile shaper. Consequently, at the breakthrough period, both saturations profiles (with and without capillarity) will be almost the same, as we can confirm from simulations results (Fig. 3.17). Consequently, if the injection time is sufficiently long so that during injection the water front is far from the wellbore at the end of injection, then the saturation distribution during flowback, when capillary pressure is included, becomes closer to the solution obtained without capillarity effects as time increases during the flowback period.

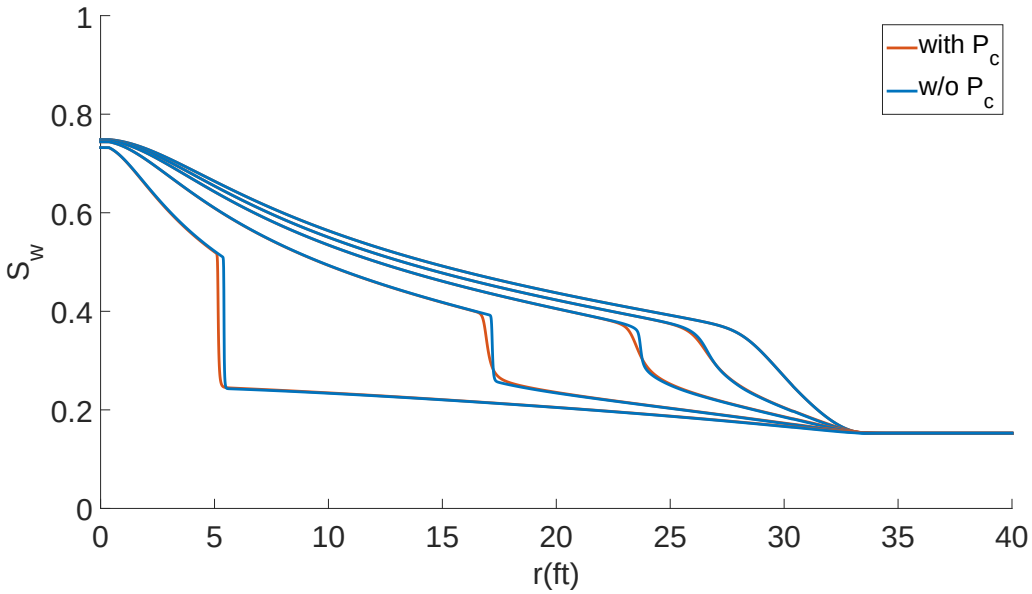

Figure 3.17: Saturation distribution obtained from IMEX, with and without capillary pressure during flowback, at different times during flowback. Here, both profiles were obtained from the same initial condition, i.e., the saturation profile at then of of falloff, where capillary effects were considered during injection and falloff.

Considering this wave behavior in addition to the fact the wellbore pressure is not very sensitive to slight variations in the saturation distribution at locations in the reservoir far from the well, it may be possible to ignore capillarity effects on the wellbore pressure during flowback, provided that the water front moves far from the well during injection. However, this conjecture does not mean that capillary pressure can be ignored in constructing the injection and falloff solutions as the solution at the end of falloff provides the initial condition for constructing the solution during production.

Similarly to injection, during the production period we have a convection-dispersion non-linear problem, but with the following initial and boundary conditions,

$$\begin{cases} S_w(r,0) = S_w(r,t_{foff}) = S_w(r,\Delta t_{prod}=0), & r_w \le r \le \infty, \\ r\frac{\partial S_w(r_w,t)}{\partial r} = 0 \quad (p_c = 0), & t > 0, \\ \lim_{r\to\infty} S_w = S_{iw}, & t \ge 0. \end{cases} \tag{3.156}$$

Note; here we neglect outlet end effect and assume that the water saturation gradient is

$$F_w = f_w + \epsilon k f_w k_{ro} \boxed{r \frac{dP_c}{dS_w} \frac{\partial S_w}{\partial r}} \qquad \text{(3.2 revisited)}$$

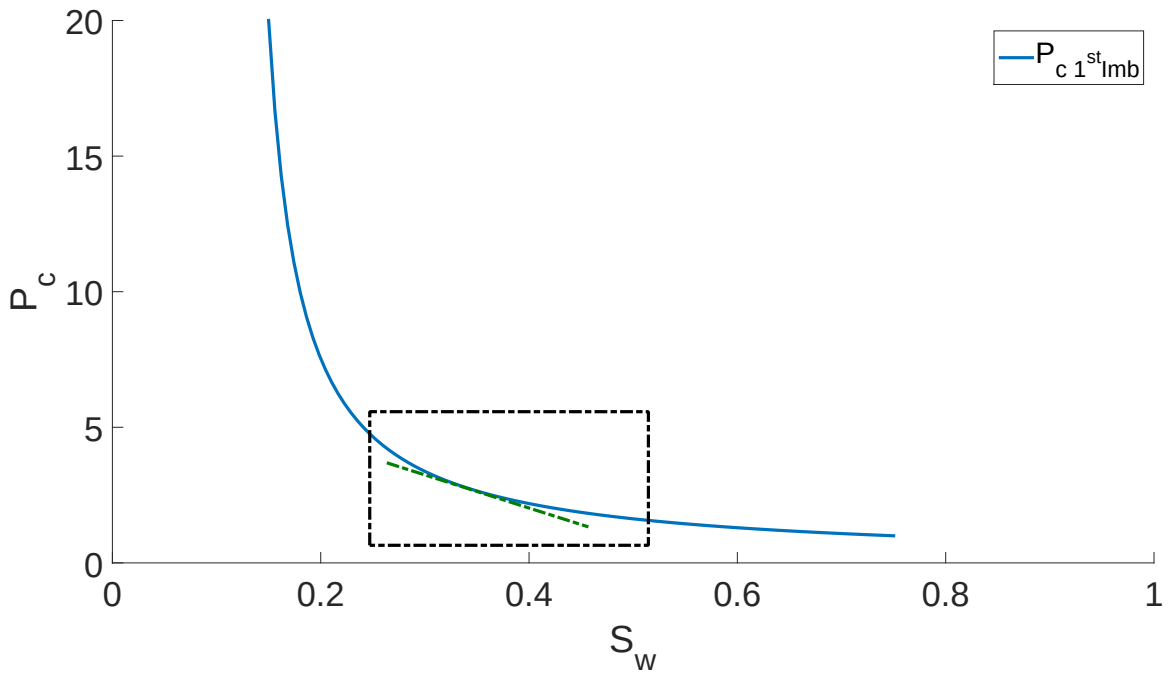

(a)

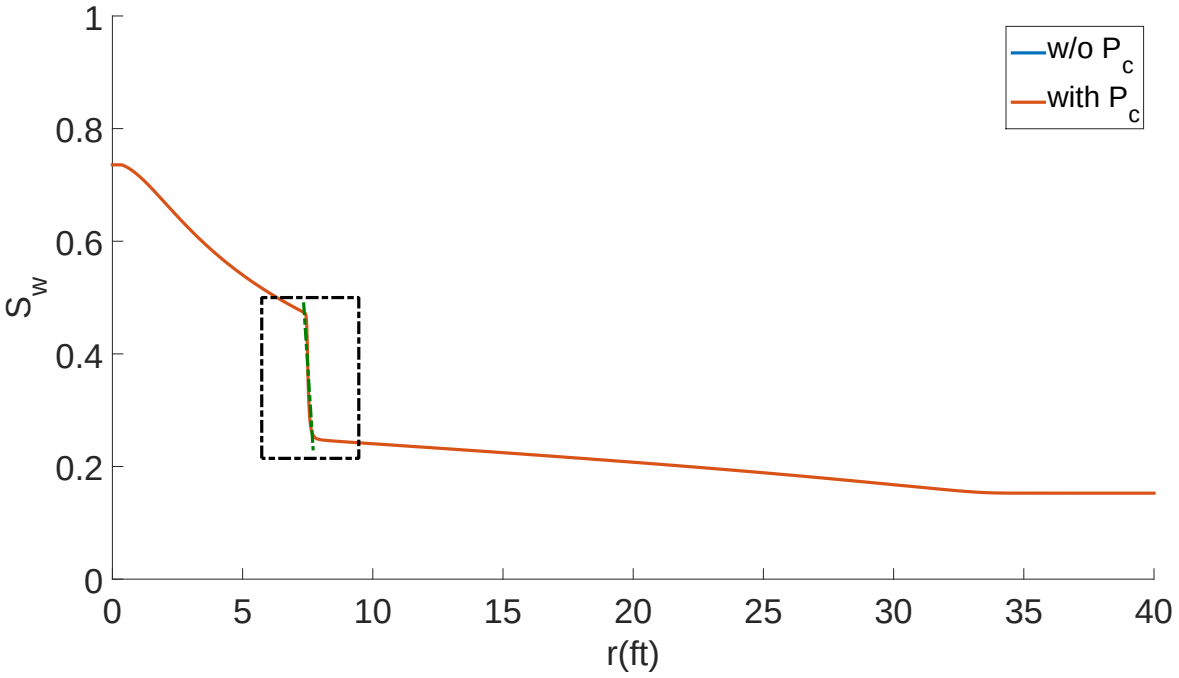

(b)

Figure 3.18: Capillary pressure curve (a) and saturation profile (b) after 12 hours flowing back.The dashed green lines represent the capillary pressure derivative (a) and the saturation gradient (b) at the saturation at the shock front at time t during the flowback.

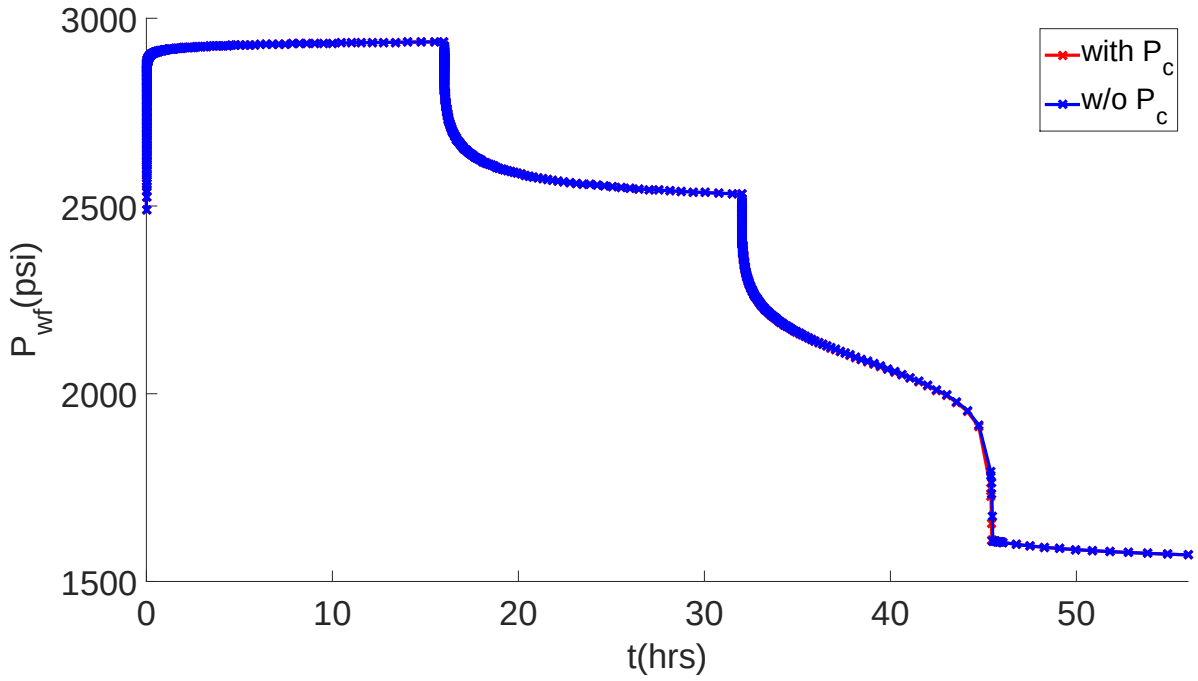

(a)

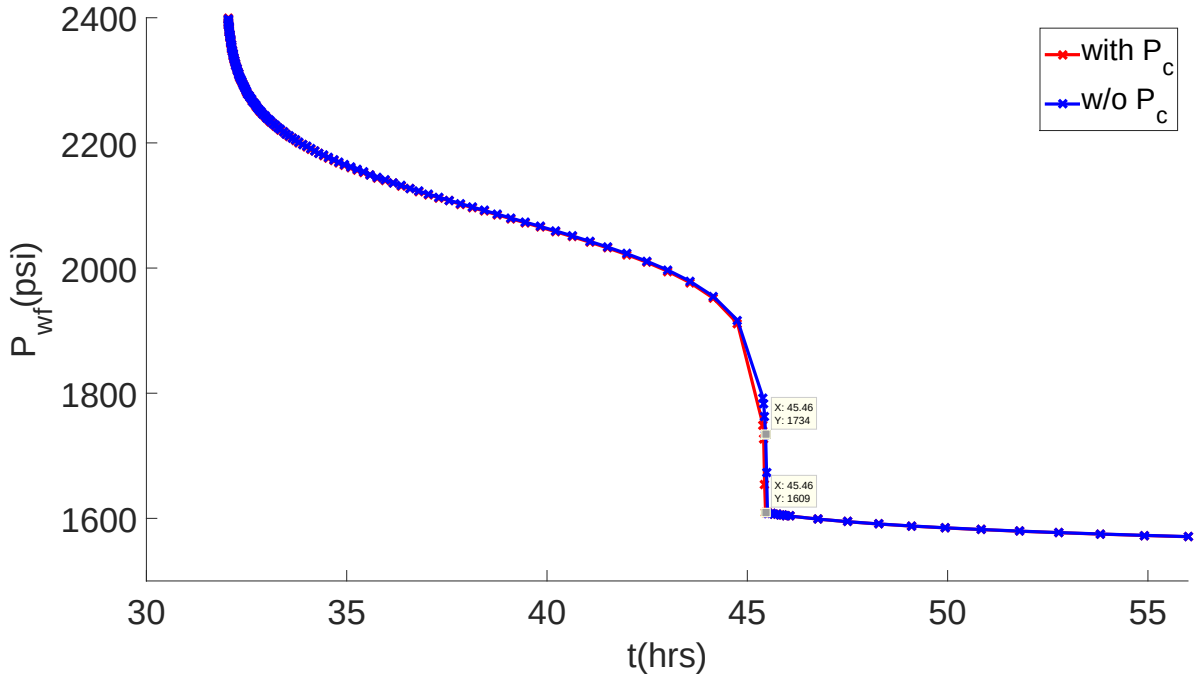

(b)

Figure 3.19: Wellbore pressure history during an IFPT from IMEX (a) and the zoom in the wellbore pressure history during flowback (b) to show the discrepancy on pressure caused by neglecting capillary pressure effects during the flowback. Here, capillary pressure is considered for the injection and falloff periods in both cases. X corresponds to time while Y corresponds to pressure. At $X = 45.46$ there is a 125 psi discrepancy in the wellbore pressure when neglecting capillary pressure effects, which represents 5% of the initial pressure, 2500 psi.

zero at the wellbore (second condition in Eq. 3.156), which gives us an unique solution, but not the true solution [5]. This assumption implies that the capillary pressure gradient is zero at the wellbore, which does guarantee pressure continuity and means that $F_w(r_w, t) = f_w(r_w, t)$. This equality will be useful later when developing a closed form for the inner solution thorough material balance. Considering everything discussed, let us divide the production period in three stages:

- **Stage 1: Before wave breaking time, $t \in (t_{foff}, t_{bt})$**. In this period, the saturation solutions with and without capillary pressure overlaps, we can use the Buckley-Leverett hyperbolic equation (Eq. 3.1) to estimate saturation profile.

- **Stage 2: Between wave breaking time and shock breakthrough, $t \in (t_{bt}, t_{BT})$**. During this stage we do need to consider the dispersive term in the saturation governing equation (Eq. 3.21). Similarly to injection, we can apply the method of matched asymptotic expansion to find the saturation profile for any time after the wave breaking time and before the oil front breakthrough.

- **Stage 3: After shock breakthrough, $t > t_{BT}$** Here, as in Stage 1, we solve Eq. 3.1 to estimate the saturation distribution.

Now, before discuss each stage in details, let us show how to find the saturation wave braking time, t_{bt}. The breaking time is the earliest time at which a gradient catastrophe occurs, .i.e., when a shock (the sharp oil front) is formed in the reservoir. Before the breaking time, the physical and non-physical saturation distributions without capillary pressure effects are the same, and the capillary effects could be considered negligible, as we can see in Fig. 3.17, in which the last four curves (from left to right) corresponds to saturation profiles for two different times before wave breaking time. We can see that for both times, the saturation profile with and without capillary pressure overlaps.

Breaking Time The breaking time is given by

$$t_{bt} = \frac{-1}{\min \frac{dc(S_{w0}(r_0^2))}{d(r_0^2)}}, \tag{3.157}$$

for $\frac{dc(S_{w0}(r_0^2))}{dr_0^2} < 0$, where

$$\frac{dc(S_{w0}(r_0))}{d(r_0^2)} = \frac{dc(S_w(r, t_{foff}))}{d(r^2)} = \frac{\theta q_{prod}}{\pi\phi h}\frac{d^2 f_w}{dS_w^2}\frac{dS_w}{d(r^2)} = \frac{\theta q_{prod}}{\pi\phi h}\frac{d^2 f_w}{dS_w^2}\frac{dS_w}{d\Delta\Psi_D}\frac{d\Delta\Psi_D}{d(r^2)}, \tag{3.158}$$

with

$$\frac{d\Delta\Psi_D}{dS_w} = -\frac{f_w k_{ro}\frac{dP_c}{dS_w}}{\Delta\Psi(r_{skin}, t_{foff})} \tag{3.159}$$

and

$$\frac{d\Delta\Psi_D}{d(r^2)} = \frac{d\Delta\Psi_D^0}{d(r^2)} + \frac{d\Delta\Psi_D^1}{d(r^2)}. \tag{3.160}$$

The minimum is given by $\frac{d}{d(r_0^2)}\left(\frac{dc(S_0(r_0))}{d(r_0^2)}\right) = 0$,

$$\begin{aligned}\frac{d^2 c(S_{w0}(r_0))}{d(r_0^2)^2} &= \frac{\theta q_{prod}}{\pi\phi h}\left[\frac{d^2 f_w}{dS_w^2}\frac{d^2 S_w}{d(r^2)^2} + \frac{d^3 f_w}{dS_w^3}\left(\frac{dS_w}{d(r^2)}\right)^2\right] \\ &= \frac{\theta q_{prod}}{\pi\phi h}\left\{\frac{d^2 f_w}{dS_w^2}\left[\frac{d^2 S_w}{d\Delta\Psi_D^2}\left(\frac{d\Delta\Psi_D}{d(r^2)}\right)^2 + \frac{dS_w}{d\Delta\Psi_D}\frac{d^2\Delta\Psi_D}{d(r^2)^2}\right]\right. \\ &\qquad \left. + \frac{d^3 f_w}{dS_w^3}\left(\frac{dS_w}{d\Delta\Psi_D}\frac{d\Delta\Psi_D}{d(r^2)}\right)^2\right\}.\end{aligned} \tag{3.161}$$

The breaking time expression can be derived following the derivation in Knobel [58] for Cartesian coordinates. Defining the speed

$$c(S_w(r,t)) = \frac{\theta q_t}{\pi\phi h}\frac{df_w(S_w(r,t))}{dS_w}, \tag{3.162}$$

we can rewrite Eq. 3.1 as

$$\frac{\partial S_w(r,t)}{\partial t} + c(S_w(r,t))\frac{\partial S_w(r,t)}{\partial(r^2)} = 0. \tag{3.163}$$

Characteristics are curves in the plan (r^2,t) which transmit the initial saturation profile, $S_w(r^2,0) = S_{w0}(r_0^2)$, forward in time. Along the characteristic curves, the partial differential equation (Eq. 3.163) becomes an ordinary differential; $\frac{dr^2(t)}{dt} = c(S_w(r^2,t))$. A characteristic curve (r^2(t),t) starting at the point (r_0^2,0) is given by

$$r^2 = c(S_{w0}(r_0^2))t + r_0^2, \tag{3.164}$$

where $r_0^2 = r^2(0)$. Since $\frac{dS_w(r^2(t),t)}{dt} = 0$ along $\frac{dr^2(t)}{dt} = c(S_w(r^2,t))$, - i.e. $S_w(r^2(t),t)$ is constant this particular curve starting at (r_0^2,t) - we have $S_w(r^2,t) = S_w(r_0^2,0) = S_{w0}(r_0^2)$ at the point (r^2,t). $r_0^2 = (r^2,t)$ determines the strating point $(r_0^2,0)$ of the characteristic passing thorough (r^2,t), defined implicitly by Eq. 3.164. Taking the partial derivative of Eq. 3.164 with respect to r^2,

$$\frac{\partial r^2}{\partial(r^2)} = \frac{\partial(c(S_{w0}(r_0^2)t + r_0^2)}{\partial(r^2)}, \tag{3.165}$$

gives

$$1 = \frac{\partial(c(S_{w0}(r_0^2))}{\partial(r_0^2)}\frac{\partial r_0^2}{\partial(r^2)}t + \frac{\partial r_0^2}{\partial(r^2)}. \tag{3.166}$$

Solving Eq. 3.166 for $\frac{\partial r_0^2}{\partial(r^2)}$, we get

$$\frac{\partial r_0^2}{\partial(r^2)} = \frac{1}{1 + \frac{\partial(c(S_{w0}(r_0^2))}{\partial r_0^2}t}. \tag{3.167}$$

Substituting Eq. 3.167 in the derivative of S_w with respect to r^2 and using $S_w(r^2,t) = S_{w0}(r_0^2)$ at (r^2,t), yields,

$$\frac{\partial S_w(r^2,t)}{\partial(r^2)} = \frac{\partial S_{w0}(r_0^2)}{\partial(r_0^2)}\frac{\partial r_0^2}{\partial(r^2)} = \frac{\frac{\partial S_{w0}(r_0^2)}{\partial(r_0^2)}}{1 + \frac{\partial(c(S_{w0}(r_0^2))}{\partial(r_0^2)}t}. \tag{3.168}$$

When the denominator in Eq. 3.168 goes to 0, we have a gradient catastrophe, i.e., $\frac{\partial S_w}{\partial(r^2)} \to \infty$. When $\frac{\partial(c(S_{w0}(r_0^2))}{\partial(r_0^2)} \geq 0$, that would not happen. The denominator goes to zero, as $t \to \frac{-1}{\frac{\partial(c(S_{w0}(r_0^2))}{\partial(r_0^2)}}$, for $\frac{\partial(c(S_{w0}(r_0^2))}{\partial(r_0^2)} < 0$. Considering we are looking for the earliest time $t$he wave breaks, the breaking time (t_{bt}) is given by Eq. 3.157. Fig. 3.20 shows water saturation profiles

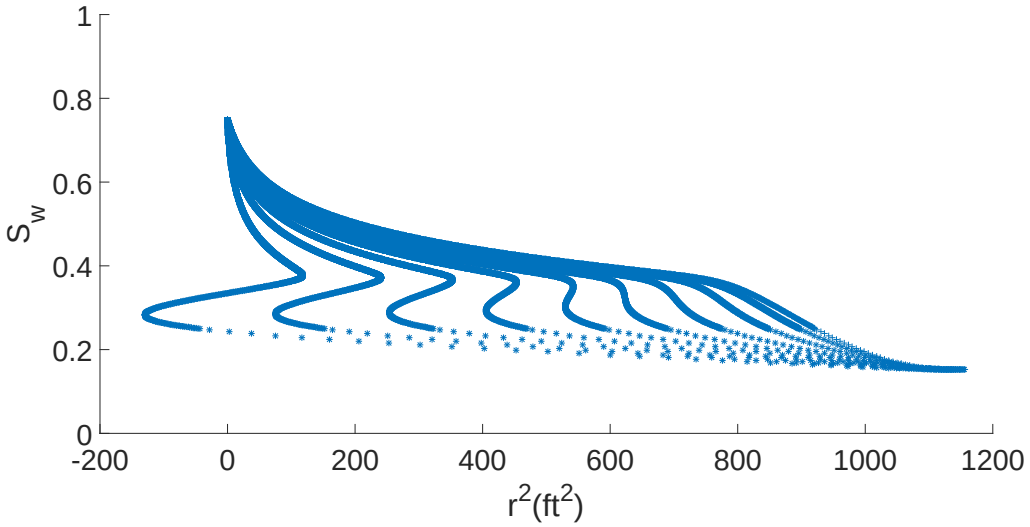

Figure 3.20: Physical water saturation profiles before and non-physical multivalued water saturation profiles at different times before and after t_{bt}, respectively, during the flowback period. The last curve in the right side is the profile at the earliest time and the flow is towards the well from right to left. We can see that the wave is breaking at time when the "oil front" is about 600 ft^2 in this case.

at different times before and after t_{bt} obtained by flowing back the water saturations using the characteristic equation (Eq. 3.164).

Stage 1: Before wave breaking time, $t \in (t_{foff}, t_{bt})$ As discussed, before the wave breaking time, .i.e., before a sharp oil front is formed in the reservoir, we can solve the Buckley-Leverett equation (Eq. 3.1) instead of Eq. 3.21, since their solutions are equivalent during this period. Letting $\epsilon \to 0$ in Eq. 3.21, we have the following Cauchy problem,

$$\begin{cases} \frac{\partial S_w}{\partial t} + \frac{\theta q}{\phi 2\pi r h}\frac{\partial f_w(S_w)}{\partial r} = 0, \\ S_w(r, t_{foff}) = S_w(r_0), \qquad r > r_w \end{cases} \tag{3.169}$$

whose strong solution can be obtained by the application of the Method of Characteristics and is given by

$$r^2(S_w, t) = r_0^2 + \frac{\theta q_{prod}}{\pi\phi h}\frac{df_w(S_w)}{dS_w}(t - t_{foff}), \tag{3.170}$$

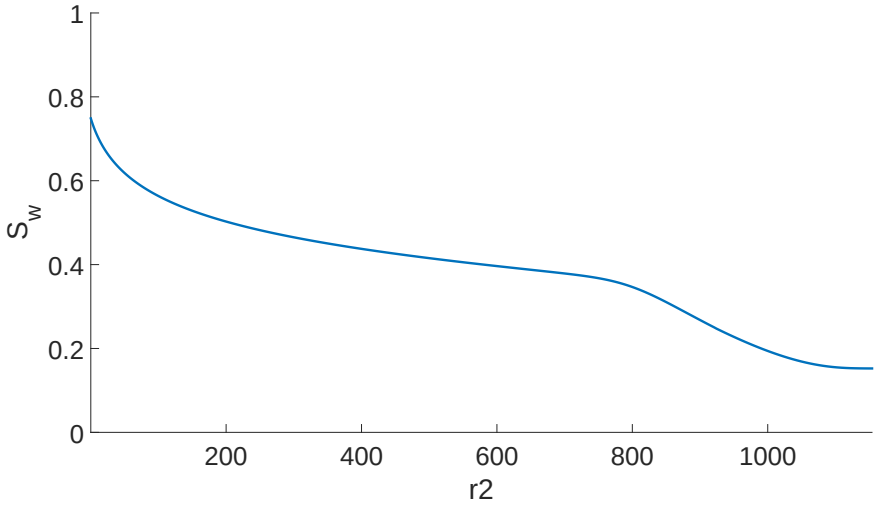

Figure 3.21: Saturation profile at a time t before the wave breaking time.

for any $S_w \in (S_{iw}, 1 - S_{or})$, where $r_0 = r(S_w, t_{foff})$. Remember that $q_{prod} < 0$, which means that the saturation waves are travelling towards the wellbore, they are flowing back.

Stage 2: Between wave breaking time and shock breakthrough, $t \in (t_{bt}, t_{BT})$ We can develop a solution analogue to the one described for the injection period by employing the flowback solution presented in Chapter 2 as the outer solution, with same initial condition for both outer and global solution, adopting a transient traveling wave as the inner solution. This approximate solution obtained with the method of matched asymptotic expansion would be valid for any time after the Buckley-Leverett saturation wave (outer solution) breaking time. Fig. 3.21 shows the saturation profile in the reservoir at a time t before the wave breaking time.

Outer solution, S_w^{BL} After the gradient catastrophe occurs, we need to solve the system of equations showed in Chapter 2 to get the shock position and the shock saturations. If the initial condition for production was the same without p_c, we would have the expression derived in Chapter 2, which is untrue. So, we need to derive an equation to find the shock position with the initial condition as the saturation distribution at the end of the falloff. As explained in Chapter 2, since the solution must satisfy the weak form of the BL equation,

the area under the discontinuous saturation profile (weak solution) must be the same as the area under the multivalued wave profile in Fig. 3.22, which we know satisfies conservation of mass [102]. Therefore, the conservation law implies that we must have,

$$\int_{S_w^+}^{S_w^*}(r^2 - r_s^2)dS_w = \int_{S_w^*}^{S_w^-}(r_s^2 - r^2)dS_w, \tag{3.171}$$

at a time t such that $A_1 = A_2$, where

$$r^2 = \left(r_{foff}^2 - \frac{\theta q_{prod}\Delta t_{prod}}{\pi\phi h}\frac{df_w}{dS_w}\right). \tag{3.172}$$

Eq. 3.171 can be rearranged as

$$\int_{S_w^+}^{S_w^-}(r^2 - r_s^2)dS_w = 0. \tag{3.173}$$

Inserting Eq. 3.172 into Eq. 3.174, yields

$$\int_{S_w^+}^{S_w^-}(r_{foff}^2 - \frac{\theta q_{prod}\Delta t_{prod}}{\pi\phi h}\frac{df_w}{dS_w} - r_s^2)dS_w = 0, \tag{3.174}$$

leading to

$$r_s^2(t) = \frac{\int_{S_w^+}^{S_w^-} r_{foff}^2 dS_w}{[S_w^- - S_w^+]} - \frac{\theta q_{prod}\Delta t_{prod}}{\pi\phi h}\frac{[f_w(S_w^-) - f_w(S_w^+]}{[S_w^- - S_w^+]}. \tag{3.175}$$

We also know that the saturation position ahead the shock is given by,

$$r_s^2 = r_{foff}^2(S_w^+) - \frac{\theta q_{prod}\Delta t_{prod}}{\pi\phi h}\frac{df_w}{dS_w}(S_w^+), \tag{3.176}$$

while the saturation position behind the shock is,

$$r_s^2 = r_{foff}^2(S_w^-) - \frac{\theta q_{prod}\Delta t_{prod}}{\pi\phi h}\frac{df_w}{dS_w}(S_w^-), \tag{3.177}$$

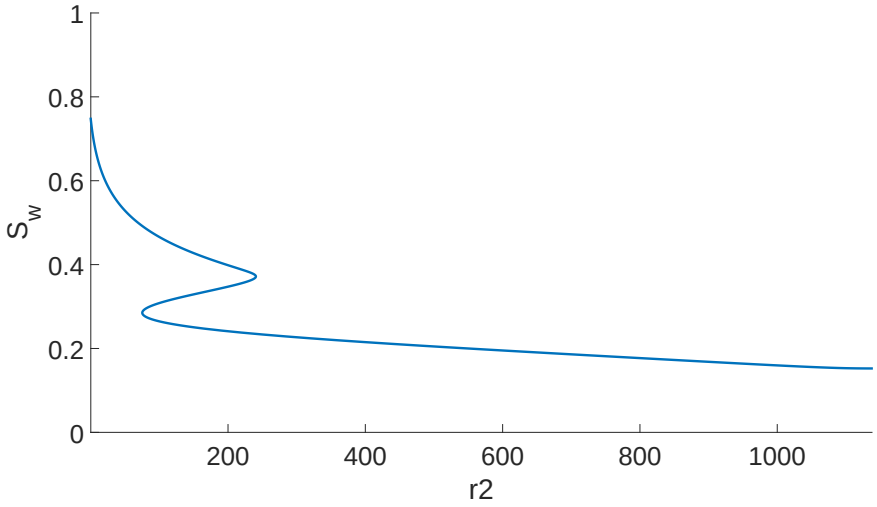

(a)

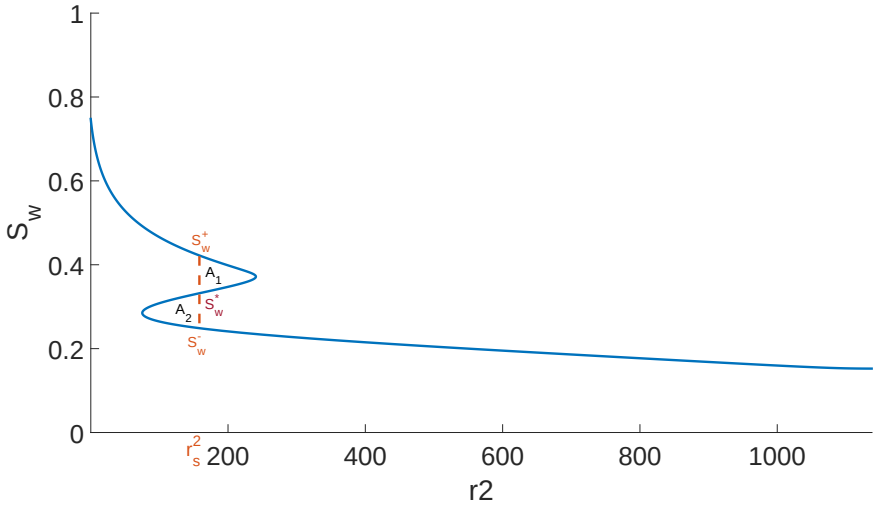

(b)

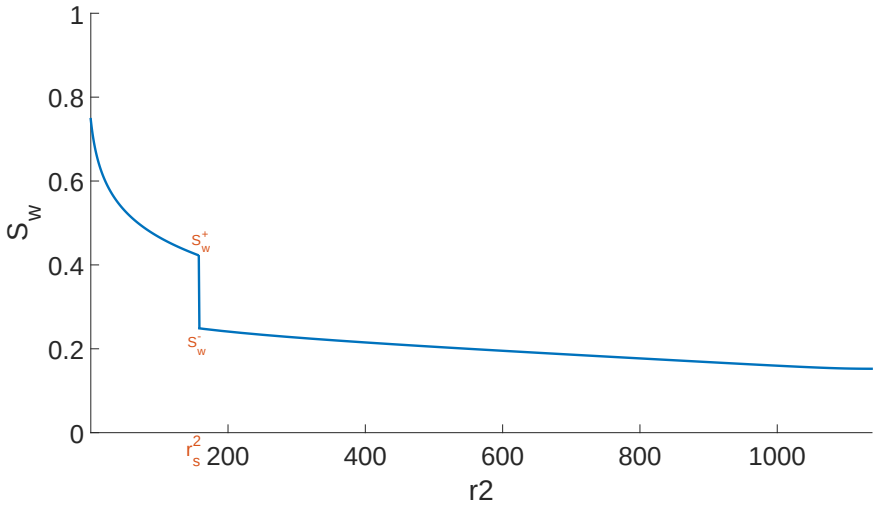

(c)

Figure 3.22: Non-physical multivalued saturation profile during flowback (a), area equality shock fitting (b) and physical solution (c).

where $S_w^+ > S_w^* > S_w^-$. We can solve this system numerically using Newton-Raphson's method [90].

Inner Solution, S_w^{SL} Once again, to find the inner solution, and subsequently, the global saturation distribution, we define the traveling wave stretching coordinate w, defined by Eq. 3.37 to transform the governing PDE (Eq. 3.21) from $(r,t) \to (w,\tau)$, where $w = w(r,t)$ and $\tau = t$. In this case, $S_w = S_w(w,\tau)$ and w depends on τ. Using the chain rule and Eq.3.37, we obtain

$$\frac{\partial S_w}{\partial t} = \frac{\partial S_w}{\partial \tau} + \frac{\partial S_w}{\partial w}\frac{\partial w}{\partial \tau} = \frac{\partial S_w}{\partial \tau} - \frac{1}{\epsilon}\frac{\partial S_w}{\partial w}\frac{dr_s^2}{d\tau} = \frac{\partial S_w}{\partial \tau} - \frac{1}{\epsilon}\frac{\partial S_w}{\partial w}\frac{\theta q_{prod}}{\pi\phi h}\frac{[f_w(S_w^-) - f_w(S_w^+)]}{[S_w^- - S_w^+]}, \tag{3.178}$$

where the equality used Eq. 3.175 to find $\frac{dr_s^2}{d\tau} = \frac{dr_s^2}{dt}\frac{dt}{d\tau}$. Rearranging Eq. 3.178 and using Eq. 3.178, Eq. 3.40 and Eq. 3.41, Eq 3.21 can be rewritten as follows

$$\epsilon\frac{\pi\phi h}{\theta q_{prod}}\frac{\partial S_w}{\partial \tau} - \frac{[f_w(S_w^-) - f_w(S_w^+)]}{[S_w^- - S_w^+]}\frac{\partial S_w}{\partial w} + \frac{\partial f_w}{\partial w} - \frac{\partial}{\partial w}\left(2r^2k(r)\frac{\partial \Psi}{\partial w}\right) = 0. \tag{3.179}$$

Letting $\epsilon \to 0$ in Eq. 3.179, we have

$$-\frac{[f_w(S_w^-(\tau)) - f_w(S_w^+(\tau))]}{[S_w^-(\tau) - S_w^+(\tau)]}\frac{\partial S_w}{\partial w} + \frac{\partial f_w}{\partial w} - \frac{\partial}{\partial w}\left(2r_s^2(\tau)k(r_s(\tau))\frac{\partial \Psi}{\partial w}\right) = 0, \tag{3.180}$$

where $r^2 = \epsilon w + r_S^2(\tau) \to r_s^2(\tau)$ as $\epsilon \to 0$; $r_s^2(\tau)$ is

$$r_s^2(\tau) = \frac{\int_{S_w^+(\tau)}^{S_w^-(\tau)} r_{foff}^2 dS_w}{[S_w^-(\tau) - S_w^+(\tau)]} - \frac{\theta q_{prod}\tau}{\pi\phi h}\frac{[f_w(S_w^-(\tau)) - f_w(S_w^+(\tau)]}{[S_w^-(\tau) - S_w^+(\tau)]}. \tag{3.181}$$

Integrating Eq. 3.180 with to respect to w gives

$$-\frac{[f_w(S_w^-(\tau)) - f_w(S_w^+(\tau))]}{[S_w^-(\tau) - S_w^+(\tau)]}S_w + f_w - \left(2r_s^2(\tau)k\frac{\partial \Psi}{\partial w}\right) = b(\tau), \tag{3.182}$$

We can find the $b(\tau)$ from the boundary conditions:

$$\lim_{w\to\infty} S_w(\tau, w) = S_w^-(\tau) \tag{3.183}$$

and

$$\lim_{w\to-\infty} S_w(\tau, w) = S_w^+(\tau), \tag{3.184}$$

for $\tau > 0$. Since, as discussed when developing the injection solution, we assume that S_w goes asymptotically to $Sw^-(\tau)$ and $Sw^+(\tau)$, such that $\frac{\partial S_w}{\partial w} \to 0$ as $w \to \pm\infty$, we have $\frac{\partial \Psi}{\partial w} = \frac{\partial \Psi}{\partial S_w}\frac{\partial S_w}{\partial w} \to 0$ as $w \to \pm\infty$. So, letting $w \to -\infty$ in Eq. 3.182 gives

$$b(\tau) = -\frac{[f_w(S_w^-(\tau)) - f_w(S_w^+(\tau))]}{[S_w^-(\tau) - S_w^+(\tau)]} S_w^+(\tau) + f_w(S_w^+(\tau)). \tag{3.185}$$

Using Eq. 3.185 together with Eq. 3.182 and rearranging the resulting equation, yields

$$2r_s^2(\tau)k(r_s^2(\tau))\frac{d\Psi}{dS_w}\frac{\partial S_w}{\partial w} = -\frac{[f_w(S_w^-(\tau)) - f_w(S_w^+(\tau))]}{[S_w^-(\tau) - S_w^+(\tau)]}(S_w - S_w^+(\tau)) + (f_w - f_w(S_w^+(\tau))), \tag{3.186}$$

which can be rearranged and integrated from wellbore to w to give

$$2r_s^2(\tau)k(r_s^2(\tau))\int_{S_{w,well}}^{S_w} \frac{\frac{d\Psi}{dS_w}}{(f_w - f_w(S_w^+(\tau))) - \frac{[f_w(S_w^- r_s^2(\tau)) - f_w(S_w^+ r_s^2(\tau))]}{[S_w^- r_s^2(\tau) - S_w^+ r_s^2(\tau)]}(S_w - S_w^+ r_s^2(\tau))} dS_w = w - w_{well}, \tag{3.187}$$

at any $\tau > 0$ where $S_w = S_w(\tau, w)$ and $S_{w,well} = S_w(\tau, w_{well}) = S_w(\tau, w(r_w, \tau))$. $S_{w,well}$ can be determined by a material balance analogous to what was done to derive the injection period solution.

Matching Saturation, S_w^{SH} The matching saturation S_w^{SH} defined using the matching principle by applying Prandtl's technique [72] in the production period is given by

$$S_w^{SH}(r,t) = \begin{cases} S_w^-(t) & r^2 \geq r_s^2(t) \\ S_w^+(t) & r_w^2 \leq r^2 < r_s^2(t). \end{cases} \tag{3.188}$$

Material Balance In this case, the amount of water injected minus the amount produced must be the same as the amount of mobile water present in the reservoir, i.e,

$$q_{inj}t_{inj} - \int_{t_{foff}}^{t} q_{prod}F_w(S_w(r_w,t))dt = \int_{r_w}^{\infty}(S_w(r,t) - S_{iw})2\pi rhdr, \tag{3.189}$$

where $S_w(r,t)$ is the water saturation value during the flowback period. The same statement is true for the saturation solution neglecting the capillary pressure effects:

$$q_{inj}t_{inj} - \int_{t_{foff}}^{t} q_{prod}f_w(S_w^{BL}(r_w,t))dt = \int_{r_w}^{\infty}(S_w^{BL}((r,t)) - S_{iw})2\pi rhdr. \tag{3.190}$$

Solving both Eqs. 3.189 and 3.190 for $q_{inj}t_{inj}$, gives

$$\begin{aligned} &\int_{t_{foff}}^{t} q_{prod}F_w(S_w(r_w,t))dt + \int_{r_w}^{\infty}(S_w(r,t) - S_{iw})2\pi rhdr = \\ &\int_{t_{foff}}^{t} q_{prod}f_w(S_w^{BL}(r_w,t))dt + \int_{r_w}^{\infty}(S_w^{BL}((r,t)) - S_{iw})2\pi rhdr. \end{aligned} \tag{3.191}$$

Using Eq. 3.31 in Eq. 3.191and rearranging the resulting equation gives

$$\int_{r_w^2}^{\infty}(S_w^{SL}(r,t) - S_w^{SH}(r,t))\pi d(r^2) + q_{prod}\int_{t_{foff}}^{t} F_w(S_w(r_w,t)) - f_w(S_w^{BL}(r_w,t))dt = 0. \tag{3.192}$$

At $r = r_w$, we assumed that $p_c = 0$, which means $F_w = f_w$. So, we can rewrite Eq. 3.192 as

$$\int_{r_w^2}^{\infty}(S_w^{SL} - S_w^{SH})\pi d(r^2) + q_{prod}\int_{t_{foff}}^{t} f_w(S_w(r_w,t)) - f_w(S_w^{BL}(r_w,t))dt = 0. \tag{3.193}$$

We can approximate the water fractional flow by using a Taylor expansion around S_w^{BL},

$$f_w(S_w) \approx f_w(S_w^{BL} + S_w^{SL} - S_w^{SH}) \approx f_w(S_w^{BL}) + (S_w^{SL} - S_w^{SH})\frac{df_w(S_w^{BL})}{dS_w}. \tag{3.194}$$

Note that Eq. 3.194 is different from the approximation made by Deng and King [38] for the injection case. In that they assumed that the term $\frac{df_w(S_w^{BL})}{dS_w}$ is a constant equal to the shock speed by using the method of matched asymptotic expansion to find a composite solution for f_w. Their approximation is only valid and equivalent to the Taylor expansion for this very specific injection case. Their procedure would give the incorrect water fractional flow value for the production period, where both shock saturations are mobile. Using Eq. 3.194 in Eq. 3.193, yields,

$$\int_{r_w^2}^{\infty}(S_w^{SL} - S_w^{SH})d(r^2) + \frac{q_{prod}}{\pi}\int_{t_{foff}}^{t}(S_w^{SL}(r_w,t) - S_w^{SH}(r_w,t))\frac{df_w(S_w^{BL}(r_w,t))}{dS_w}dt = 0, \tag{3.195}$$

which can be rearranged as

$$\int_{r_w^2}^{\infty} S_w^{SL}d(r^2) + \frac{q_{prod}}{\pi}\int_{t_{foff}}^{t} S_w^{SL}(r_w,t)\frac{df_w(S_w^{BL}(r_w,t))}{dS_w}dt = S_w^{+}(t)(r_s^2 - r_w^2) + S_w^{-}(t)\int_{r_s^2}^{\infty} d(r^2) + \frac{q_{prod}}{\pi}\int_{t_{foff}}^{t} S_w^{+}(t)\frac{df_w(S_w^{BL}(r_w,t))}{dS_w}dt, \tag{3.196}$$

using Eq. 3.188 and assuming $S_w^{SH}(r_w,t) = S_w^{+}(t)$ for $t < t_{BT}$. For $t \geq t_{TB}$, as mentioned previously, we will not use the composition solution obtained using the method of asymptotic expansion. So, we do not need to solve Eq. 3.195 after the oil shock breakthrough. When neglecting hysteresis effects in the relative permeability curves, $S_w^{BL}(r_w,t) = 1 - S_{or}$ and

Eq. 3.196 becomes

$$\int_{r_w^2}^{\infty} S_w^{SL} d(r^2) + \frac{q_{prod}}{\pi} \frac{df_w(1-S_{or})}{dS_w} \int_{t_{foff}}^{t} S_w^{SL}(r_w,t)dt = S_w^+(t)(r_s^2 - r_w^2) + S_w^-(t) \int_{r_s^2}^{\infty} d(r^2) + \frac{q_{prod}}{\pi} \frac{df_w(1-S_{or})}{dS_w} \int_{t_{foff}}^{t} S_w^+(t)dt. \tag{3.197}$$

Since $\frac{df_w(1-S_{or})}{dS_w} = 0$ for our S-shaped f_w curve, we have

$$\int_{r_w^2}^{\infty} S_w^{SL} d(r^2) = S_w^+(t)(r_s^2(t) - r_w^2) + S_w^-(t) \int_{r_s^2(t)}^{\infty} d(r^2), \tag{3.198}$$

for $t < t_{BT}$. t_{BT} can be obtained from the solution without capillary pressure, the outer solution, by solving the system of Eqs. 3.175, 3.176 and 3.177 for t at $r_s = r_w$. We can rewrite Eq. 3.198 as

$$\int_{r_w^2}^{\infty} S_w^{SL} d(r^2) = S_w^+(t)(r_s^2(t) - r_w^2) + \left(S_w^-(t) \int_{r_w^2}^{\infty} dr^2 - S_w^-(t) \int_{r_w^2}^{r_s^2(t)} d(r^2) \right). \tag{3.199}$$

Using Eq. 3.38 in Eq. 3.199, it follows that

$$\int_{r_w^2}^{\infty} S_w^{SL} d(r^2) = (S_w^+(t) - S_w^-(t))(r_s^2(t) - r_w^2)CDt + S_w^-(t) \int_{r_w^2}^{\infty} d(r^2). \tag{3.200}$$

Transforming Eq. 3.200 from $(r,t) \rightarrow (w,\tau)$ and using Eq. 3.37, Eq. 3.200 becomes

$$\epsilon \int_{-\frac{CD\tau}{\epsilon}}^{\infty} S_w^{SL}(w)dw = (S_w^+(t) - S_w^-(t))CD\tau + \epsilon S_w^-(t) \int_{-\frac{CD\tau}{\epsilon}}^{\infty} dw. \tag{3.201}$$

From Eq. 3.186,

$$dw = 2r_s^2(\tau)k(r_s^2(\tau)) \frac{\frac{d\Psi}{dS_w}}{-\frac{[f_w(S_w^-(\tau)) - f_w(S_w^+(\tau))]}{[S_w^-(\tau) - S_w^+(\tau)]}(S_w^{SL} - S_w^+(\tau)) + (f_w - f_w(S_w^+(\tau)))} \tag{3.202}$$

Substituting Eq. 3.202 in Eq. 3.201 gives

$$\epsilon 2r_s^2 k(r_s^2) \int_{S_w^{SL}(-\frac{CD\tau}{\epsilon})}^{S_w^-} \frac{S_w^{SL}\frac{d\Psi}{dS_w}}{-\frac{[f_w(S_w^-(\tau))-f_w(S_w^+(\tau))]}{[S_w^-(\tau)-S_w^+(\tau)]}(S_w^{SL}-S_w^+(\tau))+(f_w-f_w(S_w^+(\tau)))} dS_w^{SL}$$
$$= (S_w^+ - S_w^-)CD\tau + \epsilon S_w^- \int_{-\frac{CD\tau}{\epsilon}}^{\infty} dw. \tag{3.203}$$

Dividing Eq. 3.203 by ϵS_w^- and solving the resulting equation for $\int_{-\frac{CD\tau}{\epsilon}}^{\infty} dw$ gives

$$\int_{-\frac{CD\tau}{\epsilon}}^{\infty} dw = \frac{2r_s^2 k(r_s^2)}{S_w^-} \int_{S_w^{SL}(-\frac{CD\tau}{\epsilon})}^{S_w^-} \frac{S_w^{SL}\frac{d\Psi}{dS_w}}{-\frac{[f_w(S_w^-(\tau))-f_w(S_w^+(\tau))]}{[S_w^-(\tau)-S_w^+(\tau)]}(S_w^{SL}-S_w^+(\tau))+(f_w-f_w(S_w^+(\tau)))} dS_w^{SL}$$
$$- \frac{(S_w^+ - S_w^-)CD\tau}{\epsilon S_w^-}. \tag{3.204}$$

Setting $S_w = S_w^-$ in the upper limits of the integrals of Eq. 3.187 and exchanging the two sides of the equation yields,

$$\int_{-\frac{CD\tau}{\epsilon}}^{\infty} dw = 2r_s^2 k(r_s^2) \int_{S_w^{SL}(-\frac{CD\tau}{\epsilon})}^{S_w^-} \frac{\frac{d\Psi}{dS_w}}{-\frac{[f_w(S_w^-)-f_w(S_w^+)]}{[S_w^- - S_w^+]}(S_w^{SL}-S_w^+)+(f_w-f_w(S_w^+))} dS_w^{SL}. \tag{3.205}$$

As the left sides of Eqs 3.204 and 3.205 are the same, the right sides of these two equations must be equal which gives

$$2r_s^2 k(r_s^2) \int_{S_w^{SL}(-\frac{CD\tau}{\epsilon})}^{S_w^-} \frac{\frac{d\Psi}{dS_w}}{D(S_{iw}-S_w^{SL})+f_w} dS_w^{SL} = -\frac{(S_w^+ - S_w^-)CD\tau}{\epsilon S_w^-}$$
$$+ \frac{2r_s^2 k(r_s^2)}{S_w^-} \int_{S_w^{SL}(-\frac{CD\tau}{\epsilon})}^{S_w^-} \frac{S_w^{SL}\frac{d\Psi}{dS_w}}{-\frac{[f_w(S_w^-)-f_w(S_w^+)]}{[S_w^- - S_w^+]}(S_w^{SL}-S_w^+)+(f_w-f_w(S_w^+))} dS_w^{SL}, \tag{3.206}$$

Multiplying Eq. 3.206 by ϵS_w^- and rearranging the resulting equation gives

$$2r_s^2 k(r_s^2)\epsilon \int_{S_w^{SL}(-\frac{CD\tau}{\epsilon})}^{S_w^-} \frac{(S_w^{SL}-S_w^-)\frac{d\Psi}{dS_w}}{-\frac{[f_w(S_w^-)-f_w(S_w^+)]}{[S_w^- - S_w^+]}(S_w^{SL}-S_w^+)+(f_w-f_w(S_w^+))} dS_w^{SL} = (S_w^+ - S_w^-)CD\tau. \tag{3.207}$$

Once the value $S_w^{SL}(-\frac{CD\tau}{\epsilon})$ (i.e., the inner solution saturation in the wellbore, $S_w^{SL}(w_{well})$) is determined numerically by solving Eq. 3.207 using the bisection method [90] at each time τ, Eq. 3.187 is used to determine the saturation profile in the stabilized zone.

Stage 3: After shock breakthrough, $t > t_{BT}$ After the oil front breakthrough, the capillary pressure effects become negligible as the shock dematerializes (and consequently, the high saturation gradient values that were present in the shock layer vanish). Thus, we can use the saturation profile at $t = t_{BT}$ as initial condition to find the saturation distribution during flowback after oil breakthrough by solving $S_w(r,t) = S_w^{BL}(r,t)$, similarly as done before the wave breaking time.

Here, as in Stage 1, we solve Eq. 3.1 to estimate the saturation distribution $S_w(r,t)$ for any $t > t_{BT}$, where the initial condition is given by the saturation distribution at the time of breakthrough. In this case we have the following Cauchy problem,

$$\begin{cases} \frac{\partial S_w}{\partial t} + \frac{\theta q}{\phi 2\pi r h}\frac{\partial f_w(S_w)}{\partial r} = 0, \\ S_w(r, t_{BT}) = S_w(r_0), \qquad r > r_w, \end{cases} \tag{3.208}$$

whose strong solution is given by

$$r^2(S_w, t) = r_0^2 + \frac{\theta q_{prod}}{\pi\phi h}\frac{df_w(S_w)}{dS_w}(t - t_{foff}), \tag{3.209}$$

for any $S_w \in (S_{iw}, S_{w,well})$, where $r_0 = r(S_w, t_{BT})$. Remember, t_{BT} can be obtained from the solution without capillary pressure, the outer solution, by solving the system of Eqs. 3.175, 3.176 and 3.177 for t at $r_s = r_w$.

Note on Heterogeneity If there is a skin zone, the heterogeneity in the absolute permeability will affect only the solution with capillary effect, which might leading to a difference between both saturation distributions (with and without capillary effects) at the moment those waves reach the skin radius and this discrepancy should reflect in the wellbore pressure

drop as well. We would not be able to see that in numerical simulation if use skin factor instead of actually"adding" a skin zone in the numerical grid. The steady-state theory predicts sharp changes in saturation when regions of permeability change are traversed. The static capillary continuity criterion requires an a step-like change in saturation across the jump from high permeability to low permeability [25, 26], i.e., across the skin zone interface. Chaouche et al. [26] showed that heterogeneities effects mitigate as the flow rate increases. Considering we are already assuming a steady-state condition around the wellbore and that the well test flow rate condition is high enough, we have one more argument in favor of neglecting capillary pressure while estimating saturation distribution and wellbore pressure response during the flowback period. However, as we can see in Fig. 3.2, for a short period of time around the oil front breakthrough time, there is a large discrepancy in the wellbore pressure. If we want to estimate capillary pressure curves, we need to consider capillary pressure. To do that, we have one more condition, mass conservation across the skin zone interface, the fluid flux condition [100],

$$F_w(r_{skin}^-, t) = F_w(r_{skin}^+, t), \tag{3.210}$$

which is obtained form the integral form of integral form of Eq. 3.21,

$$\frac{d}{dt}\int_{a^2}^{b^2} S_w(r,t)\pi d(r^2) = \frac{q_t}{\phi h}(F_w(a,t) - F_w(b,t)), \tag{3.211}$$

which we split into two regions for a fixed point $(r_{skin}, t) \in (a, b)$ to obtain

$$\frac{d}{dt}\Big(\int_{a^2}^{r_{skin}^{-2}} S_w(r,t)\pi d(r^2) + \int_{r_{skin}^{+2}}^{b^2} S_w(r,t)\pi d(r^2)\Big) = \frac{q_t}{\phi h}(F_w(a,t) - F_w(b,t)), \tag{3.212}$$

where $r^-_{skin} = r_{skin} - \epsilon$ and $r^+_{skin} = r_{skin} + \epsilon$, with constant ϵ. Applying Leibniz rule in the integrals of Eq. 3.212

$$\int_{a^2}^{r^{-2}_{skin}} \frac{\partial S_w(r,t)}{\partial t} d(r^2) + S_w(r^-_{skin},t)\frac{dr^{-2}_{skin}}{dt} + \int_{r^{+2}_{skin}}^{b^2} \frac{\partial S_w}{\partial t}(r,t)d(r^2) - S_w(r^+_{skin},t)\frac{dr^{+2}_{skin}}{dt} = \frac{q_t}{\phi\pi h}(F_w(a,t) - F_w(b,t)), \quad (3.213)$$

Letting $a \to r^-_{skin}$, $b \to r^+_{skin}$ and $\epsilon \to 0$ in Eq. 3.213 and simplifying,

$$F_w(S_w(r^-_{skin},t)) - F_w(S_w(r^+_{skin},t)) = \frac{\pi\phi h}{\theta q_{prod}}\frac{dr^2_{skin}}{dt}(S_w(r^-_{skin},t) - S_w(r^+_{skin},t)). \quad (3.214)$$

Since $\frac{dr^2_{skin}}{dt} = 0$, we have

$$F_w(S_w(r^-_{skin},t)) - F_w(S_w(r^+_{skin},t)) = 0. \quad (3.215)$$

Throughout this work we have assumed that porosity is homogeneous in the reservoir; that is the basis for the analytical solutions derived for the Buckley-Leverett equation. When we assume that the only rock property that changes in the skin zone is the absolute permeability, we need to guarantee pressure continuity across the skin radius [100]. Here, as is typically done, we assume that one capillary pressure curve applies throughout the reservoir including the skin zone, which means there will not be a discontinuity at saturation in the interface, i.e., $S^(_w w_{skin}) = S^-_w(w_{skin}) = S^+_w(w_{skin})$. We can use Eq. 3.53,

$$2r_s^2 k \int_{S_{iw}}^{S_w} \frac{\frac{d\Psi}{dS_w}}{D(S_{iw} - S_w) + f_w} dS_w = w - w_0, \quad (3.216)$$

to find the saturation distribution in the non-skin zone region, then we need to solve Eq. 3.216 at $w_{skin} = w(r_{skin}, t)$ to find $S_w(r_{skin}, t)$,

$$2r_s^2 k \int_{S_{iw}}^{S_w(w_{skin})} \frac{\frac{d\Psi}{dS_w}}{D(S_{iw} - S_w) + f_w} dS_w = w_{skin} - w_0, \quad (3.217)$$

and then calculate the saturation distribution in the other region with,

$$2r_s^2 k_s \int_{S_w(w_{skin})}^{S_w} \frac{\frac{d\Psi}{dS_w}}{D(S_{iw} - S_w) + f_w} dS_w = w - w_{skin}. \tag{3.218}$$

When the reservoir permeability is modified by the drilling fluid invasion, it is usually assumed that it does not affect the capillary pressure curve when running numerical simulations. Therefore, we would not be able to see an interface jump in saturation across the skin zone. However, we could only know if this assumption is indeed reasonable and how it would affect the wellbore pressure response through real/lab data analysis. In the case of considering two different capillary pressure curves, both given by

$$p_c(S_w, r) = \sigma \sqrt{\frac{\phi}{k(r)}} J(S_w), \tag{3.219}$$

for a damaged reservoir, to guarantee pressure continuity (i.e, $p_c(S_w(r_{skin}^-, t)) = p_c(S_w(r_{skin}^+, t))$), we must have [100],

$$J(S_w(r_{skin}^+, t)) = \sqrt{\frac{k_s}{k}} J(S_w(r_{skin}^-, t)). \tag{3.220}$$

So, if we knew the J-curve, we could find $S_w(r_{skin}^+, t)$.

3.1.2 Wellbore Pressure History

As shown in Chapter 2, the IFPT pressure solutions used in this work are derived following the Peres and Reynolds [78] procedure, which assumes the validity the Thompson and Reynolds [98] steady-state theory. As mentioned previously, after finding the saturation distribution, we can obtain the wellbore pressure by applying the pressure solutions presented by Peres et al. [82], Chen [28], Chen et al. [31].

Injection: During injection at a constant flow rate, $q_t(r_w, t)$ RB/D, where $t = 0$ at the beginning of the water injection, by integrating the pressure gradient expression for the total liquid flow rate given by Darcy's law as in Thompson and Reynolds [98], Peres and

Reynolds [79], given by

$$q_t = -\frac{k(r)hr}{\alpha}\left(\lambda_o \frac{\partial p_o}{\partial r} + \lambda_w \frac{\partial p_w}{\partial r}\right). \tag{3.221}$$

Substituting $p_w = p_o - p_c$ into Eq. 3.221, yields

$$q_t = -\frac{k(r)hr}{\alpha}\left(\lambda_o \frac{\partial p_o}{\partial r} + \lambda_w \frac{\partial (p_o - p_c)}{\partial r}\right), \tag{3.222}$$

or equivalently

$$q_t = -\frac{k(r)hr}{\alpha}\left(\lambda_t \frac{\partial p_o}{\partial r} - \lambda_w \frac{\partial p_c}{\partial r}\right). \tag{3.223}$$

Eq. 3.223 can be rearranged to obtain

$$\frac{\partial p_o}{\partial r} = -\frac{\alpha q_t}{k(r)hr\lambda_t} + \frac{\lambda_w}{\lambda_t}\frac{dp_c}{dS_w}\frac{\partial S_w}{\partial r}. \tag{3.224}$$

Integrating Eq. 3.224 assuming an infinite-acting reservoir, the bottom hole pressure difference from the reservoir initial pressure (p_{oi}) can be expressed as

$$\Delta p_{wf}(t) = p_{wf}(t) - p_{oi} = \int_{r_w}^{\infty} \frac{\alpha q_t(r,t)}{h\lambda_t(r,t)k(r)}\frac{dr}{r} - \int_{r_w}^{\infty} f_w \frac{dp_c}{dS_w}\frac{\partial S_w}{\partial r} dr, \tag{3.225}$$

where it is assumed that $p_o(r_w, t) = p_w(r_w, t)$, i.e., $p_c = 0$ at $r = r_w$, to satisfy the compatibility condition [92], i,e, to guarantee phases pressure continuity at the wellbore ($r = r_w$). Although this statement seems to contradict the discussion presented when solving for saturation, it is an assumption that simplifies the pressure governing equation and gives us an solution. Since the numerical simulator - our only validation tool available - assumes the same as we do, it is not possible for us to show here that this assumption gives indeed an accurate wellbore pressure response estimate. Eq. 3.225 can be rewritten as

$$\Delta p_{wf}(t) = \int_{r_w}^{\infty} \frac{\alpha q_t(r,t)}{h\lambda_t(r,t)k(r)}\frac{dr}{r} - \int_{r_w}^{r_{wf(t)}} f_w \frac{dp_c}{dS_w}\frac{\partial S_w}{\partial r} dr, \tag{3.226}$$

by assuming that

$$-\int_{r_{wf(t)}}^{\infty} f_w \frac{dp_c}{dS_w}\frac{\partial S_w}{\partial r}dr = 0, \tag{3.227}$$

considering $f_w(S_{iw}) = 0$ and $\frac{\partial S_w}{\partial r} = 0$ for $r > r_{wf}(t)$, since the water in the region ahead of the water front foot is assumed immobile. r_{wf} can be defined as the position at which $S_w - S_{iw} < \delta$, where δ is a very small number. Using the [98] steady-state theory, which assumes that, $q_t(r,t) = q(r_w,t)$, for $r \leq r_{wf}(t)$, Eq. 3.226 becomes

$$\Delta p_{wf}(t) = \frac{\alpha q_{r_w,t}}{h}\int_{r_w}^{r_{wf}(t)} \frac{1}{\lambda_t(r,\Delta t_{prod})k(r)}\frac{dr}{r} + \frac{\alpha}{h}\int_{r_{wf}(t)}^{\infty}\frac{q_t(r,t)}{\lambda_t(r,t)k(r)}\frac{dr}{r} - \int_{r_w}^{r_{wf}(t)} f_w\frac{dp_c}{dS_w}\frac{\partial S_w}{\partial r}dr, \tag{3.228}$$

where for any practical set of values of physical properties, [78] indicate that this assumption is valid. Adding and subtracting the term

$$\frac{\alpha}{h}\int_{r_w}^{r_{wf}(t)}\frac{q_t(r_w,t)}{\hat{\lambda}_o k(r)}\frac{dr}{r},$$

where $\hat{\lambda}_o = \frac{k_{ro}(S_{wi})}{\mu_o}$ is the endpoint oil mobility at $S_w = S_{wi}$, Eq. 3.228 can be rewritten as

$$\begin{aligned}\Delta p_{wf}(t) =& \frac{\alpha}{h}\int_{r_w}^{\infty}\frac{q_t(r,t)}{\hat{\lambda}_o(r,t)k(r)}\frac{dr}{r} + \frac{\alpha q_t(r_w,t)}{h}\int_{r_w}^{r_{wf}(t)}\left(\frac{1}{\lambda_t(r,t)} - \frac{1}{\hat{\lambda}_o}\right)\frac{dr}{k(r)r} - \int_{r_w}^{r_{wf}(t)} f_w\frac{dp_c}{dS_w}\frac{\partial S_w}{\partial r}dr \\ =& \Delta\hat{p}_o(t) + \frac{\alpha q_t(r_w,t)}{h\hat{\lambda}_o}\int_{r_w}^{r_{wf}(t)}\Big(\frac{\hat{\lambda}_o}{\lambda_t(r,t)} - 1\Big)\frac{1}{k(r)}\frac{dr}{r} - \int_{r_w}^{r_{wf}(t)} f_w\frac{dp_c}{dS_w}\frac{\partial S_w}{\partial r}dr.\end{aligned} \tag{3.229}$$

$\Delta\hat{p}_o(t)$ is the single-phase oil transient pressure drop, the known pressure drop solution that is obtained if we inject oil into an oil reservoir (injection period), whose well known

approximate solution is given by [89]

$$\Delta\hat{p}_o(t) = p_{wf,o}(t) - p_{oi} = \frac{\alpha q_t}{kh\hat{\lambda}_o}\left[\frac{1}{2}\ln\left(\frac{\beta k\hat{\lambda}_o t}{\phi\hat{c}_{to}r_w^2}\right) + 0.4045 + s\right]. \tag{3.230}$$

Here, β is a unit conversion factor which in oil field units is 0.0002637 and the single-phase total compressibility is

$$\hat{c}_{to} = c_o(1 - S_{or}) + c_w S_{wi} + c_r. \tag{3.231}$$

Falloff: During falloff, differently as presented in Chapter 2, we de not assume that the saturation distribution remains constant and equal to the distribution at the end of injection period. Therefore, the bottom hole pressure drop during falloff can be expressed as

$$\Delta p_{ws}(\Delta t_{foff}) = p_{ws}(\Delta t_{foff}) - p_{oi} = \int_{r_w}^{\infty} \frac{\alpha q_s(r, \Delta t_{foff})}{h\lambda_t(r, \Delta t_{foff})k(r)}\frac{dr}{r} - \int_{r_w}^{\infty} f_w \frac{dp_c}{dS_w}\frac{\partial S_w}{\partial r}dr, \tag{3.232}$$

where $\Delta t_{foff} = 0$ at the beginning of the falloff period and $p_{ws}(\Delta t_{foff})$ denotes the falloff pressure at time Δt_{foff}. Eq. 3.232 can be rewritten as

$$\begin{aligned}\Delta p_{ws}(\Delta t_{foff}) = \frac{\alpha}{h}\int_{r_w}^{r_{wf}(\Delta t_{foff})} \frac{q_s(r, \Delta t_{foff})}{\lambda_t(r, \Delta t_{foff}))k(r)}\frac{dr}{r} + \frac{\alpha}{h}\int_{r_{wf}(\Delta t_{foff})}^{\infty} \frac{q_s(r, \Delta t_{foff})}{\lambda_t(r, \Delta t_{foff}))k(r)}\frac{dr}{r} \\ - \int_{r_w}^{r_{wf}(\Delta t_{foff})} f_w \frac{dp_c}{dS_w}\frac{\partial S_w}{\partial r}dr,\end{aligned} \tag{3.233}$$

where $q_s(r, \Delta t_{foff})$ is the total flow rate profile at shut-in time, Δt_{foff}. Following Peres et al. [81] and Chen [28], we add and subtract the term

$$\frac{\alpha}{h}\int_{r_w}^{r_{wf}(\Delta t_{foff})} \frac{q_{os}(r, \Delta t_{foff})}{\hat{\lambda}_o k(r)}\frac{dr}{r}$$

to Eq. 3.233 and rearrange the resulting equation to obtain

$$\begin{aligned}
\Delta p_{ws}(\Delta t_{foff}) &= p_{ws}(\Delta t_{foff}) - p_{oi} \\
&= \int_{r_w}^{\infty} \frac{\alpha q_s(r,\Delta t_{foff})}{h\hat{\lambda}_o k(r)} \frac{dr}{r} - \int_{r_w}^{r_{wf}(\Delta t_{foff})} f_w \frac{dp_c}{dS_w}\frac{\partial S_w}{\partial r} dr \\
&+ \frac{\alpha}{h\hat{\lambda}_o} \int_{r_w}^{r_{wf}(\Delta t_{foff})} \left(\frac{\hat{\lambda}_o}{\lambda_t(r,\Delta t_{foff})} q_s(r,\Delta t_{foff}) - q_{os}(r,\Delta t_{foff}) \right) \frac{1}{k(r)} \frac{dr}{r} \\
&= \Delta \hat{p}_{os}(\Delta t_{foff}) - \int_{r_w}^{r_{wf}(\Delta t_{foff})} f_w \frac{dp_c}{dS_w}\frac{\partial S_w}{\partial r} dr \\
&+ \frac{\alpha}{h\hat{\lambda}_o} \int_{r_w}^{r_{wf}(\Delta t_{foff})} \left(\frac{\hat{\lambda}_o}{\lambda_t(r,\Delta t_{foff})} q_s(r,\Delta t_{foff}) - q_{os}(r,\Delta t_{foff}) \right) \frac{1}{k(r)} \frac{dr}{r}.
\end{aligned} \tag{3.234}$$

Here $q_s(r,\Delta t_{foff}) = q_{os}(r,\Delta t_{foff})$ in the uninvaded zone, i.e., for $r > r_{wf}(\Delta t_{foff})$, where $q_{os}(r,\Delta t_{foff})$ is the single-phase rate profile obtained during falloff after injecting oil at the rate q_{inj} [82]. Since we are considering only infinite-acting behavior, where the single oil phase pressure drop that would be obtained if we had injected oil and then shut the well can be defined from the superposition of two constant flow rates solutions, i.e.,

$$\Delta \hat{p}_{os} = p_{wf,o}(\Delta t_{foff}) - p_{oi} = \frac{\alpha q_{inj}}{2kh\hat{\lambda}_o} \ln\left(\frac{t_{inj} + \Delta t_{foff}}{\Delta t_{foff}}\right), \tag{3.235}$$

with the rate schedule

$$q_t(r_w,t) = \begin{cases} q_{inj} > 0, & 0 < t \le t_{inj} \\ 0, & t_{inj} < t \le t_{inj} + t_{foff}, \end{cases} \tag{3.236}$$

where t_{foff} is the total time at the end of the falloff period and $\Delta t_{foff} = 0$ at the beginning of the falloff period. As rate superposition applies for single-phase flow, following Peres et al.

[81] and Chen [28], we use rate superposition to approximate the rate profiles as

$$q_s(r,\Delta t_{foff}) = q_{inj}\Bigg[\exp\bigg(-\frac{\phi c_t(r,\Delta t_{foff})r^2}{4\beta k\lambda_t(r,\Delta t_{foff})(t_{inj}+\Delta t_{foff})}\bigg) - \exp\bigg(-\frac{\phi c_t(r,\Delta t_{foff})r^2}{4\beta k\lambda_t(r,\Delta t_{foff})\Delta t_{foff}}\bigg)\Bigg] \tag{3.237}$$

and the single oil phase flow rate

$$q_{os}(r,\Delta t_{foff}) = q_{inj}\Bigg[\exp\bigg(-\frac{\phi \hat{c}_{to} r^2}{4\beta k\hat{\lambda}_o(t_{inj}+\Delta t_{foff})}\bigg) - \exp\bigg(-\frac{\phi \hat{c}_{to} r^2}{4\beta k\hat{\lambda}_o\Delta t_{foff}}\bigg)\Bigg], \tag{3.238}$$

with

$$c_t(r,\Delta t_{foff}) = c_o S_o(r,\Delta t_{foff}) + c_w S_w(r,\Delta t_{foff}) + c_r. \tag{3.239}$$

Production: During production at a constant flow rate $q_{prod} = q_t(r_w,\Delta t_{prod})$ RB/D, where $\Delta t_{prod} = 0$ at the beginning of the flowback period, the bottom hole pressure drop can be expressed as [28, 31]

$$\Delta p_{wf}(\Delta t_{prod}) = p_{oi} - p_{wf}(\Delta t_{prod}) = -\int_{r_w}^{\infty}\frac{\alpha q_t(r,\Delta t_{prod})}{h\lambda_t(r,\Delta t_{prod})k(r)}\frac{dr}{r} + \int_{r_w}^{\infty} f_w\frac{dp_c}{dS_w}\frac{\partial S_w}{\partial r}dr, \tag{3.240}$$

Let $r_{f,inj}$ be the radius of the water front at the end of injection period, then for any time Δt_{prod}, such that, $q_t(r,t) = q_{prod}$ for $r \le r_{inj}(t_{inj})$, Eq. 3.240 becomes

$$\begin{aligned}\Delta p_{wf}(\Delta t_{prod}) = &-\frac{\alpha q_{prod}}{h}\int_{r_w}^{r_{wf}(t_{foff})}\frac{1}{\lambda_t(r,\Delta t_{prod})k(r)}\frac{dr}{r} - \frac{\alpha}{h}\int_{r_{wf}(t_{foff})}^{\infty}\frac{q_t(r,\Delta t_{prod})}{\lambda_t(r,\Delta t_{prod})k(r)}\frac{dr}{r}\\ &+\int_{r_w}^{r_{wf}(t_{foff})} f_w\frac{dp_c}{dS_w}\frac{\partial S_w}{\partial r}dr,\end{aligned} \tag{3.241}$$

where the Thompson and Reynolds [98] steady-state theory was applied to calculate the pressure drop with time in each stage of well testing by integrating Darcy's equation, ignoring capillary and gravitational effects. Obviously, the former assumption is not valid for the

whole production process. However, as shown by Chen [28], the steady-state solution will be reached in a short time after the production starts, if the injected water bank is not extensive. By adding and subtracting the term

$$\frac{\alpha}{h}\int_{r_w}^{r_{wf}(t_{foff})}\frac{q_{prod}}{\hat{\lambda}_o k(r)}\frac{dr}{r},$$

where $\hat{\lambda}_o$ is the endpoint oil mobility at $S_w = S_{wi}$, which means that $\lambda_t(r, \Delta t_{prod}) = \hat{\lambda}_o$ for $r > r_{wf}(t_{foff})$, Eq. 3.241 can be rewritten as

$$\begin{aligned}\Delta p_{wf}(\Delta t_{prod}) &= -\frac{\alpha}{h}\int_{r_w}^{\infty}\frac{q_t(r,\Delta t_{prod})}{\hat{\lambda}_o k(r)}\frac{dr}{r} + \int_{r_w}^{r_{wf}(t_{foff})} f_w \frac{dp_c}{dS_w}\frac{\partial S_w}{\partial r}dr \\ &\quad - \frac{\alpha q_{prod}}{h}\int_{r_w}^{r_{wf}(t_{foff})}\left(\frac{1}{\lambda_t(r,\Delta t_{prod})} - \frac{1}{\hat{\lambda}_o}\right)\frac{dr}{k(r)r} \\ &= -\Delta\hat{p}_{op}(\Delta t_{prod}) + \int_{r_w}^{r_{wf}(t_{foff})} f_w \frac{dp_c}{dS_w}\frac{\partial S_w}{\partial r}dr \\ &\quad - \frac{\alpha q_{prod}}{h\hat{\lambda}_o}\int_{r_w}^{r_{wf}(t_{foff})}\left(\frac{\hat{\lambda}_o}{\lambda_t(S_w(r,\Delta t_{prod}))} - 1\right)\frac{1}{k(r)}\frac{dr}{r}, \end{aligned} \tag{3.242}$$

where we have assumed that Δt_{prod} is sufficiently large so that $q_t(r, \Delta t_{prod}) = q_{prod}$ for $r \geq r_{wf}(t_{foff})$. The single-phase oil solution that would be obtained if we had injected oil into a oil reservoir, shut the well and the produced it, $\Delta\hat{p}_o(\Delta t_{prod})$, can be determined by the superposition of three constant flow rate solutions

$$\begin{aligned}\Delta\hat{p}_{op}(\Delta t_{prod}) = \frac{\alpha}{kh\hat{\lambda}_o}\Bigg\{&\frac{q_{inj}}{2}\ln\left(\frac{t_{inj}+t_{foff}+\Delta t_{prod}}{t_{foff}+\Delta t_{prod}}\right) \\ &+ q_{prod}\left[\frac{1}{2}\ln\left(\frac{\beta k\hat{\lambda}_o}{\phi\hat{c}_{to}r_w^2}\Delta t_{prod}\right) + 0.4045 + s\right]\Bigg\},\end{aligned} \tag{3.243}$$

with the rate schedule:

$$q_t(r_w,t)=\begin{cases} q_{inj}>0, & 0<t\leq t_{inj} \\ 0, & t_{inj}<t\leq t_{foff} \\ q_{prod}<0, & t>t_{foff}. \end{cases} \tag{3.244}$$

3.1.3 Note on Hysteresis Effects

As shown in Chapter 2, the fluid saturation distribution for the IFPT can be determined assuming two different fractional curves, as consequence of two pairs of relative permeability curves, imbibition and drainage, and also two capillary pressure curves (Fig. 3.23). Figs. 3.24 and 3.25 show the wellbore water saturation the wellbore pressure response, respectively, during an IFPT with and without hysteresis effect, with capillary pressure included obtained, from a case run in IMEX.

3.2 Validation

We have compared our pressure and saturation solution solution including capillary pressure effects with the commercial numerical simulator IMEX, using the properties shown in Table 3.1. Fig. 3.26 compares the saturation distribution obtained from our analytical solution with the one obtained with IMEX while Fig. 3.29 shows the comparison of the wellbore pressure response from our analytical solution and IMEX during injection test. To be able to match saturation and pressure obtained from our solution with IMEX, we have to use a very refined grid (0.01 ft) around the wellbore - in the zone invaded by water -and then increase it exponential to a very large external radius (10,000 times the wellbore radius) to reproduce a a infinite acting reservoir. In addition, we have to start with very short time steps, 10^{-7} day.

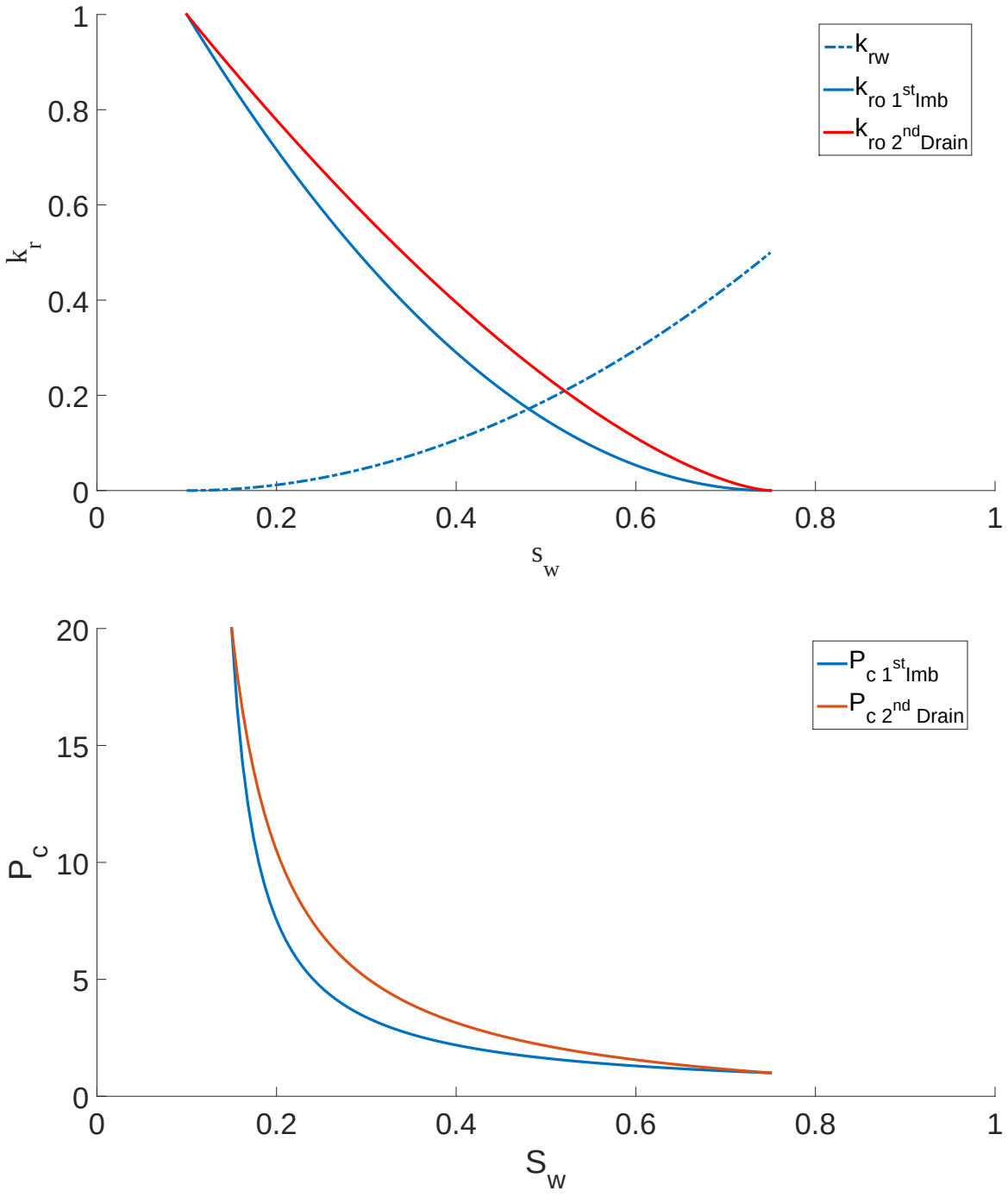

Figure 3.23: Relative permeability and capillary pressure curves for first imbibition and second drainage.

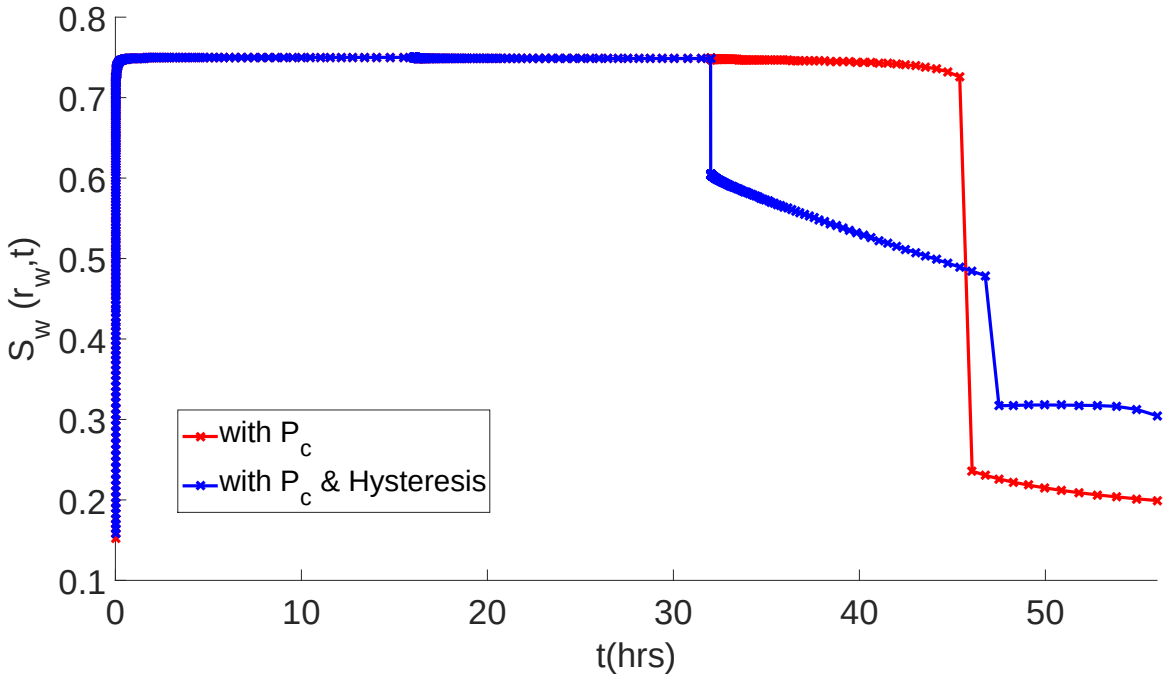

Figure 3.24: Wellbore saturation during an IFPT with and without hysteresis effect. Results obtained from IMEX. Here, $t_{inj} = 16h$ and $t_{foff} = 32$.

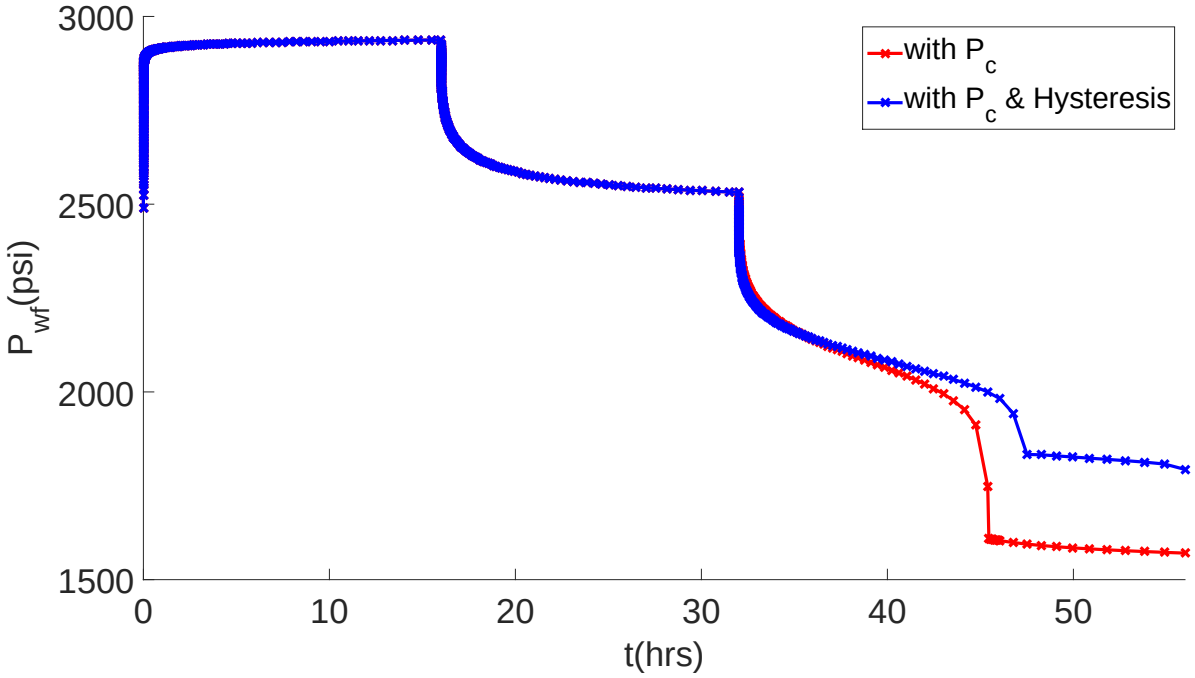

Figure 3.25: Wellbore pressure response during an IFPT with and without hysteresis effect. Results obtained from IMEX. Here, $t_{inj} = 16h$ and $t_{foff} = 32$

Table 3.1: Reservoir, rock and fluid properties for simulation and analytical solution.

Property	Value	Unit
q_t	3000	RB/DAY
h	60	ft
r_w	0.35	ft
r_e	6800	ft
k	300	md
s	0	
S_{iw}	0.10	
S_{or}	0.25	
p_i	2500	psi
ϕ	0.22	
B_o	1.003	RB/STB
B_w	1.002	RB/STB
c_o	8.0×10^{-6}	1/psi
c_w	3.02×10^{-6}	1/psi
c_r	5.0×10^{-6}	1/psi
μ_o	3.0	cp
μ_w	0.5	cp
λ	2	
p_t	0.5	psi

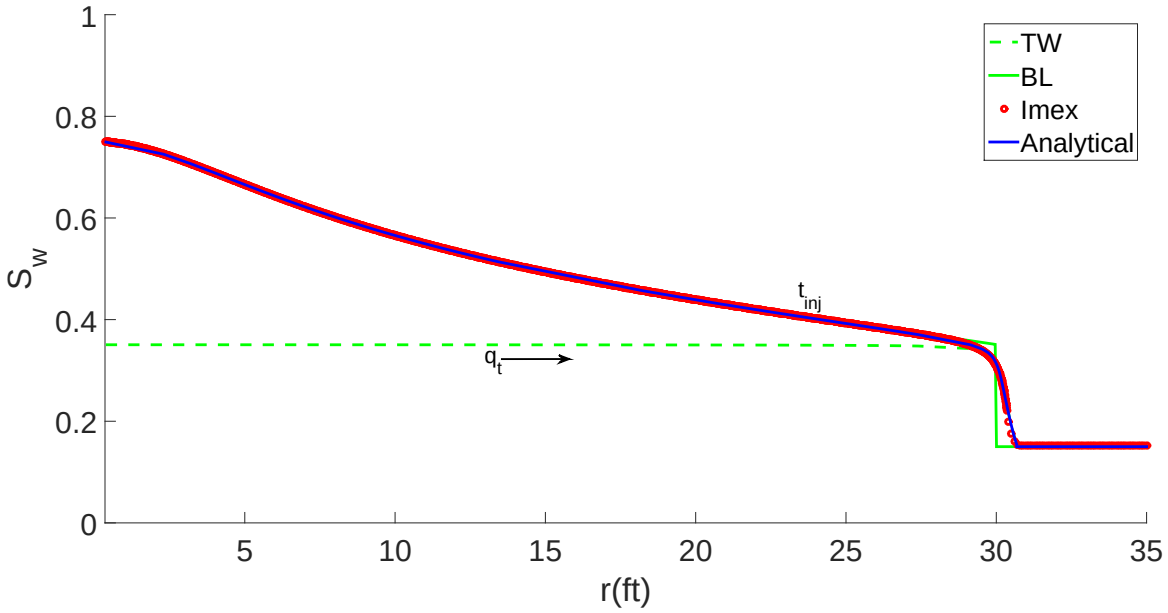

Figure 3.26: Comparison of the saturation distribution from analytical solution and IMEX during the injection period with capillary pressure. The discontinuous green line represents the traveling wave (TW) while the continuous green line (BL) represents the outer solution, i.e., the saturation distribution in the reservoir when there is no capillary pressure effects.

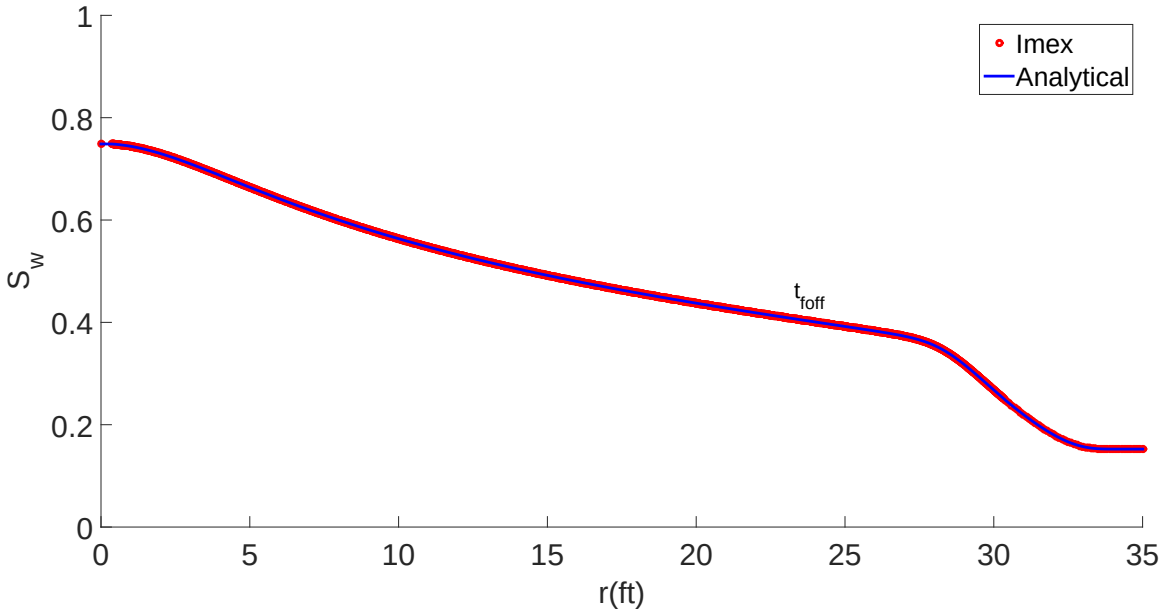

Figure 3.27: Comparison of the saturation distribution from analytical solution and IMEX during the falloff period with capillary pressure.

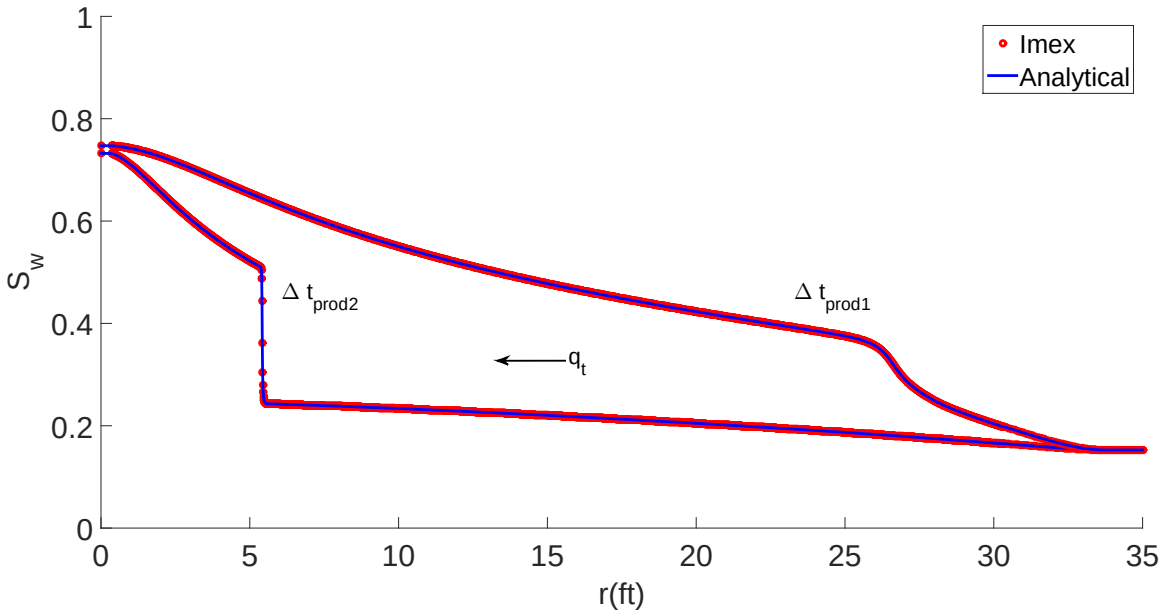

Figure 3.28: Comparison of the saturation distribution from analytical solution and IMEX during the production period with capillary pressure at two different times, before (right curve) and after (left curve) wave breaking time.

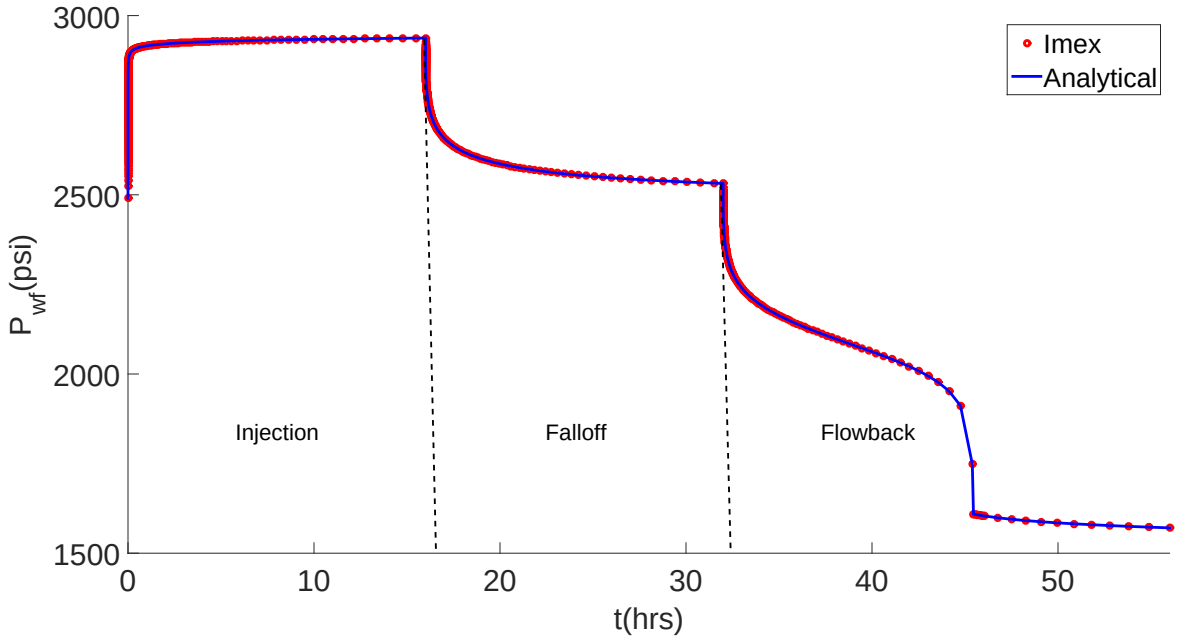

Figure 3.29: Comparison of the wellbore pressure response from analytical solution and IMEX during the injection ($t \in (0, 16)$), falloff ($t \in (16, 32)$) and production ($t > 32$) test with capillary pressure.

3.3 Example

"I wasn't meant for reality, but life came and found me."

— Fernando Pessoa, *The Book of Disquiet*

In the example, we use our expanded approximate analytical solution for the wellbore pressure response durning an injection-falloff-production test including capillary pressure effects as the forward model to estimate permeabilities, relative permeabilities curves and capillary pressure curve, i.e, the

$$\vec{m} = [k, s, a_w, p_t, \lambda]^T, \tag{3.245}$$

using the procedure presented in Chapter 2. Here, we provide a synthetic example where we first compute "true pressure data" by running a commercial simulator using a very fine grid and very small time steps using specified (true) values. As in Chapter 2, we assume a skin zone of a given radius and then for the given value of skin factor, compute the value of skin

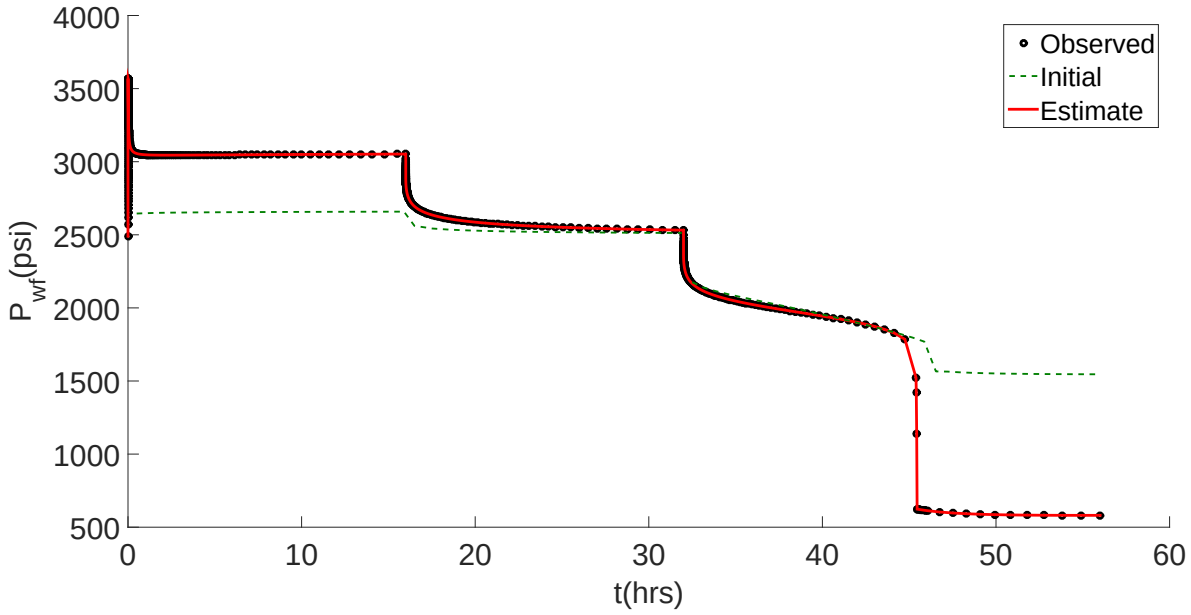

Figure 3.30: Bottom hole pressure data match for the injection-falloff-production test including capillary pressure effects.

Table 3.2: Estimated model parameters based on the approximate analytical solution for injection-falloff-production test.

Parameter	k (md)	Skin	a_w	p_t	λ
True	300.00	5.00	0.5	0.5	2
Initial Guess	600.00	0.00	0.8	1	1
Estimate	299.5	5.02	0.48	0.51	1.97

zone permeability, k_s, using Hawkins's formula [50] for input into the reservoir simulator. The radius of the skin zone is equal to1 foot and includes the 100 radial gridblocks closest to the wellbore. The reservoir, rock and fluid properties are those shown in Table 2.1. The observed pressure data are generated by adding uncorrelated Gaussian noise with mean zero and variance 1 psi^2 to the true pressure data. We only match observed pressure data corresponding to times more 0.5 hour after each flow rate change. Table 3.2 presents the values of model parameters estimated from the TRR algorithm where the bounds specified on the parameters are given in Table 3.3; $\epsilon = 10^{-4}$ and $sv = 10^{-3}$. Fig. 3.30 shows the bottom hole pressure match for the IFPT data while Fig. 3.31 shows the estimated relative permeability and capillary pressure curves.

Table 3.3: Parameter bounds for the injection-falloff-production test.

Parameter	k (md)	Skin	a_w	p_t	λ
Lower bound	0	-60	0.05	0.01	0.04
Upper bound	∞	60	1.00	20	4.00

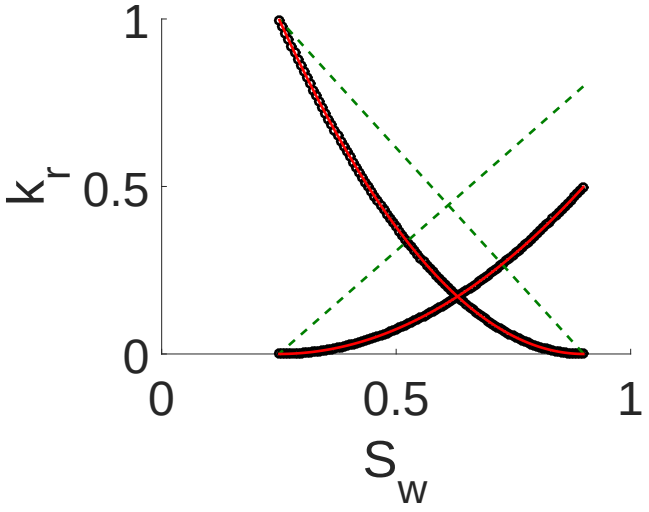

(a)

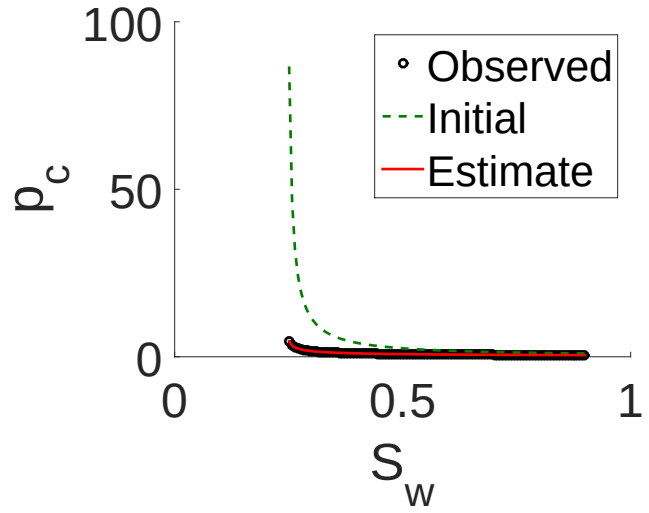

(b)

Figure 3.31: Estimated relative permeability (a) and capillary pressure (b) curves based on model parameters obtained from IFPT data match. The green dashed lines represent the curves computed based on the initial guess for model parameters and the circles, represents the true curves.

CHAPTER 4

PRESSURE RESPONSE WITH CO_2 PRESENCE

"Observe now with what skill, with what art,

I make the biggest transition in this book."

— "Brás Cubas"

in *Memórias Póstumas de Brás Cubas* by Machado de Assis

In this chapter we provide analytical solutions for the wellbore pressure during an injection-falloff test under radial flow conditions in a homogeneous porous media where the injected fluid is carbonated water. For both the injection and falloff periods, we assume an isothermal process with thermodynamic equilibrium, a linear adsorption isotherm and that viscosities depend only on the CO_2 concentration. We also neglect CO_2 diffusion, gravity effects and capillarity effects. For the injection period, we first determine the saturation and concentration distributions with time in the reservoir by applying the method of characteristics (MOC) to solve the appropriate system of hyperbolic conservation equations where we assume incompressible fluids. In solving for water saturation and CO_2 concentration in water, we neglect the change in water volume due to the variation of the CO_2 concentration in water. Similar to what was done in the previous chapters, after solving for the saturation and concentration profiles, the pressure solution can be obtained by integrating Darcy's law, from the wellbore radius to infinity while assuming an infinite-acting reservoir and invoking the Thompson-Reynolds steady-state theory. Because Darcy's law does not assume incompressible flow, the pressure solution generated does not assume incompressible flow. To obtain an analytical expression for the wellbore pressure, we again assume that for injection and falloff, the total flow rate profile in the reservoir is constant in a region from the wellbore to a radius greater than the radius of the flood front. During the falloff stage, it

is assumed that there is no change in saturation in the reservoir, which is reasonable because we neglect capillary pressure, the gravity force and fluid compressibilities when determining the saturation profile. Based on this assumptions, we generate analytical solutions for a carbonated water injection and falloff test and compare these solutions to those obtained with a commercial reservoir simulator using very fine spatial grids and very small time steps. This comparison and results from matching data suggest that the analytical solutions presented can be used reliably to analyze pressure data obtained during carbonated water injection and falloff tests.

We focus on the development of an approximate analytical solution to calculate wellbore pressure during a carbonated water injection and falloff test in a oil reservoir where the connate water may or may not contain dissolved CO_2. As we focus on carbonated water injection (also known as orcoflooding), the straightforward application of the results is limited to a special case; however, it is straightforward to apply the solution procedure developed in this work to other EOR problems such as polymer injection or the problem where gas (or water) is injected into an oil reservoir where the injected and in situ fluids are at different temperatures. Carbonated water injection (CWI) has been applied successfully since the 1950's, where results for some fields in Oklahoma and Texas showed that CWI gave an incremental increase in oil recovery that was 50% to 80% higher than was achievable by conventional waterflooding [51, 33]. Thus, it may prove useful to have analytical solutions that can be used to analyze pressure data obtained during a carbonated water injection-falloff test.

Injection-falloff testing when the injected fluid is either water or carbonated water is particularly important for offshore reservoirs which contain oil and gas with very high CO_2 content such the subsalt reservoirs offshore Brazil, where carbon dioxide concentrations can exceed 50%. In this environment, a conventional well test on an exploratory well cannot be run because the produced gas cannot be released since the emission of gas with a high concentration of CO_2 to the atmosphere is harmful to the environment as well as a significant health hazard to workers; hence, there is a need to develop techniques for analyzing pressure

data from injection-falloff tests. Injecting water which contains dissolved CO_2 (carbonated water) not only avoids the negative environmental impact that occurs with a drill-stem test but also may increase oil recovery because any dissolved CO_2 in the injected water that is transferred to the oil phase decreases oil viscosity and residual oil saturation. There are three different scenarios for the water injection when comparing the initial and injected CO_2 concentration in the water phase ($C_{CO_2}^{wi}$ and $C_{CO_2}^{w,inj}$, respectively):

Case 1: $C_{CO_2}^{w,inj} < C_{CO_2}^{wi}$ In this case, the residual oil saturation will increase during the injection due to an increase in the interfacial tension due to the decrease in the CO_2 concentration in the oil and connate water phases. Similarly, the oil viscosity will increase while the water viscosity will decrease, leading to a more unfavorable mobility ratio. We will not consider this case in this work because it would not be recommended in practice.

Case 2: $C_{CO_2}^{w,inj} = C_{CO_2}^{wi}$ In this case, we only have one fractional flow curve and the carbonated water flooding problem reduces to solving the well-known Buckley-Leverett problem. An analytical solution for injection-falloff wellbore pressure response can be found in Peres and Reynolds [79] and Peres et al. [82].

Case 3: $C_{CO_2}^{w,inj} > C_{CO_2}^{wi}$ This is the case we will focus on in this work. When injecting water with a higher concentration of CO_2 than in the connate water, some of the CO_2 that is contained in the injected water will transfer to the oil phase which causes the residual oil saturation will decrease due to a lower interfacial tension. Moreover, the oil viscosity will decrease while the water viscosity will increase, leading to a more favorable mobility ratio.

For injection tests, Peres and Reynolds [79] developed a analytical solution for the wellbore pressure during water injection, for both horizontal and vertical wells, using the Thompson and Reynolds [98] steady-state theory. Intuitively, the assumption that this steady-state zone exists appears to be more tenuous as the total compressibility of the system increases. However, it has been shown to yield accurate analytical pressure solutions

even for gas-condensate systems [99]. In the vertical well case, Peres and Reynolds [79] showed that their solution yields the injection solution of Bratvold and Horne [17] provided one makes the Bratvold and Horne assumption that the injection solution is a unique function of the Boltzmann transform which is valid for a finite wellbore radius well except at early times. Bratvold and Horne [17] as well as Abbaszadeh and Kamal [1] generated an approximation to the falloff pressure response by analogy with the shut-in solution for a single-phase composite reservoir, whereas Peres et al. [82] approximated the falloff pressure solution by applying superposition in an approximate way. Pope [84] presented an analytical solution to saturation and concentration distributions during carbonated water injection into an oil reservoir, but he ignored the CO_2 adsorption phenomenon and the dependence of the water-oil surface tension on carbon dioxide concentration in his solution. Bedrikovetsky [11] presented an analytical solution to the hyperbolic system that governs oil displacement by chemical solutions considering the phenomena that Pope [84] neglected, but none of these authors referenced in this paragraph has considered the effect of CO_2 in the wellbore pressure response as in Machado et al. [69, 70].

Here, we first present an approximate analytical solution for the wellbore pressure during a water injection and falloff well test in a reservoir containing CO_2-rich oil and irreducible water saturation, where the carbon dioxide can be present at distinct concentrations in both phases, water and oil. Then, we show that our analytical solution is highly accurate by comparing it to the results obtained from a commercial numerical simulator. Finally, using our analytical solution as the forward model, we show that the data obtained from the commercial numerical simulator can be analyzed to estimate reservoir permeability, the mechanical skin factor and end-point mobilities.

4.1 Mathematical Model

"Young man, in mathematics you don't understand things.

You just get used to them."

— John von Neumann

4.1.1 Saturation/Composition Profile

We assume that the initial pressure is high enough so that no CO_2 gas phase is formed anywhere in the reservoir. Therefore, we have two-phase flow with three components, water, oil and CO_2. Assuming a one-dimensional homogeneous reservoir with incompressible fluids, without capillary or gravity effects, the mass balance equation, using radial coordinates, leads to the following Buckley and Leverett [21] equation:

$$\frac{\partial S_w}{\partial t} + \frac{\theta q_t}{2\pi r h \phi} \frac{\partial f_w(S_w, C^w_{CO_2})}{\partial r} = 0, \tag{4.1}$$

which can be rewritten as

$$\frac{\partial S_w}{\partial t} + \frac{\theta q_t}{\phi \pi h} \left(\frac{\partial f_w(S_w, C^w_{CO_2})}{\partial S_w} \frac{\partial S_w}{\partial r^2} + \frac{\partial f_w(S_w, C^w_{CO_2})}{\partial C^w_{CO_2}} \frac{\partial C^w_{CO_2}}{\partial r^2} \right) = 0, \tag{4.2}$$

where S_w is the water saturation and $C^w_{CO_2}$ is the CO_2 concentration in the water in $\frac{lbm}{ft^3}$; time is in hours; q_t is the total liquid rate in RB/D; r and h, the reservoir radius and thickness, are in feet, $\theta = 5.6146/24$ is a unit conversion factor and ϕ is porosity. Neglecting capillary and gravity effects, the water fractional flow curve is

$$f_w = \frac{\frac{k_{rw}}{\mu_w}}{\frac{k_{rw}}{\mu_w} + \frac{k_{ro}}{\mu_o}}, \tag{4.3}$$

where the oil and water viscosities (μ_w and μ_o) are in centipoise and assumed to be a function of CO_2 concentration in each phase. Dissolved carbon dioxide changes the water fractional flow curve (Fig. 4.1) by increasing water viscosity [55], decreasing oil viscosity and lowering the interfacial tension between the two phases, i.e., reducing residual oil saturation [11],

leading to

$$\frac{\partial f_w(S_w, C^w_{CO_2})}{\partial C^w_{CO_2}} = \frac{\partial f_w}{\partial \mu_w}\frac{\partial \mu_w}{\partial C^w_{CO_2}} + \frac{\partial f_w}{\partial \mu_o}\frac{\partial \mu_o}{\partial C^w_{CO_2}} + \frac{\partial f_w}{\partial S_{or}}\frac{\partial S_{or}}{\partial C^w_{CO_2}} < 0, \tag{4.4}$$

where the inequality follows from the fact that the terms $\frac{\partial \mu_w}{\partial C^w_{CO_2}}$, $\frac{\partial f_w}{\partial \mu_o}$ and $\frac{\partial f_w}{\partial S_{or}}$ in Eq. 4.4 are positive while the terms $\frac{\partial f_w}{\partial \mu_w}$, $\frac{\partial \mu_o}{\partial C^w_{CO_2}}$ and $\frac{\partial S_{or}}{\partial C^w_{CO_2}}$ are negative. For simplicity, we again assume that relative permeabilities can be represented by the power law model given by

$$k_{rw} = a_w\left(\frac{S_w - S_{iw}}{1 - S_{iw} - S_{or}}\right)^{n_w} \tag{4.5}$$

and

$$k_{ro} = a_o\left(\frac{1 - S_w - S_{or}}{1 - S_{iw} - S_{or}}\right)^{n_o}, \tag{4.6}$$

with $a_w = k_{rw}(S_w = 1 - S_{or})$ and $a_o = k_{ro}(S_w = S_{iw})$, where S_{or} denotes residual oil saturation and S_{iw} denotes irreducible water saturation.

Following the assumptions made by Pope [84] in his analytical model for saturation distribution during carbonated waterflood, we assume an isothermal process with thermodynamic equilibrium, neglecting the CO_2 diffusion and the volume that carbon dioxide occupies in water. The mass conservation equation for the carbon dioxide in radial coordinates is then given by [45]

$$\frac{\partial(S_w C^w_{CO_2} + S_o C^o_{CO_2} + C^M_{CO_2})}{\partial t} + \frac{\theta q_t}{2\pi r h \phi}\frac{\partial(f_w C^w_{CO_2} + f_o C^o_{CO_2})}{\partial r} = 0, \tag{4.7}$$

where $C^M_{CO_2}$ is the mass of CO_2 adsorbed in the rock per rock pore volume. We assume a linear equilibrium relationship between $C^o_{CO_2}$ and $C^w_{CO_2}$ defined by

$$C^o_{CO_2} = K_{wo-CO_2} C^w_{CO_2}, \tag{4.8}$$

where $C^o_{CO_2}$ is the CO_2 concentration in the oil phase in lbm/ft^3 and K_{wo-CO_2} is the water/oil-CO_2 partition coefficient [46] - which is assumed to be constant - with a linear adsorption

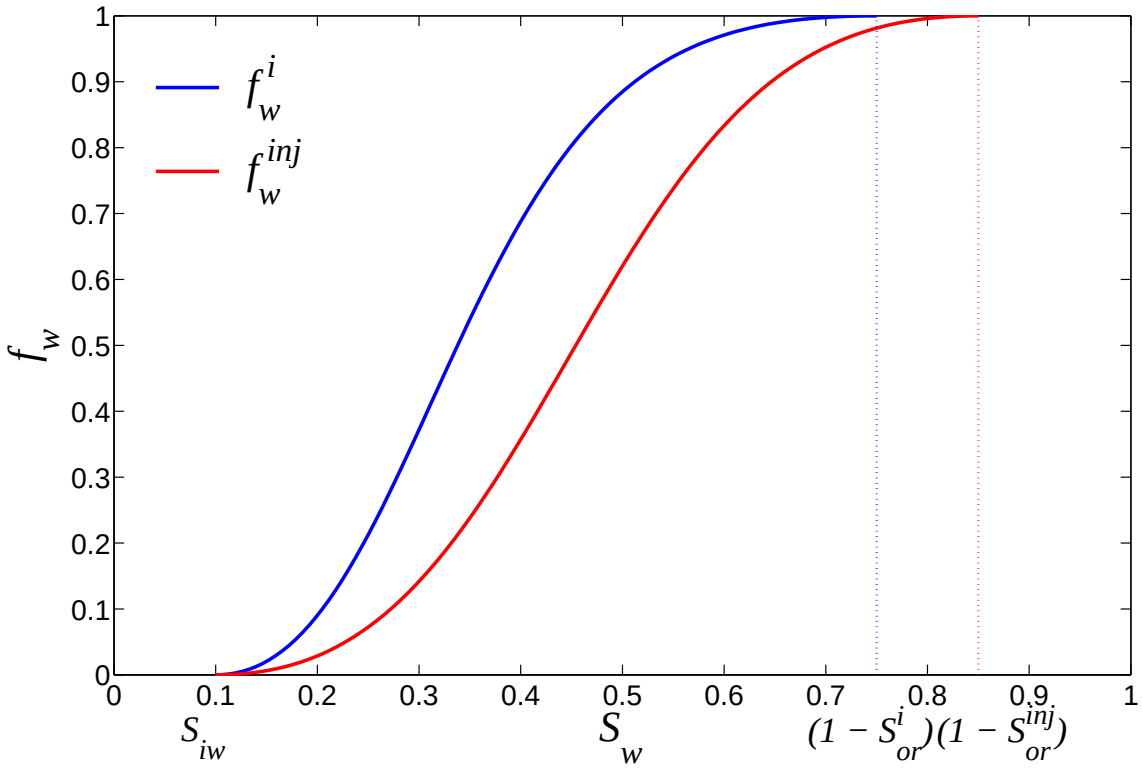

(a)

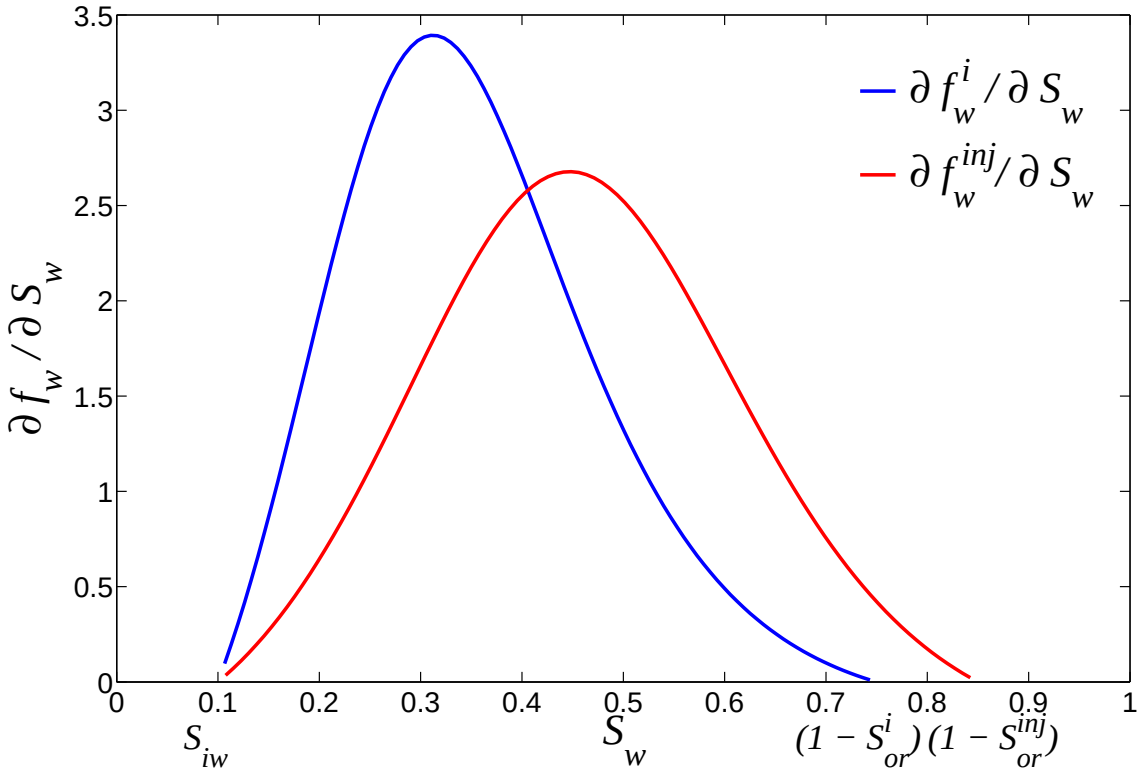

(b)

Figure 4.1: Water fractional flow curves for initial and injection CO_2 concentrations (a) and its derivatives (b).

isotherm [11] given by

$$C^M_{CO_2} = \frac{\rho_M(1-\phi)}{\phi} K_s C^w_{CO_2}, \tag{4.9}$$

where ρ_M is the matrix density in lbm-rock/ft^3 and K_s is the adsorption constant in ft^3/lbm-rock [59]. Using $S_o + S_w = 1$, $f_w + f_o = 1$ and Eq. 3.1, Eq. 4.7 can be rearranged as

$$\left(S_w + (1-S_w)\frac{dC^o_{CO_2}}{dC^w_{CO_2}} + \frac{dC^M_{CO_2}}{dC^w_{CO_2}}\right)\frac{\partial C^w_{CO_2}}{\partial t} + \frac{\theta q_t}{\phi 2\pi r h}\left(f_w + (1-f_w)\frac{dC^o_{CO_2}}{dC^w_{CO_2}}\right)\frac{\partial C^w_{CO_2}}{\partial r} + \left(C^w_{CO_2} - C^o_{CO_2}\right)\left(\frac{\partial S_w}{\partial t} + \frac{\theta q_t}{\phi 2\pi r h}\frac{\partial f_w}{\partial r}\right) = 0. \tag{4.10}$$

From Eq. 4.1 we can see that the third term in E.q 4.10 vanishes, leading to

$$\left(S_w + (1-S_w)\frac{dC^o_{CO_2}}{dC^w_{CO_2}} + \frac{dC^M_{CO_2}}{dC^w_{CO_2}}\right)\frac{\partial C^w_{CO_2}}{\partial t} + \frac{\theta q_t}{\phi 2\pi r h}\left(f_w + (1-f_w)\frac{dC^o_{CO_2}}{dC^w_{CO_2}}\right)\frac{\partial C^w_{CO_2}}{\partial r} = 0. \tag{4.11}$$

Computing the ordinary derivatives in Eq. 4.11 from Eqs. 4.8 and 4.9, we can rewrite Eq. 4.11 as

$$\frac{\partial C^w_{CO_2}}{\partial t} + \frac{\theta q_t}{\pi h \phi}\frac{\left(f_w + (1-f_w)K_{wo-CO_2}\right)}{\left(S_w + (1-S_w)K_{wo-CO_2} + \frac{\rho_M(1-\phi)K_s}{\phi}\right)}\frac{\partial C^w_{CO_2}}{\partial (r^2)} = 0. \tag{4.12}$$

From Eqs. 4.2 and 4.12, the carbonated water flow is governed by the following system of equations,

$$\vec{u}_t + A\vec{u}_{r^2} = \vec{0}, \tag{4.13}$$

where

$$\vec{u} = \begin{pmatrix} S_w \\ C^w_{CO_2} \end{pmatrix}, \tag{4.14}$$

$$A = \frac{\theta q_t}{\pi h \phi}\begin{pmatrix} \frac{\partial f_w}{\partial S_w} & \frac{\partial f_w}{\partial C^w_{CO_2}} \\ 0 & \frac{f_w + (1-f_w)K_{wo-CO_2}}{S_w + (1-S_w)K_{wo-CO_2} + \frac{\rho_M(1-\phi)K_s}{\phi}} \end{pmatrix}, \tag{4.15}$$

and the subscripts t and r^2 in Eq. 4.13 refers to partial derivatives.To find the saturation and

concentration profiles with time, we can use the eigenvalues of matrix A, which are given by

$$\lambda_1 = \frac{\theta q_t}{\pi h \phi} \frac{\partial f_w}{\partial S_w} \tag{4.16}$$

and

$$\lambda_2 = \frac{\theta q_t}{\pi h \phi} \left(\frac{f_w + (1 - f_w) K_{wo-CO_2}}{S_w + (1 - S_w) K_{wo-CO_2} + \rho_M \frac{1-\phi}{\phi} K_s} \right), \tag{4.17}$$

with the corresponding left eigenvectors given by,

$$\vec{l_1} = \begin{pmatrix} \lambda_1 - \lambda_2 \\ \frac{\theta q_t}{\pi h \phi} \frac{\partial f_w}{\partial C^w_{CO_2}} \end{pmatrix} \tag{4.18}$$

and

$$\vec{l_2} = \begin{pmatrix} 0 \\ 1 \end{pmatrix}, \tag{4.19}$$

obtained from $\vec{l}A = \lambda \vec{l}$, which, as shown bellow, allows us to decouple the system of equations given by Eq. 4.13 into

$$\begin{pmatrix} \lambda_2 \\ C^w_{CO_2} \end{pmatrix}_t + \begin{pmatrix} \lambda_1 & 0 \\ 0 & \lambda_2 \end{pmatrix} \begin{pmatrix} \lambda_2 \\ C^w_{CO_2} \end{pmatrix}_{(r^2)} = \vec{0}. \tag{4.20}$$

To transform Eq. 4.13 into Eq. 4.20, we need to decouple the system of hyperbolic equations given in Eq. 4.13. The eigenvalues are not equal, the left eigenvectors (Eqs. 4.18 and 4.19) are linearly independent and can be used to diagonalize A [63]. Therefore,

$$\Lambda = QAQ^{-1}, \tag{4.21}$$

where the rows vectors of Q are the transposes of the left eigenvectors of A and Λ is the

diagonal matrix of eigenvalues of A. Substituting $A = Q^{-1}\Lambda Q$ into Eq. 4.13, yields

$$\vec{u}_t + Q^{-1}\Lambda Q\vec{u}_{(r^2)} = \vec{0}. \tag{4.22}$$

Multiplying Eq. 4.22 by Q, we get

$$Q\vec{u}_t + \Lambda Q\vec{u}_{(r^2)} = \vec{0}, \tag{4.23}$$

or, equivalently,

$$\begin{pmatrix} \lambda_1 - \lambda_2 & \frac{\theta q_t}{\pi h\phi}\frac{\partial f_w}{\partial C^w_{CO_2}} \\ 0 & 1 \end{pmatrix} \begin{pmatrix} S_w \\ C^w_{CO_2} \end{pmatrix}_t + \begin{pmatrix} \lambda_1 & 0 \\ 0 & \lambda_2 \end{pmatrix} \begin{pmatrix} \lambda_1 - \lambda_2 & \frac{\theta q_t}{\pi h\phi}\frac{\partial f_w}{\partial C^w_{CO_2}} \\ 0 & 1 \end{pmatrix} \begin{pmatrix} S_w \\ C^w_{CO_2} \end{pmatrix}_{(r^2)} = \vec{0}. \tag{4.24}$$

The first equation of the system in Eq. 4.23 is

$$(\lambda_1 - \lambda_2)\frac{\partial S_w}{\partial t} + \frac{\theta q_t}{\pi h\phi}\frac{\partial f_w}{\partial C^w_{CO_2}}\frac{\partial C^w_{CO_2}}{\partial t} + \lambda_1\left((\lambda_1 - \lambda_2)\frac{\partial S_w}{\partial (r^2)} + \frac{\theta q_t}{\pi h\phi}\frac{\partial f_w}{\partial C^w_{CO_2}}\frac{\partial C^w_{CO_2}}{\partial (r^2)}\right) = 0. \tag{4.25}$$

Following Boughrara [14]'s solution for cold water injection, differentiating Eq. 4.17 with respect to $C^w_{CO_2}$, we have

$$\frac{\partial \lambda_2}{\partial C^w_{CO_2}} = \frac{\theta q_t}{\pi h\phi}\frac{1 - K_{wo-CO_2}}{S_w + (1 - S_w)K_{wo-CO_2} + \rho_M\frac{1-\phi}{\phi}K_s}\frac{\partial f_w}{\partial C^w_{CO_2}}, \tag{4.26}$$

or,

$$\frac{\theta q_t}{\pi h\phi}\frac{\partial f_w}{\partial C^w_{CO_2}} = \frac{S_w + (1 - S_w)K_{wo-CO_2} + \rho_M\frac{1-\phi}{\phi}K_s}{1 - K_{wo-CO_2}}\frac{\partial \lambda_2}{\partial C^w_{CO_2}}. \tag{4.27}$$

Now taking the derivative of Eq. 4.17 with respect to S_w, leads to

$$\frac{\partial \lambda_2}{\partial S_w} = \frac{\theta q_t}{\pi h\phi}\frac{1 - K_{wo-CO_2}}{S_w + (1 - S_w)K_{wo-CO_2} + \rho_M\frac{1-\phi}{\phi}K_s}\left(\frac{\partial f_w}{\partial S_w} - \frac{f_w + (1 - f_w)K_{wo-CO_2}}{S_w + (1 - S_w)K_{wo-CO_2} + \rho_M\frac{1-\phi}{\phi}K_s}\right), \tag{4.28}$$

which can be rewritten as

$$\frac{\partial \lambda_2}{\partial S_w} = \frac{1 - K_{wo-CO_2}}{S_w + (1 - S_w)K_{wo-CO_2} + \rho_M \frac{1-\phi}{\phi} K_s}(\lambda_1 - \lambda_2). \tag{4.29}$$

Eq. 4.29 can be rearranged to obtain

$$\lambda_1 - \lambda_2 = \frac{S_w + (1 - S_w)K_{wo-CO_2} + \rho_M \frac{1-\phi}{\phi} K_s}{1 - K_{wo-CO_2}} \frac{\partial \lambda_2}{\partial S_w}. \tag{4.30}$$

Substituting Eqs. 4.27 and 4.30 in Eq. 4.25, yields

$$\begin{aligned} &\left(\frac{S_w + (1 - S_w)K_{wo-CO_2} + \rho_M \frac{1-\phi}{\phi} K_s}{1 - K_{wo-CO_2}} \frac{\partial \lambda_2}{\partial S_w} \right) \frac{\partial S_w}{\partial t} \\ &+ \frac{S_w + (1 - S_w)K_{wo-CO_2} + \rho_M \frac{1-\phi}{\phi} K_s}{1 - K_{wo-CO_2}} \frac{\partial \lambda_2}{\partial C^w_{CO_2}} \frac{\partial C^w_{CO_2}}{\partial t} \\ +\lambda_1 \Bigg[&\left(\frac{S_w + (1 - S_w)K_{wo-CO_2} + \rho_M \frac{1-\phi}{\phi} K_s}{1 - K_{wo-CO_2}} \frac{\partial \lambda_2}{\partial S_w} \right) \frac{\partial S_w}{\partial (r^2)} + \frac{\theta q}{\pi h \phi} \frac{\partial f_w}{\partial C^w_{CO_2}} \frac{\partial C^w_{CO_2}}{\partial (r^2)} \Bigg] = 0, \end{aligned} \tag{4.31}$$

which, upon simplification using Eq. 4.27, gives

$$\frac{\partial \lambda_2}{\partial S_w} \frac{\partial S_w}{\partial t} + \frac{\partial \lambda_2}{\partial C^w_{CO_2}} \frac{\partial C^w_{CO_2}}{\partial t} + \lambda_1 \left(\frac{\partial \lambda_2}{\partial S_w} \frac{\partial S_w}{\partial (r^2)} + \frac{\partial \lambda_2}{\partial C^w_{CO_2}} \frac{\partial C^w_{CO_2}}{\partial (r^2)} \right) = 0. \tag{4.32}$$

Eq. 4.32 can be rewritten as

$$\frac{\partial \lambda_2}{\partial t} + \lambda_1 \frac{\partial \lambda_2}{\partial (r^2)} = 0. \tag{4.33}$$

Also note that Eq. 4.12 is equivalent to

$$\frac{\partial C^w_{CO_2}}{\partial t} + \lambda_2 \frac{\partial C^w_{CO_2}}{\partial (r^2)} = 0. \tag{4.34}$$

Therefore, Eq. 4.23 is equivalent to the decoupled system given by Eqs. 4.33 and 4.34, which can be written as

$$\vec{v}_t + \Lambda \vec{v}_{(r^2)} = \vec{0}, \tag{4.35}$$

where

$$\vec{v} = \begin{pmatrix} \lambda_2 \\ C^w_{CO_2} \end{pmatrix}. \tag{4.36}$$

Defining $\vec{v} = (\lambda_2, C^w_{CO_2})^T$, the total derivative of each element of the vector $\vec{v}$ with respect to time is given by

$$\frac{dv_i}{dt} = \frac{\partial v_i}{\partial t} + \frac{dr_i^2}{dt}\frac{\partial v_i}{\partial (r^2)}, \quad \text{for} \quad i = 1, 2. \tag{4.37}$$

When $\frac{dv_i}{dt} = 0$, the right hand side of Eq. 4.37 must be equal to the i row in the left hand side of Eq. 4.35,

$$\frac{dr_i^2}{dt} = \lambda_i, \quad \text{for} \quad i = 1, 2, \tag{4.38}$$

where $\frac{dr_i^2}{dt}$ defines the speed of the waves [58]. That means, this system of partial differential equations (Eq. 4.35) can be reduced to a system of ordinary differential equations along the families of characteristic curves $\frac{dr_i^2}{dt}$ [66]. In this case,

$$\frac{d\lambda_2}{dt} = 0 \quad \text{along} \quad \frac{dr^2}{dt} = \lambda_1 \tag{4.39}$$

and

$$\frac{dC^w_{CO_2}}{dt} = 0 \quad \text{along} \quad \frac{dr^2}{dt} = \lambda_2, \tag{4.40}$$

where integrating these differential equations along their characteristic direction, gives the Riemann invariants, $R_1 = \lambda_2$ and $R_2 = C^w_{CO_2}$, which are constants along their respective families of characteristic curves.

Injection: The injection period of the test at a constant flow rate equal to q_{inj} is a non-strictly hyperbolic Riemann problem governed by Eq. 4.13 with the following initial and boundary conditions (Fig. 1.1),

$$\begin{cases} t = 0, r \geq r_w : S_w = S_{iw},\ C^w_{CO_2} = C^{wi}_{CO_2} \\ r = r_w, t > 0 : S_w = 1 - S_{or}(C^w_{CO_2}),\ C^w_{CO_2} = C^{winj}_{CO_2}, \end{cases}$$

and can be solved with the method of characteristics. Solving Eq. 4.38, we find both families of characteristic curves,

$$r_i^2(t) = \lambda_i(t - \tau) + \xi \quad \text{for} \quad i = 1, 2, \tag{4.41}$$

for any starting point (ξ,τ) in the (r^2, t) plane. To construct a physical solution for this Riemann problem, the velocity constraint (or compatibility condition) must be satisfied. The velocity constraint states that the wave velocities should decrease monotonically from downstream to upstream [76]. As we can see in Fig. 4.2, where we have plotted the fractional flow curves and the eigenvalues with saturation for both concentrations, initial and injected, if we start from the initial point (I), the point most upstream from the wellbore, to satisfy the monotonic condition, we have jump to S_{wf} - whose slope is tangent to the initial fractional flow curve - and then another jump from S_w^i to S_w^{inj}, following the line λ_2 = constant and whose slop is tangent to the injected fractional flow curve. The former represents the water saturation front - the moving boundary between noninvaded and invaded zone in the reservoir - and the latter represents the discontinuity between initial concentration and injection concentration. Any other path chosen satisfying the Oleinik entropy condition [74] would not satisfy the compatibility condition (the velocity constraint), leading to a multivalued non-physical saturation/composition profile in the reservoir. Therefore, the solution to this problem will consist of two discontinuities: a contact discontinuity between CO_2 injection and initial concentrations and one semi-shock in saturation caused by the fact that some saturation waves traveling from the wellbore moves with a higher speed than other saturations which are also traveling from the well due the S-shape of the water fractional flow curve. To be a unique admissible entropy solution, this semi-shock must satisfy the

Oleinik Entropy condition [74], given by

$$\frac{f_w(S_w^-, C_{CO_2}^{wi}) - f_w(S_w, C_{CO_2}^{wi})}{S_w^- - S_w} \geq \frac{f_w(S_w^-, C_{CO_2}^{wi}) - f_w(S_{iw}, C_{CO_2}^{wi})}{S_w^- - S_{iw}} \tag{4.42}$$

and

$$\frac{f_w(S_w^-, C_{CO_2}^{wi}) - f_w(S_{iw}, C_{CO_2}^{wi})}{S_w^- - S_{iw}} \geq \frac{f_w(S_w, C_{CO_2}^{wi}) - f_w(S_{iw}, C_{CO_2}^{wi})}{S_w - S_{iw}}, \tag{4.43}$$

for any $S_w \in (S_{iw}, S_w^-)$ [7], where S_w^- represents the saturation behind the shock. Fig. 4.2b shows the unique wave velocity path from the initial saturation,S_{iw}, to the injected saturation, $1 - S_{or}^{inj}$, that satisfies the velocity constraint, with the following switching points: S_{iw}, S_{wf}, S_w^i, S_w^{inj} and $1 - S_{or}$. Fig. 4.2a presents the contact and semi-shock discontinuities in the water fractional flow curves. The jump in $C_{CO_2}^w$ concentration from $C_{CO_2}^{wi}$ to $C_{CO_2}^{winj}$ will occur in the contact between connate water and injected water along $\lambda_2 = \text{constant}$,

$$\lambda_2(S_w^{inj}, C_{CO_2}^{winj}) = \frac{\theta q_t}{\pi h \phi}\left(\frac{f_w(S_w^{inj}) - f_w(S_w^i)}{S_w^{inj} - S_w^i}\right) = \lambda_2(S_w^i, C_{CO_2}^{wi}). \tag{4.44}$$

Shock waves and contact discontinuities are transition surfaces across which the mass flux is continuous, but unlike shock discontinuities, there is no fluid flow or component transport across contact discontinuity surfaces, i.e., mass flux is zero (velocity is zero) across the contact discontinuity [93, 60]. In addition, we have a semi-shock - also known as tangent shock - instead of shock by itself, because the saturation wave traveling behind the shock has the same speed as the semi-shock [87, 88], i.e.,

$$\frac{\theta q_t}{\pi h \phi}\frac{\partial f_w}{\partial S_w}(S_{wf}) = \frac{\theta q_t}{\pi h \phi}\left(\frac{f_w(S_{wf}) - f_w(S_{iw})}{S_{wf} - S_{iw}}\right) > \frac{\theta q_t}{\pi h \phi}\frac{\partial f_w}{\partial S_w}(S_{iw}). \tag{4.45}$$

The slope of the line contacting $(S_w^i, C_{CO_2}^{wi})$ to $(S_w^{inj}, C_{CO_2}^{winj})$ given by λ_2 can only be less or equal the slope of the injection water fractional curve at $(S_w^{inj}, C_{CO_2}^{winj})$, given by $\frac{\theta q_{inj}}{\phi \pi h}\frac{\partial f_w(S_w^{inj}, C_{CO_2}^{winj})}{\partial S_w}$. If $\lambda_2 < \frac{\theta q_{inj}}{\phi \pi h}\frac{\partial f_w(S_w^{inj}, C_{CO_2}^{winj})}{\partial S_w}$, the speed of the wave behind of contact

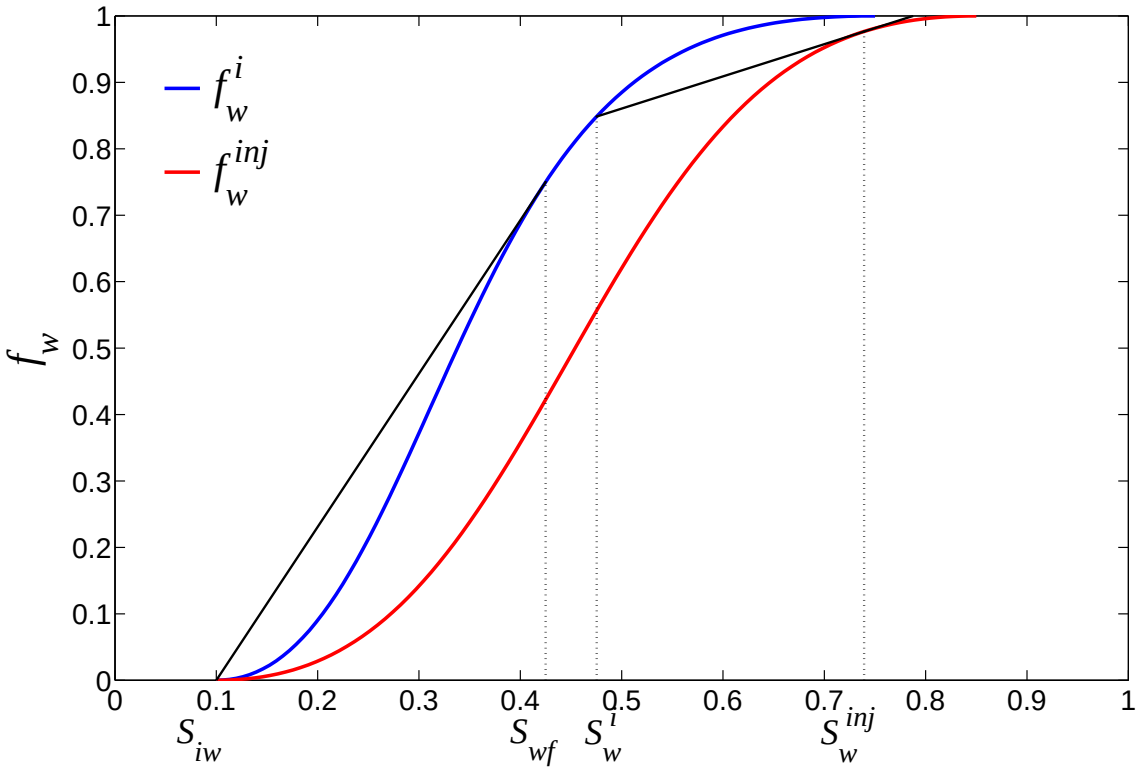

(a)

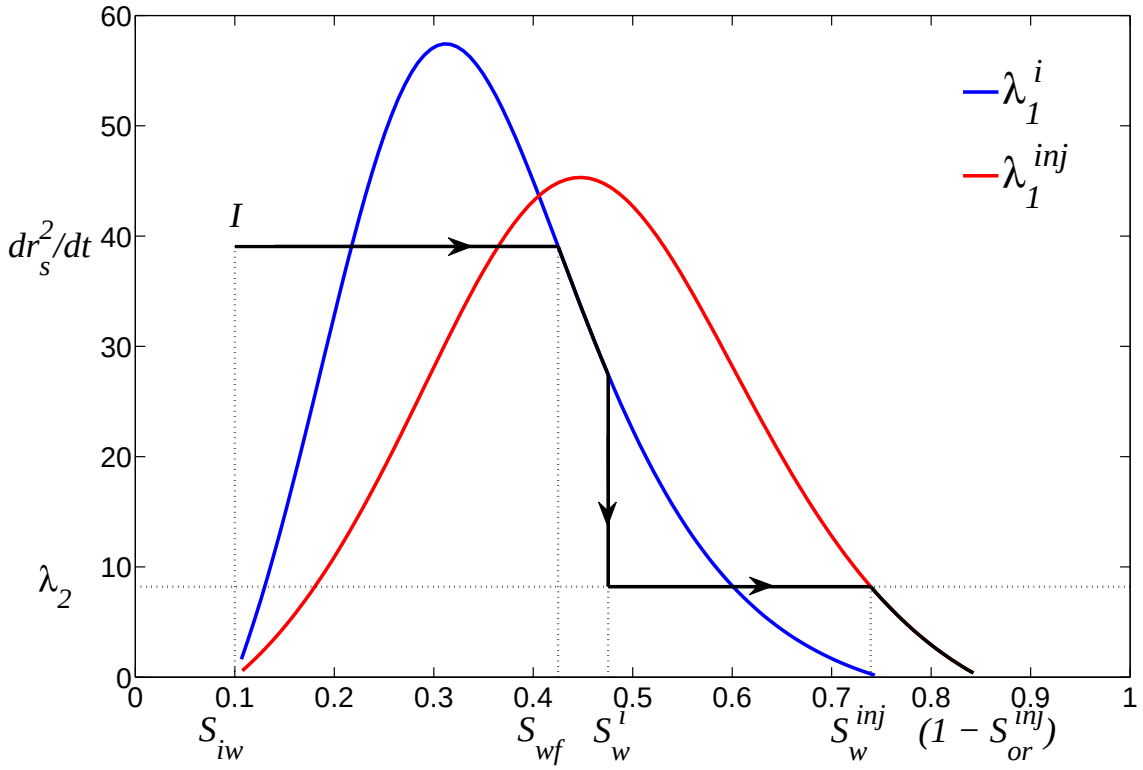

(b)

Figure 4.2: Contact and semi-shock discontinuities in the water fractional flow curves (a) and the wave velocity path solution from S_{iw} to $1 - S_{or}^{inj}$, showing the switching points - S_{wf}, S_w^i and S_w^{inj} - that satisfy the velocity constraint (b).

discontinuity would be higher than the speed of the contact discontinuity, which goes against the monotonic condition. Therefore, to satisfy the velocity constraint, λ_2 must corresponds to a line in the (S_w,f_w) plane whose slope is tangent to f_w^{inj} curve, i.e,

$$\lambda_2 = \frac{\theta q_{inj}}{\phi \pi h} \frac{\partial f_w(S_w^{inj}, C_{CO_2}^{winj})}{\partial S_w}, \tag{4.46}$$

which represents a line of slope $\frac{\partial f_w(S_w^{inj}, C_{CO_2}^{winj})}{\partial S_w}$ in the (S_w,f_w) plane that passes through point

$$(S_w, f_w) = \left(- \frac{K_{wo-CO_2} + \rho_M \frac{1-\phi}{\phi} K_s}{1 - K_{wo-CO_2}}, - \frac{K_{wo-CO_2}}{1 - K_{wo-CO_2}} \right). \tag{4.47}$$

The jump in the CO_2 concentration causes a jump in saturation, given by

$$\lambda_2 = \frac{\theta q_{inj}}{\phi \pi h} \frac{f_w(S_w^{inj}, C_{CO_2}^{winj}) - f_w(S_w^i, C_{CO_2}^{wi})}{S_w^{inj} - S_w^i}. \tag{4.48}$$

Once Eq. 4.46 and 4.47 are solved together numerically (or graphically) to find S_w^{inj} and λ_2, Eq. 4.48 can be solved numerically (or graphically) to find S_w^i. Because S_w^i moves with a higher speed than the contact discontinuity ($\lambda_2 < \frac{\theta q_{inj}}{\phi \pi h} \frac{\partial f_w(S_w^i, C_{CO_2}^{wi})}{\partial S_w}$, as we can see in Fig. 4.2), a region of constant saturation equal to S_w^i is formed ahead of the concentration front. The speed of the semi-shock that is formed at the water front is given by

$$\frac{dr_{f,inj}^2}{dt} = \frac{\theta q_{inj}}{\phi \pi h} \frac{f_w(S_{wf}, C_{CO_2}^{wi}) - f_w(S_{iw}, C_{CO_2}^{wi})}{S_{wf} - S_{iw}}, \tag{4.49}$$

which does satisfy the Oleinik entropy condition [74] for any $S_w \in (S_w^i, S_{iw})$; hence this shock wave solution is the unique solution. Since this semi-shock has a higher speed than S_w^i, a rarefaction wave is formed between the constant zone and the water front. In summary, the saturation distribution solution during the injection period consists of a $(1 - S_{or}^{inj}) - S_w^{inj} \rightarrow S_w^i - S_{wf} \rightarrow S_{iw}$ configuration, where S_{or}^{inj} corresponds to $S_{or}(C_{CO_2}^w)$. Here, "–" represents a rarefaction fan and "→" represents a shock or discontinuity. In another words, the solution consists of a family of rarefaction waves carrying the CO_2 injection concentration,

a contact discontinuity, a constant zone at S_w^i, a family of rarefaction waves carrying the CO_2 initial concentration, a semi-shock and a uniform region at initial condition, S_{iw}. The r^2-t diagram with the characteristic curves corresponding to this solution is shown in Fig. 4.3. In Fig. 4.3, from upstream to downstream, the injection period is composed of a family of rarefaction waves carrying $C_{CO_2}^{winj}$, a contact discontinuity, a constant zone ($S_w = S_w^i$), a family of rarefaction waves carrying $C_{CO_2}^{wi}$, a semi-shock and another region of constant saturation equal to S_{iw}. Translating into the language of mathematics, the unique solution for the injection period has the form

$$C_{CO_2}^{w}(r,t) = \begin{cases} C_{CO_2}^{winj}, & r_w^2 \leq r^2 < r_w^2 + \frac{\theta q_{inj}}{\phi \pi h} \frac{\partial f_w(S_w^{inj}, C_{CO_2}^{winj})}{\partial S_w} t \\ C_{CO_2}^{wi}, & r_w^2 + \frac{\theta q_{inj}}{\phi \pi h} \frac{\partial f_w(S_w^{inj}, C_{CO_2}^{winj})}{\partial S_w} t \leq r^2 \end{cases} \tag{4.50}$$

and

$$S_w(r,t) = \begin{cases} \left(\frac{df_w^{inj}}{dS_w}\right)^{-1} \left(\frac{\phi \pi h}{\theta q_{inj}} \frac{(r^2 - r_w^2)}{t}\right), & r_w^2 \leq r^2 < r_w^2 + \frac{\theta q_{inj} t}{\phi \pi h} \frac{\partial f_w(S_w^{inj}, C_{CO_2}^{winj})}{\partial S_w} \\ S_w^i, & r_w^2 + \frac{\theta q_{inj} t}{\phi \pi h} \frac{\partial f_w(S_w^{inj}, C_{CO_2}^{winj})}{\partial S_w} \leq r^2 < r_w^2 + \frac{\theta q_{inj}}{\phi \pi h} \frac{\partial f_w(S_w^{i}, C_{CO_2}^{wi})}{\partial S_w} \\ \left(\frac{df_w^{i}}{dS_w}\right)^{-1} \left(\frac{\phi \pi h}{\theta q_{inj}} \frac{(r^2 - r_w^2)}{t}\right), & r_w^2 + \frac{\theta q_{inj} t}{\phi \pi h} \frac{\partial f_w(S_w^{i}, C_{CO_2}^{wi})}{\partial S_w} \leq r^2 < r_w^2 + \frac{\theta q_{inj} t}{\phi \pi h} \frac{\partial f_w(S_{wf}, C_{CO_2}^{wi})}{\partial S_w} \\ S_{wi}, & r_w^2 + \frac{\theta q_{inj} t}{\phi \pi h} \frac{\partial f_w(S_{wf}, C_{CO_2}^{wi})}{\partial S_w} \leq r^2. \end{cases} \tag{4.51}$$

The concentration and saturation profiles for the end of injection period are shown in Fig. 4.4, where r_d is the concentration front position, given by

$$r_d^2(t) = r_w^2 + \frac{\theta q_{inj} t}{\phi \pi h} \frac{\partial f_w(S_w^{inj}, C_{CO_2}^{winj})}{\partial S_w} = r_w^2 + \frac{\theta q_{inj} t}{\phi \pi h} \frac{f_w(S_w^{inj}, C_{CO_2}^{winj}) - f_w(S_w^{i}, C_{CO_2}^{wi})}{S_w^{inj} - S_w^{i}}, \tag{4.52}$$

r_{iw} is the position of the constant zone,

$$r_{iw}^2(t) = r_w^2 + \frac{\theta q_{inj} t}{\phi \pi h} \frac{\partial f_w(S_w^{i}, C_{CO_2}^{wi})}{\partial S_w}, \tag{4.53}$$

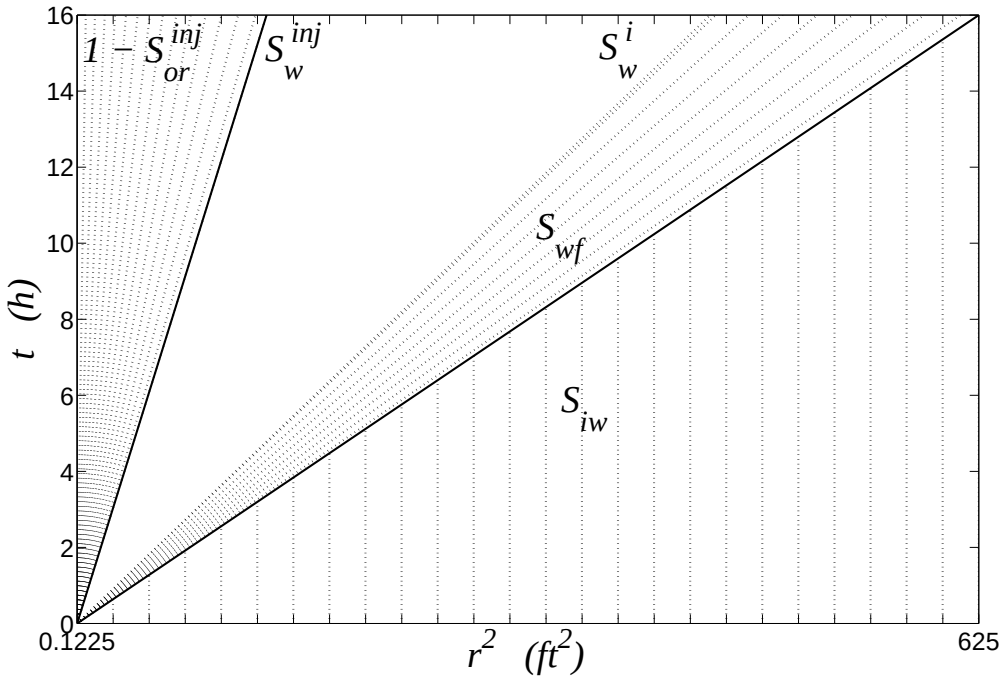

Figure 4.3: Characteristic lines of the injection problem in the r^{2}t-plane. From upstream to downstream, the injection period is composed of a family of rarefaction waves carrying $C_{CO_2}^{winj}$, a contact discontinuity, a constant zone ($S_w = S_w^i$), a family of rarefaction waves carrying $C_{CO_2}^{wi}$, a semi-shock and another region of constant saturation equal to S_{iw}.

and $r_{f,inj}$ is the water front position,

$$r_{f,inj}^2(t) = r_w^2 + \frac{\theta q_{inj} t}{\phi \pi h} \frac{\partial f_w(S_{wf}, C_{CO_2}^{wi})}{\partial S_w} = r_w^2 + \frac{\theta q_{inj} t}{\phi \pi h} \frac{f_w(S_{wf}, C_{CO_2}^{wi}) - f_w(S_{iw}, C_{CO_2}^{wi})}{S_{wf} - S_{iw}}. \quad (4.54)$$

Note in in Fig. 4.4 that CO_2 from the injected water is transfered to the oil in place in the region behind the concentration front.

In the derivations showed above, we have assumed that $S_{wf} < S_w^i$. However, depending on the shape of the initial and injection fractional flow curves and on the point (S_w, f_w) given by Eq. 4.47 (i.e, depending on the rock-fluid properties combination), the point in the initial fractional flow curve to which the slope of a line starting from S_{iw} would be tangent could be greater than S_w^i. In this case, $S_{wf} = S_w^i$. If that is the case, the solution to the system of hyperbolic equation is slightly different from the one we just described. The family of rarefaction waves carrying the initial concentration vanishes but the solution still consists of two discontinuities: a contact discontinuity between CO_2 injection and initial concentrations

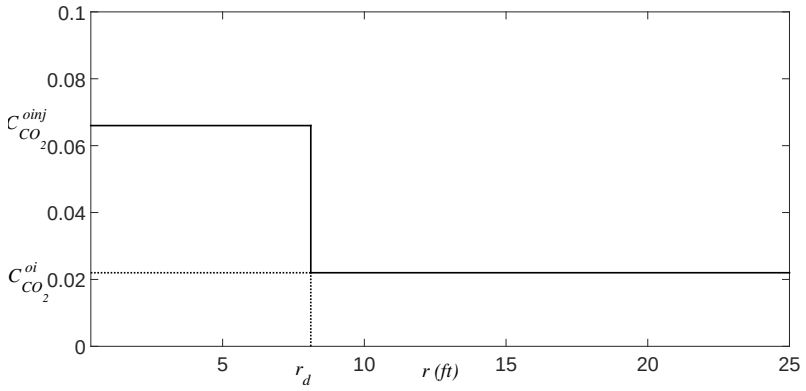

(a)

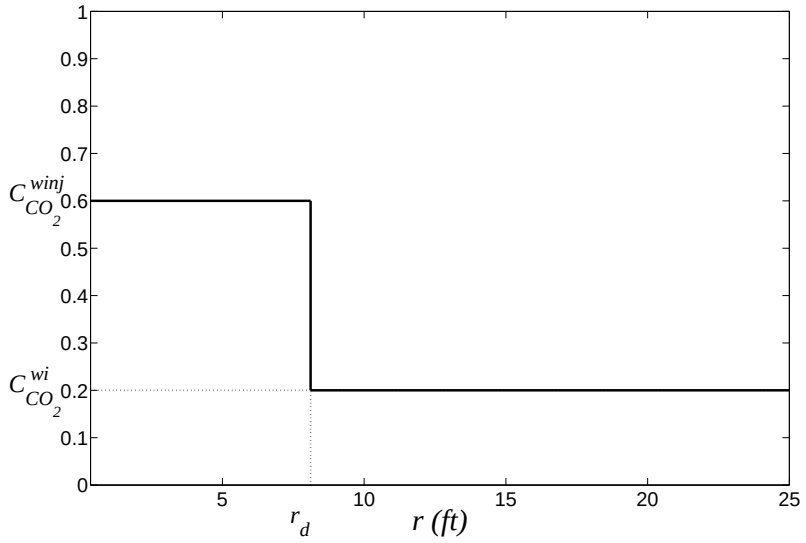

(b)

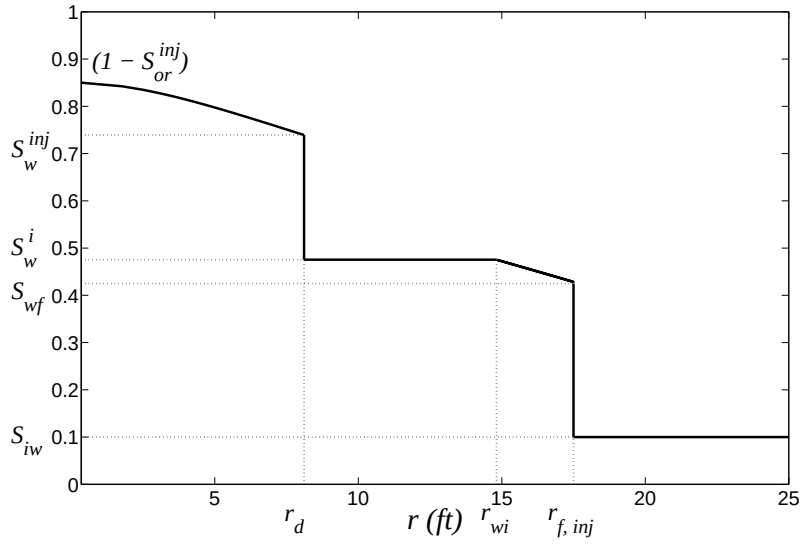

(c)

Figure 4.4: CO_2 concentration profile in the oil (a) and the water (b) phase together with the saturation profile (c) at the end of the injection period. Note; CO_2 from the injected water is transfered to the oil in place in the region behind the concentration front.

and one shock in saturation caused by the fact that the constant region moves with a higher speed than the initial water saturation. In this case we have shock instead of semi-shock since $\frac{\theta q_{inj}}{\phi\pi h}\frac{\partial f_w(S_w^i,C_{CO_2}^{wi})}{\partial S_w} > \frac{\theta q_{inj}}{\phi\pi h}\frac{f_w(S_w^i,C_{CO_2}^{wi})-f_w(S_{iw},C_{CO_2}^{wi})}{S_w^i-S_{iw}} > \frac{\theta q_{inj}}{\phi\pi h}\frac{\partial f_w(S_{iw},C_{CO_2}^{wi})}{\partial S_w}$. Fig. 4.5b shows the unique wave velocity path from from the initial saturation, S_{iw}, to the injected saturation, $1-S_{or}^{inj}$, that satisfies the velocity constraint, with the following switching points: S_{iw}, S_w^i, S_w^{inj} and $1-S_{or}$. Fig. 4.5a presents the contact and shock discontinuities in the water fractional flow curves. The speed of the shock which is formed ahead of the constant zone in this case is given by

$$\frac{dr_{f,inj}^2}{dt} = \frac{\theta q_{inj}}{\phi\pi h}\frac{f_w(S_w^i,C_{CO_2}^{wi}) - f_w(S_{iw},C_{CO_2}^{wi})}{S_w^i - S_{iw}}, \tag{4.55}$$

which does satisfy the Oleinik entropy condition [74] for any $S_w \in (S_w^i, S_{iw})$; hence is unique. In summary, the saturation distribution solution during the injection period in this case consists of a $(1-S_{or}^{inj}) - S_w^{inj} \rightarrow S_w^i \rightarrow S_{iw}$ configuration. In another words, the solution consists of a family of rarefaction waves, a contact discontinuity, a constant zone, a shock and a uniform region at initial condition, S_{iw}.

The(r^2-t)-diagram with the characteristic curves corresponding to this solution is shown in Fig. 4.6. In Fig. 4.6, from upstream to downstream, the injection period is composed of a family of rarefaction waves, a contact discontinuity, a constant zone ($S_w = S_w^i$), a shock and another region of constant saturation equal to S_{iw}. Note; in this case, the region corresponding to the family of rarefaction waves from S_{wf} to S_{iw} carrying the initial concentration is not present, since $S_{wf} = S_{iw}$. Translating into the language of mathematics, the unique solution for the injection period in this case has the form

$$C_{CO_2}^w(r,t) = \begin{cases} C_{CO_2}^{winj}, & r_w^2 \le r^2 < r_w^2 + \frac{\theta q_{inj} t}{\phi\pi h}\frac{\partial f_w(S_w^{inj},C_{CO_2}^{winj})}{\partial S_w} \\ C_{CO_2}^{wi}, & r_w^2 + \frac{\theta q_{inj} t}{\phi\pi h}\frac{\partial f_w(S_w^{inj},C_{CO_2}^{winj})}{\partial S_w} \le r^2 \end{cases} \tag{4.56}$$

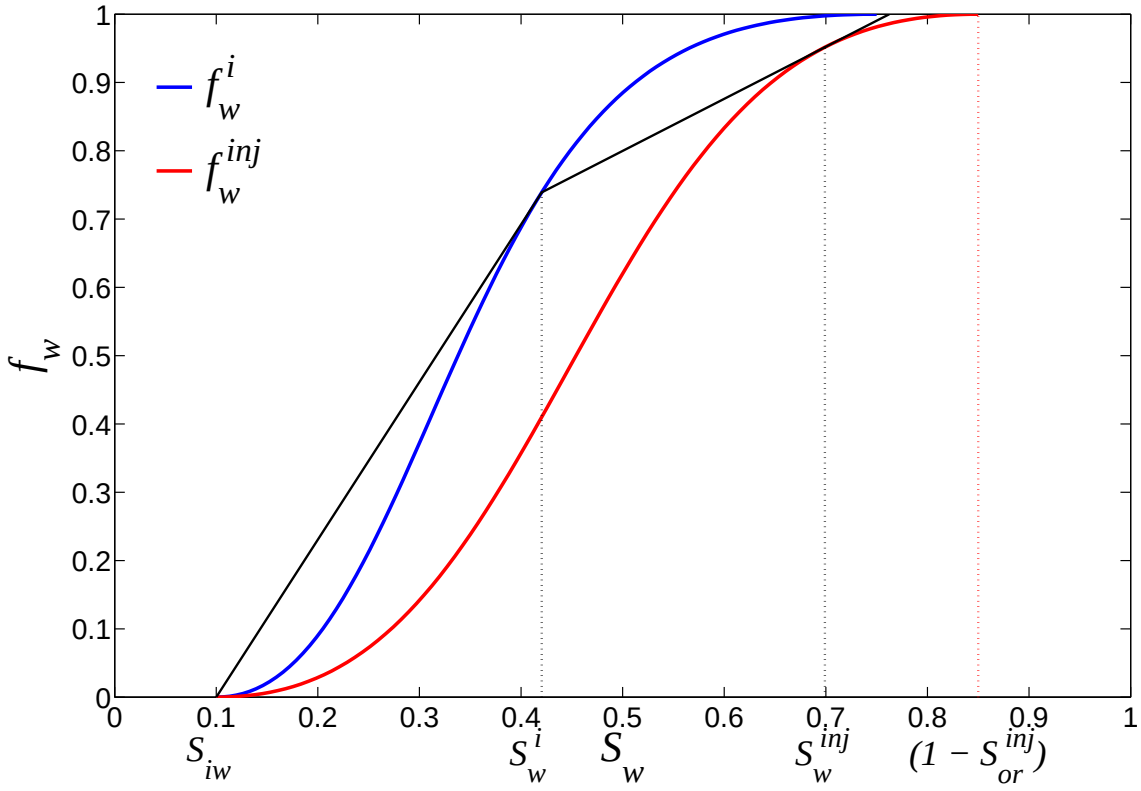

(a)

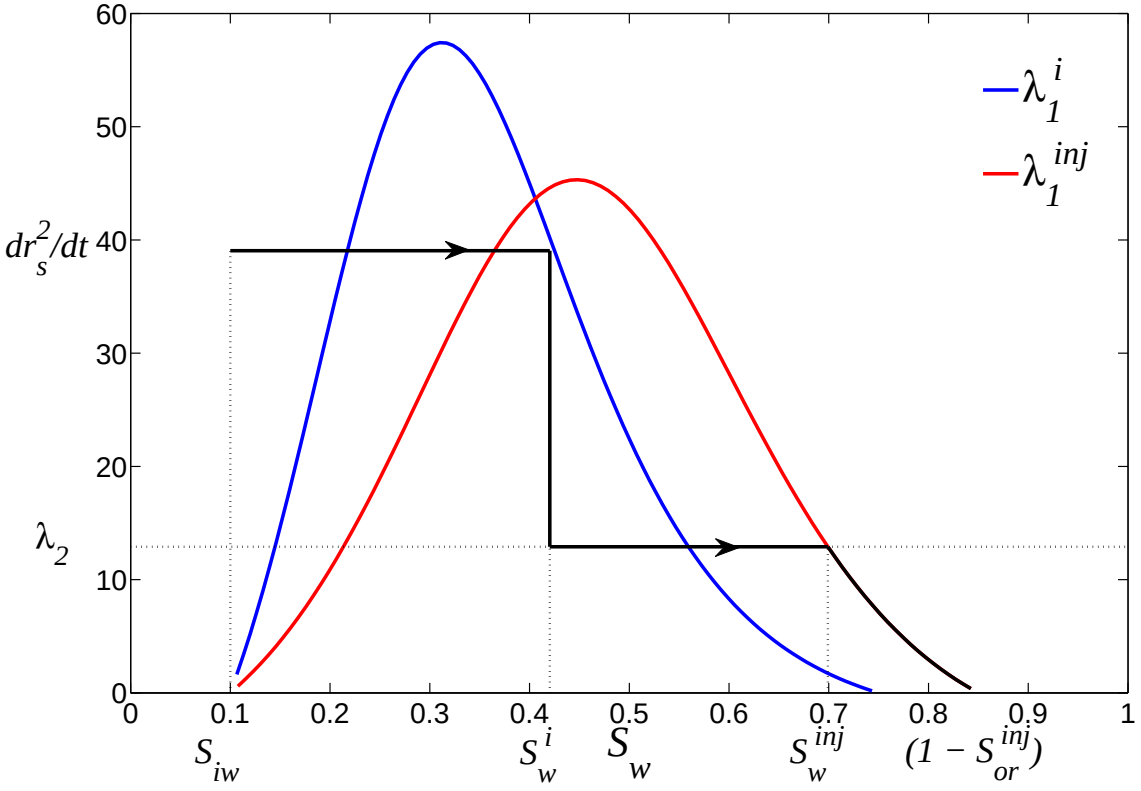

(b)

Figure 4.5: Contact and shock discontinuities in the water fractional flow curves (a) and the wave velocity path solution from S_{iw} to $1 - S_{or}^{inj}$, showing the switching points - S_w^i and S_w^{inj} - that satisfy the velocity constraint (b) for the case when $S_{wf} = S_w^i$.

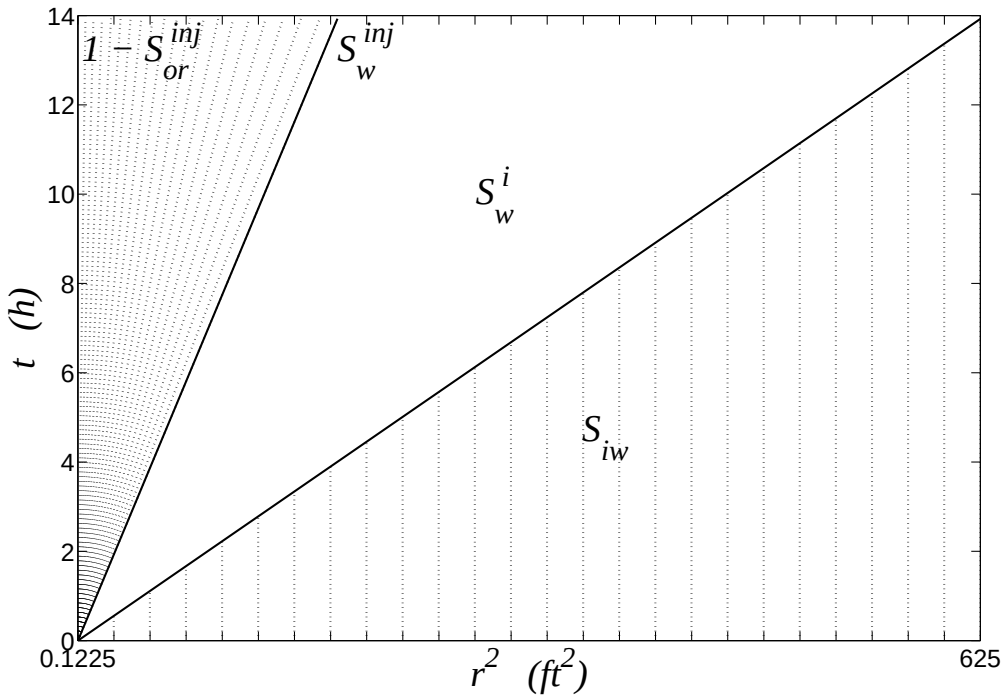

Figure 4.6: Characteristic lines of the injection problem in the r^2t-plane for the case when $S_{wf} = S_w^i$. From upstream to downstream, the injection period is composed of a family of rarefaction waves, a contact discontinuity, a constant zone ($S_w = S_w^i$), a shock and another region of constant saturation equal to S_{iw}.

and

$$S_w(r,t) = \begin{cases} \left(\frac{df_w^{inj}}{dS_w}\right)^{-1}\left(\frac{\phi\pi h}{\theta q_{inj}}\frac{(r^2-r_w^2)}{t}\right), & r_w^2 \le r^2 < r_w^2 + \frac{\theta q_{inj} t}{\phi\pi h}\frac{\partial f_w(S_w^{inj},C_{CO_2}^{winj})}{\partial S_w} \\ S_w^i, & \frac{\theta q_{inj} t}{\phi\pi h}\frac{\partial f_w(S_w^{inj},C_{CO_2}^{winj})}{\partial S_w} \le r^2 - r_w^2 < \frac{\theta q_{inj} t}{\phi\pi h}\frac{f_w(S_w^i,C_{CO_2}^{wi}) - f_w(S_{iw},C_{CO_2}^{wi})}{S_w^i - S_{iw}} \\ S_{wi}, & r_w^2 + \frac{\theta q_{inj} t}{\phi\pi h}\frac{f_w(S_w^i,C_{CO_2}^{wi}) - f_w(S_{wi},C_{CO_2}^{wi})}{S_w^i - S_{wi}} \le r^2. \end{cases} \tag{4.57}$$

The concentration and saturation profiles for this case at the end of injection period are shown in Fig. 4.7, where the water front position in this case is given by

$$r_{f,inj}^2(t) = r_w^2 + \frac{\theta q_{inj} t}{\phi\pi h}\frac{f_w(S_w^i, C_{CO_2}^{wi}) - f_w(S_{iw}, C_{CO_2}^{wi})}{S_w^i - S_{iw}}. \tag{4.58}$$

Note in Fig. 4.7 that CO_2 from the injected water is transfered to the oil in place in the region behind the concentration front.

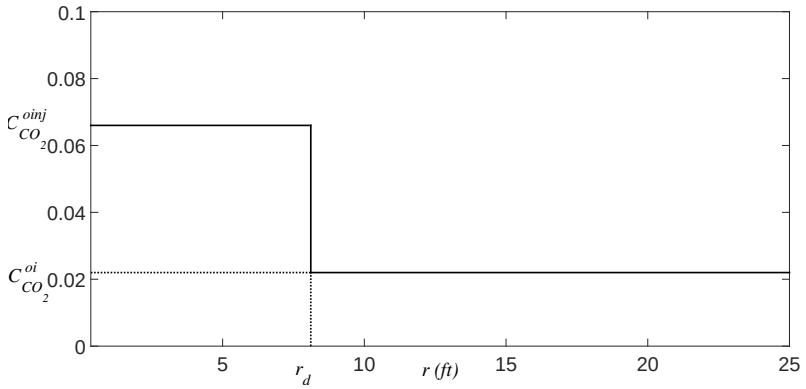

(a)

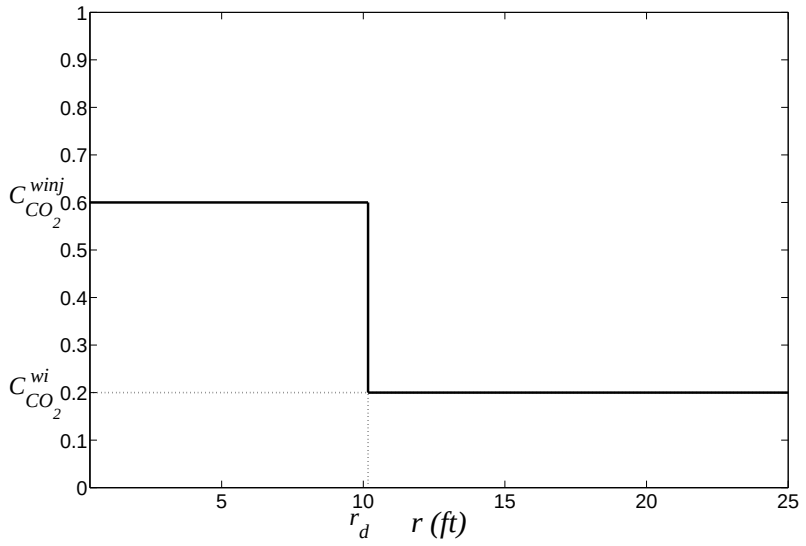

(b)

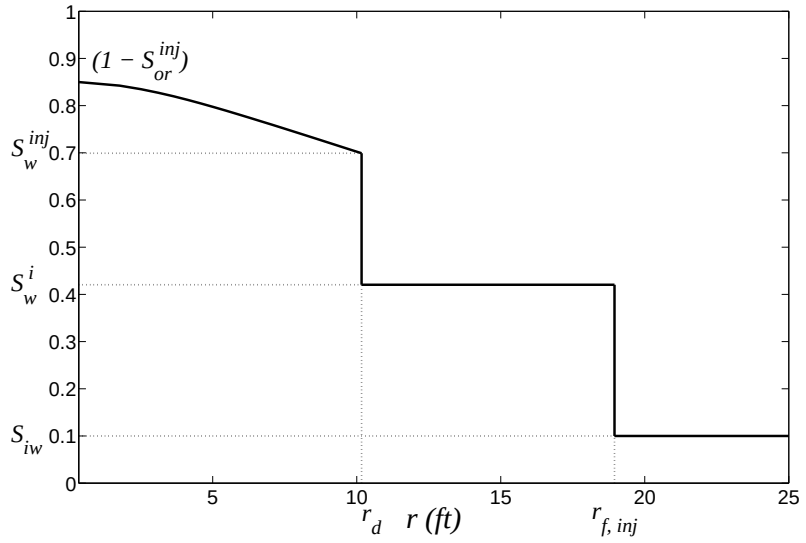

(c)

Figure 4.7: CO_2 concentration profile in the oil (a) and the water (b) phase together with the saturation profile (c) at the end of the injection period for the case when $S_{wf} > S_w^i$. Note; CO_2 from the injected water is transfered to the oil in place in the region behind the concentration front.

Falloff: During the falloff stage, it is assumed that there is no fluid movement in the reservoir, which is reasonable as we neglect capillary pressure, gravity force and fluid compressibilities. Although it is possible to consider the diffusion of CO_2, for short falloff periods, as we believe the wellbore pressure is be insensitive to this effect. Therefore, we also neglect the component redistribution in the reservoir.

4.1.2 Wellbore Pressure History

Injection: During injection at a constant flow rate $q_{inj} = q_t(r_w, t)$ RB/D, where $t = 0$ at the beginning of the water injection, by integrating Darcy's law as in Thompson and Reynolds [98] and Peres and Reynolds [79], the bottom hole pressure difference from the reservoir initial pressure (p_i) can be expressed as

$$\Delta p_{wf}(t) = p_{wf}(t) - p_i = \int_{r_w}^{\infty} \frac{\alpha q_t(r,t)}{h\lambda_t(r,t)k(r)} \frac{dr}{r}, \tag{4.59}$$

where α is a unit conversion factor with $\alpha = 141.2$ when oil field units are used, $q_{inj} > 0$,

$$k(r) = \begin{cases} k_{skin}, & r_w < r \leq r_{skin} \\ k, & r > r_{skin} \end{cases} \tag{4.60}$$

and $\lambda_t = \frac{k_{ro}}{\mu_o} + \frac{k_{rw}}{\mu_w}$. Taking the derivative of Eq. 4.59 with respect to the logarithm of time, $\ln t$, we have

$$\frac{\partial \Delta p_{wf}(t)}{\partial \ln t} = \frac{\alpha}{h} \int_{r_w}^{\infty} \frac{1}{r} \left(\frac{\partial q_t(r,t)}{\partial \ln t} - \frac{q_t(r,t)}{\lambda_t(r,t)} \frac{\partial \lambda_t(r,t)}{\partial \ln t} \right) \frac{1}{\lambda_t(r,t)k(r)} dr. \tag{4.61}$$

Let $r_{f,inj}(t)$ be the radius of the water front at any time t during the injection period. Using the Thompson and Reynolds [98] steady theory, which assumes that, $q_t(r,t) = q_{inj}$,

for $r \leq r_{f,inj}(t)$, Eq. 4.59 becomes

$$\Delta p_{wf}(t) = \frac{\alpha q_{inj}}{h} \int_{r_w}^{r_{f,inj}(t)} \frac{1}{\lambda_t(r,t)k(r)} \frac{dr}{r} + \frac{\alpha}{h} \int_{r_{f,inj}(t)}^{\infty} \frac{q_t(r,t)}{\lambda_t(r,t)k(r)} \frac{dr}{r}, \tag{4.62}$$

where for any reasonable set of parameters, Peres and Reynolds [79] indicate that the flood front is within an steady-state zone. Adding and subtracting the term

$$\frac{\alpha}{h} \int_{r_w}^{r_{finj}(t)} \frac{q_{inj}}{\hat{\lambda}_o k(r)} \frac{dr}{r}$$

to Eq. 4.62, where $\hat{\lambda}_o = \frac{k_{ro}(S_{iw}, C^{oi}_{CO_2})}{\mu_o(C^{oi}_{CO_2})}$ is the endpoint oil mobility at $S_w = S_{iw}$ and $C^o_{CO_2} = C^{oi}_{CO_2}$, Eq. 4.62 can be rewritten as

$$\begin{aligned}\Delta p_{wf}(t) =& \frac{\alpha q_{inj}}{h} \int_{r_w}^{r_{f,inj}(t)} \left(\frac{1}{\lambda_t(r,t)} - \frac{1}{\hat{\lambda}_o}\right) \frac{dr}{k(r)r} + \frac{\alpha}{h} \int_{r_w}^{\infty} \frac{q_t(r,t)}{\hat{\lambda}_o(r,t)k(r)} \frac{dr}{r} \\ =& \Delta \hat{p}_o + \frac{\alpha q_{inj}}{h\hat{\lambda}_o} \int_{r_w}^{r_{wf}(t)} \left(\frac{\hat{\lambda}_o}{\lambda_t(r,t)} - 1\right) \frac{1}{k(r)} \frac{dr}{r}. \end{aligned} \tag{4.63}$$

The single-phase oil transient pressure drop ($\Delta \hat{p}_o$) can be approximated as

$$\Delta \hat{p}_o = p_{wf,o}(t) - p_i = \frac{\alpha q_{inj}}{kh\hat{\lambda}_o} \left[\frac{1}{2} \ln \left(\frac{\beta k \hat{\lambda}_o t}{\phi \hat{c}_{to} r_w^2}\right) + 0.4045 + s\right], \tag{4.64}$$

where β is a unit conversion factor which in oil field units with time in hours is equal to 0.0002637 and

$$\hat{c}_{to} = c_o(1 - S_{iw}) + c_w S_{iw} + c_r, \tag{4.65}$$

with the oil compressibility (c_o) and the water compressibility (c_w) being functions of $C^{oi}_{CO_2}$ and $C^{wi}_{CO_2}$, respectively, are assumed to be known.

Falloff: During falloff, assuming that the saturation distribution remains constant and equal to the distribution at the end of injection period, the bottom hole pressure drop can be expressed as

$$\Delta p_{ws}(\Delta t_{foff}) = p_{ws}(\Delta t_{foff}) - p_i = \int_{r_w}^{\infty} \frac{\alpha q_s(r, \Delta t_{foff})}{h\lambda_t(r, t_{inj})k(r)} \frac{dr}{r}, \tag{4.66}$$

where $\Delta t_{foff} = 0$ at the beginning of the falloff period, $p_{ws}(\Delta t_{foff})$ denotes the falloff pressure at time Δt_{foff} and t_{inj} is the time at the end of the injection period. Taking the derivative of Eq. 4.66 with respect to the logarithm of time, $\ln \Delta t_{foff}$, we have

$$\frac{\partial \Delta p_{ws}(\Delta t_{foff})}{\partial \ln \Delta t_{foff}} = \frac{\alpha}{h} \int_{r_w}^{\infty} \frac{1}{r} \frac{\partial q_s(r, \Delta t_{foff})}{\partial \ln \Delta t_{foff}} \frac{1}{k(r)\lambda_t(r, t_{inj})} dr. \tag{4.67}$$

Eq. 4.66 can be rewritten as

$$\Delta p_{ws}(\Delta t_{foff}) = \frac{\alpha}{h} \int_{r_w}^{r_{f,inj}(t_{inj})} \frac{q_s(r, \Delta t_{foff})}{\lambda_t(r, t_{inj})k(r)} \frac{dr}{r} + \frac{\alpha}{h} \int_{r_{f,inj}(t_{inj})}^{\infty} \frac{q_s(r, \Delta t_{foff})}{\lambda_t(r, t_{inj})k(r)} \frac{dr}{r}, \tag{4.68}$$

where q_s is the total flow rate profile during the shut-in period. Following Peres et al. [82], we add and subtract the term

$$\frac{\alpha}{h} \int_{r_w}^{r_{f,inj}(t)} \frac{q_{os}(r, \Delta t_{foff})}{\hat{\lambda}_o k(r)} \frac{dr}{r}$$

to Eq. 4.68 and rearrange the resulting equation to obtain

$$\Delta p_{ws}(\Delta t_{foff}) = \Delta \hat{p}_{os}(\Delta t_{foff}) + \frac{\alpha}{h\hat{\lambda}_o} \int_{r_w}^{r_{f,inj}(t_{inj})} \left(\frac{\hat{\lambda}_o}{\lambda_t(r, t_{inj})} q_s(r, \Delta t_{foff}) - q_{os}(r, \Delta t_{foff}) \right) \frac{dr}{k(r)r}. \tag{4.69}$$

This result assumes that for $r > r_{f,inj}(t_{inj})$, $q_s(r, \Delta t_{foff}) = q_{os}(r, \Delta t_{foff})$, where $q_{os}(r, \Delta t_{foff})$

is the single-phase rate profile obtained during falloff after injecting oil at the rate q_{inj}. We are considering only infinite-acting behavior. So that the single oil phase pressure drop can be defined from the superposition of two constant flow rate solutions is given by

$$\Delta\hat{p}_{os}(\Delta t_{foff}) = p_{wf,o}(\Delta t_{foff}) - p_i = \frac{\alpha q_{inj}}{2kh\hat{\lambda}_o} \ln\left(\frac{t_{inj} + \Delta t_{foff}}{\Delta t_{foff}}\right), \tag{4.70}$$

with the rate schedule

$$q(r_w, t) = \begin{cases} q_{inj} > 0 & 0 < t \leq t_{inj} \\ 0 & t_{inj} < t \leq t_{inj} + t_{foff}, \end{cases} \tag{4.71}$$

where t_{foff} is the time at the end of the falloff period. As rate superposition applies for single-phase flow [82],

$$q_{os}(\Delta t_{foff}) = q_{inj}\left[\exp\left(-\frac{\phi\hat{c}_{to}r^2}{4\beta\hat{\lambda}_o(t_{inj} + \Delta t_{foff})}\right) - \exp\left(-\frac{\phi\hat{c}_{to}r^2}{4\beta\hat{\lambda}_o\Delta t_{foff}}\right)\right]. \tag{4.72}$$

Following Peres et al. [82], we use rate superposition to approximate the multiphase rate profiles as

$$q_s(\Delta t_{foff}) = q_{inj}\left[\exp\left(-\frac{\phi c_t(r, t_{inj})r^2}{4\beta\lambda_t(r, t_{inj})(t_{inj} + \Delta t_{foff})}\right) - \exp\left(-\frac{\phi c_t(r, t_{inj})r^2}{4\beta\lambda_t(r, t_{inj})\Delta t_{foff}}\right)\right], \tag{4.73}$$

with

$$c_t(r, \Delta t_{foff}) = c_o(C^o_{CO_2}(r, t_{inj}))S_o(r, t_{inj}) + c_w(C^w_{CO_2}(r, t_{inj}))S_w(r, t_{inj}) + c_r. \tag{4.74}$$

4.2 Validation

"The model is great but

there seems to be something wrong with the reservoir."

—L. P. Dake in *The Practice of Reservoir Engineering*

We compared our analytical solution with the commercial numerical simulator GEM, using the properties shown in Table 4.1. To match our solution with GEM, we have to use very small time steps as well as highly refined radial grids. We also have to keep the water viscosity independent of concentration and disregard the carbon dioxide adsorption in the rock. Fig. 4.8 presents the comparison between the concentration (in molar fraction) and saturation distributions obtained from our solution with the reservoir numerical simulator at the end of the injection period. We can see, except near the contact discontinuity, there is a very good agreement between the solution we developed and the numerical simulator results, which suffers from numerical dispersion. The accentuated difference between our concentration/saturation distributions and the numerical distribution obtained from the commercial simulator around the contact discontinuity is driven by the fact that while our solubility model is linear, the solubility model used by the simulator is non-linear, which results in a rarefaction wave. Although we could develop a solution using the same model as the simulator, the wellbore pressure shown in Fig. 4.9 which is the variable of interest does not seems to be sensitive to the difference between the two concentration/saturation profiles. Fig. 4.9 presents the comparison between the bottom hole pressure obtained from our solution with the reservoir numerical simulator during the whole carbonated water injection and falloff test. Our pressure solution is in agreement with the GEM result throughout the injection period, we believe it is not necessary to complicate the analytical model. Our model underestimate the wellbore pressure in the early times of falloff period. We believe this occurs because we assume an oil constant compressibility equal to the initial oil compressibility for the single-phase pressure drop term (Eq. 4.70) while the wellbore pressure is reflecting injected oil compressibility in the beginning of the falloff. Since in the falloff, the multiphase

Table 4.1: Reservoir, rock and fluid properties for simulation and analytical solution.

Property	Value	Unit
q_{inj}	3500	RB/DAY
h	60	ft
r_w	0.35	ft
r_e	6800	ft
k	300	md
s	5	
a_w	0.5	
a_o	1	
n_w	2	
n_o	2	
$C^{wi}_{CO_2}$	0.19	lb/ft^3 (0.0013 molar fraction)
$C^{winj}_{CO_2}$	14.76	lb/ft^3 (0.106 molar fraction)
S_{iw}	0.10	
S_{or}	0.25	
p_i	2500	psi
T	200	°F
ϕ	0.22	
$c_o(C^{wi}_{CO_2})$	8.0×10^{-6}	1/psi
$c_w(C^{wi}_{CO_2})$	3.02×10^{-6}	1/psi
c_r	5.0×10^{-6}	1/ft
$\mu_o(C^{wi}_{CO_2})$	3.28	cp
$\mu_o(C^{winj}_{CO_2})$	1.06	cp
μ_w	0.5	cp
ρ_M	130	lb/ft^3
K_s	0	ft^3 /lb-rock
K_{wo-CO_2}	0.11	

pressure drop (last term in Eq. 4.69) is negligible compared to the the single-phase term, our model fail to estimate the correct pressure. We could try to fix this disagreement by trying to development and early and long time solution for falloff or using a numerical method to calculate the wellbore pressure, but since we could estimate the reservoir parameters (as we will show in the next section, Section **Example**), we believe that is unnecessary.

To be consistent with standard pressure transient analysis procedures, Fig. 4.10 presents the log-log diagnostic plots of injection (top) and falloff (bottom) of the pressure data, with $s = 0$. We can see that at early times of injection, there is a plateau (stabilization)

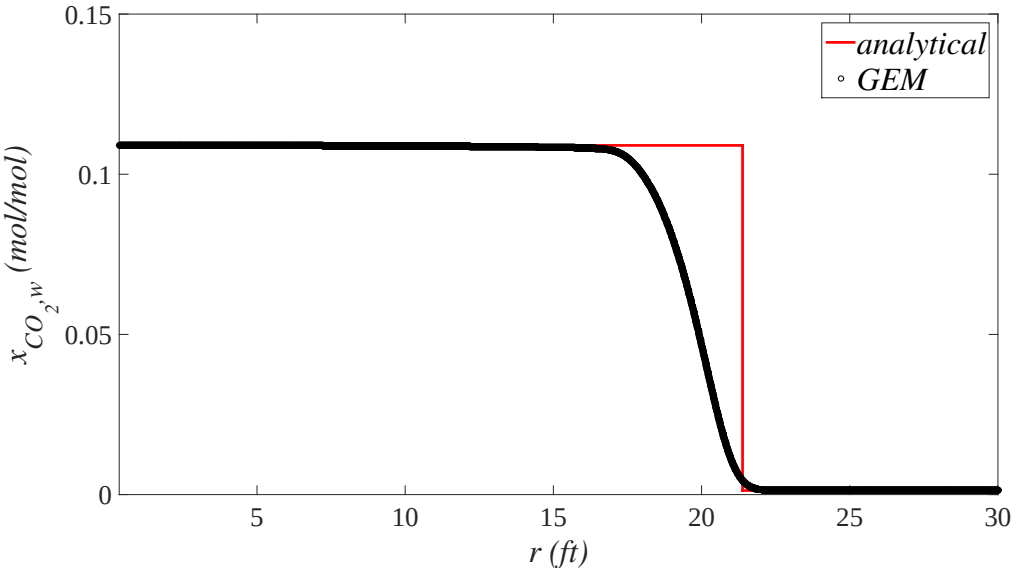

(a)

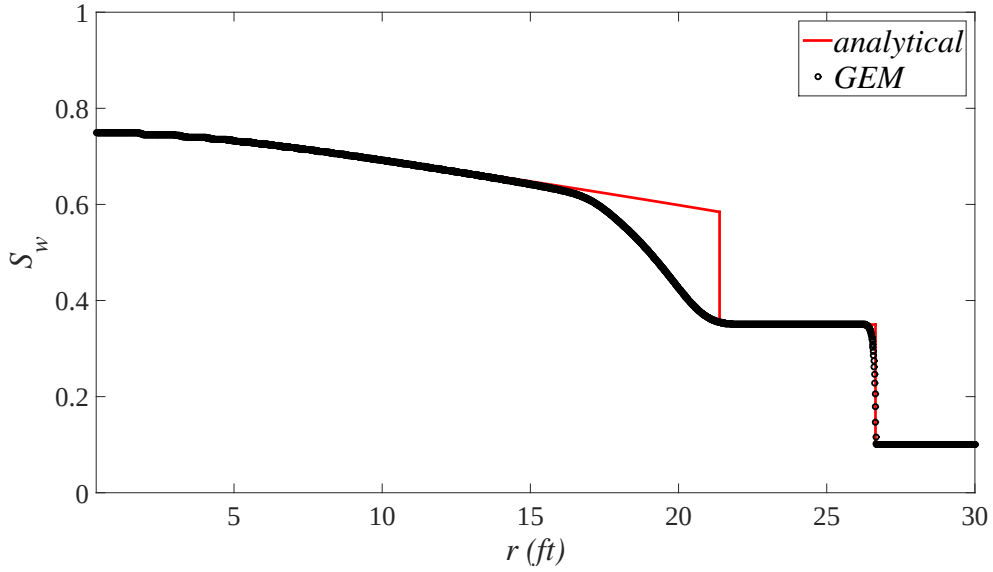

(b)

Figure 4.8: Comparison between the concentration (a) and saturation (b) distributions obtained from our solution with the reservoir numerical simulator at the end of the injection period.

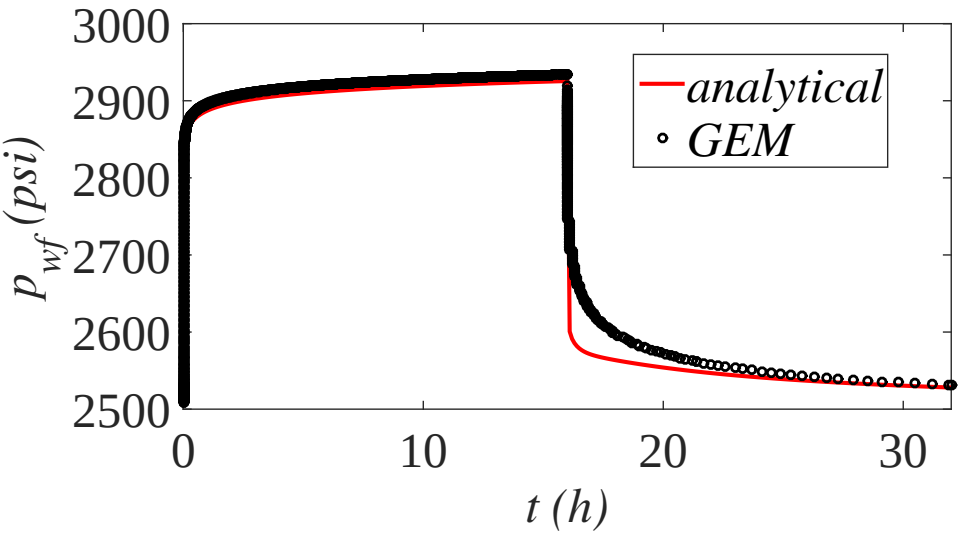

Figure 4.9: Comparison between the bottom hole pressure obtained from our solution with the reservoir numerical simulator during carbonated water injection and falloff.

in the wellbore pressure derivative plot. The true original end-point oil mobility is

$$\lambda_o(S_{iw}, C^{wi}_{CO_2})^{true} = \frac{k_{ro}(S_{iw})}{\mu_o(C^{wi}_{CO_2})} = \frac{1}{3.28} = 0.305 \tag{4.75}$$

and the true end-point water mobility is

$$\lambda_w(1 - S_{or}, C^{w,inj}_{CO_2})^{true} = \frac{k_{rw}(1 - S_{or})}{\mu_w} = \frac{0.5}{0.5} = 1. \tag{4.76}$$

As $t \to 0$, the integral in Eq. 4.63 becomes negligible and $\Delta p_{wf}(t) \approx \Delta p_{wo}(t)$. Consequently, at very early times of injection, the solution reflects the the original total mobility (i.e., the end-point oil mobility with initial CO_2 concentration) through the semi-log slope exhibited by the pressure derivative given by

$$\lambda_o(S_{iw}, C^{wi}_{CO_2})) = \frac{\alpha q_{inj}}{\frac{\partial \Delta p_{wf}(t)}{\partial \ln t} 2kh} = \frac{141.2 \times 3500}{\frac{\partial \Delta p_{wf}(t)}{\partial \ln t} \times 2 \times 300 \times 60} = \frac{13.73}{\frac{\partial \Delta p_{wf}(t)}{\partial \ln t}} \tag{4.77}$$

From Fig. 4.10(a), at very early times,

$$\frac{\partial \Delta p_{wf}(t)}{\partial \ln t} \approx 40. \tag{4.78}$$

Inserting Eq. 4.78 in Eq. 4.77 and comparing it with Eq. 4.75, we have $\lambda_o(S_{iw}, C^{wi}_{CO_2})^{est} = 0.343 \approx 0.305 = \lambda_o(S_{iw}, C^{wi}_{CO_2}))^{true}$. At late times, we find that the derivative shows stabilized radial flow, which by inspection reflects the end-point water mobility at the CO_2 concentration of the injected fluid. Let us use the Boltzmann transform given by $\xi = \frac{r^2}{4t}$ to change variables of Eq. 4.63 [12],

$$\Delta p_{wf}\Big(\frac{r_w^2}{4t}\Big) = \Delta p_{wf,o}\Big(\frac{r_w^2}{4t}\Big) + \frac{\alpha q_{inj}}{kh\hat{\lambda}_o}\int\limits_{\frac{r_w^2}{4t}}^{\xi_{wf}} \Big(\frac{\hat{\lambda}_o}{\lambda_t(r,t)} - 1\Big)\frac{d\xi}{2\xi}, \tag{4.79}$$

where

$$\xi_{wf} = \frac{r_{wf}^2}{4t} = \frac{r_w^2}{4t} + \frac{\theta q_{inj}}{4\phi\pi h}\frac{\partial f_w(S_{wf}, C^{wi}_{CO_2})}{\partial S_w}. \tag{4.80}$$

For a finite wellbore radius, at late times, $\frac{r_w^2}{4t} << \frac{\theta q_{inj}}{4\phi\pi h}\frac{\partial f_w(S_{wf}, C^{wi}_{CO_2})}{\partial S_w}$ and $\xi_{wf} \approx \frac{\theta q_{inj}}{4\phi\pi h}\frac{\partial f_w(S_{wf}, C^{wi}_{CO_2})}{\partial S_w}$. In this period, we can assume that the saturation profile can be approximated by the profile that would be obtained if water were injected from a line source well; in this case ξ_{wf} is stationary and $\lambda_t(r,t) = \lambda_t(\xi)$. Under these assumptions, taking the derivative of Eq. 4.79 with respect of $\ln t$ by applying the Leibniz's rule, yields

$$\begin{aligned}
\frac{\partial \Delta p_{wf}\Big(\frac{r_w^2}{4t}\Big)}{\partial \ln t} &= \frac{\partial \Delta p_{wf,o}\Big(\frac{r_w^2}{4t}\Big)}{\partial \ln t} + \frac{\alpha q_{inj}}{kh\hat{\lambda}_o}\frac{\partial}{\partial \ln t}\int\limits_{\frac{r_w^2}{4t}}^{\xi_{wf}} \Big(\frac{\hat{\lambda}_o}{\lambda_t(\xi)} - 1\Big)\frac{d\xi}{2\xi} \\
&= \frac{\partial \Delta p_{wf,o}\Big(\frac{r_w^2}{4t}\Big)}{\partial \ln t} + \frac{\alpha q_{inj} t}{2kh\hat{\lambda}_o}\Big(-\frac{\hat{\lambda}_o}{\lambda_t(\frac{r_w^2}{4t})} + 1\Big)\frac{4t}{r_w^2}(-\frac{r_w^2}{4t^2}) \\
&= \frac{\partial \Delta p_{wf,o}\Big(\frac{r_w^2}{4t}\Big)}{\partial \ln t} + \frac{\alpha q_{inj}}{2kh\hat{\lambda}_o}\Big(\frac{\hat{\lambda}_o}{\lambda_t(\frac{r_w^2}{4t})} - 1\Big).
\end{aligned} \tag{4.81}$$

As $\lambda_t(\frac{r_w^2}{4t}) = \lambda_w(1 - S_{or}, C^{w,inj}_{CO_2})$ and

$$\frac{\partial \Delta p_{wf,o}\Big(\frac{r_w^2}{4t}\Big)}{\partial \ln t} = \frac{\alpha q_{inj}}{kh\hat{\lambda}_o}\frac{\partial}{\partial \ln t}\left[\frac{1}{2}\ln\left(\frac{\beta k\hat{\lambda}_o t}{\phi\hat{c}_{to} r_w^2}\right) + 0.4045 + s\right] = \frac{\alpha q_{inj}}{2kh\hat{\lambda}_o}, \tag{4.82}$$

Eq. 4.81 can be rewritten as

$$\frac{\partial \Delta p_{wf}(t)}{\partial \ln t} = \frac{\alpha q_{inj}}{2kh\hat{\lambda}_w}, \tag{4.83}$$

which indicates that the solution does reflect the injected water properties through the semi-log slope exhibited by the pressure derivative. We can evaluate the end-point water mobility by rearranging Eq. 4.83:

$$\lambda_w(1 - S_{or}, C_{CO_2}^{w,inj}) = \frac{\alpha q_{inj}}{\frac{\partial \Delta p_{wf}(t)}{\partial \ln t} 2kh} = \frac{141.2 \times 3500}{\frac{\partial \Delta p_{wf}(t)}{\partial \ln t} \times 2 \times 300 \times 60} = \frac{13.73}{\frac{\partial \Delta p_{wf}(t)}{\partial \ln t}}. \tag{4.84}$$

From Fig. 4.10(a), at late times,

$$\frac{\partial \Delta p_{wf}(t)}{\partial \ln t} \approx 13.6. \tag{4.85}$$

Inserting Eq. 4.85 in Eq. 4.84 and comparing it with Eq. 4.76, we have $\lambda_w(1-S_{or}, C_{CO_2}^{w,inj})^{est} = 1.01 \approx 1 = \lambda_w(1 - S_{or}, C_{CO_2}^{w,inj})^{true}$. During the falloff period, we can see that the pressure derivative is constant at late times and; during this time period, the solution seems to reflect the end-point oil mobility at initial CO_2 concentration. At late times, as $q_s(r, \Delta t_{foff}) \rightarrow 0$ and $q_{os}(r, \Delta t_{foff}) \rightarrow 0$ for $r \in (r_w, r_{f,inj}(t_{inj}))$, the integral in Eq. 4.69 vanishes and $\Delta p_{ws}(\Delta t_{foff}) = \Delta \hat{p}_{os}(\Delta t_{foff})$; which implies that, at late times, the solution reflects the original oil in place properties through the semi-log slope exhibited by the pressure derivative given by the derivative of Eq. 4.70 with respect of the logarithmic of t_e,

$$\frac{\partial \Delta p_{ws}(\Delta t_{foff})}{\partial \ln t_e} = \frac{\partial \Delta p_{os} \Delta(\Delta t_{foff})}{\partial \ln t_e} = \frac{\alpha q_{inj}}{2kh\lambda_o(S_{iw}, C_{CO_2}^{wi})}, \tag{4.86}$$

where

$$t_e = \frac{t_{inj} \Delta t_{foff}}{t_{inj} + \Delta t_{foff}}. \tag{4.87}$$

Solving Eq. 4.86 for the end-point oil mobility, we have

$$\lambda_o(S_{iw}, C_{CO_2}^{wi}) = \frac{\alpha q_{inj}}{\frac{\partial \Delta p_{ws}(\Delta t_{foff})}{\partial \ln t_e} 2kh} = \frac{141.2 \times 3500}{\frac{\partial \Delta p_{wf}(\Delta t_{foff})}{\partial \ln t_e} \times 2 \times 300 \times 60} = \frac{13.73}{\frac{\partial \Delta p_{ws}(\Delta t_{foff})}{\partial \ln t_e}} \tag{4.88}$$

From Fig. 4.10(b), at late times,

$$\frac{\partial \Delta p_{ws}(t)}{\partial \ln t} \approx 45.9. \tag{4.89}$$

Inserting Eq. 4.89 in Eq. 4.88 and comparing it with Eq. 4.75, we have $\lambda_o(S_{iw}, C^{wi}_{CO_2})^{est} = 0.299 \approx 0.305 = \lambda_o(S_{iw}, C^{wi}_{CO_2}))^{true}$. These observations are consistent with results on water injection obtained by [18] and [79]. For a detailed discussion on the wellbore pressure information in the case $s \neq 0$, please see Peres and Reynolds [79], Boughrara [14].

4.3 Example

"And if there is something here,
just one little thing out of a whole mess of things,
maybe we can pass it on to someone else. "
— "Guy Montag" in *Fahrenheit 451* by Ray Bradbury

In this case, the approximate analytical solution for the wellbore pressure response while injecting carbonated water injection followed by falloff is used as the forward model with the model parameters k, s and a_w to be estimated, i.e.,

$$\vec{m} = [k, s, a_w]^T, \tag{4.90}$$

using the procedure presented in Chapter 2. Here, we provide a synthetic example where we first compute "true pressure data" by running a commercial simulator using a very fine grid and very small time steps using specified (true) values of absolute permeability, skin factor and end-point mobilities (where a_o is equal 1). In this simulation, again we assume a skin zone of given radius and then for the given value of skin factor, compute the value of skin zone permeability, k_s, using Hawkins's formula [50] for input into the reservoir simulator. The radius of the skin zone is equal to 1 feet and includes the 100 radial gridblocks closest to the wellbore. The reservoir, rock and fluid properties are those shown in Table 4.1. The observed pressure data are generated by adding uncorrelated Gaussian noise with

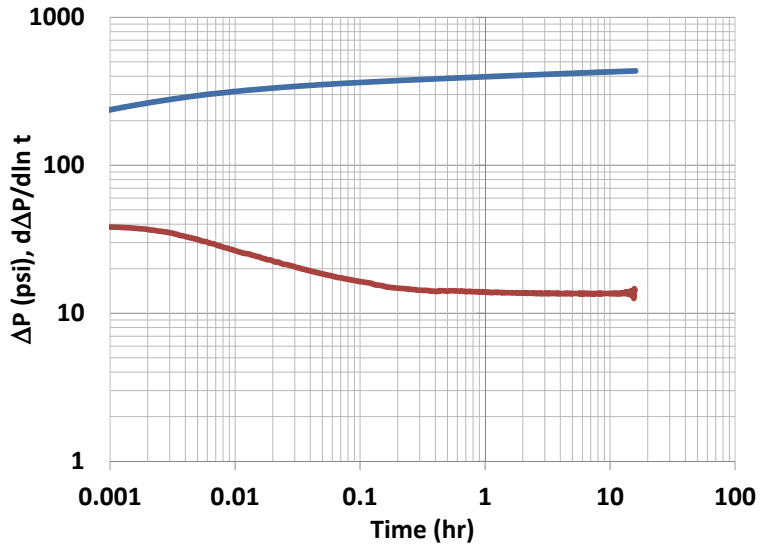

(a)

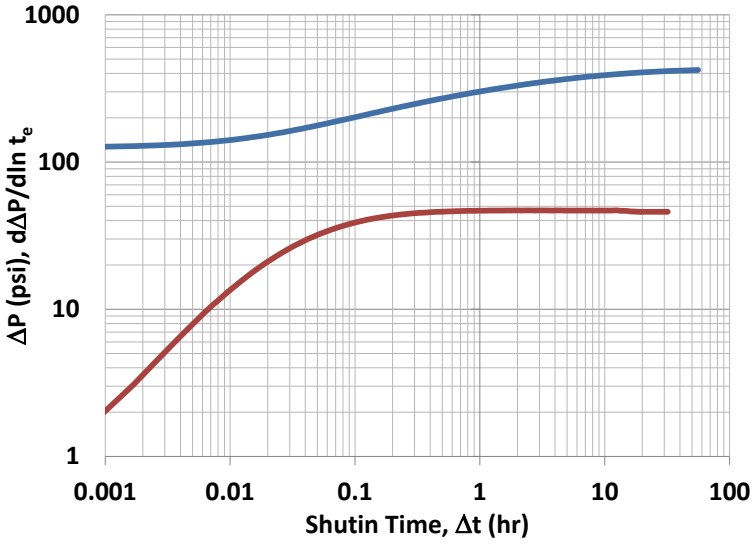

(b)

Figure 4.10: Log-log diagnostic plots of injection (a) and falloff (b) of the wellbore pressure (blue curves) and the wellbore pressure derivatives (red curves) with time.

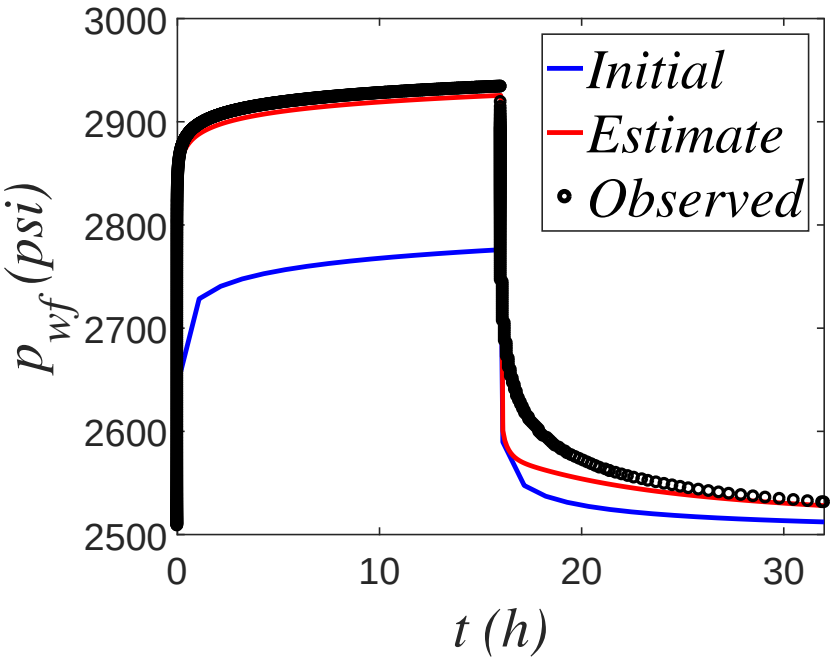

Figure 4.11: Bottom hole pressure data match for the injection-falloff test.

Table 4.2: Estimated model parameters based on the approximate analytical solution for injection-falloff test.

Parameter	k (md)	Skin Factor	a_w
True	300.00	5.00	0.500
Initial Guess	600.00	0.00	0.800
Estimate	302.11	5.04	0.496

mean zero and variance 1 psi^2 to the true pressure data. We only match observed pressure data corresponding to times more 0.5 hour after each flow rate change. Table 4.2 presents the values of model parameters estimated from the Trust-Region-Reflective Least Squares Algorithm algorithm [35] where the bounds specified on the parameters are given in Table 4.3. $\epsilon = 10^{-4}$. Fig. 4.11 shows the bottom hole pressure match for the test data.

Table 4.3: Parameter bounds for the injection-falloff test.

Parameter	k (md)	Skin Factor	a_w
Lower bound	0	-60	0.05
Upper bound	∞	60	1.00

"Maybe I'll leave out the previous chapter[s].
Among other reasons because in the last lines
there's a phrase that's close to being nonsense
and I don't want to provide food for future critics."
— "Brás Cubas"
in *Memórias Póstumas de Brás Cubas* by Machado de Assis

CHAPTER 5

DISCUSSIONS AND CONCLUSIONS

"How much bettter it would have been to have said things smoothly,
without all these jolts!"
— "Brás Cubas"

"Given the possibility that one of my readers
might have skipped the previous chapter[s],
I must observe that it's necessary to read it
in order to understand what I said..."
— "Brás Cubas"
in *Memórias Póstumas de Brás Cubas* by Machado de Assis

In this work an approximate semi-analytical solution was developed for an injection-falloff-production test which allows the governing relative permeabilities during the flow back period to be different from the relative permeabilities during injection. Contrary to what [28] has concluded in his dissertation, we have shown that hysteresis effects does affect the wellbore pressure during flowback, even when the reservoir is water wet. The weak solution we construct for the saturation equation for the flowback period satisfies the Oleinik entropy condition and hence is unique.

By comparing results with those from a commercial simulator, we show that our approximate semi-analytical solution yields an accurate prediction of the saturation profile and bottom-hole pressure during an IFPT. The saturation solution during flowback can be constructed either with front-tracking or the simpler and more computationally efficient area equality method derived in the text. Finally, we show that the approximate analytical

pressure solution developed can be used to match data from an IFPT to estimate absolute permeability, skin factor and the parameters for in-situ relative permeabilities. Next, we were able to show the importance of capillary effects in wellbore pressure during flowback and we successfully included these effects in the IFPT model.

In addition, an accurate approximate analytical solution was constructed for wellbore pressure during carbonated water injection test followed by a falloff well test in a reservoir containing oil and water where carbon dioxide can be present in both the in-situ oil and water phases as well as in the injected water. After validating our solution by comparing the bottom-hole pressure data calculated from the analytical model with the bottom-hole pressure obtained from a commercial numerical simulator, we showed that our solution can be used as the forward model in a least-squares optimization algorithm to estimate skin factor, reservoir absolute permeability and fluid end-point mobilities. The wellbore pressure data sensitivity to the exponents parameters of the relative permeability curves during an injection-falloff test is insignificant. Therefore, trying to completely characterize relative permeability without the flowback would be really difficulty. However, end-point mobilities could be estimated.

5.1 Future Work

"E agora, José"

—Carlos Drummond de Andrade, *José*

"Si a partir de mañana decidiera vivir una vida tranquila
y dejara de ser soñador, para ser un sujeto más serio,
todo el mundo mañana me podría decir: "se agotaron tus pilas,
te has quedado sin luz, ya no tienes valor, se acabó tu misterio"."

—Alberto Cortez, *A partir de mañana*

We have developed analytical models for water injection and carbonated water injection tests. The wellbore pressure profile when gases, such as CO_2 and N_2 are injected

into an oil reservoir are also very relevant to the oil industry, and our method can be used to develop models for this cases. To do that, we can solve the system of n-equations for n components given by the mass balance equation, using radial coordinates [76]:

$$\frac{\partial C_i}{\partial t} + \frac{\theta q_t}{2\pi r h \phi}\frac{\partial F_i(C_i, T)}{\partial r} = 0, \text{ for } i = 1, \ldots, n \tag{5.1}$$

where and T is the temperature in °F and C_i is the overall concentration of component i, given by

$$C_i = c_{ig} S_g + c_{io}(1 - S_g) \tag{5.2}$$

and F_1 is the overall fractional flow of component 1, given by

$$F_i = c_{ig} f_g + c_{io}(1 - f_g), \tag{5.3}$$

defining the volume fraction of component i in the gas phase, c_{ig}, and in the oil phase, c_{io}, as

$$c_{ip} = \frac{\frac{x_{i,p}}{\rho_{ci}}}{\rho_{m,p}}, \text{ for } p = g, o. \tag{5.4}$$

Here, $x_{i,p}$ is the mole fraction of component i in the phase p, ρ_{ci} is the component molar density and $\rho_{m,p}$ is the phase molar density. We would again the Corey-type relative permeabilities given by

$$k_{rg} = \begin{cases} 0, & S_g \leq S_{gc} \\ (\frac{S_g - S_{gc}}{1 - S_{gc} - S_{or}})^{n_g}, & S_{gc} < S_g \leq 1 - S_{or} \\ 1, & S_g > 1 - S_{or} \end{cases} \tag{5.5}$$

and

$$k_{ro} = \begin{cases} 1, & S_g \leq S_{gc} \\ (\frac{1-S_g-S_{or}}{1-S_{gc}-S_{or}})^{n_o}, & S_{gc} < S_g \leq 1 - S_{or} \\ 0, & S_g > 1 - S_{or}, \end{cases} \tag{5.6}$$

where S_g is the gas saturation and S_{gc} is the critical gas saturation. From Eqs. 5.5 and 5.6, it follows that

$$f_g = \begin{cases} 0, & S_g \leq S_{gc} \\ \frac{(S_g-S_{gc})^{n_g}}{(1-S_g-S_{or})^{n_o}(1-S_{gc}-S_{or})^{(n_g-n_o)}\frac{\mu_g}{\mu_o}+(S_g-s_{gc})^{n_g}}, & S_{gc} < S_g \leq 1 - S_{or} \\ 1, & S_g > 1 - S_{or}. \end{cases} \tag{5.7}$$

The system of equations in E.q 5.1 can be solved by using the method of characteristics, assuming a one-dimensional homogeneous reservoir with incompressible fluids and constant molar density, and neglect capillary effects, gravity effects, volume changing on mixing and diffusion. Once we have the concentration distribution in the reservoir, we can integrate the pressure gradient given by Darcy's law, assuming viscosities depending on composition, to find the wellbore pressure. Considering that water-alternating-gas flooding has shown better performance than continuous gas flooding in many applications cases [27], it seems necessary to extend the solutions for wellbore pressure response presented in this work, and the solutions to be developed, to include the effects of three mobile phases in the reservoir. This can be done by adding one more equation to the system of governing hyperbolic equations, and then, we can use the method of characteristics to find the three-phase saturation distribution in the reservoir.

Thermal effects caused by the temperature difference between injected fluid and the reservoir should also be considered, assuming convection is the only significant heat exchange mechanism in the reservoir during injection [83] and falloff , i.e., neglecting heat loss and

heat diffusion, the heat equation can be written as [59],

$$\frac{\partial T}{\partial t} + \frac{\theta q_t}{2\pi r h \phi}\left(\frac{(M_g - M_o)f_g + M_o}{(M_g - M_o)S_g + M_o + \frac{(1-\phi)}{\phi}M_r}\right)\frac{\partial T}{\partial t} = 0, \tag{5.8}$$

where M is the volumetric heat capacity defined by product of the phase density with the phase specific heat, i.e.,$M_{phase} = \rho_{phase}C_{p,phase}$. The procedure for solving the system of hyperbolic equations for the case of pure water injection or a 2-component reservoir (gas and oil) is analogous to what was shown for carbonated water injection. This solution just need to be validated against a thermal reservoir numerical simulator to verify that it can used to be used as forward model to analyze injection-falloff tests.

Ultimately, if the goal is to pursue the estimation in-situ of relative permeabilities, the flowback wellbore pressure solution must be developed for all cases. In doing that, we will observe that there are characteristic curves of different families crossing each other in the r-t plane. We have developed solutions for this problem intuitively, but the main challenge is how to prove that these solutions are the unique solutions.

Finally, let us not forget that all the solutions developed in this work were based on the assumption of an infinite acting homogeneous reservoir with radial flow from and towards a vertical well with constant flow rate periods. Chen [28] has showed the IFPT test and data analysis are still applicable under stable fluctuations in the flow rate, but large rapid changes in the flow may affect the accuracy of the parameter estimates. The solutions need to be expanded to be able applied to more complex tests, as to heterogeneous reservoir rock characterization and to horizontal wells multiphase testing with diverse flow regimes.

"Writing long books is a laborious and impoverishing act of foolishness:
expanding in five hundred pages an idea that could be perfectly explained in a few minutes.
A better procedure is to pretend that those books already exist
and to offer a summary,a commentary."

— Jorge Luis Borges

BIBLIOGRAPHY

[1] M. Abbaszadeh and M. Kamal. Pressure-transient testing of water injection wells. *SPE Reservoir Engineering*, 4(1):115–124, 1989.

[2] Milton Abramowitz and Irene A Stegun. *Handbook of mathematical functions: with formulas, graphs, and mathematical tables*, volume 55. Courier Corporation, 1964.

[3] R. Al-Hussainy, H. J. Ramey, and P. B Crawford. The flow of real gases through porous media. *Society of Petroleum Engineers*, May 1966. doi:10.2118/1243-A-PA.

[4] A. J. Al-Khalifa, R. N. Horne, and K. Aziz. In-place determination of reservoir relative permeability using well test analysis. *Society of Petroleum Engineers*, January 1987. doi:10.2118/16774-MS.

[5] Khalid Aziz and Antonin Settari. *Petroleum reservoir simulation*. Chapman & Hall, 1979.

[6] JC Bacri, M Rosen, and D Salin. Capillary hyperdiffusion as a test of wettability. *EPL (Europhysics Letters)*, 11(2):127, 1990.

[7] Donald P. Ballou. Solutions to nonlinear hyperbolic Cauchy problems without convexity conditions. *Trans. Amer. Math. Soc.*, 152:441–460, 1970.

[8] Grigory Isaakovich Barenblatt, Vladimir Mordukhovich Entov, and Viktor Mikhaĭ Ryzhik. *Theory of fluid flows through natural rocks*.

[9] Abelardo Borges Barreto, Jr. *Solução da equação da difusividade hidráulica não-linear do gás através de funções de green*. PhD thesis, Universidade Estadual do Norte Fluminense Darcy Ribeiro, 2011.

[10] P. Bedrikovetsky, J. R. P. Rodrigues, and P. R. F. Britto. Analytical model for the waterflood honouring capillary pressure (with applications to laboratory studies). *Society of Petroleum Engineers*, January 1996. doi:10.2118/36130-MS.

[11] Pavel Bedrikovetsky. *Mathematical Theory of Oil and Gas Recovery: With Applications to ex-USSR Oil and Gas Fields (Petroleum Engineering and Development Studies)*. Springer, 1st ed. edition, 12 1993. ISBN 9789048143009.

[12] RB Bird, WE Stewart, EN Lightfoot, and Robert E Meredith. Transport phenomena. *Journal of The Electrochemical Society*, 108(3):78C–79C, 1961.

[13] A. A. Boughrara, A. M. M. Peres, S. Chen, A. A. V. Machado, and A. C. Reynolds. Approximate analytical solutions for the pressure response at a water injection well. *SPE Journal*, 12(1):19–34, 2007.

[14] Amina Boughrara. *Injection/Falloff Testing of Vertical and Horizontal Wells*. Ph.D. thesis, The University of Tulsa, Tulsa, Oklahoma, 2006.

[15] F. Bratvedt, K. Bratvedt, C. F. Buchholz, L. Holden, H. Holden, and N. H. Risebro. A new front-tracking method for reservoir simulation. *SPE Reservoir Engineering*, 7 (1):107–116, February 1992.

[16] F. Bratvedt, T. Gimse, and C. Tegnander. Streamline computations for porous media flow including gravity. *Transport in Porous Media*, 25(1):63–85, 1996.

[17] R. B. Bratvold and R. N. Horne. Analysis of pressure-falloff tests following cold water injection. *SPE Formation Evaluation*, 5(3):293–302, 1990.

[18] Reidar Bratvold. *An Analytical Study of Pressure Response Following Cold Water Injection*. Ph.D. thesis, Stanford University, Stanford, California, 1989.

[19] D. Brook. On the distinction between the conditional probability and the joint probability approaches in the specification of nearest-neighbour systems. *Biometrika*, 51(3 and 4):481–483, 1964.

[20] R.H. Brooks and A.T Corey. Hydraulic properties of porous media. *Hydrology Paper No. 3*, 1964.

[21] S. E. Buckley and M. C. Leverett. Mechanism of fluid displacement in sands. *SPE*, 1941.

[22] Richard L Burden and J Douglas Faires. 2.1 the bisection algorithm. numerical analysis. *Prindle, Weber & Schmidt, Boston, MA., pp. x*, 1985.

[23] Eugene Butkov. *Mathematical Physics (1968).* Addison-Wesley Publishing Company, Incorporated.

[24] Horatio Scott Carslaw and John Conrad Jaeger. *Conduction of heat in solids*. Clarendon Press, 1960.

[25] M Chaouche, N Rakotomalala, D Salin, and YC Yortsos. Capillary effects in immiscible flows in heterogeneous porous media. *EPL (Europhysics Letters)*, 21(1):19, 1993.

[26] M Chaouche, N Rakotomalala, D Salin, B Xu, and YC Yortsos. Capillary effects in drainage in heterogeneous porous media: continuum modelling, experiments and pore network simulations. *Chemical engineering science*, 49(15):2447–2466, 1994.

[27] Bailian Chen and Albert C Reynolds. Ensemble-based optimization of the water-alternating-gas-injection process. *SPE Journal*, 21(03):786–798, 2016.

[28] Shi Chen. *A Well Test for In-Situ Determination of Relative Permeability Curves*. Ph.D. dissertation, The University of Tulsa, Tulsa, Oklahoma, 2005.

[29] Shi Chen, Gaoming Li, Alvaro Peres, and A. C. Reynolds. A well test for in-situ determination of relative permeability curves. In *Proceedings of the SPE Annual Technical Conference and Exhibition*, 2005.

[30] Shi Chen, Gaoming Li, and Albert Coburn Reynolds. Analytical solution for injection-falloff-production. *SPE Conference Paper*, 2006. doi:10.2118/103271-MS.

[31] Shi Chen, Gaoming Li, Alvaro Peres, and A. C. Reynolds. A well test for in-situ determination of relative permeability curves. *SPE Reservoir Evaluation & Engineering*, 11(1):95–107, 2008.

[32] Yan Chen, Dean S. Oliver, and Dongxiao Zhang. Data assimilation for nonlinear problems by ensemble Kalman filter with reparameterization. *Journal of Petroleum Science and Engineering*, 66:1–14, 2007.

[33] R. J. Christensen. Carbonated waterflood results–Texas and Oklahoma. In *Annual Meeting of Rocky Mountain Petroleum Engineers of AIME*. Society of Petroleum Engineers, 1961.

[34] Kevin D Cole, James V Beck, A Haji-Sheikh, and Bahman Litkouhi. *Heat conduction using Greens functions*. Taylor & Francis, 2010.

[35] T. F. Coleman and Y. Li. On the convergence of reflective Newton methods for large-scale nonlinear minimization subject to bounds vol. 67. *Ithaca, NY, USA: Cornell University*, 1994.

[36] Royal Eugene Collins. *Flow of fluids through porous materials*. Petroleum Publishing Co., Tulsa, OK, 1976.

[37] A. T. Corey. The interrelation between gas and oil relative permeabilities. *Producers Monthly*, 19:3841, November 1954.

[38] L. Deng and M. J. King. Capillary corrections to buckley-leverett flow. *Society of Petroleum Engineers*, 2015. doi:10.2118/175150-MS.

[39] William E. Boyce & Richard C. DiPrima. *Elementary Differential Equations and Boundary Value Problems*. Wiley, 8 edition, 2005.

[40] Erle C Donaldson, Nina Ewall, and Baljit Singh. Characteristics of capillary pressure curves. *Journal of Petroleum Science and Engineering*, 6(3):249–261, 1991.

[41] Jim Douglas Jr, PM Blair, and RJ Wagner. Calculation of linear waterflood behavior including the effects of capillary pressure. 1958.

[42] Dean G Duffy. *Greens functions with applications*. CRC Press, 2015.

[43] Dmitry Eydinov, Guohua Gao, Gaoming Li, and A.C. Reynolds. Simultaneous estimation of relative permeability and porosity/permeability fields by history matching production data. *Journal of Canadian Petroleum Technology*, 48(12):13–25, December 2009.

[44] Guohua Gao and A. C. Reynolds. An improved implementation of the LBFGS algorithm for automatic history matching. *SPE Journal*, 11(1):5–17, 2006.

[45] Don W. Green and G. Paul Willhite. *Enhanced oil recovery (SPE textbook series) Volume 6*. Henry L. Doherty Memorial Fund of AIME, Society of Petroleum Engineers, 1 1998. ISBN 9781555630775.

[46] A. T. Grogan and W. V. Pinczewski. The role of molecular diffusion processes in tertiary CO_2 flooding. *Society of Petroleum Engineers*, May 1987. doi:10.2118/12706-PA.

[47] Thomas Hahn. The cuba library. *Nuclear Instruments and Methods in Physics Research Section A: Accelerators, Spectrometers, Detectors and Associated Equipment*, 559(1): 273–277, 2006.

[48] Richard Hamming. *Numerical methods for scientists and engineers*. Courier Corporation, 2012.

[49] D. G. Hatzignatiou and A. C. Reynolds. Determination of effective or relative permeability curves from well tests. *SPE Journal*, 1(1):69–82, 1996.

[50] M. F. Jr. Hawkins. A note on the skin effect. *Trans. AIME*, 207:356–357, 1956.

[51] C. W. Hickok and H. J. Ramsay Jr. Case histories of carbonated waterfloods in Dewey-Bartlesville field. In *SPE Secondary Recovery Symposium*. Society of Petroleum Engineers, 1962.

[52] Mark H Holmes. *Introduction to perturbation methods*, volume 20. Springer Science & Business Media, 2012.

[53] Mehdi Matt Honarpour, F Koederitz, and A Herbert. Relative permeability of petroleum reservoirs. 1986.

[54] F. Hussain, Y. Cinar, and P. Bedrikovetsky. A semi-analytical model for two phase immiscible flow in porous media honouring capillary pressure. *Transport in Porous Media*, 92:187–212, March 2011.

[55] Akand W Islam and Eric S Carlson. Viscosity models and effects of dissolved CO_2. *Energy & Fuels*, 26(8):5330–5336, 2012.

[56] R. Juanes and T. Patzek. Analytical solution to the riemann problem of three-phase flow in porous media. *Transport in Porous Media*, 55:47, 2004.

[57] MJ King and VA Dunayevsky. Why waterflood works: a linearized stability analysis. In *SPE Annual Technical Conference and Exhibition*. Society of Petroleum Engineers, 1989.

[58] Roger Knobel. *An Introduction to the Mathematical Theory of Waves (Student Mathematical Library, V. 3)*. American Mathematical Society, first edition, 9 1999. ISBN 9780821820391.

[59] Larry W. Lake. *Enhanced Oil Recovery*. Society of Petroleum Engineers, 2010. ISBN 9781555633059.

[60] Lev Davidovich Landau, JS Bell, MJ Kearsley, LP Pitaevskii, EM Lifshitz, and JB Sykes. *Electrodynamics of continuous media*, volume 8. elsevier, 2013.

[61] G Peter Lepage. Gp lepage, j. comput. phys. 27, 192 (1978). *J. Comput. Phys.*, 27: 192, 1978.

[62] GP Lepage. Report clns-80/447. *Cornell Univ., Ithaca, NY*, 1980.

[63] R. Leveque. *Numerical Methods for Conservation Laws*. Birkhuser, 2nd edition, 8 2005. ISBN 9783764327231.

[64] K. Li. Generalized capillary pressure and relative permeability model inferred from fractal characterization of porous media. 2004. doi:10.2118/89874-MS.

[65] K. Li and R. N. Horne. Numerical simulation with input consistency between capillary pressure and relative permeability. 2004. doi:10.2118/79716-MS.

[66] J. David Logan. *An Introduction to Nonlinear Partial Differential Equations*. Wiley, 1994.

[67] Cíntia G Machado and Albert C Reynolds. Approximate semi-analytical solution for injection–falloff–production well test: An analytical tool for the in situ estimation of relative permeability curves. *Transport in Porous Media*, pages 1–25, 2017. doi: 10.1007/s11242-017-0955-4.

[68] Cintia G. Machado and Albert C. Reynolds. Application of the method of matched asymptotic expansions to solve a non-linear pseudo-parabolic equation: The saturation convection-dispersion equation. In Ilkay Bakrtaş, editor, *Pertubation Methods*. Accepted for publication in InTech Open Science, To appear in 2018. ISBN 978-953-51-6198-1.

[69] Cíntia G. Machado, Mohammadreza M. Firoozabad, and Albert C. Reynolds. CO_2 effects on wellbore pressure response during injection-falloff test. In *SPE Europec featured at 79th EAGE Conference and Exhibition*. Society of Petroleum Engineers, 2017. doi: 10.2118/185824-MS.

[70] Cíntia G. Machado, Mohammadreza M. Firoozabad, and Albert C. Reynolds. Carbon dioxide effects on wellbore-pressure response during injection/falloff test. *SPE Journal*, 2018. doi:10.2118/185824-PA.

[71] Takao Nanba and RN Horne. Estimation of water and oil relative permeabilities from pressure transient analysis of water injection well data. In *SPE Annual Technical Conference and Exhibition*. Society of Petroleum Engineers, 1989.

[72] Ali Hasan Nayfeh. *Introduction to perturbation techniques*. Wiley, New York, 1981. ISBN 0-471-08033-0. A Wiley-Interscience publication.

[73] RA Novy, PG Toledo, HT Davis, and LE Scriven. Capillary dispersion in porous media at low wetting phase saturations. *Chemical engineering science*, 44(9):1785–1797, 1989.

[74] Olga Arsen'evna Oleinik. Discontinuous solutions of non-linear differential equations. *Uspekhi Matematicheskikh Nauk*, 12(3):3–73, 1957.

[75] Dean S Oliver, Albert C Reynolds, and Ning Liu. *Inverse theory for petroleum reservoir characterization and history matching*. Cambridge University Press, 2008.

[76] Franklin Mattes Orr. *Theory of gas injection processes*. Tie-Line Publications, 2007.

[77] A. M. M. Peres and A. C. Reynolds. Injectivity and falloff tests on horizontal wells. TUPREP research report, The University of Tulsa, 2001.

[78] A. M. M. Peres and A. C. Reynolds. Theory and analysis of injectivity tests on horizontal wells. In *Proceedings of the SPE Annual Technical Conference and Exhibition*, number SPE 71582, 2001.

[79] A. M. M. Peres and A. C. Reynolds. Theory and analysis of injectivity tests on horizontal wells. *SPE Journal*, 8(2):147–159, 2003.

[80] A. M. M. Peres, K. V. Serra, and A. C. Reynolds. Supplement to SPE 18113, toward a unified theory of well testing for nonlinear-radial-flow problems with application to interference tests. *SPE General*, 1989. SPE 20402-MS.

[81] A. M. M. Peres, A. A. Boughrara, and A. C. Reynolds. Rate superposition for generating pressure falloff solutions for vertical and horizontal wells. In *Proceedings of the SPE Annual Technical Conference and Exhibition*, number SPE 90907, 2004.

[82] A. M. M. Peres, A. Boughrara, and A. C. Reynolds. Rate superposition for generating pressure falloff solutions for vertical and horizontal wells. *SPE Journal*, 11(3):364–374, 2006.

[83] R. J. Platenkamp. Temperature distribution around water injectors: Effects on injection performance. *SPE Journal*, 1985.

[84] G. A. Pope. The application of fractional flow theory to enhanced oil recovery. *Society of Petroleum Engineers*, June 1980. doi:10.2118/7660-PA.

[85] W.R. Purcell. Capillary pressures-their measurement using mercury and the calculation of permeability. 1949.

[86] L. A. Rapoport and W. J Leas. Properties of linear waterfloods. *Society of Petroleum Engineers*, 1953. doi:10.2118/213-G.

[87] Hyun-Ku Rhee, Rutherford Aris, and Neal R. Amundson. *First-order partial differential equations: Volume I theory and application of single equations*. Dover Publications, 2001.

[88] Hyun-Ku Rhee, Rutherford Aris, and Neal R. Amundson. *First-order partial differential equations: Volume II theory and application of hyperbolic system of quasilinear equations*. Dover Publications, 2013.

[89] A. J. Rosa, R. S. Carvalho, and J. A. D. Xavier. *Engenharia de Reservatórios de Petróleo*. Rio de Janeiro, 2005.

[90] Márcia A Gomes Ruggiero and Vera Lúcia da Rocha Lopes. *Cálculo numérico: aspectos teóricos e computacionais*. Makron Books do Brasil, 1997.

[91] K. V. Serra, A. M. M. Peres, and A. C. Reynolds. Well test analysis for solution gas-drive reservoirs–part i: Determination of relative and absolute permeabilities. *SPE Formation Evaluation*, 5(2):124–132, 1990.

[92] Antonin Settari and Khalid Aziz. A computer model for two-phase coning saturation. *SPE Journal*, 1974.

[93] Vishnu D Sharma. *Quasilinear hyperbolic systems, compressible flows, and waves*. CRC Press, 2010.

[94] E. P. S. Sousa, A. B. Barreto Jr., and A. M. M. Peres. Finite-wellbore-radius solution for gas wells by green's functions. *SPE Journal*, 2015. doi:10.2118/169323-PA.

[95] Emilio Paulo dos Santos Sousa. Aplicação das funções de green no estudo do comportamento de testes de pressão em reservatórios de gás: poço vertical com efeitos de estocagem e dano de formação. Master's thesis, Universidade Estadual do Norte Fluminense, 2014.

[96] M. B. Standing. Notes on relative permeability relationships. Technical report, U. of Trondheim, Norway, 1975.

[97] Harald Stehfest. Algorithm 368: Numerical inversion of laplace transforms [d5]. *Communications of the ACM*, 13(1):47–49, 1970.

[98] L. G. Thompson and A. C. Reynolds. Well testing for radially heterogeneous reservoirs under single and multiphase flow conditions. *SPE Formation Evaluation*, 12(1):57–64, 1997.

[99] L. G. Thompson and A. C. Reynolds. Pressure transient analysis for gas condensate reservoirs. *In Situ*, 21(2):101–144, 1997.

[100] CJ Van Duijn, Johannes Molenaar, and MJ De Neef. The effect of capillary forces on immiscible two-phase flow in heterogeneous porous media. *Transport in porous media*, 21(1):71–93, 1995.

[101] Milton Van Dyke. *Perturbation methods in fluid mechanics/Annotated edition*, volume 75. 1975.

[102] G. B. Whitham. *Linear and Nonlinear Waves*. Wiley-Interscience, 1 edition, 7 1999. ISBN 9780471359425.

[103] Thomas Williams, C Kelley, et al. Gnuplot 4.4: an interactive plotting program. official gnuplot documentation, 2010.

[104] Stephen Wright and Jorge Nocedal. Numerical optimization. *Springer Science*, 35 (67-68):7, 1999.

[105] YC Yortsos and AS Fokas. An analytical solution for linear waterflood including the effects of capillary pressure. *Society of Petroleum Engineers Journal*, 23(01):115–124, 1983.

APPENDIX A

DETAILS ON THE NUMERICAL COMPUTATIONS

"It is a mistake to think you can solve any major problems just with potatoes."

— Douglas Adams in *Life, the Universe and Everything*

In this Appendix, we discuss the numerical methods used in this work to compute our analytical solutions in Fortran 90 and to perform the pressure transient data analysis. The numerical details that have been already discussed in the main text are not repeated here.

A.1 Solving Single Equations

We have implemented the bisection method given in [22] with a convergence tolerance on the relative error solution equal to 10^{-6} to solve Eqs. 2.15, 3.68, 3.207, 4.45, 4.46 and 4.47.

A.2 System of Equations to find the Shock Position

We implemented the Newton-Raphson method [90] with the analytical derivatives (given by Eqs. A.14, A.15, A.16, A.17, A.18, A.19,A.20, A.21 and A.22) and a convergence tolerance on the relative error of the solution equal to 10^{-6} to solve the non-linear system of equations given by Eqs. 2.36, 2.38 and 2.40 to find the shock position and its saturation at a time t. Note; as stated in Chapter 2, we only need to solve this system 3 times, then we can fit a polynomial of order 2 that can be used to evaluate the shock positions and

saturations explicitly at any time where they are needed. To constrain the equations, we use a log-transform to replace each independent variable m_i by

$$x_i(m_i) = \ln\left(\frac{m_i - m_{i,lb}}{m_{i,ub} - m_i}\right), \tag{A.9}$$

where $m_{i,lb}$ and $m_{i,ub}$, respectively, are the lower and upper bounds on the variable m_i discussed in Chapter 2. The solution of the system of equations to find the shock position is found in the log-transform space using an analytical Jacobian, J_{3x3}. The residual equations (R_i, for $i = 1, 2, 3$) - which given by Eqs. 2.36, 2.38 and 2.40 - are rewritten here as,

$$\begin{aligned} R_1(r_s^2, S_w^-, S_w^+, t) = r_s^2 - r_w^2 - \frac{\theta q_{t,prod}(t - t_{foff})}{\pi h \phi} \frac{[f_w(S_w^-) - f_w(S^+)]}{[S_w^- - S_w^+]} \\ - \frac{\theta q_{inj} t_{inj}}{\pi h \phi} \frac{(f_w(S_{wf}) - f_w(S_w^+) - (S_{wf} - S_w^-)\frac{df_w}{dS_w}(S_{wf}))}{[S_w^- - S_w^+]}, \end{aligned} \tag{A.10}$$

$$R_2(r_s^2, S_w^+, t) = r_s^2 - r_{prod}^2(S_w^+) = r_s^2 - r_w^2 - \frac{\theta(q_{inj} t_{inj} + q_{t,prod}(t - t_{foff}))}{\phi h \pi} \frac{df_w(S_w^+)}{dS_w} \tag{A.11}$$

and

$$R_3(r_s^2, S_w^-, t) = r_s^2 - r_{prod}^2(S_w^-) = r_s^2 - r_w^2 - \frac{\theta q_{inj} t_{inj}}{\phi h \pi} \frac{df_w(S_{wf})}{dS_w} - \frac{q_{t,prod}(t - t_{foff})}{\phi h \pi} \frac{df_w(S_w^-)}{dS_w}. \tag{A.12}$$

The derivative of the residual equations with respect to each transformed model parameter x_i are computed by the chain rule and are be given by

$$\frac{\partial R_i}{\partial x_i} = \frac{\partial R_i}{\partial m_i} \frac{\partial m_i}{\partial x_i} = \frac{\partial R_i}{\partial m_i} \frac{(m_{i,ub} - m_i)(m_i - m_{i,lb})}{m_{i,ub} - -m_{i,lb}}, \quad \text{for } i = 1, 2, 3. \tag{A.13}$$

The derivative of A.10 with respect of r_s^2 is given by

$$\frac{\partial R_1(r_s^2, S_w^-, S_w^+, t)}{\partial r_s^2} = 1, \tag{A.14}$$

the derivative of A.10 with respect of S_w^+ is given by

$$\frac{\partial R_1(r_s^2, S_w^-, S_w^+, t)}{\partial S_w^+} = -\frac{\theta q_{t,prod}(t - t_{foff})}{\pi h \phi}\left(\frac{-\frac{\partial f_w(S^+)}{S_w+}[S_w^- - S_w^+] + [f_w(S_w^-) - f_w(S^+)]}{[S_w^- - S_w^+]^2}\right)$$
$$- \frac{\theta q_{inj} t_{inj}}{\pi h \phi}\left\{\frac{-\frac{\partial f_w(S^+)}{S_w+}[S_w^- - S_w^+] + [f_w(S_{wf}) - f_w(S_w^+) - (S_{wf} - S_w^-)\frac{df_w}{dS_w}(S_{wf})]}{[S_w^- - S_w^+]^2}\right\} \quad \text{(A.15)}$$

and the derivative of Eq. A.10 with respect of S_w^- is given by

$$\frac{\partial R_1(r_s^2, S_w^-, S_w^+, t)}{\partial S_w^-} = -\frac{\theta q_{t,prod}(t - t_{foff})}{\pi h \phi}\left(\frac{\frac{\partial f_w(S^-)}{S_w-}[S_w^- - S_w^+] - [f_w(S_w^-) - f_w(S^+)]}{[S_w^- - S_w^+]^2}\right)$$
$$- \frac{\theta q_{inj} t_{inj}}{\pi h \phi}\left\{\frac{\frac{df_w}{dS_w}(S_{wf})[S_w^- - S_w^+] - [f_w(S_{wf}) - f_w(S_w^+) - (S_{wf} - S_w^-)\frac{df_w}{dS_w}(S_{wf})]}{[S_w^- - S_w^+]^2}\right\}. \quad \text{(A.16)}$$

The derivative of Eq. A.11 with respect of r_s^2 is given by

$$\frac{\partial R_2(r_s^2, S_w^+, t)}{\partial r_s^2} = 1, \quad \text{(A.17)}$$

the derivative of Eq. A.11 with respect of S_w^+ is given by

$$\frac{\partial R_2(r_s^2, S_w^+, t)}{\partial S_w^+} = -\frac{\partial r_{prod}^2(S_w^+)}{\partial S_w^+} = -\frac{\theta(q_{inj} t_{inj} + q_{t,prod}(t - t_{foff}))}{\phi h \pi}\frac{\partial}{\partial S_w^+}\left(\frac{df_w(S_w^+)}{dS_w}\right) \quad \text{(A.18)}$$

and the derivative of Eq. A.11 with respect of S_w^- is given by

$$\frac{\partial R_2(r_s^2, S_w^+, t)}{\partial S_w^-} = 0. \quad \text{(A.19)}$$

The derivative of Eq. A.12 with respect of r_s^2 is given by

$$\frac{\partial R_3(r_s^2, S_w^-, t)}{\partial r_s^2} = 1, \quad \text{(A.20)}$$

the derivative of Eq. A.12 with respect of S_w^+ is given by

$$\frac{\partial R_3(r_s^2, S_w^-, t)}{\partial S_w^+} = 0 \quad \text{(A.21)}$$

and the derivative of Eq. A.12 with respect of S_w^- is given by

$$\frac{\partial R_3(r_s^2, S_w^-, t)}{\partial S_w^-} = -\frac{\partial r_{prod}^2(S_w^-)}{\partial S_w^-} = -\frac{\theta q_{t,prod}(t - t_{foff})}{\phi h \pi} \frac{\partial}{\partial S_w^-} \left(\frac{df_w(S_w^-)}{dS_w} \right). \tag{A.22}$$

To find the breakthrough time, $r_s = r_w$ is fixed and the time became the independent variable m_1. In this case, the derivative of A.10 with respect of t_{BT} is given by

$$\frac{\partial R_1(r_s^2, S_w^-, S_w^+, t)}{\partial t_{BT}} = -\frac{\theta q_{t,prod}}{\phi h \pi} \frac{[f_w(S_w^-) - f_w(S_w^+)]}{[S_w^- - S_w^+]}, \tag{A.23}$$

the derivative of Eq. A.11 with respect of t_{BT} is given by

$$\frac{\partial R_2(r_s^2, S_w^+, t)}{\partial t_{BT}} = -\frac{\partial r_{prod}^2(S_w^+)}{\partial t} = -\frac{\theta q_{t,prod}}{\phi h \pi} \frac{df_w(S_w^+)}{dS_w} \tag{A.24}$$

and the derivative of Eq. A.12 with respect of t_{BT} is given by

$$\frac{\partial R_3(r_s^2, S_w^-, t)}{\partial t_{BT}} = -\frac{\partial r_{prod}^2(S_w^-)}{\partial t} = -\frac{\theta q_{t,prod}}{\phi h \pi} \frac{df_w(S_w^-)}{dS_w}. \tag{A.25}$$

The reader should keep in mind that $q_{inj} > 0$ and $q_{t,prod} < 0$.

A.3 Wellbore Pressure drop

We generate an array of N points of equally spaced saturations and then calculate their positions explicitly using Eq. 2.19 instead of using an uniformly-spaced array for radius to avoid the computational cost of solving 2.19 numerically for water saturation at each point r. We have modified the numerical integration method Simpson 1/3 Rule [48] to use this non-uniformly spaced points for the radius array that is obtained from the uniform saturation array by using a polynomial interpolation of order 2 with varying $h_i = r_{i+1} - r_i$

given by

$$P_2(r,\vec{m},S_w,t)=\sum_{i}^{i+2} f(r_i,\vec{m},S_w(r_i),t)\frac{\prod_{k=i,k\neq i}^{i+2}(r-r_k)}{\prod_{k=i,k\neq i}^{i+2}(r_i-r_k)}$$
$$=f(r_i,\vec{m},S_w(r_i),t)\frac{(r-r_{i+1})(r-r_{i+2})}{(r_i-r_{i+1})(r_i-r_{i+2})}$$
$$+f(r_{i+1},\vec{m},S_w(r_{i+1}),t)\frac{(r-r_i)(r-r_{i+2})}{(r_{i+1}-r_i)(r_{i+1}-r_{i+2})}$$
$$+f(r_{i+2},\vec{m},S_w(r_{i+2}),t)\frac{(r-r_{i+1})(r-r_i)}{(r_{i+2}-r_i)(r_{i+2}-r_{i+1})}, \tag{A.26}$$

where $f(r_i,\vec{m},S_w(r_i),t)$ is the integrand which varies for each test period. Remember that each r_i is obtained from its corresponding saturation at time t. Integrating Eq. A.26 from r_i to r_{i+2}, yields

$$\int_{r_i}^{r_{i+2}} P_2(r,\vec{m},S_w,t)dr=\int_{r_i}^{r_{i+2}}\left[f(r_i,\vec{m},S_w(r_i),t)\frac{(r-r_{i+1})(r-r_{i+2})}{(r_i-r_{i+1})(r_i-r_{i+2})}\right.$$
$$+f(r_{i+1},\vec{m},S_w(r_i),t)\frac{(r-r_i)(r-r_{i+2})}{(r_{i+1}-r_i)(r_{i+1}-r_{i+2})}$$
$$\left.+f(r_{i+2},\vec{m},S_w(r_{i+2}),t)\frac{(r-r_{i+1})(r-r_i)}{(r_{i+2}-r_i)(r_{i+2}-r_{i+1})}\right]dr$$
$$=\left[f(r_i,\vec{m},S_w(r_i),t)\frac{(\frac{r^3}{3}-\frac{r^2}{2}(r_{i+2}+r_{i+1})+r(r_{i+1}r_{i+2}))}{(r_i-r_{i+1})(r_i-r_{i+2})}\right.$$
$$+f(r_{i+1},\vec{m},S_w(r_{i+1}),t)\frac{(\frac{r^3}{3}-\frac{r^2}{2}(r_{i+2}+r_i)+r(r_ir_{i+2}))}{(r_{i+1}-r_i)(r_{i+1}-r_{i+2})}$$
$$\left.+f(r_{i+2},\vec{m},S_w(r_{i+2}),t)\frac{(\frac{r^3}{3}-\frac{r^2}{2}(r_i+r_{i+1})+r(r_{i+1}r_i))}{(r_{i+2}-r_i)(r_{i+2}-r_{i+1})}\right]_{r_i}^{r_{i+2}}$$
$$=f(r_i,\vec{m},S_w(r_i),t)\frac{(\frac{(r_{i+2}^3-r_i^3)}{3}-\frac{(r_{i+2}^2-r_i^2)}{2}(r_{i+2}+r_{i+1})+(r_{i+2}-r_i)(r_{i+1}r_{i+2}))}{(r_i-r_{i+1})(r_i-r_{i+2})}$$
$$+f(r_{i+1},\vec{m},S_w(r_{i+1}),t)\frac{(\frac{(r_{i+2}^3-r_i^3)}{3}-\frac{(r_{i+2}^2-r_i^2)}{2}(r_{i+2}+r_i)+(r_{i+2}-r_i)(r_ir_{i+2}))}{(r_{i+1}-r_i)(r_{i+1}-r_{i+2})}$$
$$+f(r_{i+2},\vec{m},S_w(r_{i+2}),t)\frac{(\frac{(r_{i+2}^3-r_i^3}{3}-\frac{r_{i+2}^2-r_i^2}{2}(r_i+r_{i+1})+(r_{i+2}-r_i)(r_{i+1}r_i))}{(r_{i+2}-r_i)(r_{i+2}-r_{i+1})}. \tag{A.27}$$

Finally, using Eq. A.27, we can approximate the integral of the function $f(r, \vec{m}, S_w, t)$ in the interval (r_0, r_N) by

$$\int_{r_0}^{r_N} f(r,\vec{m},S_w,t)dr \approx \sum_{l=1}^{l=\frac{N}{2}} \int_{r_{2l-2}}^{r_{2l}} P_2(r,\vec{m},S_w,t)dr$$
$$= \sum_{l=1}^{l=\frac{N}{2}} \Bigg[f(r_{2l-2},\vec{m},S_w(r_{2l-2}),t) \frac{(\frac{(r_{2l}^3 - r_{2l-2}^3)}{3} - \frac{(r_{2l}^2 - r_{2l-2}^2)}{2}(r_{2l}+r_{2l-1}) + (r_{2l}-r_{2l-2})(r_{2l-1}r_{2l}))}{(r_{2l-2}-r_{2l-1})(r_{2l-2}-r_{2l})}$$
$$+ f(r_{2l-1},\vec{m},S_w(r_{2l-1}),t) \frac{(\frac{(r_{2l}^3 - r_{2l-2}^3)}{3} - \frac{(r_{2l}^2 - r_{2l-2}^2)}{2}(r_{2l}+r_{2l-2}) + (r_{2l}-r_{2l-2})(r_{2l-2}r_{2l}))}{(r_{2l-1}-r_{2l-2})(r_{2l-1}-r_{2l})}$$
$$+ f(r_{2l},\vec{m},S_w(r_{2l}),t) \frac{(\frac{(r_{2l}^3 - r_{2l-2}^3}{3} - \frac{r_{2l}^2 - r_{2l-2}^2}{2}(r_{2l-2}+r_{2l-1}) + (r_{2l}-r_{2l-2})(r_{2l-1}r_{2l-2}))}{(r_{2l}-r_{2l-2})(r_{2l}-r_{2l-1})} \Bigg]. \tag{A.28}$$

Note; $N = \sum_0^N i$ - where i specifies our integration points - must be even. We have used $N = 100$ in this work. We first have tried to use the trapezoidal rule, but to be able to obtain an accurate pressure solution with the trapezoidal rule (in this case to be able to validate our solution with IMEX) led to an expensive computational cost, we needed to use 10 times more points than we use in this modified Simpson's rule.

To obtain a more accurate integration, we divide our integrand into segments to avoid integrating over discontinuities. For the pure water injection problems, if the water/oil front is inside the skin zone, we use the 3 segments: (r_w, r_s), (r_s, r_{skin}) and $(r_{skin}, r_{f,inj})$. If the water/oil front is outside the skin zone, we have: (r_w, r_{skin}), (r_{skin}, r_s) and $(r_s, r_{f,inj})$. For the carbonated water problems, we solve in similar way but we increment the number of segments accordingly with the saturation self-similar solution "number of segments" (see Figs. 4.4 and 4.7 in Chapter 4).

To check our pressure matching while regressing at each iteration, we call the open-source software Gnuplot [103] from our Fortran code. The final estimated data is exported to DAT files to be stored and also may be upload in the software Matlab.

A.4 Saturation during Falloff with p_c

To evaluate the saturation distribution during falloff, we first need to evaluate $\Delta\overline{\Psi_D^0}(r,s)$ and $\Delta\overline{\Psi_D^1}(r,s)$ in the Laplace domain and then invert it numerically. Once we have $G(r,t_{foff})$, we need to perform a two-dimensional numerical integration from t_{inj} to t_{foff} and from r_w to r to find $\Delta\Psi_D^1(r,t_{foff})$ for each radius r.

Modified Bessels Funtions We have implemented the zeroth and first order modified Bessel functions of first and second kind by using the polynomial approximations given in Abramowitz and Stegun [2] to evaluate $\Delta\overline{\Psi_D^0}(s)$ and $\Delta\overline{G}(s)$ in the Laplace domain.

Numerical Laplace Inversion To invert Eq. 3.111 and the first term in Eqs. 3.150 and 3.151 for the saturation distribution during at end of the falloff period given in Chapter 3, we implemented the well-known Stehfest Algorithm [97], with $N = 14$. This algorithm is appropriate for smooth functions, without rapid oscillations. Given a function $\overline{F}(s)$, $F(t)$ at any time t can be obtained from

$$F(t) = \frac{\ln 2}{t}\sum_{i=1}^{N} V_i \overline{F}\left(\frac{\ln 2}{t} i\right), \tag{A.29}$$

where

$$V_i = (-1)^{i+\frac{1}{2}}\frac{\ln 2}{t}\sum_{i=1}^{\min(i,\frac{n}{2})}, \quad \text{for } i = 1, ..., N \tag{A.30}$$

and $N \in [8, 16]$ must be pair. The propety $\sum_{i=1}^{N} V_i = 0$ can be used to validate the implementation of Eq. A.30.

Multidimensional Numerical Integration For the two-dimensional numerical integration, we use the Vegas algorithm from CUBA library [47] with relative error equal to 10^{-6}. As Hahn [47] stated,

> "Vegas algorithm is a Monte Carlo algorithm that uses importance sampling as a variance-reduction technique. Vegas iteratively builds up a piecewise constant

weight function, represented on a rectangular grid. Each iteration consists of a sampling step followed by a refinement of the grid. The exact details of the algorithm can be found in [61, 62] and shall not be reproduced here."

We would like to point out that while our full non-linear regression can be run within a few seconds for the cases without capillary pressure and within minutes for the cases that include capillary pressure, the numerical simulator take minutes just to run one forward model simulation.

A.5 History Matching

For the pressure transient data analysis,to avoid finding the second-order derivatives, the Hessian was approximated as

$$H(\vec{m}) \approx G^T C_D^{-1} G, \tag{A.31}$$

where G is the sensitivity matrix whose individual elements are

$$g(\vec{m})_{ij} = \frac{\partial \Delta p_{wf}(\vec{m})}{\partial m_j}. \tag{A.32}$$

and C_D, the covariance of error matrix, is a diagonal matrix with the i diagonal given by σ_1^2 and $\vec{m}$ the vector of model parameter to be estimated [75]. Following the procedure adopted by Chen [28] and Gao and Reynolds [44], an unconstrained optimization process is obtained by applying a logarithmic transformation to replace each model parameter m_i by

$$x_i(m_i) = \ln\left(\frac{m_i - m_{i,min}}{m_{i,max} - m_i}\right), \tag{A.33}$$

to avoid obtaining non-physical values of the parameters, where $m_{i,min}$ and $m_{i,max}$ are the minimum and maximum values allowed to parameter m_i. The injection pressure drop deriva-

tives with respect to each new model parameter will be given by

$$\frac{\partial \Delta p_{wf}}{\partial x_i} = \frac{\partial \Delta p_{wf}}{\partial m_i}\frac{\partial m_i}{\partial x_i} = \frac{\partial \Delta p_{wf}}{\partial m_i}\frac{(m_{i,max} - m_i)(m_i - m_{i,min})}{m_{i,max} - m_{i,min}}, \tag{A.34}$$

where solving Eq. A.33 for m_i gives

$$m_i(x_i) = \frac{\exp(x_i)m_{i,max} + m_{i,min}}{1 + \exp(x_i)}. \tag{A.35}$$

The history matching is done in the log-transform space using the gradient-based method Levenberg-Marquadt, which was implemented in Fortran 90 together with the analytical derivatives presented in for the the transient data analysis of IPFT when neglecting capillary pressure. The Levenberg-Marquadt method first choose a step size and then the direction while line search first choose a step direction and then the size [104]. The Levenberg-Marquadt algorithm is similar to the gradient-based Gauss-Newton method, but more robust, since it handle the situation when the approximate Hessian matrix might be singular. where each iteration of the non-linear regression is given be the solution of the following equation,

$$(\lambda^k I + H^k(\vec{x}^k))\delta\vec{x}^{k+1} = -\nabla O(\vec{x}^k), \tag{A.36}$$

where $\lambda > 0$ may vary along iterations and $O(\vec{x}^k)$ is the least-square objective function at iteration k. A factor of 10 was used to decreased or increased λ, according to the drop or rise in the objective function, where we start with 10^5. The convergence criteria for the minimization of the objective function was defined as

$$\frac{\mid O(x^k) - O(x^{k-1}) \mid}{\mid O(x^k) \mid + 10^{-8}} < \epsilon_1 \tag{A.37}$$

or

$$\frac{\mid x^k - x^{k-1} \mid}{\mid x^k \mid + 10^{-8}} < \epsilon_2, \tag{A.38}$$

with $\epsilon_1 = 10^{-3}$ and $\epsilon_2 = 10^{-4}$.

APPENDIX B

ANALYTICAL DERIVATIVES FOR THE IFPT WITHOUT CAPILLARY PRESSURE

"Of course this is the material that goes in the second appendix.
What did you expect to find here?"
— Richard Redner in *TU thesis template*

In this appendix, we provide the derivatives for the IFPT analytical solution presented in Chapter 2 to be used within optimization gradient-based methods. Although the finite difference method to evaluate the gradients of our analytical functions is simpler to implement and not computationally expensive, it can be unstable and it may require some experiments to find the appropriate perturbation values for each parameter to be estimated. Therefore, we recommend the use of analytical derivatives derivatives when evaluating the sensitivity matrix for the non-linear regression. However, one should be careful when deriving and implementing the analytical derivatives, since they lead to complex and lengthly expressions.

B.1 Injection

For the injection period the observed data is the bottom hole pressure and the model parameters to be estimated may be the components of the vector $\vec{m}_{inj}$, given by

$$\vec{m}_{inj} = [k, s, a_w, n_w, n_o]^T, \tag{B.39}$$

where the last 6 paramaters pertain to the imbibition water-oil relative permeability curves. The derivative of the pressure drop with respect to the model parameter k is obtained by

differentiating Eq. 2.62 and is given by

$$\frac{\partial \Delta p_{wf}}{\partial k} = \frac{\partial \Delta \hat{p}_o}{\partial k} + \frac{\alpha q_{inj}}{h\hat{\lambda}_o}\frac{\partial}{\partial k}\int_{r_w}^{r_{f,inj}(t)} \Big(\frac{\hat{\lambda}_o}{\lambda_t(r,t)} - 1\Big)\frac{1}{k(r)}\frac{dr}{r}, \tag{B.40}$$

where differentiating Eq. 3.230 with respect to absolute permeability we find that

$$\begin{aligned}\frac{\partial \Delta \hat{p}_o}{\partial k} &= -\frac{\alpha q_{inj}}{k^2 h\hat{\lambda}_o}\left[\frac{1}{2}\ln\left(\frac{\beta k\hat{\lambda}_o t}{\phi \hat{c}_{to} r_w^2}\right) + 0.4045 + s\right] + \frac{\alpha q_{inj}}{2k^2 h\hat{\lambda}_o} \\ &= -\frac{\alpha q_{inj}}{k^2 h\hat{\lambda}_o}\left[\frac{1}{2}\ln\left(\frac{\beta k\hat{\lambda}_o t}{\phi \hat{c}_{to} r_w^2}\right) - 0.0955 + s\right].\end{aligned} \tag{B.41}$$

Substituting Eq. B.41 into Eq. B.40 and taking the derivative of the second term on the right-hand side of Eq. B.40 yields

$$\frac{\partial \Delta p_{wf}}{\partial k} = \frac{\partial \Delta \hat{p}_o}{\partial k} - \frac{\alpha q_{inj}}{h\hat{\lambda}_o k^2}\Big[\Big(\frac{s}{\ln(\frac{r_{skin}}{r_w})} + 1\Big)\int_{r_w}^{r_{skin}} \Big(\frac{\hat{\lambda}_o}{\lambda_t(r,t)} - 1\Big)\frac{dr}{r} + \int_{r_{skin}}^{r_{f,inj}(t)} \Big(\frac{\hat{\lambda}_o}{\lambda_t(r,t)} - 1\Big)\frac{dr}{r}\Big], \tag{B.42}$$

for $r_{f,inj}(t) \geq r_{skin}$. Otherwise,

$$\frac{\partial \Delta p_{wf}}{\partial k} = \frac{\partial \Delta \hat{p}_o}{\partial k} - \frac{\alpha q_{inj}}{h\hat{\lambda}_o k^2}\left(\frac{s}{\ln(\frac{r_{skin}}{r_w})} + 1\right)\int_{r_w}^{r_{f,inj}(t)} \Big(\frac{\hat{\lambda}_o}{\lambda_t(r,t)} - 1\Big)\frac{dr}{r}. \tag{B.43}$$

The derivative of the permeability with respect to the skin permeability is given by

$$k_s = \frac{k}{\frac{s}{\ln(\frac{r_{skin}}{r_w})} + 1} \tag{B.44}$$

and the derivative of the skin permeability with respect to the skin factor is given by

$$\frac{\partial k_s}{\partial s} = -\frac{k}{\ln(\frac{r_{skin}}{r_w})}\frac{1}{\big(\frac{s}{\ln(\frac{r_{skin}}{r_w})} + 1\big)^2}, \tag{B.45}$$

Here, we applied the Hawkin's formula [1956]

$$s = \left(\frac{k}{k_s} - 1\right) \ln\left(\frac{r_{skin}}{r_w}\right), \tag{B.46}$$

where s is the skin factor, k is the absolute permeability, k_s is the the permeability within the skin radius, i.e., $r \leq r_{skin}$. The pressure drop derivative with the model parameter s is given by

$$\frac{\partial \Delta p_{wf}}{\partial s} = \frac{\partial \Delta \hat{p}_o}{\partial s} + \frac{\alpha q_{inj}}{h\hat{\lambda}_o} \frac{\partial}{\partial s} \int_{r_w}^{r_{f,inj}(t)} \Big(\frac{\hat{\lambda}_o}{\lambda_t(r,t)} - 1\Big) \frac{1}{k(r)} \frac{dr}{r}, \tag{B.47}$$

where the single oil phase pressure drop derivative with respect to skin is

$$\frac{\partial \Delta \hat{p}_o}{\partial s} = \frac{\alpha q_{inj}}{kh\hat{\lambda}_o}. \tag{B.48}$$

Substituting Eq. B.48 in Eq. B.47 and taking the derivative of its second term in the right-hand side yields

$$\frac{\partial \Delta p_{wf}}{\partial s} = \frac{\alpha q_{inj}}{kh\hat{\lambda}_o} + \frac{\alpha q_{inj}}{h\hat{\lambda}_o k_s^2} \frac{k}{\ln(\frac{r_{skin}}{r_w})} \frac{1}{\left(\frac{s}{\ln(\frac{r_{skin}}{r_w})} + 1\right)^2} \int_{r_w}^{rint(t)} \Big(\frac{\hat{\lambda}_o}{\lambda_t(r,t)} - 1\Big) \frac{dr}{r}, \tag{B.49}$$

where

$$rint(t) = \begin{cases} r_{f,inj}(t) & r_{f,inj}(t) < r_{skin} \\ r_{skin} & r_{f,inj}(t) \geq r_{skin}. \end{cases} \tag{B.50}$$

The derivative of the pressure drop with respect to the model parameter a_w is given by

$$\frac{\partial \Delta p_{wf}}{\partial a_w} = \frac{\alpha q_{inj}}{h\hat{\lambda}_o} \frac{\partial}{\partial a_w} \int_{r_w}^{r_{f,inj}(t)} \Big(\frac{\hat{\lambda}_o}{\lambda_t(r,t)} - 1\Big) \frac{1}{k(r)} \frac{dr}{r}. \tag{B.51}$$

Applying the Leibniz rule to the right-hand side of Eq. B.51 yields

$$\frac{\partial \Delta p_{wf}}{\partial a_w} = \frac{\alpha q_{inj}}{h\hat{\lambda}_o}\Bigg[\int_{r_w}^{r_{f,inj}(t)} \frac{\partial}{\partial a_w}\Big(\frac{\hat{\lambda}_o}{\lambda_t(r,t)} - 1\Big)\frac{dr}{k(r)r} + \frac{\Big(\frac{\hat{\lambda}_o}{\lambda_t(r_{f,inj},t)} - 1\Big)}{k(r_{f,inj})r_{f,inj}}\frac{\partial r_{f,inj}}{\partial a_w}\Bigg], \tag{B.52}$$

where the total mobility and water front radius derivative with respect a_w are

$$\frac{\partial \lambda_t}{\partial a_w} = \frac{1}{\mu_w}\left(\frac{S_w - S_{iw}}{1 - S_{iw} - S_{or}}\right)^{n_w} \tag{B.53}$$

and

$$\frac{\partial r_{f,inj}}{\partial a_w} = \frac{\frac{\theta q_{inj} t}{\phi \pi h}\frac{\partial}{\partial a_w}\left(\frac{df_w(S_{wfinj})}{dS_w}\right)}{2\big(r_w^2 + \frac{\theta q_{inj} t}{\phi \pi h}\frac{df_w(S_{wfinj})}{dS_w}\big)^{\frac{1}{2}}}. \tag{B.54}$$

Inserting Eqs. B.53 and B.54 in Eq. B.52, we have

$$\begin{aligned}\frac{\partial \Delta p_{wf}}{\partial a_w} =& -\frac{\alpha q_{inj}}{h}\int_{r_w}^{r_{f,inj}(t)} \frac{1}{\lambda_t(r,t)^2}\frac{1}{\mu_w k(r)}\left(\frac{S_w(r,t) - S_{wi}}{1 - S_{wi} - S_{or}}\right)^{n_w}\frac{dr}{r} \\ &+ \frac{\alpha\theta q_{inj}^2 t}{\pi h^2 \hat{\lambda}_o \phi}\Big(\frac{\hat{\lambda}_o}{\lambda_t(r_{f,inj},t)} - 1\Big)\frac{1}{k(r_{f,inj})r_{f,inj}}\frac{\frac{\partial}{\partial a_w}\big(\frac{df_w}{dS_w}(S_{wfinj})\big)}{2\big(r_w^2 + \frac{\theta q_{inj} t}{\phi \pi h}\frac{df_w}{dS_w}(S_{wfinj})\big)^{\frac{1}{2}}},\end{aligned} \tag{B.55}$$

where

$$\begin{aligned}\frac{\partial}{\partial a_w}\left(\frac{df_w}{dS_w}\right) =& \, a_o\mu_o\mu_w\left(\frac{S_{or} + S_{wfinj} - 1}{S_{iw} + S_{or} - 1}\right)^{n_o}\left(\frac{S_{iw} - S_{wfinj}}{S_{iw} + S_{or} - 1}\right)^{n_w} \\ &\times [S_{iw}n_o + n_w(S_{or} + S_{wfinj} - 1) - n_o S_{wfinj}] \\ &\times \left\{\frac{\Big[\mu_o a_w\left(\frac{S_{iw} - S_{wfinj}}{S_{iw} + S_{or} - 1}\right)^{n_w} - a_o\mu_w\left(\frac{S_{or} + S_{wfinj} - 1}{S_{iw} + S_{or} - 1}\right)^{n_o}\Big]}{(S_{iw} - S_{wfinj})(S_{or} + S_{wfinj} - 1)\Big[a_o\mu_w\left(\frac{S_{or} + S_{wfinj} - 1}{S_{iw} + S_{or} - 1}\right)^{n_o} + \mu_o a_w\left(\frac{S_{iw} - S_{wfinj}}{S_{iw} + S_{or} - 1}\right)^{n_w}\Big]^3}\right\}.\end{aligned} \tag{B.56}$$

The derivative of the pressure drop with respect to the model parameter n_w is given by

$$\frac{\partial \Delta p_{wf}}{\partial n_w} = \frac{\alpha q_{inj}}{h\hat{\lambda}_o} \frac{\partial}{\partial n_w} \int_{r_w}^{r_{f,inj}(t)} \Big(\frac{\hat{\lambda}_o}{\lambda_t(r,t)} - 1 \Big) \frac{1}{k(r)} \frac{dr}{r}. \tag{B.57}$$

Applying the Leibniz rule to the right-hand side of Eq. B.57 yields

$$\frac{\partial \Delta p_{wf}}{\partial n_w} = \frac{\alpha q_{inj}}{h\hat{\lambda}_o} \Bigg[\int_{r_w}^{r_{f,inj}(t)} \frac{\partial}{\partial n_w} \Big(\frac{\hat{\lambda}_o}{\lambda_t(r,t)} - 1 \Big) \frac{dr}{k(r)r} + \frac{\Big(\frac{\hat{\lambda}_o}{\lambda_t(r_{f,inj},t)} - 1 \Big)}{k(r_{f,inj}) r_{f,inj}} \frac{\partial r_{f,inj}}{\partial n_w} \Bigg], \tag{B.58}$$

where the derivative of total mobility and water front radius with respect to n_w are

$$\frac{\partial \lambda_t}{\partial n_w} = \frac{a_w}{\mu_w} \left(\frac{S_w - S_{iw}}{1 - S_{iw} - S_{or}} \right)^{n_w} \ln \left(\frac{S_w - S_{iw}}{1 - S_{iw} - S_{or}} \right) \tag{B.59}$$

and

$$\frac{\partial r_{f,inj}}{\partial n_w} = \frac{\frac{\theta q_{inj} t}{\phi \pi h} \frac{\partial}{\partial n_w} \left(\frac{df_w}{dS_w}(S_{wfinj}) \right)}{2\big(r_w^2 + \frac{\theta q_{inj} t}{\phi \pi h} \frac{df_w(S_{wfinj})}{dS_w} \big)^{\frac{1}{2}}}. \tag{B.60}$$

Inserting Eqs. B.59 and B.60 into Eq. B.58, we have

$$\begin{aligned} \frac{\partial \Delta p_{wf}}{\partial n_w} = & - \frac{\alpha q_{inj}}{h} \int_{r_w}^{r_{f,inj}(t)} \frac{1}{\lambda_t(r,t)^2} \frac{a_w}{\mu_w} \left(\frac{S_w - S_{iw}}{1 - S_{iw} - S_{or}} \right)^{n_w} \ln \left(\frac{S_w - S_{iw}}{1 - S_{iw} - S_{or}} \right) \frac{dr}{k(r)r} \\ & + \frac{\alpha \theta q_{inj}^2 t}{\pi h^2 \hat{\lambda}_o \phi} \Big(\frac{\hat{\lambda}_o}{\lambda_t(r_{f,inj},t)} - 1 \Big) \frac{1}{k(r_{f,inj}) r_{f,inj}} \frac{\frac{\partial}{\partial n_w} \big(\frac{df_w}{dS_w}(S_{wfinj}) \big)}{2\big(r_w^2 + \frac{\theta q_{inj} t}{\phi \pi h} \frac{df_w}{dS_w}(S_{wfinj}) \big)^{\frac{1}{2}}}, \end{aligned} \tag{B.61}$$

where

$$\frac{\partial}{\partial n_w}\left(\frac{df_w}{dS_w}(S_{wfinj})\right) = -a_o\mu_o\mu_w a_w \left(\frac{S_{or}+S_{wf}-1}{S_{iw}+S_{or}-1}\right)^{n_o}\left(\frac{S_{iw}-S_{wf}}{S_{iw}+S_{or}-1}\right)^{n_w}$$
$$\times\left\{\frac{(S_{or}+S_{wf}-1)\left[a_o\mu_w\left(\frac{S_{or}+S_{wf}-1}{S_{iw}+S_{or}-1}\right)^{n_o}+\mu_o a_w\left(\frac{S_{iw}-S_{wf}}{S_{iw}+S_{or}-1}\right)^{n_w}\right]}{(S_{iw}-S_{wf})(S_{or}+S_{wf}-1)\left[a_o\mu_w\left(\frac{S_{or}+S_{wf}-1}{S_{iw}+S_{or}-1}\right)^{n_o}+\mu_o a_w\left(\frac{S_{iw}-S_{wf}}{S_{iw}+S_{or}-1}\right)^{n_w}\right]^3}+\right.$$
$$\left.\frac{-\ln\left(\frac{S_{iw}-S_{wf}}{S_{iw}+S_{or}-1}\right)(S_{iw}n_o+n_w(S_{or}+S_{wf}-1)-n_oS_{wf})}{(S_{iw}-S_{wf})(S_{or}+S_{wf}-1)\left[a_o\mu_w\left(\frac{S_{or}+S_{wf}-1}{S_{iw}+S_{or}-1}\right)^{n_o}+\mu_o a_w\left(\frac{S_{iw}-S_{wf}}{S_{iw}+S_{or}-1}\right)^{n_w}\right]^3}\right.$$
$$\left.\times\left[\mu_o a_w\left(\frac{S_{iw}-S_{wf}}{S_{iw}+S_{or}-1}\right)^{n_w}-a_o\mu_w\left(\frac{S_{or}+S_{wf}-1}{S_{iw}+S_{or}-1}\right)^{n_o}\right]\right\}. \tag{B.62}$$

The pressure drop derivative with the model parameter n_o is given by

$$\frac{\partial\Delta p_{wf}}{\partial n_o} = \frac{\partial}{\partial n_o}\left[\frac{\alpha q_{inj}}{h\hat{\lambda}_o}\int_{r_w}^{r_{f,inj}(t)}\Big(\frac{\hat{\lambda}_o}{\lambda_t(r,t)}-1\Big)\frac{1}{k(r)}\frac{dr}{r}\right]. \tag{B.63}$$

Applying the Leibniz rule to the second term on the right-hand side of Eq. B.63 yields

$$\frac{\alpha q_{inj}}{h\hat{\lambda}_o}\left\{\int_{r_w}^{r_{f,inj}(t)}\frac{\partial}{\partial n_o}\Big(\frac{\hat{\lambda}_o}{\lambda_t(r,t)}-1\Big)\frac{1}{k(r)}\frac{dr}{r}+\left[\Big(\frac{\hat{\lambda}_o}{\lambda_t(r_{f,inj},t)}-1\Big)\frac{1}{k(r_{f,inj})}\frac{1}{r_{f,inj}}\right]\frac{\partial r_{f,inj}}{\partial n_o}\right\}, \tag{B.64}$$

where the derivative of the total mobility and the water front radius with respect to n_o are

$$\frac{\partial\lambda_t}{\partial n_o} = \frac{a_o}{\mu_o}\left(\frac{1-S_w-S_{or}}{1-S_{iw}-S_{or}}\right)^{n_o}\ln\left(\frac{1-S_w-S_{or}}{1-S_{iw}-S_{or}}\right) \tag{B.65}$$

and

$$\frac{\partial r_{f,inj}}{\partial n_o} = \frac{\frac{\theta q_{inj}t}{\phi\pi h}\frac{\partial}{\partial n_o}\big(\frac{df_w}{dS_w}(S_{wfinj})\big)}{2\big(r_w^2+\frac{\theta q_{inj}t}{\phi\pi h}\frac{df_w}{dS_w}(S_{wfinj})\big)^{\frac{1}{2}}}. \tag{B.66}$$

Then, using Eqs. B.65, B.66 and Eq. B.64 in Eq. B.63, we have

$$\frac{\partial \Delta p_{wf}}{\partial n_o} = -\frac{\alpha q_{inj}}{h\hat{\lambda}_o}\int_{r_w}^{r_{f,inj}(t)}\left(\frac{\hat{\lambda}_o}{\lambda_t(r,t)^2}\right)\frac{a_o}{\mu_o}\left(\frac{1-S_w-S_{or}}{1-S_{iw}-S_{or}}\right)^{n_o}\ln\left(\frac{1-S_w-S_{or}}{1-S_{iw}-S_{or}}\right)\frac{1}{k(r)}\frac{dr}{r}$$
$$+\frac{\alpha\theta q_{inj}^2 t}{\pi h^2\hat{\lambda}_o\phi}\Big(\frac{\hat{\lambda}_o}{\lambda_t(r_{f,inj},t)}-1\Big)\frac{1}{k(r_{f,inj})r_{f,inj}}\frac{\frac{\partial}{\partial n_o}\left(\frac{df_w}{dS_w}(S_{wfinj})\right)}{2\Big(r_w^2+\frac{\theta q_{inj}t}{\phi\pi h}\frac{df_w}{dS_w}(S_{wfinj})\Big)^{\frac{1}{2}}}, \tag{B.67}$$

where

$$\frac{\partial}{\partial n_o}\left(\frac{df_w}{dS_w}(S_{wfinj})\right) = a_o\mu_o\mu_w a_w\left(\frac{S_{or}+S_{wf}-1}{S_{iw}+S_{or}-1}\right)^{n_o}\left(\frac{S_{iw}-S_{wf}}{S_{iw}+S_{or}-1}\right)^{n_w}$$
$$\times\Bigg\{\frac{(S_{wf}-S_{iw})\left[a_o\mu_w\left(\frac{S_{or}+S_{wf}-1}{S_{iw}+S_{or}-1}\right)^{n_o}+\mu_o a_w\left(\frac{S_{iw}-S_{wf}}{S_{iw}+S_{or}-1}\right)^{n_w}\right]}{(S_{iw}-S_{wf})(S_{or}+S_{wf}-1)\left[a_o\mu_w\left(\frac{S_{or}+S_{wf}-1}{S_{iw}+S_{or}-1}\right)^{n_o}+\mu_o a_w\left(\frac{S_{iw}-S_{wf}}{S_{iw}+S_{or}-1}\right)^{n_w}\right]^3}+$$
$$\frac{-\ln\left(\frac{S_{or}+S_{wf}-1}{S_{iw}+S_{or}-1}\right)\left[S_{iw}n_o+n_w(S_{or}+S_{wf}-1)-n_oS_{wf}\right]}{(S_{iw}-S_{wf})(S_{or}+S_{wf}-1)\left[a_o\mu_w\left(\frac{S_{or}+S_{wf}-1}{S_{iw}+S_{or}-1}\right)^{n_o}+\mu_o a_w\left(\frac{S_{iw}-S_{wf}}{S_{iw}+S_{or}-1}\right)^{n_w}\right]^3}$$
$$\times\left[\mu_o a_w\left(\frac{S_{iw}-S_{wf}}{S_{iw}+S_{or}-1}\right)^{n_w}-a_o\mu_w\left(\frac{S_{or}+S_{wf}-1}{S_{iw}+S_{or}-1}\right)^{n_o}\right]\Bigg\}. \tag{B.68}$$

B.2 Falloff

For the pressure drop equation for the falloff period, the derivatives with respect to model parameters can be obtained in a similar way to those for the injection period. First, we can take the derivative of the single oil phase pressure drop with respect to k,

$$\frac{\partial\Delta\hat{p}_o}{\partial k} = -\frac{\alpha q_{inj}}{2k^2h\hat{\lambda}_o}\ln\left(\frac{t_{inj}+\Delta t_{foff}}{\Delta t_{foff}}\right), \tag{B.69}$$

and with respect to a_o,

$$\frac{\partial\Delta\hat{p}_o}{\partial a_o} = -\frac{\alpha q_{inj}}{2kh\hat{\lambda}_o^2\mu_o}\ln\left(\frac{t_{inj}+\Delta t_{foff}}{\Delta t_{foff}}\right). \tag{B.70}$$

The derivative of the pressure drop with respect to the model parameter k is given by

$$\frac{\partial \Delta p_{wf}}{\partial k} = \frac{\partial \Delta \hat{p}_o}{\partial k} + \frac{\alpha}{h\hat{\lambda}_o}\frac{\partial}{\partial k}\int_{r_w}^{r_{f,inj}(t_{inj})}\left(\frac{\hat{\lambda}_o}{\lambda_t(r,t_{inj})}q_s(r,\Delta t_{foff}) - q_{os}(r,\Delta t_{foff})\right)\frac{1}{k(r)}\frac{dr}{r}. \quad \text{(B.71)}$$

Taking the derivative of the second term in the right-hand side of Eq. B.71 yields

$$\begin{aligned}\frac{\partial \Delta p_{wf}}{\partial k} =& \frac{\partial \Delta \hat{p}_o}{\partial k} - \frac{\alpha}{h\hat{\lambda}_o k^2}\left[\left(\frac{s}{\ln(\frac{r_{skin}}{r_w})}+1\right)\int_{r_w}^{r_{skin}(t_{inj})}\left(\frac{\hat{\lambda}_o}{\lambda_t(r,t_{inj})}q_s(r,\Delta t_{foff}) - q_{os}(r,\Delta t_{foff})\right)\frac{dr}{r}\right.\\ &\left. + \int_{r_{skin}}^{r_{f,inj}(t_{inj})}\left(\frac{\hat{\lambda}_o}{\lambda_t(r,t_{inj})}q_s(r,\Delta t_{foff}) - q_{os}(r,\Delta t_{foff})\right)\frac{dr}{r}\right]\\ &+ \frac{\alpha}{h\hat{\lambda}_o}\int_{r_w}^{r_{f,inj}(t_{inj})}\left(\frac{\hat{\lambda}_o}{\lambda_t(r,t_{inj})}\frac{\partial q_s}{\partial k}(r,\Delta t_{foff})\frac{\partial q_{os}}{\partial k}(r,\Delta t_{foff})\right)\frac{dr}{rk(r)}, \end{aligned} \quad \text{(B.72)}$$

for $r_{f,inj}(t_{inj}) > r_{skin}$. Otherwise, i.e., for $r_{f,inj}(t_{inj}) \leq r_{skin}$

$$\begin{aligned}\frac{\partial \Delta p_{wf}}{\partial k} =& \frac{\partial \Delta \hat{p}_o}{\partial k} - \frac{\alpha}{h\hat{\lambda}_o k^2}\left(\frac{s}{\ln(\frac{r_{skin}}{r_w})}+1\right)\int_{r_w}^{r_{f,inj}(t_{inj})}\left(\frac{\hat{\lambda}_o}{\lambda_t(r,t_{inj})}q_s(r,\Delta t_{foff}) - q_{os}(r,\Delta t_{foff})\right)\frac{dr}{r}\\ &+ \frac{\alpha}{h\hat{\lambda}_o}\int_{r_w}^{r_{f,inj}(t_{inj})}\left(\frac{\hat{\lambda}_o}{\lambda_t(r,t_{inj})}\frac{\partial q_s}{\partial k}(r,\Delta t_{foff})\frac{\partial q_{os}}{\partial k}(r,\Delta t_{foff})\right)\frac{dr}{rk(r)}, \end{aligned} \quad \text{(B.73)}$$

where

$$\frac{\partial q_{os}}{\partial k} = \frac{q_{inj}\phi\hat{c}_{to}r^2}{4\beta k^2\hat{\lambda}_o}\left[\frac{\exp\left(-\frac{\phi\hat{c}_{to}r^2}{4\beta k\hat{\lambda}_o(t_{inj}+\Delta t_{foff})}\right)}{t_{inj}+\Delta t_{foff}} - \frac{\exp\left(-\frac{\phi\hat{c}_{to}r^2}{4\beta k\hat{\lambda}_o\Delta t_{foff}}\right)}{\Delta t_{foff}}\right] \quad \text{(B.74)}$$

and

$$\frac{\partial q_s}{\partial k} = \frac{q_{inj}\phi c_t(r,t_{inj})r^2}{4\beta k^2\lambda_t(r,t_{inj})}\left[\frac{\exp\left(-\frac{\phi c_t(r,t_{inj})r^2}{4\beta k\lambda_t(r,t_{inj})(t_{inj}+\Delta t_{foff})}\right)}{t_{inj}+\Delta t_{foff}} - \frac{\exp\left(-\frac{\phi c_t(r,t_{inj})r^2}{4\beta k\lambda_t(r,t_{inj})\Delta t_{foff}}\right)}{\Delta t_{foff}}\right]. \quad \text{(B.75)}$$

The pressure drop derivative with respect to the model parameter s can be written as

$$\frac{\partial \Delta p_{wf}}{\partial s} = \frac{\alpha}{h\hat{\lambda}_o}\frac{\partial}{\partial s}\int\limits_{r_w}^{r_{f,inj}(t_{inj})}\left(\frac{\hat{\lambda}_o}{\lambda_t(r,t_{inj})}q_s(r,\Delta t_{foff}) - q_{os}(r,\Delta t_{foff})\right)\frac{1}{k(r)}\frac{dr}{r}, \tag{B.76}$$

which yields

$$\frac{\partial \Delta p_{wf}}{\partial s} = \frac{\alpha}{h\hat{\lambda}_o k_s^2}\frac{k}{\ln(\frac{r_{skin}}{r_w})}\frac{1}{(\frac{s}{\ln(\frac{r_{skin}}{r_w})}+1)^2}\int\limits_{r_w}^{rint(t_{inj})}\left(\frac{\hat{\lambda}_o}{\lambda_t(r,t_{inj})}q_s(r,\Delta t_{foff}) - q_{os}(r,\Delta t_{foff})\right)\frac{dr}{r}, \tag{B.77}$$

with

$$rint(t_{inj}) = \begin{cases} r_{f,inj}(t_{inj}) & r_{f,inj}(t_{inj}) \le r_{skin} \\ r_{skin} & r_{f,inj}(t_{inj}) > r_{skin}. \end{cases} \tag{B.78}$$

For model parameter a_w, the pressure drop derivative is expressed as

$$\frac{\partial \Delta p_{wf}}{\partial a_w} = \frac{\alpha}{h\hat{\lambda}_o}\frac{\partial}{\partial a_w}\int\limits_{r_w}^{r_{f,inj}(t_{inj})}\left(\frac{\hat{\lambda}_o}{\lambda_t(r,t_{inj})}q_s(r,\Delta t_{foff}) - q_{os}(r,\Delta t_{foff})\right)\frac{1}{k(r)}\frac{dr}{r}, \tag{B.79}$$

which yields

$$\begin{aligned}\frac{\partial \Delta p_{wf}}{\partial a_w} = \frac{\alpha}{h}&\int\limits_{r_w}^{r_{f,inj}(t_{inj})}\left\{-\frac{q_s(r,\Delta t_{foff})}{\lambda_t^2(r,t_{inj})} + \frac{q_{inj}\phi c_t(r,t_{inj})r^2}{4\beta k\lambda_t^3(r,t_{inj})}\right.\\
&\left.\times\left[\left(\frac{\exp\left(-\frac{\phi c_t(r,t_{inj})r^2}{4\beta k\lambda_t(r,t_{Inj})(t_{inj}+\Delta t_{foff})}\right)}{(t_{inj}+\Delta t_{foff})}\right) - \left(\frac{\exp\left(-\frac{\phi c_t(r,t_{inj})r^2}{4\beta k\lambda_t(r,t_{inj})\Delta t_{foff}}\right)}{\Delta t_{foff}}\right)\right]\right\}\frac{\frac{\partial \lambda t}{\partial aw}(r,t_{inj})}{k(r)}\frac{dr}{r}\\
&+\frac{\alpha\theta q_{inj}t_{inj}}{\pi h^2\hat{\lambda}_o\phi}\frac{\left(\frac{\hat{\lambda}_o}{\lambda_t(r_{f,inj},t_{inj})}q_s(r_{f,inj},\Delta t_{foff}) - q_{os}(r_{f,inj},\Delta t_{foff})\right)}{k(r_{f,inj})r_{f,inj}}\frac{\frac{\partial}{\partial a_w}\left(\frac{df_w(S_{wfinj})}{dS_w}\right)}{2\left(r_w^2+\frac{\theta q_{inj}t_{inj}}{\phi\pi h}\frac{df_w(S_{wfinj})}{dS_w}\right)^{\frac{1}{2}}}.\end{aligned} \tag{B.80}$$

The pressure drop derivative with respect to the model parameter n_w is given by

$$\frac{\partial \Delta p_{wf}}{\partial n_w} = \frac{\alpha}{h\hat{\lambda}_o}\frac{\partial}{\partial n_w}\int_{r_w}^{r_{f,inj}(t_{inj})}\left(\frac{\hat{\lambda}_o}{\lambda_t(r,t_{inj})}q_s(r,\Delta t_{foff}) - q_{os}(r,\Delta t_{foff})\right)\frac{1}{k(r)}\frac{dr}{r}, \tag{B.81}$$

which leads to

$$\begin{aligned}\frac{\partial \Delta p_{wf}}{\partial n_w} = \frac{\alpha}{h}\int_{r_w}^{r_{f,inj}(t_{inj})} a_w\left(\frac{S_w - S_{iw}}{1-S_{iw}-S_{or}}\right)^{n_o}\ln\left(\frac{S_w - S_{iw}}{1-S_{iw}-S_{or}}\right)\Bigg\{ -\frac{q_s(r,\Delta t_{foff})}{\lambda_t^2(r,t_{inj})\mu_w} \\ + \frac{q_{inj}\phi c_t(r,t_{inj})r^2}{4\beta k\mu_w\lambda_t^3(r,t_{inj})}\left[\left(\frac{\exp\left(-\frac{\phi c_t(r,t_{inj})r^2}{4\beta k\lambda_t(r,t_{Inj})(t_{inj}+\Delta t_{foff})}\right)}{(t_{inj}+\Delta t_{foff})}\right) - \left(\frac{\exp\left(-\frac{\phi c_t(r,t_{inj})r^2}{4\beta k\lambda_t(r,t_{inj})\Delta t_{foff}}\right)}{\Delta t_{foff}}\right)\right]\Bigg\}\frac{dr}{k(r)r} \\ + \frac{\alpha\theta q_{inj}t_{inj}}{\pi h^2\hat{\lambda}_o\phi}\frac{\left(\frac{\hat{\lambda}_o}{\lambda_t(r_{f,inj},t_{inj})}q_s(r_{f,inj},\Delta t_{foff}) - q_{os}(r_{f,inj},\Delta t_{foff})\right)}{k(r_{f,inj})r_{f,inj}}\frac{\frac{\partial}{\partial n_w}\left(\frac{df_w(S_{wfinj})}{dS_w}\right)}{2\left(r_w^2 + \frac{\theta q_{inj}t_{inj}}{\phi\pi h}\frac{df_w(S_{wfinj})}{dS_w}\right)^{\frac{1}{2}}}.\end{aligned} \tag{B.82}$$

The pressure drop derivative with respect to the model parameter n_o is given by

$$\frac{\partial \Delta p_{wf}}{\partial n_o} = \frac{\partial \Delta \hat{p}_o}{\partial n_o} + \frac{\alpha}{h\hat{\lambda}_o}\frac{\partial}{\partial n_o}\int_{r_w}^{r_{f,inj}(t_{inj})}\left(\frac{\hat{\lambda}_o}{\lambda_t(r,t_{inj})}q_s(r,\Delta t_{foff}) - q_{os}(r,\Delta t_{foff})\right)\frac{1}{k(r)}\frac{dr}{r}, \tag{B.83}$$

which leads to

$$\begin{aligned}\frac{\partial \Delta p_{wf}}{\partial n_o} = \frac{\alpha}{h\hat{\lambda}_o}\int_{r_w}^{r_{f,inj}(t_{inj})} a_o\left(\frac{1-S_w-S_{or}}{1-S_{iw}-S_{or}}\right)^{n_o}\ln\left(\frac{1-S_w-S_{or}}{1-S_{iw}-S_{or}}\right)\Bigg\{ -\frac{q_s(r,\Delta t_{foff})}{\lambda_t^2(r,t_{inj})\mu_o} \\ + \frac{q_{inj}\phi c_t(r,t_{inj})r^2}{4\beta k\mu_o\lambda_t^3(r,t_{inj})}\left[\left(\frac{\exp\left(-\frac{\phi c_t(r,t_{inj})r^2}{4\beta k\lambda_t(r,t_{Inj})(t_{inj}+\Delta t_{foff})}\right)}{(t_{inj}+\Delta t_{foff})}\right) - \left(\frac{\exp\left(-\frac{\phi c_t(r,t_{inj})r^2}{4\beta k\lambda_t(r,t_{inj})\Delta t_{foff}}\right)}{\Delta t_{foff}}\right)\right]\Bigg\}\frac{\hat{\lambda}_o dr}{k(r)r} \\ + \frac{\alpha\theta q_{inj}t_{inj}}{\pi h^2\hat{\lambda}_o\phi}\frac{\left(\frac{\hat{\lambda}_o}{\lambda_t(r_{f,inj},t_{inj})}q_s(r_{f,inj},\Delta t_{foff}) - q_{os}(r_{f,inj},\Delta t_{foff})\right)}{k(r_{f,inj})r_{f,inj}}\frac{\frac{\partial}{\partial n_w}\left(\frac{df_w(S_{wfinj})}{dS_w}\right)}{2\left(r_w^2 + \frac{\theta q_{inj}t_{inj}}{\phi\pi h}\frac{df_w(S_{wfinj})}{dS_w}\right)^{\frac{1}{2}}}.\end{aligned} \tag{B.84}$$

B.3 Production

For the production period, in addition to the bottom hole pressure, the observed data includes the water cut. The model parameters to be estimated are expressed by the vector $\vec{m}_{prod}$

$$\vec{m}_{prod} = [k, s, a_w, n_w, n_o]^T, \tag{B.85}$$

where the last 3 parameters refer to a drainage process. Again, the pressure drop derivatives with respect to the model parameter can be derived in a similar way to the injection period. The pressure drop derivative with respect to the model parameter k is given by

$$\begin{aligned}\frac{\partial \Delta p_{wf}}{\partial k} =& -\frac{\alpha}{k^2 h\hat{\lambda}_o}\left\{\frac{q_{inj}}{2}\ln\left(\frac{t_{inj}+\Delta t_{foff}+\Delta t_{prod}}{\Delta t_{foff}+\Delta t_{prod}}\right)+q_{prod}\left[\frac{1}{2}\ln\left(\frac{\beta k\hat{\lambda}_o t}{\phi\hat{c}_{to}r_w^2}\right)-0.0955+s\right]\right\}\\ &-\frac{\alpha q_{prod}}{h\hat{\lambda}_o k^2}\left[\left(\frac{s}{\ln(\frac{r_{skin}}{r_w})}+1\right)\int_{r_w}^{r_{skin}}\left(\frac{\hat{\lambda}_o}{\lambda_t(r,t)}-1\right)\frac{dr}{r}+\int_{r_{skin}}^{r_{f,inj}(t_{inj})}\left(\frac{\hat{\lambda}_o}{\lambda_t(r,t)}-1\right)\frac{dr}{r}\right],\end{aligned} \tag{B.86}$$

for $r_{f,inj}(t_{inj}) \geq r_{skin}$. Otherwise,

$$\begin{aligned}\frac{\partial \Delta p_{wf}}{\partial k} =& -\frac{\alpha}{k^2 h\hat{\lambda}_o}\left\{\frac{q_{inj}}{2}\ln\left(\frac{t_{inj}+\Delta t_{foff}+\Delta t_{prod}}{\Delta t_{foff}+\Delta t_{prod}}\right)+q_{prod}\left[\frac{1}{2}\ln\left(\frac{\beta k\hat{\lambda}_o t}{\phi\hat{c}_{to}r_w^2}\right)-0.0955+s\right]\right\}\\ &-\frac{\alpha q_{prod}}{h\hat{\lambda}_o k^2}\left(\frac{s}{\ln(\frac{r_{skin}}{r_w})}+1\right)\int_{r_w}^{r_{skin}}\left(\frac{\hat{\lambda}_o}{\lambda_t(r,t)}-1\right)\frac{dr}{r}.\end{aligned} \tag{B.87}$$

The pressure drop derivative with respect to the model parameter s is defined as

$$\frac{\partial \Delta p_{wf}}{\partial s} = \frac{\alpha q_{prod}}{kh\hat{\lambda}_o}+\frac{\alpha q_{prod}}{h\hat{\lambda}_o k_s^2}\frac{k}{\ln(\frac{r_{skin}}{r_w})}\frac{1}{(\frac{s}{\ln(\frac{r_{skin}}{r_w})}+1)^2}\int_{r_w}^{rint(t_{inj})}\left(\frac{\hat{\lambda}_o}{\lambda_t(r,t)}-1\right)\frac{dr}{r}. \tag{B.88}$$

The pressure drop derivative with respect to the model parameter a_w is calculated according

to

$$\frac{\partial \Delta p_{wf}}{\partial a_w} = -\frac{\alpha q_{prod}}{h} \int_{r_w}^{r_{f,inj}(t_{inj})} \frac{1}{\lambda_t(r,t)^2} \frac{1}{\mu_w k(r)} \left(\frac{S_w(r,t) - S_{iw}}{1 - S_{iw} - S_{or}} \right)^{n_w} \frac{dr}{r}. \tag{B.89}$$

The pressure drop derivative with respect to the model parameter n_w is given by

$$\frac{\partial \Delta p_{wf}}{\partial n_w} = -\frac{\alpha q_{prod}}{h} \int_{r_w}^{r_{f,inj}(t_{inj})} \frac{1}{\lambda_t(r,t)^2} \frac{a_w}{\mu_w} \left(\frac{S_w - S_{iw}}{1 - S_{iw} - S_{or}} \right)^{n_w} \ln \left(\frac{S_w - S_{iw}}{1 - S_{iw} - S_{or}} \right) \frac{dr}{k(r) r}. \tag{B.90}$$

The pressure drop derivative with respect to the model parameter n_o is given by

$$\frac{\partial \Delta p_{wf}}{\partial n_o} = -\frac{\alpha q_{prod}}{h \hat{\lambda}_o} \int_{r_w}^{r_{f,inj}(t_{inj})} \left(\frac{\hat{\lambda}_o}{\lambda_t(r,t)^2} \right) \frac{a_o}{\mu_o} \left(\frac{1 - S_w - S_{or}}{1 - S_{iw} - S_{or}} \right)^{n_o} \ln \left(\frac{1 - S_w - S_{or}}{1 - S_{iw} - S_{or}} \right) \frac{1}{k(r)} \frac{dr}{r}. \tag{B.91}$$

If we want to estimate the parameters using all data for the whole IFPT together, we also have to consider the production pressure drop with respect to the imbibition parameters, since $r_{f,inj}(t_{inj})$ is a function of them.

The water production flow rate ($q_{w,well}$) during the production period of the IFPT is given by

$$q_{w,well} = q_{prod} f_w(S_{w,well}), \tag{B.92}$$

where the water saturation in the well ($S_{w,well}$) can be found by solving the following equation

$$R_{prod}(S_{w,well}, t_{inj}) = r_w^2 - r_{inj}^2(S_{w,well}, t_{inj}) + \frac{\theta q_{prod} \Delta t_{prod}}{\pi \phi h} \frac{df_w}{dS_w}(S_{w,well}) = 0 \tag{B.93}$$

at each time before breakthrough, and

$$R_{prod}(S_{w,well}, t_{inj}) = r_w^2 - r_{inj}^2(S_{wf}, t_{inj}) + \frac{\theta q_{prod} \Delta t_{prod}}{\pi \phi h} \frac{df_w}{dS_w}(S_{w,well}) = 0, \tag{B.94}$$

after the production shock breakthrough. The water flow rate derivative does not depend on the absolute permeability or skin permeability. Therefore, the derivatives with those two parameters are zero. The well water flow rate derivative with respect to the model parameters m_i, where, in this case,

$$\vec{m}_{prod} = [a_w, n_w, n_o]^T, \tag{B.95}$$

are given by

$$\frac{\partial q_w}{\partial m_i} = q_{prod}\left(\frac{\partial f_w(S_{w,well}, m_i)}{\partial m_i} + \frac{\partial f_w(S_{w,well}, m_i)}{\partial S_{w,well}}\frac{\partial S_{w,well}}{\partial m_i}\right), \quad \text{for } i = 1, 2, 3, \tag{B.96}$$

where the derivative of the well water saturation with respect to the model parameter m at a particular time,

$$\frac{\partial S_{w,well}}{\partial m_i} = -\frac{\frac{\partial R_{prod}}{\partial m_i}}{\frac{\partial R_{prod}}{\partial S_{w,well}}}, \tag{B.97}$$

comes from

$$\frac{dR_{prod}}{dm_i} = \frac{\partial R_{prod}}{\partial m_i} + \frac{\partial R_{prod}}{\partial S_{w,well}}\frac{\partial S_{w,well}}{\partial m_i} = 0. \tag{B.98}$$

The derivative of the water fractional flow with respect to a_w is given by

$$\frac{\partial f_w(S_{w,well}, \vec{m}_{prod})}{\partial a_w} = \frac{a_o\mu_o\mu_w\left(\frac{S_{or}+S_{wf}-1}{S_{iw}+S_{or}-1}\right)^{n_o}\left(\frac{S_{iw}-S_{wf}}{S_{iw}+S_{or}-1}\right)^{n_w}}{\left[a_o\mu_w\left(\frac{S_{or}+S_{wf}-1}{S_{iw}+S_{or}-1}\right)^{n_o} + \mu_o a_w\left(\frac{S_{iw}-S_{wf}}{S_{iw}+S_{or}-1}\right)^{n_w}\right]^2}, \tag{B.99}$$

while the derivative with respect to n_w is

$$\frac{\partial f_w(S_{w,well}, \vec{m}_{prod})}{\partial n_w} = \frac{a_o\mu_o\mu_w a_w\left(\frac{S_{or}+S_{wf}-1}{S_{iw}+S_{or}-1}\right)^{n_o}\left(\frac{S_{iw}-S_{wf}}{S_{iw}+S_{or}-1}\right)^{n_w}\ln\left(\frac{S_{iw}-S_{wf}}{S_{iw}+S_{or}-1}\right)}{\left[a_o\mu_w\left(\frac{S_{or}+S_{wf}-1}{S_{iw}+S_{or}-1}\right)^{n_o} + \mu_o a_w\left(\frac{S_{iw}-S_{wf}}{S_{iw}+S_{or}-1}\right)^{n_w}\right]^2} \tag{B.100}$$

and the derivative with respect to n_o is given by

$$\frac{\partial f_w(S_{w,well},\vec{m}_{prod})}{\partial n_o} = -\frac{a_o\mu_o\mu_w a_w\left(\frac{S_{or}+S_{wf}-1}{S_{iw}+S_{or}-1}\right)^{n_o}\left(\frac{S_{iw}-S_{wf}}{S_{iw}+S_{or}-1}\right)^{n_w}\ln\left(\frac{S_{or}+S_{wf}-1}{S_{iw}+S_{or}-1}\right)}{\left[a_o\mu_w\left(\frac{S_{or}+S_{wf}-1}{S_{iw}+S_{or}-1}\right)^{n_o}+\mu_o a_w\left(\frac{S_{iw}-S_{wf}}{S_{iw}+S_{or}-1}\right)^{n_w}\right]^2}. \quad \text{(B.101)}$$

The derivative of the function R_{prod} with respect to the well water saturation or any model parameter m_i is given by

$$\frac{\partial R_{prod}}{\partial(S_{w,well}/m_i)} = \frac{\partial r_{inj}^2}{\partial(S_{w,well}/m_i)} + \frac{\theta q_{prod}\Delta t_{prod}}{\pi\phi h}\frac{\partial}{\partial(S_{w,well}/m_i)}\left(\frac{\partial f_w}{\partial S_w}(S_{w,well}(\vec{m}_{prod}),\vec{m}_{prod})\right), \quad \text{(B.102)}$$

where before the breakthrough, we have

$$\frac{\partial r_{inj}^2}{\partial S_{w,well}} = 0 \quad \text{(B.103)}$$

and

$$\frac{\partial r_{inj}^2}{\partial m} = \frac{\theta q_{inj}\Delta t_{inj}}{\pi\phi h}\frac{\partial}{\partial m}\left(\frac{\partial f_w}{\partial S_w}(S_{wf}(m),m)\right) \quad \text{(B.104)}$$

After breakthrough, we have

$$\frac{\partial r_{inj}^2}{\partial S_{w,well}} = \frac{\theta q_{inj}\Delta t_{inj}}{\pi\phi h}\frac{\partial}{\partial S_{w,well}}\left(\frac{\partial f_w}{\partial S_w}(S_{w,well}(m),m)\right) \quad \text{(B.105)}$$

and

$$\frac{\partial r_{inj}^2}{\partial m} = \frac{\theta q_{inj}\Delta t_{inj}}{\pi\phi h}\frac{\partial}{\partial m}\left(\frac{\partial f_w}{\partial S_w}(S_{w,well}(m),m)\right). \quad \text{(B.106)}$$

The derivative of the water front saturation with respect to the any model parameters m_i can be found from the derivative of the expression,

$$R_{S_{wf}}(S_{wf}) = \frac{\partial f_w(S_{wf})}{\partial S_w} - \frac{f_w(S_{wf})-f_w(S_{iw})}{S_{wf}-S_{iw}} = 0, \quad \text{(B.107)}$$

used to estimate S_{wf}. If we take the derivative of Eq. B.107 with respect to S_{wf}, we find

$$\frac{dR_{S_{wf}}}{dm_i} = \frac{\partial R_{S_{wf}}}{\partial m} + \frac{\partial R_{S_{wf}}}{\partial S_{wf}} \frac{\partial S_{wf}}{\partial m_i} = 0. \tag{B.108}$$

By isolating $\frac{\partial S_{wf}}{\partial m_i}$ in Eq. B.108, we have

$$\frac{\partial S_{wf}}{\partial m_i} = -\frac{\frac{\partial R_{S_{wf}}}{\partial m_i}}{\frac{\partial R_{S_{wf}}}{\partial S_{wf}}}, \tag{B.109}$$

which leads to

$$\frac{\partial S_{wf}}{\partial m_i} = \frac{\frac{\frac{\partial f_w(S_{wf})}{\partial m_i} - \frac{\partial f_w(S_{iw})}{\partial m_i}}{S_{wf} - S_{iw}} - \frac{\partial}{\partial m_i}\left(\frac{f_w(S_{wf})}{\partial S_w}\right)}{\frac{\partial}{\partial S_{wf}}\left(\frac{f_w(S_{wf})}{\partial S_w}\right)} \tag{B.110}$$

from

$$\frac{\partial R_{S_{wf}}}{\partial S_{wf}} = \frac{\partial}{\partial S_{wf}}\left(\frac{f_w(S_{wf})}{\partial S_w}\right) - \frac{\frac{\partial f_w(S_{wf})}{\partial S_{wf}} - \frac{f_w(S_{wf}) - f_w(S_{iw})}{S_{wf} - S_{iw}}}{S_{wf} - S_{iw}} = \frac{\partial}{\partial S_{wf}}\left(\frac{f_w(S_{wf})}{\partial S_w}\right), \tag{B.111}$$

where Eq. B.107 was applied, and

$$\frac{\partial R_{S_{wf}}}{\partial m_i} = \frac{\frac{\partial f_w(S_{wf})}{\partial m_i} - \frac{\partial f_w(S_{iw})}{\partial m_i}}{S_{wf} - S_{iw}} - \frac{\partial}{\partial m_i}\left(\frac{f_w(S_{wf})}{\partial S_w}\right). \tag{B.112}$$

B.4 Validation

"In cases of major discrepancy it's always reality that's got it wrong."

— Douglas Adams in *The Restaurant at the End of the Universe*

To validate the derivatives presented in this Appendix, the analytical derivatives of the observed data with respect to the model parameters were compared with the gradient obtained using finite-difference,

$$\nabla_{m_i} \Delta p_{wf,FD} = \frac{\Delta p_{wf}(m_i + \epsilon_i) - \Delta p_{wf}(m_i)}{\epsilon_i}, \tag{B.113}$$

where we tried to guarantee that the relative errors, given by

$$Rel\_Error_i = \frac{\nabla_{m_i}\Delta p_{wf,FD} - \nabla_{m_i}\Delta p_{wf}}{\nabla_{m_i}\Delta p_{wf,FD} + 10^{-14}}, \quad \text{for } i = 1, ..., n \tag{B.114}$$

were less than 0.01. To be able to match our analytical derivatives with the derivatives obtained with finite-difference, we had to use a distinct perturbation parameters ϵ_i for each model parameter m_i; we had to performed an extensive numerical experimentation to find the appropriate values for ϵ. We noticed that in same cases, by varying ϵ in one order of magnitude, the relative error could increase up to several orders of magnitude. Therefore, we recommended the use of analytical derivatives whenever is available or at least the implementation of a robust algorithm to find the perturbation parameters.

"Finally, from so little sleeping and so much reading, his brain dried up and he went completely out of his mind."

— Miguel de Cervantes Saavedra, *Don Quixote*